NORTH-WEST UNIVERSITY
YUNIBESITI YA BOKONE-BOPHIRIMA
NOORDWES-UNIVERSITEIT

Characterisation and thermodynamic stability of solvated crystal forms of mebendazole

Carel A. Swartz

2008

CHARACTERISATION AND THERMODYNAMIC STABILITY OF SOLVATED CRYSTAL FORMS OF MEBENDAZOLE

Carel André Swartz

B.Pharm

12527327

Dissertation submitted in partial fulfillment of the requirements for the degree Magister Scientiae in the Department of Pharmaceutics at the North-West University, Potchefstroom Campus.

Supervisor:	Dr. M. Brits
Co-supervisor:	Mr. Z. Perold
Assistant-suptervisor:	Me. M. Auckamp

POTCHEFSTROOM

NOVEMBER 2008

TABLE OF CONTENT

CHAPTER 2: PHYSICO-CHEMICAL AND PHARMACOLOGICAL PROPERTIES OF MEBENDAZOLE AND VARIOUS CRYSTALLINE FORMS THEREOF

ABSTRACT

Characterisation and thermodynamic stability of solvated crystal forms of mebendazole

Solid-state studies form an integral part in the research and development (R&D) of pharmaceuticals. The main objective of these studies is usually the preparation of a crystal form with improved solubility & thermodynamic stability, which will ultimately result in enhanced therapeutic efficacy.

The inclusion of specific solvent molecules into a crystal lattice may stabilise or destabilise the crystal structure (Byrn *et al.*, 1999:234). These alterations to the stability of the crystal structure may result in significant changes to the physico-chemical properties of the solid. This study focused on the ability of mebendazole to incorporate solvent molecules into its crystal lattice, and on the thermodynamic stability of these solvated systems.

A novel pseudo-polymorphic form of mebendazole (Form D) was prepared by means of accelerated recrystallisation using acetic-acid as solvent. The same method was utilised (using propionic-acid as solvent) to prepare the mebendazole propionic acid complex (referred to as Form E) previously reported by Caira *et al.* (1998:11-15).

The physico-chemical properties of the two solvated forms were investigated using DRIFT-IR, DSC, TGA, XRPD, VT-XRPD, KF, & SEM. The incorporation of the two different solvent molecules (i.e. acetic acid and propionic acid) into the crystal lattices, induced a significant difference in the dissolution profiles of the two forms in 0.1 N HCl at 37°C ($f_2 = 16$). The powder dissolution profiles of Form D indicated a 51% dissolution whereas Form E revealed a 97% dissolution after 120 minutes. The difference in the dissolution profiles was attributed to the fact that a fraction of Form D underwent a solvent mediated phase transition (in the dissolution medium) and was transformed to the poorly soluble Form A.

The thermodynamic stability of Form D and Form E was investigated. When exposed to increased temperatures both forms desolvated and were transformed into the thermodynamically stable form, Form A.

Non-isothermal studies revealed that more energy was required to initiate the desolvation of Form E, compared to the activation energy required for the desolvation of Form D. Based on this observation (and the VT-XRPD results) it was concluded that Form D was thermodynamically less stable compared to Form E.

Isothermal studies revealed that the mechanism of desolvation for Form D and Form E was temperature dependant, and that the rate of desolvation for both forms were in the order: 100°C > 90°C > 80°C.

Stability studies of mebendazole Forms D and E at: (1) 25±2 °C & 60±5 % RH, (2) 40±2 °C & 75±5 % RH, (3) 25±2 °C & 0 % RH and (4) 40±2 °C & 0 % RH – for 28 days - revealed that the rate and mechanism of desolvation of the two forms were temperature dependant. The mechanism for the desolvation of Form D, when exposed to 25±2°C & 60±5 % RH was best described by the second-order reaction (F2-model) and when exposed to 25±2°C & 0 % RH, by the Avrami-Erofeev reaction (A3/2-model). The rate of desolvation of Form D at 25±2°C & 60±5 % RH was 18 times faster compared to the desolvation of Form D at 25±2°C & 0 % RH.

The shelf-life of Form D when stored at 25±2°C & 60±5 % RH was 2.6 times lower compared to when Form D was stored at 25±2°C & 0 % RH, suggesting that the presence of moisture facilitated the desolvation process.

Desolvation of Form E was detected when it was stored at 25±2°C & 60±5 % RH, 40±2°C & 0 % RH and 40±2°C & 75±5 % RH. The rate of desolvation was in the order: 40±2°C & 75±5 % RH > 25±2°C & 60±5 % RH > 40±2°C & 0 % RH, which once again suggested that moisture might have acted as a catalyst for the desolvation of Form E.

The postulated mechanism for the desolvation of Form E when exposed to 25±2°C & 60±5 % RH was best described by the Avrami-Erofeev reaction (A3/2-model). No suitable desolvation mechanism was identified for the desolvation of Form E, when stored at 40±2°C & 75±5 % RH.

UITTREKSEL

Karakterisering en termodinamiese stabiliteit van die gesolveerde kristalvorme van mebendasool

Vaste-toestand studies vorm 'n integrale deel in die navorsing en ontwikkeling (N&O) van farmaseutiese doseervorme. Die primêre doel van vaste toestand-studies is om 'n kristalvorm met verbeterde oplosbaarheid en termodinamiese stabiliteit te berei, om sodoende verbeterde terapeutiese effektiwiteit te verseker.

Die inkorporering van `n oplosmiddel in `n kristal latwerk, verander die stabiliteit daarvan (Byrn *et al.*, 1999:234). Die verandering in die stabiliteit kan merkwaardige veranderinge in die fisies-chemiese eienskappe veroorsaak. Hierdie studie het gefokus op die potensiaal van mebendasool om as 'n gesolveerde kristalvorm te bestaan, en om dan die termodinamiese stabiliteit van hierdie gesolveerde sisteme te bepaal.

`n Nuwe pseudo-polimorfiese vorm van mebendasool (Vorm D) was berei deur middel van `n versnelde rekristallisasie metode waar asynsuur as oplosmiddel gebruik is. Dieselfde metode was gebruik (met propioonsuur as oplosmiddel) vir die bereiding van die mebendasool propioonsuur-kompleks (verwys na as Vorm E), soos gerapporteer deur Caira *et al.* (1998:11-15).

Die fisies-chemiese eienskappe van die twee gesolveerde vorme was ondersoek met DRIFT-IR, DSC, TGA, XRPD, KF en SEM. Die solvering van die kristal latwerk met asynsuur en propioonsuur afsonderlik, het merkwaardige verskille in die dissolusie-profiele van die twee vorme, in 0.1N HCl by 37°C veroorsaak (f_2 = 16). Slegs 51% van Vorm D het na 120 minute in die dissolusie medium opgelos, in vergelyking met 95% van Vorm E. Die verskille in die dissolusie profiele is toegeskryf aan die feit dat `n fraksie van Vorm D `n oplosmiddel gefasiliteerde fase omskakeling na die swak oplosbare Vorm A ondergaan het (in die dissolusie medium).

Die termodinamiese stabiliteit van Vorm D en Vorm E was ondersoek. Met blootstelling aan verhoogde temperature, het beide vorme gedesolveer en omgeskakel na Vorm A.

Non-isotermiese studies het getoon dat meer energie nodig was om desolvering van Vorm E te inisiëer in vergelyking met die aktiveringsenergie wat benodig was vir die desolvering van Vorm D. Vanuit die resultate kan afgelei word dat Vorm E termodinamies meer stabiel is as Vorm D.

Isotermiese studies het getoon dat die meganisme van desolvering van Vorm D en Vorm E temperatuur afhanklik was en dat die tempo van desolvering van beide vorme in die orde: 100 °C > 90 °C > 80 °C, was.

Versnelde stabiliteit studies op Vorm D en E by: (1) 25±2 °C & 60±5 % RH, (2) 40±2 °C & 75±5 % RH, (3) 25±2 °C & 0 % RH en (4) 40±2 °C & 0 % RH het getoon dat die tempo en meganisme van desolvering van die twee vorme temperatuur afhanklik was. Die meganisme vir die desolvering van Vorm D, na blootstelling aan 25±2 °C & 60±5 % RH was die beste beskryf deur `n tweede orde reaksie (F2-model) en wanneer blootgestel aan 25±2 °C en 0 % RH, deur die Avrami-Erofeev model (A3/2-model). Die tempo van desolvering van Vorm D by 25±2 °C & 60±5 % RH was 18 keer vinniger in vergelyking met die desolvering van Vorm D by 25±2 °C & 0 % RH.

Die rakleeftyd van Vorm D by 25±2 °C & 60±5 % RH was 2.6 keer laer in vergelyking met die rakleeftyd daarvan by 25±2 °C & 0 % RH. Hieruit is afgelei dat vog die desolveringsproses kataliseer.

Vorm E het gedesolveer by 25±2 °C & 60±5 % RH, 40±2 °C & 0 % RH en 40±2 °C & 75±5 % RH. Die tempo van desolvering was in die orde: 40±2 °C & 75±5 % RH > 25±2 °C & 60±5 % RH > 40±2 °C & 0 % RH, wat weereens daarop gedui het dat vog as katalisator opgetree het tydens die desolvering van Vorm E.

Die Avrami-Erofeev model (A3/2-model) het die desolveringsmeganisme van Vorm E by 25±2 °C & 60±5 % RH die beste beskryf. Geen desolveringsmeganisme was geïdentifiseer vir die desolvering van Vorm E by 40±2 °C & 75±5 % RH nie.

AIMS AND OBJECTIVES

Characterisation and thermodynamic stability of solvated crystal forms of mebendazole

Solid-state studies on active pharmaceutical ingredients (APIs) are becoming a more diverse and important field of focus for pharmaceutical manufactures, due to the impact of polymorphism on the physico-chemical properties of the APIs (Bernstein, 2002:27).

It was reported in the literature that mebendazole exhibited three polymorphic forms, Forms A, B and C. Form C is the pharmaceutically preferred polymorph for manufacturing due to its favoured dissolution profile and therapeutic activity. The existence of a pseudo-polymorphic form of mebendazole (propionic acid complex) has been reported (Caira *et al.*, 1998:11-15) though very little information was available on the physico-chemical properties of this form.

It is known that the inclusion of specific solvent molecules into a crystal lattice may stabilise the crystal structure (by improving either the crystal packing or intermolecular bonding) or lead to the formation of an unstable crystal structure (Byrn *et al.*, 1999:234).

This study focused on the ability of mebendazole to incorporate solvent molecules into its crystal lattice, and on the thermodynamic stability of this solvated system.

The aims of this study were achieved by pursuing the following study objectives:

- Undertake a literature overview on polymorphism and pseudo-polymorphism and the successful application of analytical techniques (such as: DRIFT-IR, XRPD, DSC, TGA, KF, etc.) to characterise and investigate the physico-chemical properties of the different crystal forms.

- Prepare and characterise the propionic-acid complex. Provide additional information with regards to the thermodynamic stability of this solvated form.

- Prepare and characterise a new acetic-acid solvate of mebendazole (Form D). To investigate the physico-chemical properties and thermodynamic stability of the new form (Form D).

- Determine the effect of the incorporated solvent molecules on the dissolution profiles of the two pseudo-polymorphs and compare it to the dissolution profiles of the non-solvated polymorphic forms of mebendazole (Forms A, B and C).

- Investigate and determine the mechanism and energies associated with the desolvation of the two solvated forms.

- Investigate the thermodynamic stability of the solvated forms when exposed to increased temperatures and moisture.

The newly acquired knowledge will provide valuable information with regards to the ability of mebendazole to incorporate solvent molecules into its crystal lattice, and on the thermodynamic stability of these solvated systems

CHAPTER 1

The importance and influence of the solid-state properties of pharmaceuticals

Introduction

During the last century, more scientists have become aware of the existence, potential and properties of different polymorphic forms since the initial observation thereof. (Bernstein, 2002:1). The term *polymorphism* (Greek: *poly* = many, *morph* = form) has a diversity of uses in the pharmaceutical-, material-, crystallographical-, microbiological and genetic- sciences. However, when used in relation to material science or crystallography, the simplest definition originated from Rosenstein and Lamy, which reads as follows: "when a substance can exist in more than one crystalline state it is said to exhibit polymorphism" (McCrone & Haleblian, 1969:911; Bernstein, 2002:1-2; 19-27).

Walter C. McCrone (1965:726-728) stated that the physico-chemical properties of polymorphs might differ to the same extent as crystals of different compounds. Seeing that most organic and inorganic pharmaceutical compounds exist in one or more crystalline state (Vippagunta *et al.*, 2001:4), it is necessary to evaluate the effect it may have on the life cycle management (LCM) of Active Pharmaceutical Ingredients (APIs), research and design (Bernstein, 2002:1-2).

1.1 The solid-state

Pharmaceutical solids can be classified as: *crystalline* (which includes polymorphs, solvates, and hydrates) or as *amorphous solids*. Figure 1.1 represents the outline to be followed in order to characterise an API. This is done by assessing the differences between the external appearance (crystal habit) and internal structure (molecular packing) of the same chemical entity (Haleblian, 1975:1269).

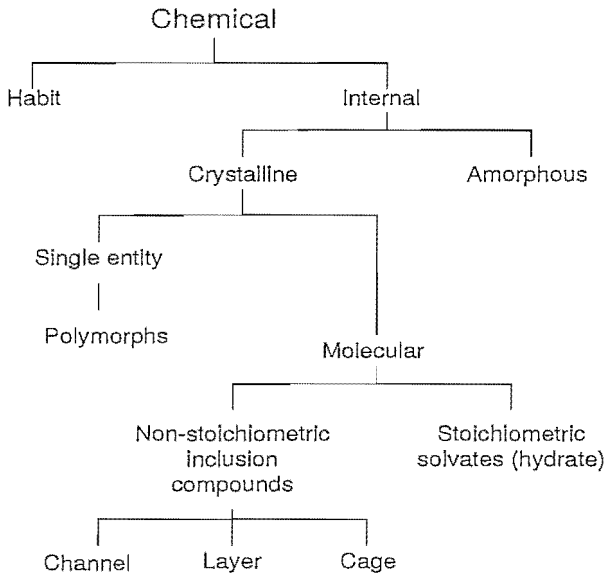

Figure 1.1 Outline differentiating between habit and crystal packing of a chemical compound (Haleblian, 1975:1270).

In order to proceed to the evaluation and classification (and subsequent influences) of these internal and external structural differences of crystal forms, it is first required to take a look into the factors which are responsible for these differences in the solid state. These factors include:

- Crystal formation;
- The forces responsible in crystal packing;
- The three dimensional characteristics of a solid;
- Crystal growth.

1.1.1 The formation and internal characteristics of a crystalline solid

The method by which crystal formation is acquired, plays an important role in the pharmaceutical industry, especially in drug design and preference polymorph manufacturing (Byrn *et al.,* 1999:15). In order to ensure that the desired crystal form is present in the final product, it is required to understand how crystals are formed, and to have some insight into the three dimensional properties of the crystal. Sections 1.1.1.1 to 1.1.1.3 will focus on the formation of crystals, whereas section 1.1.2 will detail the properties of the three dimensional structure.

1.1.1.1 Crystal formation

Crystals are defined as an orderly and infinite arrangement of molecules or atoms in a solid through the infinite repetition of a number of unit cells in a three dimensional space. This orderly arrangement of molecules or atoms plays a fundamental role in the classification of the crystalline structure (Vippagunta *et al.*, 2001:4; Byrn *et al.*, 1999:506, Sands, 1993:2).

For a single crystal to be formed, the infinite repetition in space of the same identical structural building units must occur. The structural building unit of an elemental or ionic crystal consists of a single atom or ion. In the case of organic crystals the structural building unit is one molecular unit (Byrn *et al.* 1999:1-15). Figure 1.2 illustrates crystal formation.

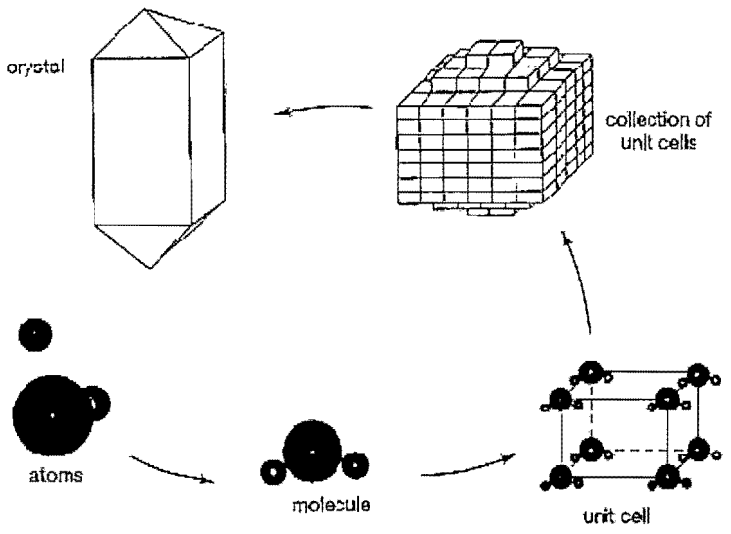

Figure 1.2 The formation of a crystal from atoms and molecules (Whitney, 2007).

The pharmaceutical industry utilises a variety of different techniques to produce different types of crystal forms. These techniques are summarised in Table 1.1.

Table 1.1 Methods for the formation of pharmaceutical solids in the industry (Byrn, 1999:16)

Pharmaceutical manufacturing methods
▪ Evaporation (including spray drying and slurry fill).
▪ Cooling a solution.
▪ Seeding a supersaturated solution with crystals of the desired form.
▪ Freeze drying (including from mixed solvents).
▪ Addition of anti-solvents.
▪ Salting out.
▪ Changing pH.
▪ Addition of reagent to produce a salt or new compound.
▪ Deliberation phase transitions during slurry, washing or drying steps.
▪ Simultaneous addition of two solvents.

1.1.1.2 Solubility and saturation conditions

Byrn *et al.* (1999:15) defined the solubility of an API as the concentration where the solution phase is in equilibrium with a given solid phase at a specific temperature and pressure. Martin (1993:212) stated that the solubility of a compound depends on the physical and chemical properties of the solute and the solvent, temperature, pressure, pH of the solvent and to a lesser extent the state of subdivision of the solute.

The formation of crystals (via recrystallisation) requires that the compound be soluble in the solvent at a specific concentration, where the solution phase is in equilibrium with the solid phase at the temperature and pressure by which the experiment is governed, to form a homogenous molecular dispersion (Martin, 1993:212; Byrn *et al.*, 1999:16).

An important factor to consider when preparing a solution for recrystallisation is the level of saturation of the solution. Three saturation conditions (or levels) exist, all differing in the concentration of the solute in the solvent. The three saturation conditions are summarised in Table 1.2 and illustrated in Figure 1. 3.

Table 1.2 Saturation conditions (Byrn *et al.*, 1999:16)

Saturation condition	Description
Saturated	The solute is in equilibrium with the solvent leaving the crystals neither dissolved nor allowing crystal growth.
Undersaturation	The concentration of the solute is less than that of the solvent forming a diluted solution where the solute crystals will dissolve.
Supersaturation	The concentration of the solute is more than that of the solvent, forming a concentrated solution where crystals will begin to grow.

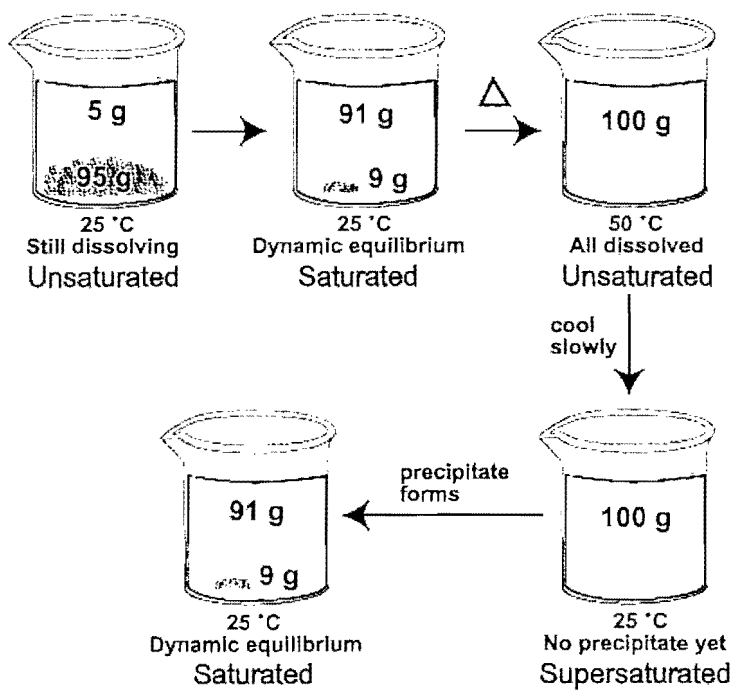

Figure 1.3 Illustration of the preparation of unsaturated, saturated and supersaturated solutions (Bishop, 2008).

1.1.1.3 Nucleation

Byrn *et al*, (1999:512) defined *nucleation* as the formation of stable molecular assemblies, leading to crystallisation. *Nucleation* normally occurs in a supersaturated solution. The first step in the formation of crystal (in a supersaturated solution) is the assembly of unit cells in the solution to form nuclei that will act as the centres of crystallisation and eventually lead to the formation of crystals (Hilfiker, 2007:34).

The nucleation process is divided into two categories, namely primary and secondary nucleation. In primary nucleation there are no traces of crystals present in the recrystallisation solution initially. During *secondary nucleation* there are crystals present in the recrystallisation solution. To ensure that crystal growth occurs during primary nucleation, the number of nuclei that needs to be formed in the recrystallisation solution (*n*) must be higher than the critical concentration (*n**), otherwise the formed nuclei will once again dissolve in the recrystallisation solvent (Figure 1.4) (Byrn *et al.*, 1999:16-18, Hilfiker, 2007:34-37).

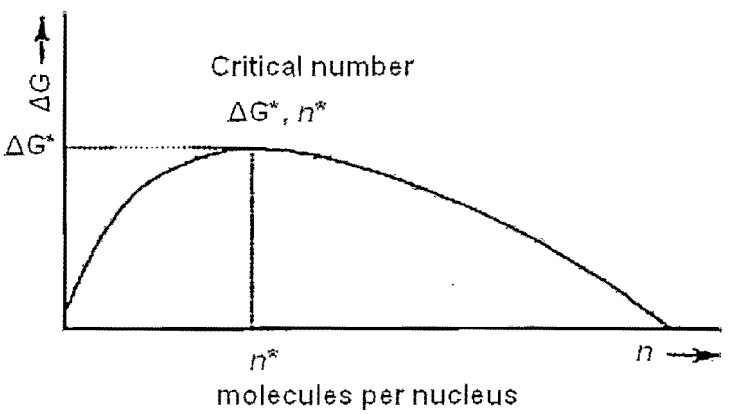

Figure 1.4 Changes in free energy (ΔG) during nucleation required for crystal formation. Molecules assemble and disassemble until a nucleus of a critical number (*n**) with an energy ΔG* is achieved, ensuring an increase in the size of the nucleus (Lieser, 1969:207).

Primary nucleation can be classified into two sub categories: i.e. *homogeneous* and *heterogeneous nucleation. Homogeneous nucleation* occurs spontaneously and can only be achieved in a small volume of recrystallisation solutions with a volume of less than 100µl. *Heterogeneous nucleation* occurs more commonly and takes place at interfaces or surfaces where it may be induced through means of foreign particles present in the recrystallisation solution (i.e. seeding) (Hilfiker, 2007:34-35).

Secondary nucleation involves the nucleation of crystals present in the recrystallisation solution by means of continuous crystallisation. The process of secondary nucleation can be initiated by deliberate seeding of the recrystallisation solution or it pursues the primary nucleation step. Secondary nucleation is affected by various factors which include: temperature, concentration gradients, crystal irregularities caused by impurities, crystal form and crystal habit (Byrn *et al.*, 1999:17). These factors can be difficult to control as the environment is ever changing and dynamic, therefore the continuous monitoring of the nucleation process is required to ensure the formation of the preferred crystal form. The factors that may influence the nucleation process are summarised in Table 1.3.

Table 1.3 Factors that influences the nucleation process (Byrn *et al.*, 1999:17)

Factors affecting nucleation
▪ Pre-existing nuclei on equipment or in air.
▪ Foreign particles of a suitable nature.
▪ Deliberate seeding with desired phase.
▪ Local hypersaturation by soluble metastable phase.
▪ Separation of a liquid phase during processing (i.e., temperature change or addition of antisolvent).
▪ Local hypersaturation at an immiscible solvent interface.
▪ Ultrasonic or shock waves.
▪ Scratched surfaces.
▪ Local temperature irregularities.
▪ Local concentration gradients (e.g., created by surface evaporation or reagent addition).

Figure 1.5 illustrates a crystallisation system where different polymorphs are formed due to a lack of control during the recrystallisation procedure. In a system where more than one crystal form is possible for an API, each of the crystal forms exists its own solubility value, which is determined by specific conditions including solvent composition, temperature and pressure. In Figure 1.5 (a) and (b) two possible crystal forms for an API is illustrated with respect to the different solubility limits, S_I and S_{II} and in Figure 1.5 (c) a mixture of the polymorphs results due to a lack of control during the crystallisation procedure (Byrn *et al.*, 1999:18-19).

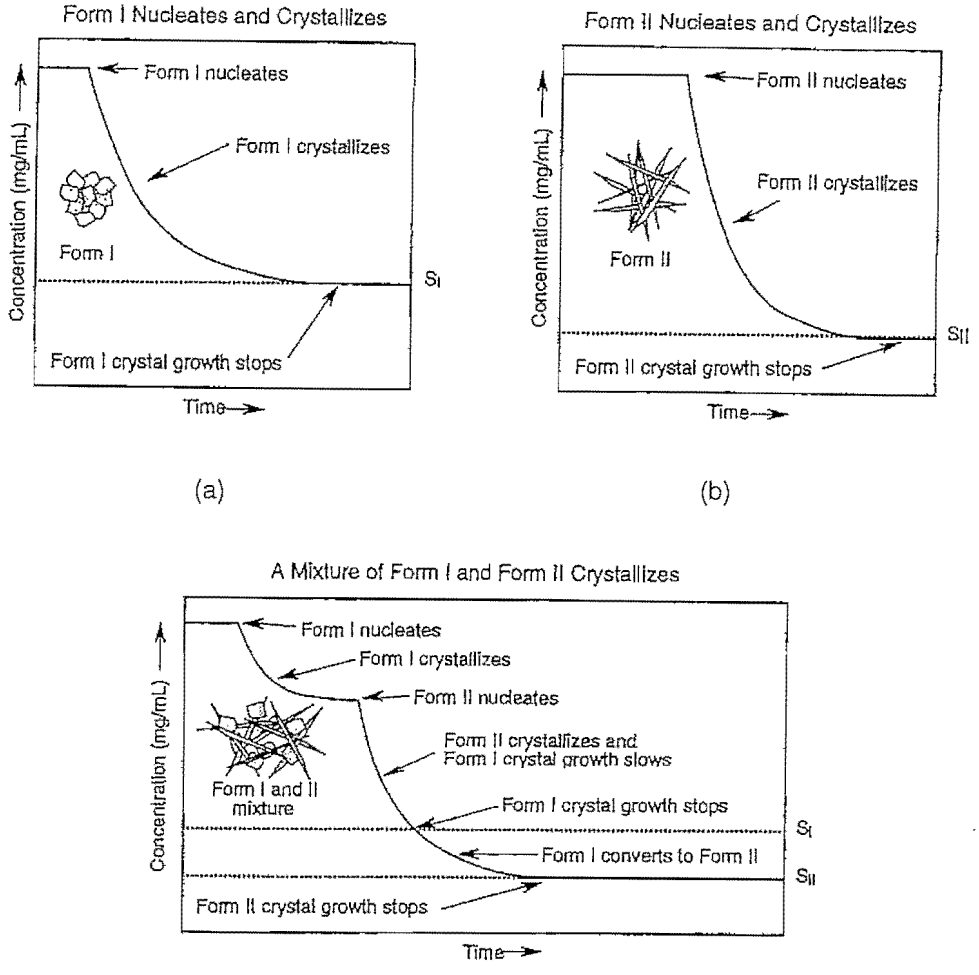

Figure 1.5 Uncontrolled crystallisation in a polymorphic system showing the different polymorphs: (a) Form I and (b) Form II or (c) the mixture of polymorphs that may form (S_I and S_{II} are the solubility limits for Forms I and II, respectively) (Byrn *et al.*, 1999:18).

Control over the nucleation process is therefore an absolute necessity to ensure the formation of the desired polymorphic form during the manufacturing thereof.

1.1.2 The three dimensional characteristics of the crystal forms

As mentioned in section 1.1, the internal structure of a solid contributes to the specific characteristics thereof. This section will discuss the three dimensional properties of unit cells and subsequently, the crystal lattice.

A *lattice point* is defined as a normal periodic arrangement of points in space connected through a three dimensional grid in various directions to form an infinite number of different lattice structures. The three dimensional points of the lattice (Figure 1.6) are defined by three fundamental translation vectors: a, b and c (Brittain, 1999:75; Byrn *et al.*, 1999:5-6).

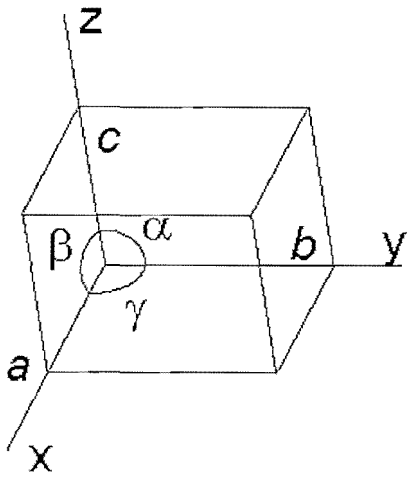

Figure 1.6 Illustration of the translation vectors and angles of a unit cell (Anon, 2007).

The *translation vectors* (a, b and c) are also known as the *crystal axes*, and creates the three adjacent edges of a parallelepiped. The smallest parallelepiped is known as the *unit cell* which has a definite volume and shape. The unit cell is not only defined by the lengths of the translation vectors, but also by the angles α, β and γ. These angles are formed by two adjacent translation vectors as defined in Table 1.4 (Brittain, 1999:75-76; Vippagunta *et al.*, 2001:3-4).

Table 1.4 Angle positions in a unit cell (Brittain, 1999:76)

Angle	Position of the angle
α	Between translation vector b and c.
β	Between translation vector a and c.
γ	Between translation vector a and b.

There are seven primitive unit cell systems which play a fundamental role in the characterisation of crystalline solids. These seven crystal systems are tabulated in Table 1.5 (Brittain, 1999:75-76; Vippagunta *et al.*, 2001:3-4).

Table 1.5 Properties of the seven fundamental systems (Brittain, 1999:77)

Crystal system	Relationship translation vectors	Relationship between unit cell angles
Cubic	$a = b = c$	$\alpha = \beta = \gamma = 90°$
Tetragonal	$a = b \neq c$	$\alpha = \beta = \gamma = 90°$
Orthorhombic	$a \neq b \neq c$	$\alpha = \beta = \gamma = 90°$
Monoclinic	$a \neq b \neq c$	$\alpha = \gamma = 90°; \beta \neq 90°$
Triclinic	$a \neq b \neq c$	$\alpha \neq \beta \neq \gamma \neq 90°$
Hexagonal	$a = b \neq c$	$\alpha = \beta = 90°; \gamma = 120°$
Trigonal	$a = b = c$	$\alpha = \beta = 90°; \gamma \neq 90°$

The properties of crystal lattices are not only defined by the *lattice translations*, but also *symmetry operations*. A *symmetry operation* is defined as an operation involved in the change of the crystal configuration, without changing the appearance of the crystal lattice. There are six known symmetry operations (Brittain, 1999:77-78; Sands, 1993:14-26):

- **Identity (E)** – Rotation of the unit cell of 360° about any axis.
- **Mirror plane (Reflection)** (σ) – Reflection of the unit cell through a plane. Reflection leaves the coordinates parallel to the plane unchanged, while changing the coordinates perpendicular to the plane.

- **Center of inversion** (i) – Changes the sign of the coordinates that define a lattice point in space.
- **Rotation axis** (C_n) – A simple counterclockwise rotation of 360° /n about an axis that passes through a lattice point.
- **Improper rotation axis (rotatory reflection axis)** (S_n) – Rotation of 360°/*n* followed by reflection in a plane perpendicular to the axis.
- **Improper rotation axis (rotatory inversion axis)** (S_n) – Rotation of 360°/*n* followed by inversion through a point on the axis.

Auguste Bravais proved that fourteen distinct space lattices exist in a three-dimensional space if the unit cell of the crystal displays symmetry (Brittain, 1999:78). The combination of the seven crystal systems (Table 1.5) together with the concept of a primitive lattice (labelled P), results in the formation of only six primitive lattices. The reason for this is attributed to the fact that hexagonal and trigonal lattices are equivalently constructed. This gives rise to the first six Bravais lattices. The other eight Bravais lattices are obtained when the six primitive Bravais lattices are considered and additional lattice points are added through centering conditions to the primitive lattices. Seven of the eight obtained lattices are labelled either body-centered (I), base-centered (C) or face-centered (F) and the last centered hexagonal lattice which is referred to as a primitive rhombohedral lattice (Brittain, 1999:78-82; Razeghi, 2002:11). Figure 1.7 illustrates an example of a face-centered cubic unit cell of a sodium chloride crystal.

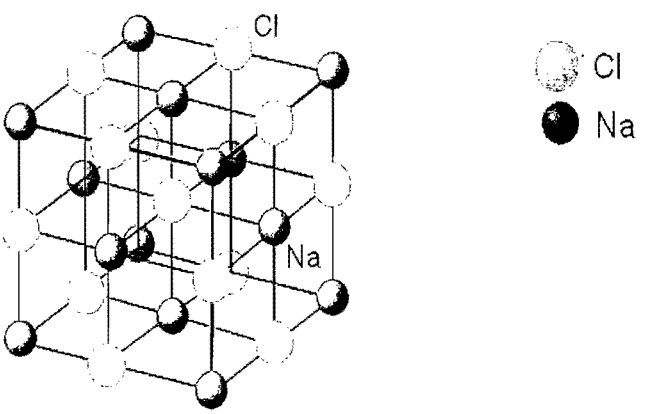

Figure 1.7 Face centered cubic unit cell of a sodium chloride crystal (Own, 2000).

The fourteen Bravias lattices are graphically illustrated in Table 1.6.

Table 1.6 The fourteen Bravais lattices (Brittain, 1999:81)

Unit cell	Bavias lattices			
	Primitive (P)	Body-centered (I)	Base-centered (C)	Face-centered (F)
Cubic	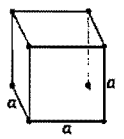	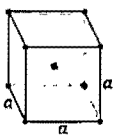		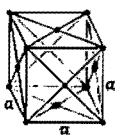
Tetragonal	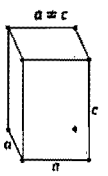	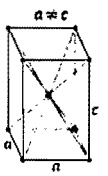		
Orthorhombic	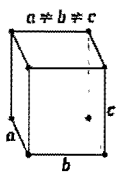	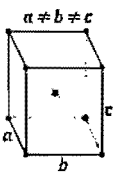	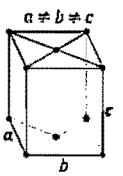	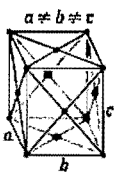
Monoclinic	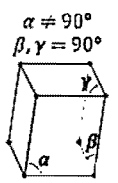		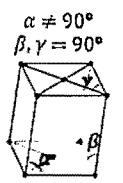	
Triclinic	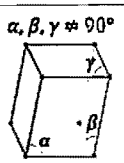			
Trigonal (Rhombohedral)	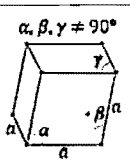			
Hexagonal	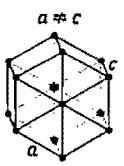			

The crystal structure of a given compound can be assigned to one of the fourteen Bravais lattices. When combining the fourteen Bravais lattices with the 32 crystallographic point groups and taking into consideration the symmetry operations, a maximum of 230 space groups are defined to the structure of a crystal. Sands (1993:71-73) defined a *space group* as a group whose elements include both the point symmetry elements and the translations of a crystal. Brittain (1999:82) defined a *space group* as the set of geometrical symmetry operations that take a three-dimensional crystal into itself and describes the spatial symmetry of the crystal (Brittain, 1999:82-84; Byrn, 1999:5).

1.1.3 Forces responsible for crystal packing

In order for molecules to exist in the solids phase, intermolecular forces must be present (Martin, 1993:22). The most common intermolecular forces include: van der Waals, London forces, dipole-dipole interactions, dispersion forces, hydrogen bonds, charge-transfer interactions and electrostatic interactions. The intermolecular forces are divided into three classes (1) non-bonded (van der Waals, London forces, etc), (2) electrostatic forces and (3) hydrogen bonding (Bernstein, 2002:152-153).

When molecules interact, both attractive and repulsive forces operate as one, affecting the potential energy of the molecules and stability of the system. These intermolecular forces in molecular crystals are weak compared to the forces involved in chemical bonding (Martin, 1993:22).

1.1.3.1 Non-covalent attractive forces

Non-covalent attraction interactions depend on dipole moments, polarity and electronic distribution in the molecules (Byrn *et al.*, 1999:7). These forces are in general weak intermolecular forces that exist between the molecules and atoms of the crystal (Bernstein, 2002:153). Several classes of van der Waals interactions exist and are tabulated in Table 1.7.

1.1.3.2 Hydrogen bonding

Hydrogen bonding exhibits the strongest and most direct intermolecular interactions (Figure 1.8). This type of bonding normally occurs between a molecule containing a hydrogen atom and a strong electronegative molecule (acceptor-donor pair), usually containing a nitrogen, oxygen or fluoride atom. When a hydrogen atom moves into contact with a strong electronegative atom, a hydrogen bond or hydrogen bridge forms between the two atoms of the molecules (Martin, 1993:23-25).

For this reason hydrogen bonding plays a more prominent role in polymorphism, especially for those compounds which contain a number of possible hydrogen bond acceptors and donors (Bernstein, 2002:54).

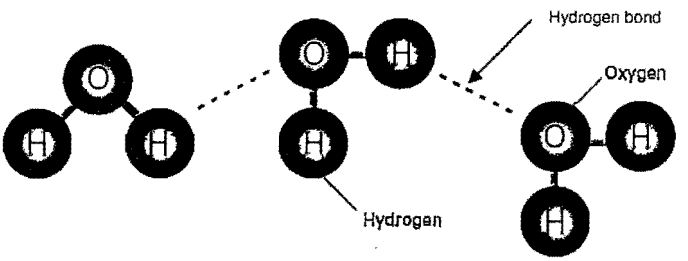

Figure 1.8 Illustration of hydrogen bonding between water molecules. The hydrogen bond that formed is indicated by the dashed-line (Anon, 2006).

The strength of the hydrogen bond between the various hydrogen donors and acceptors will not necessarily be equal (refer to Table 1.7). This is due to the fact that strong hydrogen acceptors prefer strong hydrogen donors to form a bond (Bernstein, 2002:49-55).

The incorporation of water molecules into a crystal lattice during manufacturing (i.e. wet granulation, spray drying, etc.), is not an uncommon occurrence. If a water molecule is incorporated into the crystal lattice, a *hydrated crystal lattice* is produced (Khankari *et al.*, 1995:61-62). Hydrates are discussed in more detail in section 1.3.2.

The type and extent of the inter-molecular forces present in the solid plays an important role in polymorph stability.

Table 1.7 Intermolecular forces and valence bonds (adapted from Martin, 1993:23)

Bond type	Bond Energy (approx.) (kcal/mole)
Van der Waals forces and other intermolecular attractions	
Dipole-dipole interaction, orientation effect, or Keesom force	1-10
Dipole-induced dipole interaction, induction effect or Debye force	1-10
Induced dipole-induced dipole interaction, dispersion effect or London force	1-10
Hydrogen bonds: O-H···O	6
C-H···O	2-3
O-H···N	4-7
N-H···O	2-3
F-H···F	7
Primary valence bond	
Electrocalent, ionic, heteropolar	100-200
Covalent, homopolar	50-150

1.1.4 The influence of environmental conditions on crystal habits and crystal growth

A *crystal habit* is defined as the external shape (morphology) and appearance of a crystal (Haleblain, 1975:1270; Bernstein, 2002:46). Differences in crystal habits occur when the environment in which the crystals are grown affect the crystal shape without influencing the internal structure of the crystal, resulting in the formation of a different crystal habit, but not a new polymorphic configuration. These differences in the crystal shapes are caused by interference of the crystallisation of the molecules on the different faces of the crystal (Haleblain, 1975:1270).

Crystal growth is a prominent factor affecting the habit of crystals. Crystal growth may be hindered by adjacent crystals growing simultaneously or crystals coming in contact with the wall of the container. As a result, late crystallisation may occur, leading to the formation of irregular shaped crystals in vacant spaces between already crystallised solids. Crystal growth can also be affected by the inhibitory development of plane faces in the crystal (Bernstein, 2002:46-49; Haleblian, 1975:1270-1271). Two possible types of crystal habits are possible, as illustrated in Figure 1.9.

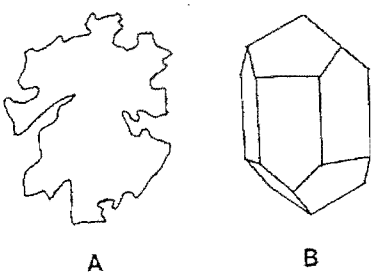

Figure 1.9 Two types of crystal habits: (A) Anhedral and (B) euhedral, which occur as an effect of crystal growth (Haleblian, 1975:1270).

Anhedral or *allotriomorphic* habits form as irregular shaped crystals. Although anhedral crystals have irregular shapes, they still display a regular arrangement of unit cells (molecules or atoms) within the lattice (Byrn *et al.*, 1999:12-15; Haleblian, 1975:1270-1271).

Euhedral or *idiomorphic* habits are distinctly shaped. There are five sub-classes of euhedral crystals: tabular, platy, prismatic, acicular and bladed (Byrn *et al.*, 1999:12-15; Haleblian, 1975:1270-1271). These different sub-classes are illustrated in Figure 1.10.

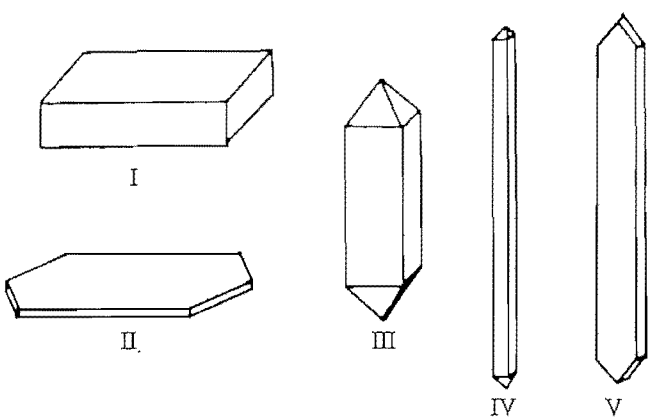

Figure 1.10 Different habits of crystals (I) Tabular, (II) Platy, (III) Prismatic, (IV) Acicular and (V) Bladed (Bernstein, 2002:47).

Aspirin is well-known for its ability to crystallise in different habits. Figure 1.11 illustrates the different crystal habits that were obtained when aspirin was recrystallised using various solvents (Byrn *et al.*, 1999:13).

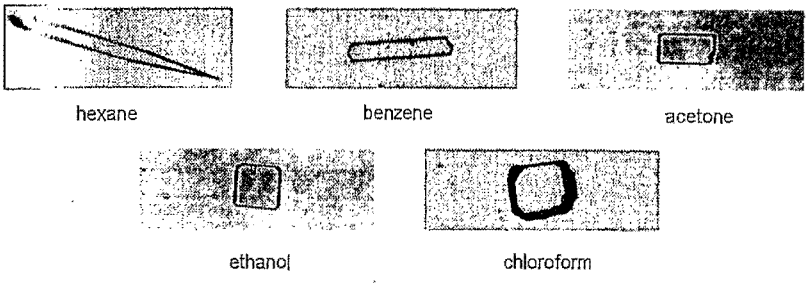

Figure 1.11 Different crystal habits for aspirin crystallised from different solvents (Byrn *et al.*, 1999:13).

Differences in habit may indicate potential differences in crystal packing. Figure 1.12 illustrates the different solvated crystal habits of β-estradiol when recrystallised from various solvents (Byrn *et al.*, 1999:13-14).

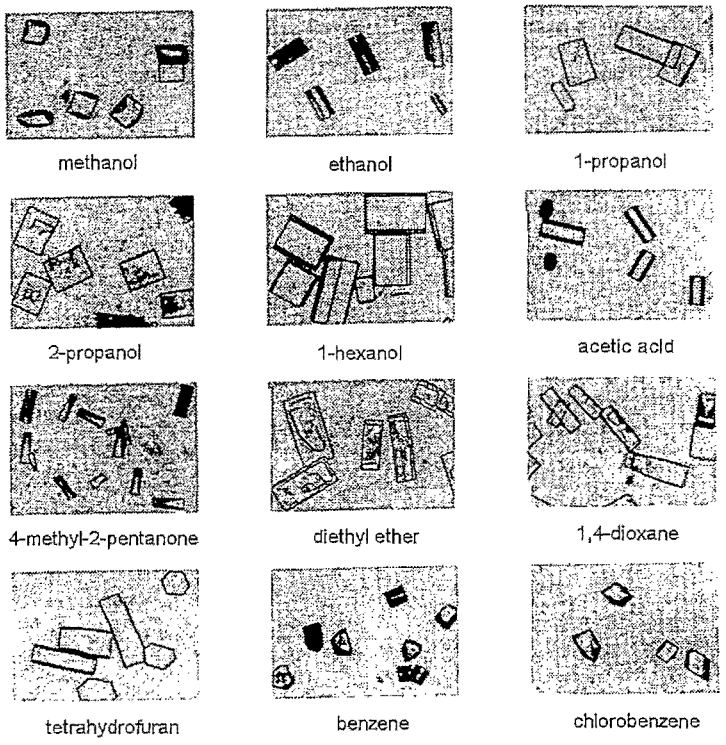

Figure 1.12 β-estradiol pseudopolymorphs formed when recrystallised from different solvents (Byrn *et al.*, 1999:14).

1.2 Polymorphism

As mentioned in section 1.1, pharmaceutical solids can be classified as: *crystalline solids* or as *amorphous solids.* Figure 1.13 summarises a classification system that may be used for the classification of solids, and will be discussed in the following sections.

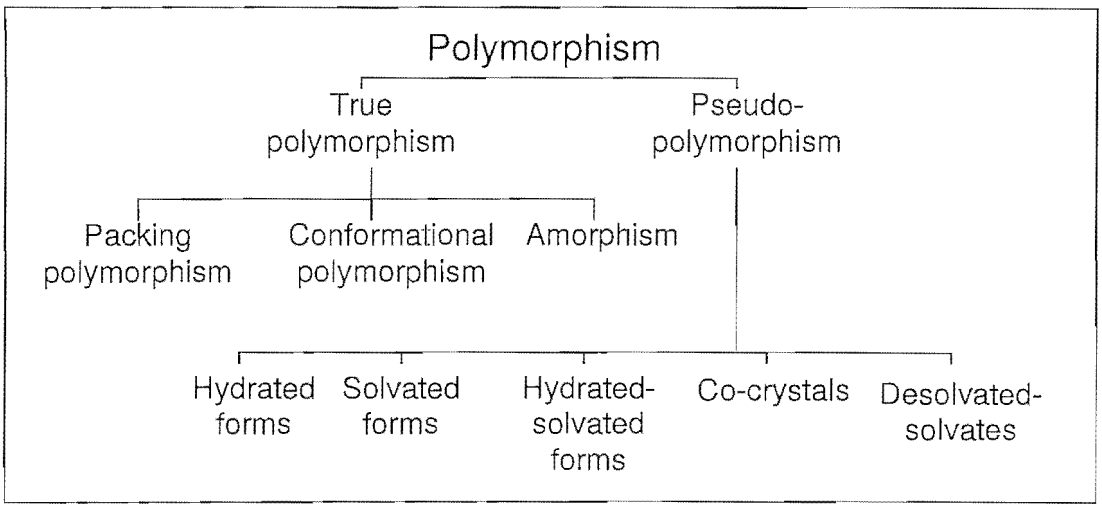

Figure 1.13 Schematic illustration of a classification system for solids.

Polymorphism or *True polymorphism* is the ability of a solid to exist in more than one crystalline phase (Bernstein, 2002:2-4). These crystalline phases differ in the arrangement of the molecules within the crystalline lattice or in the conformation of the molecules in the crystalline lattice (refer also to the formation and internal characteristics of a crystalline solid – Section 1.1.1).

Two types of polymorphism exist: *packing polymorphism* and *conformational polymorphism.* According to Vippagunta *et al.* (2001:7) there is an artificial distinction between *packing-* and *conformational polymorphism* in the sense that different packing arrangements of the molecules will involve different conformational changes of the molecules and that even the smallest conformational change of the molecules will lead to a different packing arrangement of the molecules.

1.2.1 Packing polymorphism

Packing polymorphism is a mechanism by which conformational rigid molecules are organized and packed in various ways forming different three dimensional lattices of the chemical compound (Hilfiker, 2007:22).

During a study on the different modes of intermolecular hydrogen bonding in the two polymorphic forms of *p*-nitrophenol (Figure 1.14), it was discovered that charge migration takes place within the structure from the benzene ring to the hydroxyl and nitro group that accompanies the transition from the β polymorph into the α polymorph (Kulkarni *et al.*, 1998:3498, 3503-3505).

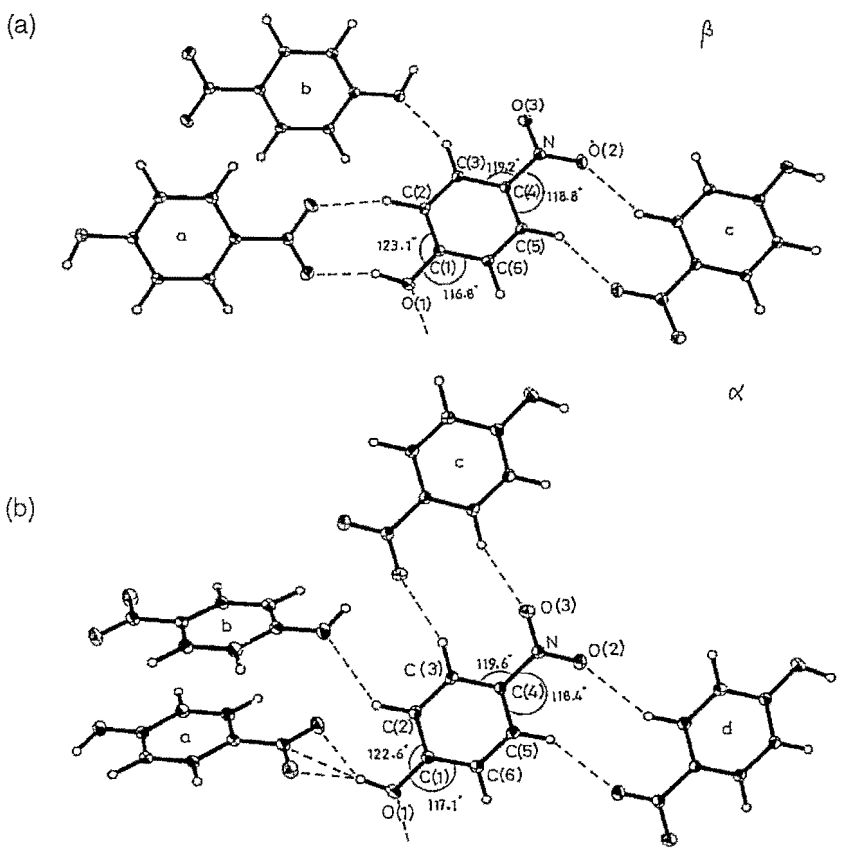

Figure 1.14 Packing polymorphism - Molecular packing diagrams for the β polymorph and α polymorphs of *p*-nitrophenol, both is showing a 50% propability displacement ellipsoids (Kulkarni *et al.*, 1998:3503).

1.2.2 Conformational polymorphism

Conformational polymorphism is a mechanism by which conformational flexible molecules are packed into different three dimensional lattices due to the ability of the molecules to fold into different conformations (Hilfiker, 2007:22).

An example of conformational polymorphism, according to Vippagunta *et al.* (2001:8) is that of piroxicam pivalate (Figure 1.15). Piroxicam pivalate has two distinctive polymorphs which show significant differences in melting points (Caira *et al.*, 1998:1608).

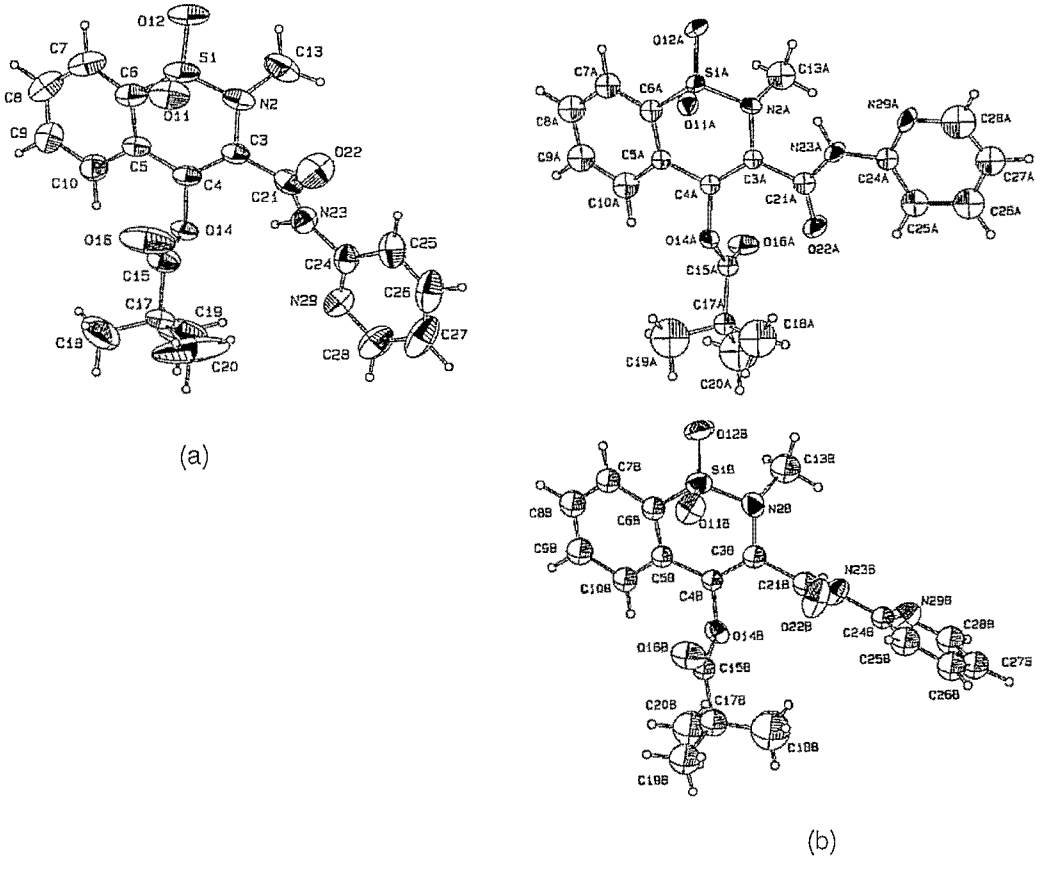

Figure 1.15 Conformational polymorphism - Molecular conformation of piroxicam pivalate polymorph 1 (a) and conformations of two independent piroxicam pivalate polymorph 2 molecules (b) (Caira *et al.*, 1998:1610).

1.3 Pseudo-polymorphism

The term *pseudo-polymorphism* has been used as a collective term for solvation of crystalline structures, second-order transitions, mesomorphism, dynamic isomerism, lattice strain effects and grain growth (Bernstein, 2002:4-8; Haleblian, 1975:1276; McCrone & Haleblian, 1969:927).

In pseudo-polymorphism the different crystal structures which are formed, are the result of hydration or solvation of the chemical entity. These crystal forms contain solvent or water molecules, depending on the solvent used during recrystallisation. If water was used as the solvent, the pseudo-polymorph is known as a *hydrate,* if an organic solvent was used the pseudo-polymorph is known as a *solvate* (Vippagunta *et al.,* 2001:4; Bernstein, 2002:4-5; McCrone & Haleblain; 1969:927).

1.3.1 Solvates

Solvates are molecular complexes which are formed when a solvent is entrapped within the crystalline lattice of an API during recrystallisation using an organic solvent or a mixture of organic solvents (Haleblian, 1975:1276; Vippagunta *et al.*, 2001:15). Solvates are formed with stoichiometric or non-stoichionetric proportions between the compound and the solvent used for recrystallisation (Haleblian, 1975:1276; Sinko, 2006:37; Vippagunta *et al.*, 2001:15).

A list of the most commonly used solvents are summarised in Table 1.8.

Table 1.8 Distribution of the 15 most popular solvents used for recrystallisation according to the Cambridge Crystallographic Database including the percentage of structures containing each of the tabulated solvents (Van der Sluis & Kroon, 1989:646)

Solvent	Occurrence (%) in literature
Water	61.4
Dichloromethane	5.9
Benzene	4.7
Methanol	4.1
Acetone	2.8
Chloroform	2.8
Ethanol	2.6
Tetrahydrofuran	2.3
Toluene	2.2
Acetonitrile	1.9
N,N-dimethylformamide	0.9
Diethylehter	0.9
Pyridine	0.7
Dimethylsulfoxide	0.5
Dioxane	0.5

An example of a solvated API is Prednisolone tert-butylacetate, which exhibits four solvated forms and one non-solvated structure. These forms are illustrated in Figure 1.16 (Byrn *et al.*, 1988:1609-1611).

The mechanism and extent of the solvent inclusion can be investigated to determine if the solvent is trapped within void spaces of the crystal lattice or whether it is bound to the crystal lattice through hydrogen bonding or van der Waal's forces. The crystal structure and solvent molecular conformation plays an integral part in the mechanism and extent of the solvent inclusion (Brittain, 1999:205; Van der Sluis & Kroon, 1989:647-651). The effect of the solvent in the crystal structure is discussed in more detail in Section 1.4.

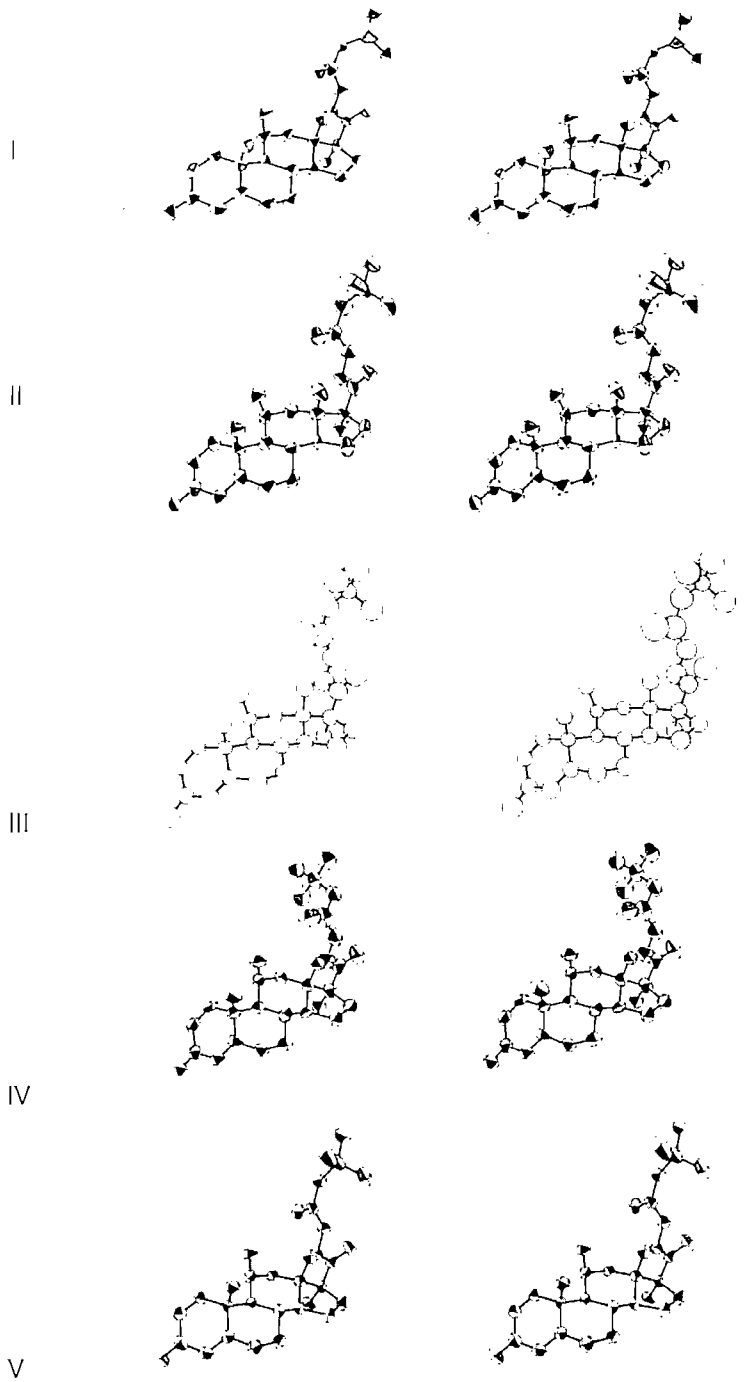

Figure 1.16 Stereoscopic views of the conformation polymorphs of prednisolone 21-tert-butylacetate: form **I, II, III, IV** (non-solvated), and **V.** The view is from approximately the same direction, perpendicular to the steroid ring nucleus (Byrn *et al.*, 1988:1611).

1.3.2 Hydrates

It is not unlikely for an API to come into contact with water during crystallisation, wet-granulation, aqueous film-coating or spray-drying during the manufacturing process, that may induce the formation of *hydrates* (Brittain, 1999:141; Khankari & Grant, 1995:61-65).

During the formation of hydrates the water molecules (due to its size and ability to exist as a hydrogen acceptor or hydrogen donor) may be incorporated into site specific areas within the crystal structure or form water channels within the crystal lattice (refer to section 1.1.3 – hydrogen bonding). Not only can the water molecules bind to other water molecules inside the crystal lattice, but the water molecules may also form covalent and / or hydrogen bonds with the functional groups of the crystal structure. The incorporation of water molecules into the crystal lattice of an anhydrous API may induce a structural change. These changes to the structure and conformation are facilitated by changes in dimension, shape, symmetry and capacity of the unit cell of the anhydrous substance (Byrn *et al.*, 1999:236-238; Kankari & Grant, 1995:61-65).

The classification of crystalline hydrates is based on the location of the water molecules in the crystal lattice (Figure 1.17). Each of these categories differs in the way that the water molecules interact with neighbouring API molecules (Brittain, 1999:141; Byrn *et al.*, 1999:236-238).

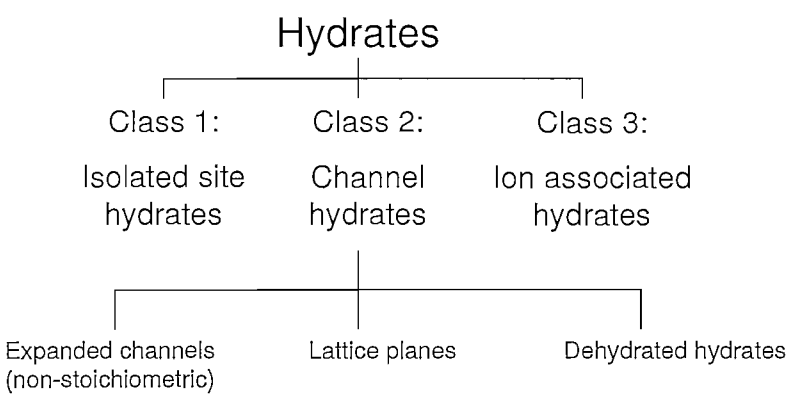

Figure 1.17 Schematic representation of the classification of hydrates (Brittain, 1999:141).

1.3.2.1 Class 1 hydrates – Isolated site hydrate

This type of hydrate exists when the water molecules are isolated from direct contact with other water molecules (Brittain, 1999:143). An example of an isolated site hydrate is: cephadrine dihydrate (Figure 1.18).

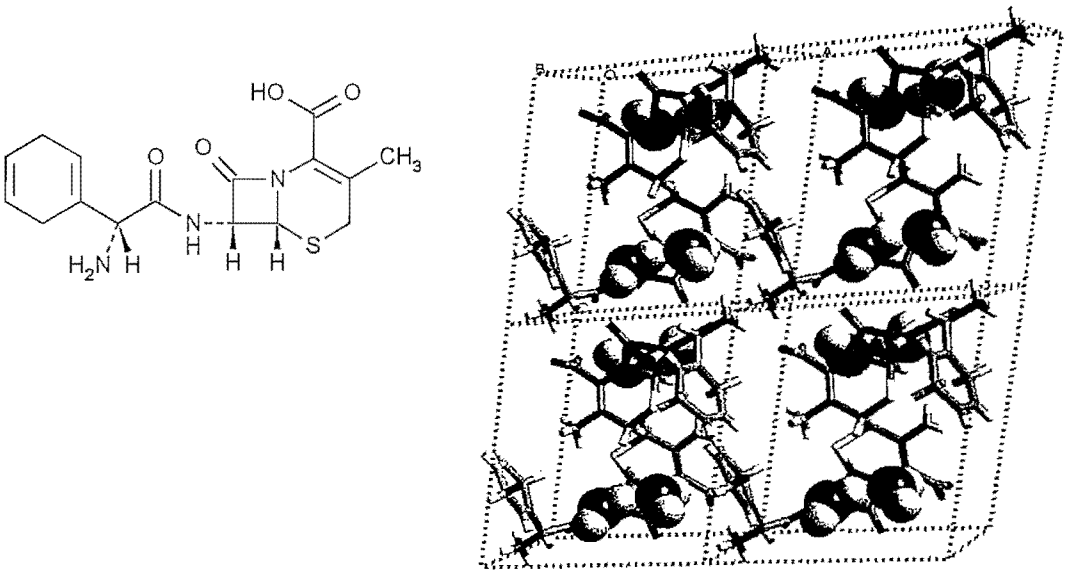

Figure 1.18 Packing diagram from single crystal data for cephadrine dihydrate. The pairs of water molecules reside in isolated lattice sites (Brittain, 1999:143).

1.3.2.2 Class 2 hydrates – Channel hydrates

When water molecules are trapped within the crystal lattice, channels or cavities may be formed within the crystal structure. These water molecules lie next to other water molecules in the lattice of adjoining unit cells and are responsible for the formation of cavities or channels in the crystal lattice (Brittain, 1999:145). According to Brittain (1999:145) these empty channels are but merely a conceptual construct, since a low-density crystalline structure with empty channels will not be physically stable without an associated change in the lattice parameters of the crystal. An example of a class-2 hydrate is ampicillin trihydrate (Figure 1.19) (Brittain, 1999:145-154).

Class 2 hydrates can be further sub-categorised into three different types: (1) expanded channel hydrates, (2) planar hydrates and (3) dehydrated hydrates (Brittain, 1999:145-154).

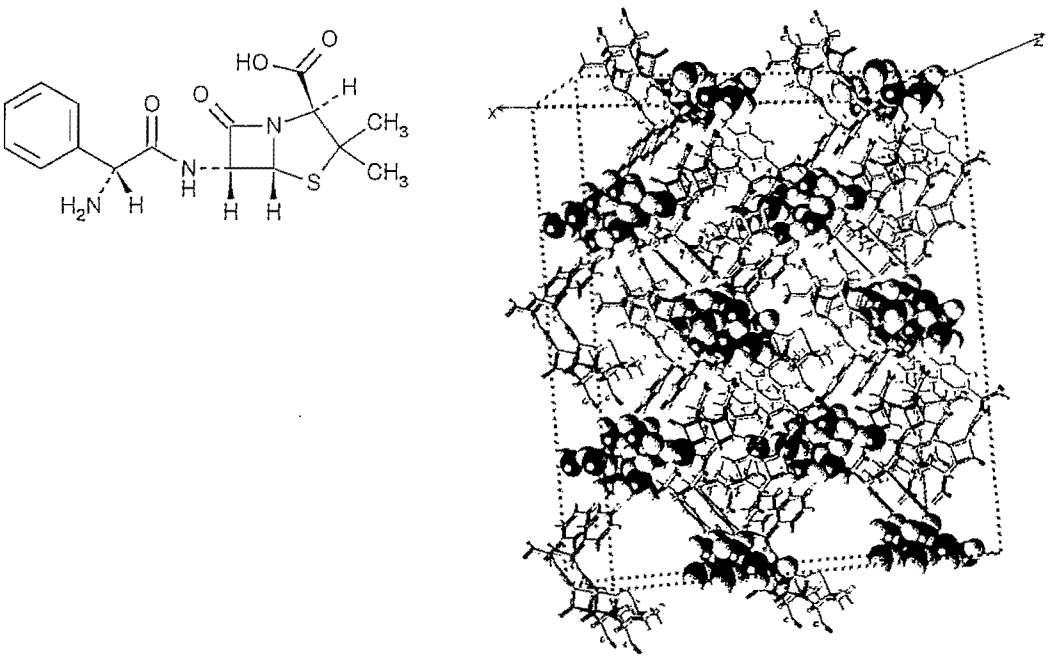

Figure 1.19 Packing diagram of ampicillin trihydrate deduced from the single crystal data. The van der Waals radii are included for the water hydrogen and oxygen and the "channels" are along the screw axes (Brittain, 1999:148).

1.3.2.2.1 Expanded channel hydrates

In certain circumstances some channel hydrates may absorb additional moisture into the channels of the crystal lattice when exposed to high humidity. Hydration of the crystal lattice may cause the lattice to expand, affecting the dimensions of the unit cell. Changes of the crystal dimensions, due to hydration can be investigated by means of XRPD analysis (Brittain, 1999:149-153).

1.3.2.2.2 Planar hydrates

In this subclass, the water molecules are trapped within the crystal lattice and are localised within a two-dimensional plane. Limited literature is available describing this phenomenon. An example of a planar hydrate is sodium ibuprofen (Figure 1.20) (Brittain, 1999:153-154).

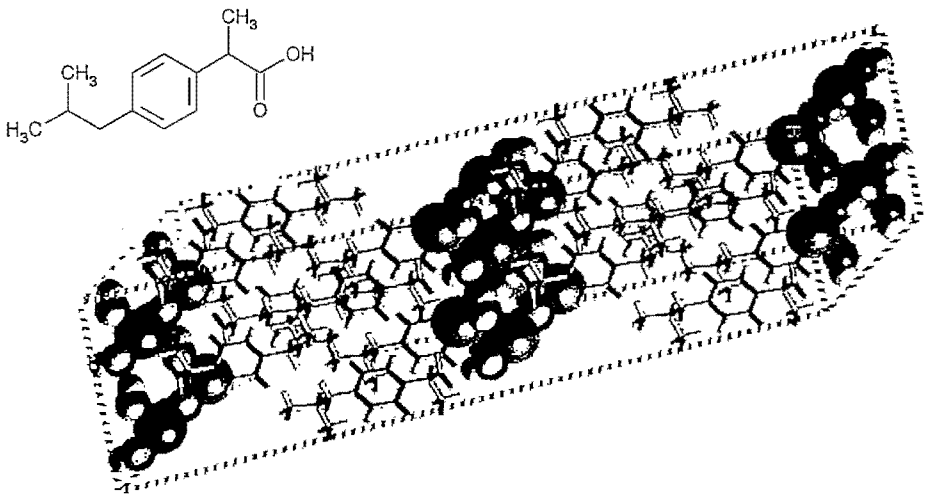

Figure 1.20 Packing diagram for sodium ibuprofen with water and sodium shown as van der Waals spheres (Brittain, 1999:153).

1.3.2.2.3 Dehydrated hydrates

Dehydration usually induces changes in the crystal lattice / structure. However, if after dehydration the crystal structure is found to be similar to that of the initial hydrated structure (but with a lower density) the dehydrated structure is classified as a *dehydrated hydrate*. If an anhydrous structure for the specific compound already exists, the structure is classified as a polymorph (Brittain, 1999:154). Similar behaviour exists for solvates (refer to section 1.4).

1.3.2.3 Class 3 hydrates – Ion-associated hydrates

Should the water molecules be bound to metal ions in the crystal structure, the crystal form is classified as a *class 3 hydrate*. The concern when forming metal-water interactions is the effect that the metal-water interaction will have on the structure and stability of the crystalline hydrate. For dehydration to occur in class 3, hydrates high temperatures are required since the interaction between the metal ion and the water molecules are relatively strong. Class 3 hydrates are normally recrystallised for pharmaceutical products exhibiting poor solubility and dissolution results. An example of a class 3 hydrate is: calteridol calsium (Figure 1.21) (Brittain, 1999:157).

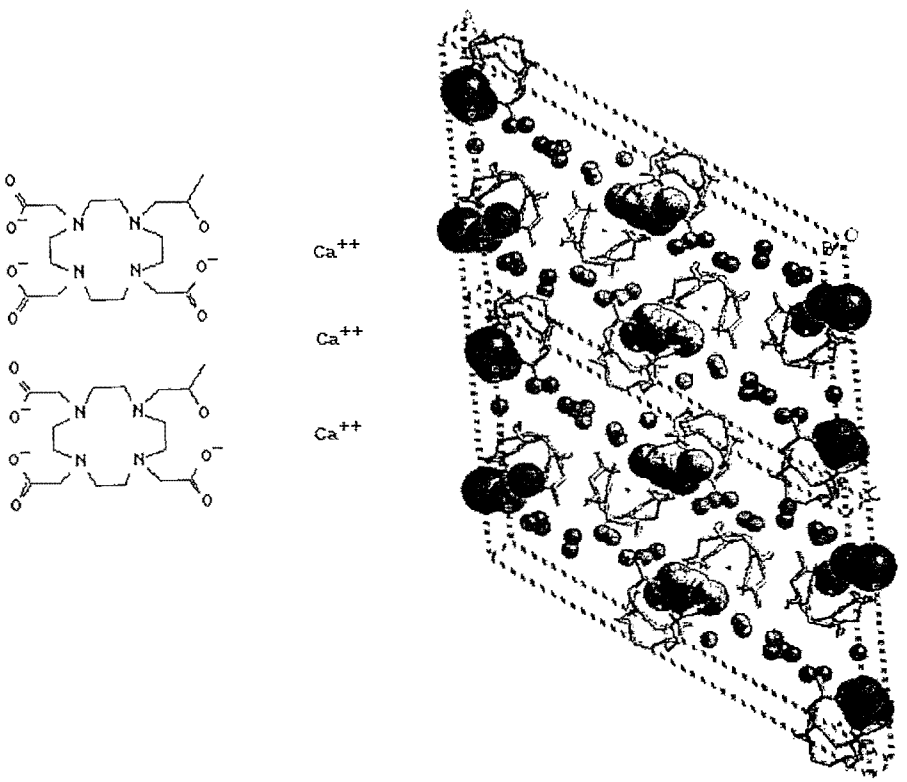

Figure 1.21 Packing diagram from single crystal data for calteridol calcium (a) reactant and (b) product. The van der Waals radii are included for the water oxygens. The radii for the oxygens directly associated with the calcium are full van der Waals radii, while the lattice and channel water oxygens are shown as one-half of the van der Waals radii for illustration purposes (Brittain, 1999:157).

1.4 Desolvated / dehydrated pseudo-polymorphs

Changes to the environment of the crystal structure (i.e. exposure to increased temperatures, pressure, etc.) may cause the entrapped solvent molecules to escape the crystal lattice, leading to a collapse of the crystalline structure or the formation of an *isomorphic desolvate* (Brittain, 1999:205; Byrn *et al.*, 1999:5-12).

When a tightly bound solvent is eliminated from the crystalline structure it normally leads to conformational change within the crystalline structure of the API giving rise to the generation of a different crystalline structure (Byrn *et al.*, 1999:293), however in certain circumstances the removal of a lightly bound solvent from a crystalline structure will not necessarily lead to a conformational change of the crystalline structure (Bernstein, 2002:4-9; Brittain, 1999:205; Van der Sluis & Kroon, 1989:651-654). This phenomenon results in the formation of a desolvated solvate or isomorphic desolvate (also refer to section 1.3.2.2.3). The crystal structure of an isomorphic solvate is retained after desolvation of the solvate, leaving the molecular packing of the crystal intact. Isomorphic desolvates are generally unstable structures and tend to undergo lattice relaxation in the absence of moisture, due to the lesser dense structure compared to the parent solvate. This may ultimately result in a decrease in the unit cell volume and an increased packing efficiency (Yu *et al.*, 1998:124). Figure 1.22 illustrates the differences between the packing of solvates and isomorphic solvates.

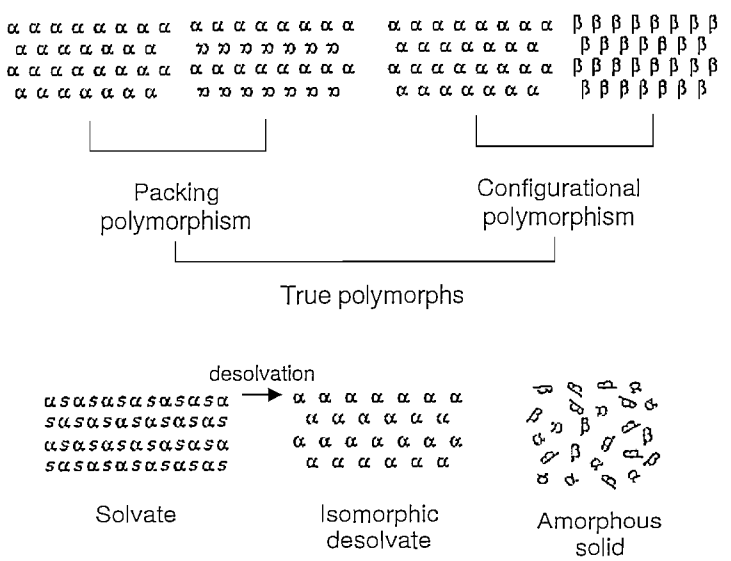

Figure 1.22 Schematic illustration of the packing of molecules in different solid forms of an API (adapted from Yu *et al.*, 1998:119).

A crystal lattice containing entrapped solvent molecules within the lattice or which has large empty channels or cavities are normally less stable than a crystal where the solvent is bound to molecules of the crystal lattice (Brittain, 1999:205; Byrn *et al.*, 1999:5-12).

1.5 Co-crystals

Co-crystals are defined as crystals that consist of an ordered arrangement of two different natural molecules that are not solvates or hydrates and that influence the hydrogen bonds in crystal structures (Byrn, *et al.,* 1999:10). These co-crystals are normally formed between hydrogen bond acceptor molecules and hydrogen bond donor molecules and may induce drug-excipient interactions. Co-crystals provide a method by which the physico-chemical properties of an API may be altered, achieving a new pharmaceutical solid (Karki *et al.*, 2007:347). Figure 1.23 illustrates an example of a co-crystal formed between a monophosphate salt and phosphoric acid showing the hydrogen bonding of the two inequivalent phosphoric acid molecules in the crystal lattice (Chen *et al.,* 2007:420).

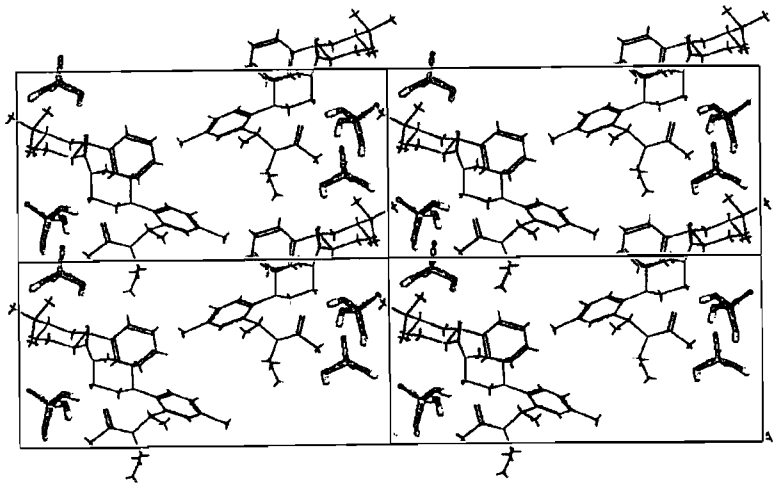

Figure 1.23 Co-crystal formed between a monophosphate salt and phosphoric acid showing the hydrogen bonding of the two inequivalent phosphoric acid molecules in the crystal lattice (Chen *et al.,* 2007:420).

1.6 Amorphous solids

Amorphous solids may be considered as super-cooled liquids in which the molecules are in a somewhat random manner similar to the liquid state (Sinko, 2006:37). The physico-chemical properties of amorphous solids differ from crystalline solids. Amorphous forms are usually shapeless solids and can be distinguished from normal crystalline structures on the basis that they lack a distinct XRPD pattern when compared to crystalline solids (Byrn *et al.,* 1999:22). The most commonly known amorphous solid is glass where the atoms and molecules exist in a totally non-uniform array. Glass exhibits no faces, habits or polymorphism. Examples of pharmaceutical amorphous solids are indomethacin (see Figure 1.31) and the antibacterial azlocillin sodium (Bernstein, 2002:245; Brittain, 1999:8-9; Byrn *et al.*, 1999:22,249; Haleblian, 1975:1272).

Amorphous solids can be prepared by means of rapid-cooling (amorphous form of chloramphenicol palmitate), lyophilisation (amorphous forms of fluprednisolone), spray drying, removal of solvent from a solvate, precipitation by changing pH, grinding, granulation and milling. A more recent technique developed to prepare amorphous solids is through means of supercritical fluids (Byrn *et al.,* 1999:22; Bernstein, 2002:254). The most commonly used methods by which amorphous solids are prepared in the pharmaceutical industry are illustrated in Figure 1.24 (Hancock & Zografi, 1997:1).

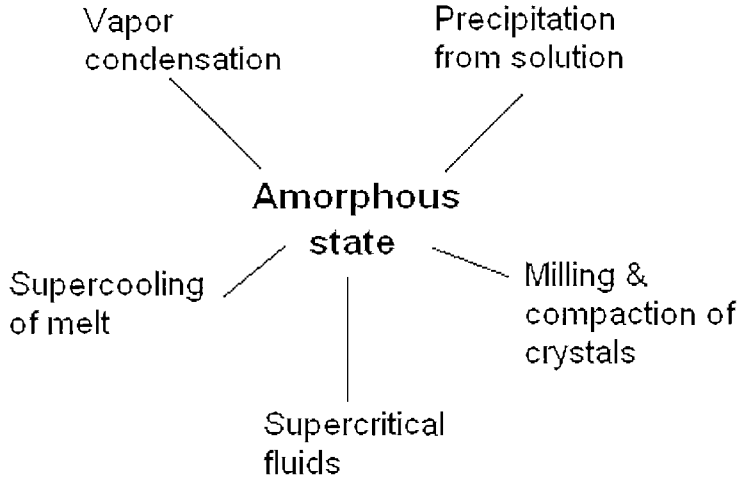

Figure 1.24 The most commonly used methods by which amorphous solids are prepared in the pharmaceutical industry (adapted from Hancock & Zografi, 1997:1).

No crystal is perfect and the lack of perfection is the result of a disorder within the molecules of the crystal lattice. When the entire crystalline material lacks long range orders within the molecular structure, even if there are some short range orders present within the crystalline lattice, the end result will still be an amorphous solid (Figure 1.25) (Bernstein, 2002:253). Comparing amorphous solids with crystalline solids, would reveal that the amorphous solids or materials tend to be more energetic than the latter, thus resulting in the enhanced solubility and dissolution rates compared to normal crystalline solids (refer to section 1.7). It is this property of amorphous solids that give them their advantage in the pharmaceutical industry (Bernstein, 2002:253).

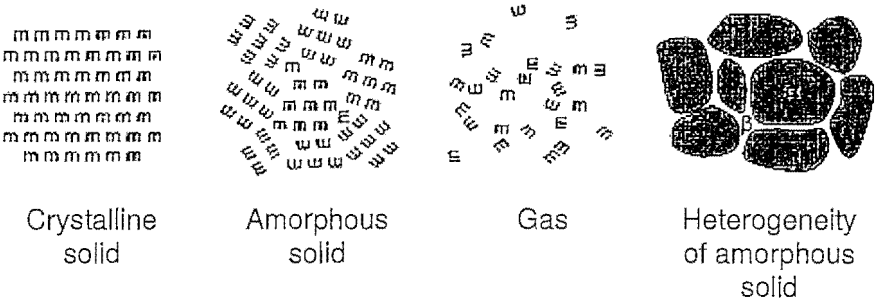

Figure 1.25 Schematic presentation of the structure of an amorphous solid in comparison with that of crystalline solids and gasses (adapted from Yu: 2001:30).

1.6.1 The glass transition temperature

Amorphous solids are further characterised by a unique thermodynamic glass transition temperature (Byrn *et al.*, 1999:22; Hilfiker, 2007:270). The *glass transition temperature* (T_g) is the temperature where amorphous solids are configurationally frozen in a glassy state and where the molecules of the amorphous solid lack the vibrational motion of molecules in a liquid state. When the temperature of an amorphous solid rises above the glass transition temperature (T_g), the molecules of the amorphous solid exhibit a substantial configurational motion, hence the amorphous solid exists in a rubbery state (Byrn *et al.*, 1999:250). Hancock and Zografi (1997:2) illustrated the differences in the formation of crystalline and amorphous solids. The rate by which the temperature was decreased during the cooling process was too fast for the amorphous solid to crystallise, resulting in the formation of a glassy state, where as the crystalline solid would have normally began to crystallise – see Figure 1.26 (Hancock and Zografi, 1997:2).

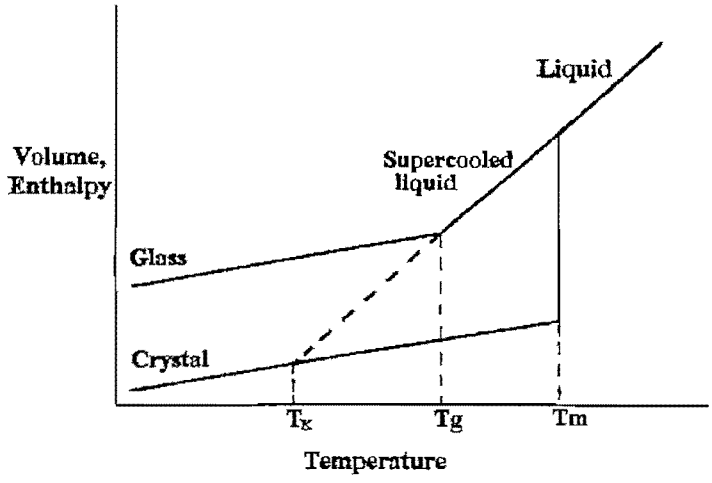

Figure 1.26 Schematic illustration of the difference in enthalpy against temperature for crystalline and amorphous solids (T_m = melting temperature, T_x = crystallisation temperature and T_g = glass transition temperature) (Hancock & Zografi, 1997:2).

1.7 The physico-chemical properties of polymorphs, pseudo-polymorphs and amorphous solids

Different polymorphs of an API differ in their physico-chemical properties. These properties are tabulated in Table 1.9. In Section 1.7.2 – Section 1.7.5 the impact of these different properties will be discussed.

Table 1.9 Physico-chemical properties that may differ between polymorphic systems of the same API (Brittain, 1999:7)

Physico-chemical properties that differ among polymorphic forms of the same active pharmaceutical ingredient
Packing properties Molar volume and density. Refractive index. Conductivity, electrical and thermal. Hygroscopicity.
Thermodynamic properties Melting and sublimation temperatures. Internal energy (i.e. Structural energy). Enthalpy (i.e. Heat content). Heat capacity. Entropy. Free energy and chemical potential. Thermodynamic activity. Vapour pressure. Solubility.
Spectroscopic properties Electronic transitions (.i.e., ultraviolet-visible absorption spectra). Vibrational transitions (i.e., infrared absorption spectra and Raman spectra). Rotational transitions (i.e., far infrared or microwave absorption spectra). Nuclear spin transitions (i.e., nuclear magnetic resonance spectra).
Kinetic properties Dissolution rate. Rates of solid state reactions. Stability.
Surface properties Surface free energy. Interfacial tension. Habit (i.e., shape).
Mechanical properties Hardness. Tensile strength. Compressibility, tabletting. Handling, flow, and blending.

1.7.1 The stability of polymorphic systems

According to Brittain (2002:23) an important discovery was made in 1897 by W.F. Ostwald on the relative stability of polymorphs and the reason for the existence of the less-stable polymorphic forms. Ostwald indicated that unstable polymorphic forms tend to exhibit a greater solubility compared to the more stable polymorphic forms of a specific API, following the initial discovery by Lehmann in 1877. Lehmann stated that the monotropic polymorphic forms exhibited a lower melting point than the enantiotropic form due to the ease by which the monotropic group could be destroyed (Buerger & Bloom, 1937:185). This became known as Ostwald's "Rule of steps" or "Law of successive reactions" (Bernstein, 2002:23). Although Ostwald's rule was tenuous and based on a limited set of observations, it is still applied to various polymorphic studies (Bernstein, 2002:23).

In an *enantiotropic system,* reversible transformations can be observed between the polymorphic forms at the transition temperature where the relative stability of the polymorphic forms invert. In a *monotropic system* a single form is always more stable than the other regardless of the temperature. In this system the less-stable forms irreversibly transform to the more stable form (Buerger & Bloom, 1937:185; Byrn *et al.*, 1999:20). Figure 1.27 illustrates the relationship between monotropic and enantiotropic systems.

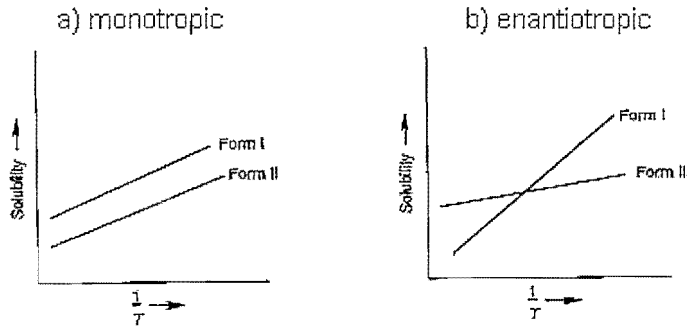

Figure 1.27 Plots of solubility versus time representing (a) a monotropic and (b) enantiotropic systems (Byrn *et al.*, 1999:20).

To aid in the characterisation, understanding and prediction of the behaviour of polymorphic systems (monotropic and enantiotropic), certain guidelines and / or "rules" were implemented. The six rules used in the determination of polymorphic behaviour are (1) Heat-of-transition rule, (2) Heat-of-fusion rule, (3) Entropy-of-fusion rule, (4) Heat-capacity rule, (5) Density rule and (6) Infrared rule (Bernstein, 2002:37-42).

1.7.1.1 Heat-of-transition rule

The rule states that if an endothermic phase transition is observed at a particular temperature below the melting point, the system is an enantiotropic system. If an exothermic phase transition is observed then no thermodynamic transition point is present and the system is monotropic (Bernstein, 2002:38).

1.7.1.2 Heat-of-fusion rule

The rule states that the polymorph with a higher melting point will exhibit a lower heat of fusion and the system is enantiotropic, but if the polymorph with the higher melting point has a higher heat of fusion then the system is monotropic (Bernstein, 2002:38).

1.7.1.3 Entropy-of-fusion rule

The rule states that the polymorph with a higher melting point will exhibit a lower entropy of fusion and is termed enantiotropic, but if the polymorph with the lower melting point has a lower entropy of fusion then the system is termed monotropic (Bernstein, 2002:40).

1.7.1.4 Heat-capacity rule

The rule states that if a polymorph has a higher melting point and heat capacity at a given temperature in comparison to the other polymorph, then the system is termed enantiotropic otherwise the system is monotropic (Bernstein, 2002:40).

1.7.1.5 Density rule

The rule states that in non-hydrogen bonded systems the polymorph with the lowest free energy at absolute zero degrees and dominated by van der Waals interactions will be the most stable polymorph with the higher density. Any other polymorphic structure from the system with a higher free energy at absolute zero degrees will have a lower density (Bernstein, 2002:40-41).

1.7.1.6 Infrared rule

The rule states that the hydrogen-bonded polymorph with the highest frequency in bond stretching will have a higher entropy value (Bernstein, 2002:41).

It is therefore clear that the stability of polymorphic systems will influence the physico-chemical properties of the API. In Section 1.7.2 – 1.7.5 the effects of polymorphic systems stability will be discussed in regards to the solubility, bioavailability, dissolution properties and physical-stability.

1.7.2 Packing symmetry, crystal density, lattice free energy and the effect thereof on physical stability

Symmetry plays an important role in crystal packing in conjunction with intermolecular forces by directly affecting the forces strength between the molecules during crystal formation. Molecules that show good symmetry allow molecules to pack tightly together, forming a close-packing arrangement that in turn ensure a stronger crystal (Byrn *et al.*, 1999:7-8). Different polymorphs contain different free energies due to different intermolecular forces and density of crystal packing between the different crystal structures. Due to these differences in the Gibbs free energies, the different crystal forms tend to exhibit differences in melting points, solubility, bio-availability, spectral properties, etc. (Byrn *et al.*, 1999:143).

The *close-packing theory* that describes the forces that hold crystals together was advanced by Kitaigorodskii in 1961 (referenced by Byrn *et al.*, 1999:8). He suggested that the packing density affect the enthalpy (ΔH) and the free energy within the crystal lattice. The packing density is indirectly proportional to the free energy in the lattice (ΔH) and the stability of the crystal configuration is indirectly proportional to the lattice free energy. This theory implied that if the packing density increased, the heat of sublimation increased (decrease in free energy) and that the polymorph should become more stable (Byrn *et al.*, 1999:7-8).

1.7.3 Solubility and bio-availability

Byrn *et al.* (1999:15) defined the solubility of an API as the concentration where the solution phase is in equilibrium with a given solid phase at a specific temperature and pressure. As mentioned in section 1.7.2, the stability of a polymorphic form increases with the increase in density and lattice strength (and subsequent decrease in free energy). Solubility is thus influenced by the strength of the intermolecular forces responsible for crystal packing. Therefore solubility is indirectly proportional to the thermodynamic stability of a solid. The least soluble polymorph is considered to be the most stable polymorphic form at a specific temperature. The other polymorphic form(s) are considered to be the metastable polymorphs (Byrn *et al.*, 1999:15-16).

It is commonly known that amorphous solids are less stable than their crystalline counterparts. This is due to the fact that amorphous solids are more energetic than the crystalline forms, thus resulting in the enhanced solubility and dissolution rates compared to normal crystalline solids. It is these properties of amorphous solids that give them their advantage in the pharmaceutical industry (Byrn *et al.*, 1999:22; Haleblian & McCrone, 1969:914; Bernstein, 2002:253-254).

Mullins and Macek (referenced by Haleblian & McCrone, 1969:914) illustrated that the bioavailability of the crystalline and amorphous form of novobiocin differed significantly, due to differences in the solubility and absorption of the two forms. The crystalline novobiocin acid showed poor absorption levels (with no therapeutic effects), where as the amorphous novobiocin acid was readily absorbed leading to adequate therapeutic levels. The difference in absorption between the two forms of novobiocin is illustrated in Figure 1.28 (Haleblian & McCrone, 1969:914).

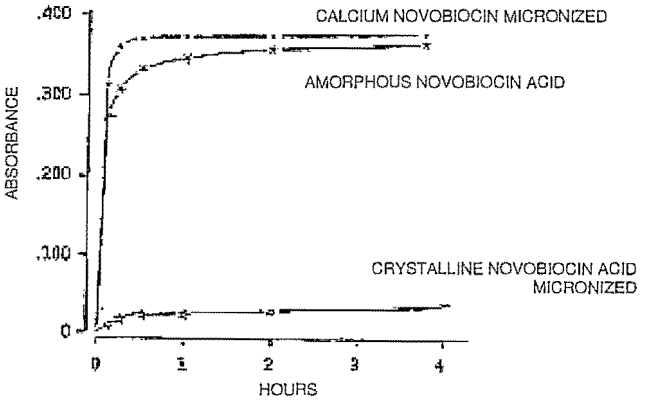

Figure 1.28 Absorbance of the two forms of novobiocin in a 0.1 N HCL solution (Haleblian & McCrone, 1969:914).

1.7.4 Dissolution

Dissolution is defined as the transfer of molecules or ions from the solid state into solution, where the extent of dissolution is governed under a given set of experimental conditions that are proportional to the solubility of the API in the solvent (Aulton, 2002:16). To demonstrate the difference in dissolution rate between two solid forms of the same API, indomethacin was used as an example (Byrn *et al.*, 1999:252-255). From the example it can be concluded that the amorphous form of indomethacin was more soluble than the crystalline forms (enhanced dissolution profile).

The factors that may affect the dissolution behaviour of an API will be discussed in Chapter 5. Figure 1.29 illustrates the solubility profile of crystalline and amorphous indomethacin.

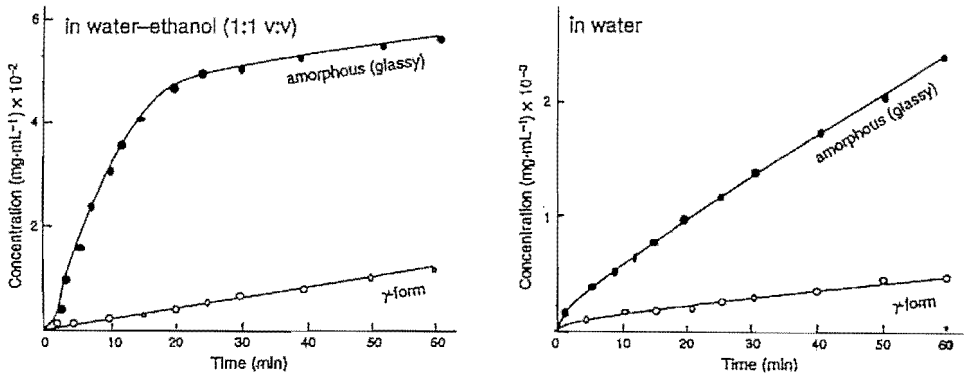

Figure 1.29 Dissolution rate curves of the amorphous and crystalline forms of indomethacin (γ-form) (Byrn *et al.*, 1999:250).

1.7.5 The effects of temperature and humidity on polymorph stability

The thermodynamic stability of the different solid forms may be influenced by a variety of environmental / induced factors, the most common being humidity and temperature. Stability studies are routinely performed by pharmaceutical industries to determine the chemical and physical stability of APIs (Wessels, 1997:427). Section 1.7.5.1 – 1.7.5.2 will discuss the influence of the mentioned factors on the stability of the polymorphic systems.

1.7.5.1 Dehydration / Desolvation of pseudo-polymorphs

As mentioned in Section 1.4, changes to the environment of the crystal structure (i.e. increase in temperature, pressure, etc.) might cause the entrapped solvent molecules of a pseudo-polymorphic form to escape the crystal lattice, leading to a collapse of the crystalline structure or the formation of an isomorphic desolvate. These changes may cause a stable hydrated / solvated form to dehydrate / desolvate (to a less stable form) or vica versa, depending on the solid phase properties, altering the APIs pharmaceutical and pharmacological properties (Khankari & Grant, 1995:61-64; Byrn *et. al.*, 1999:236-242; Singhal & Curatolo, 2004:343-344). Figure 1.30 illustrates the effect that dehydration (increased temperature) had on the stability and polymorphic conversion of ampicillin trihydrate.

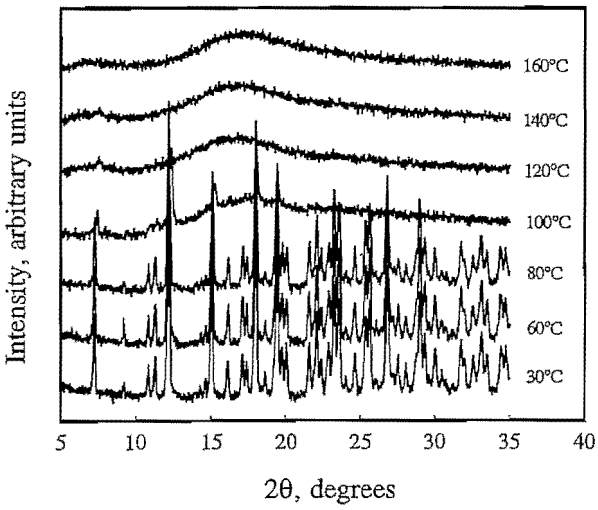

Figure 1.30 Example of effect of dehydration on stability of ampicillin trihydrate (Han *et al.*, 1998:68).

1.7.5.2 Storage conditions

An increase in temperature is not necessarily required for polymorphic conversion. When pulverised, amorphous indomethacin was exposed to ambient temperature (25°C) the amorphous indomethacin recrystallised into a crystalline phase (Figure 1.31). The amorphous form of indomethacin can thus be considered to be the meta-stable phase. Since the glass transition temperature (refer to section 1.6.1) of indometacin (30°C) is almost the same as normal ambient temperature, the phase transformation commenced within a few days (Byrn *et al.*, 1999:254).

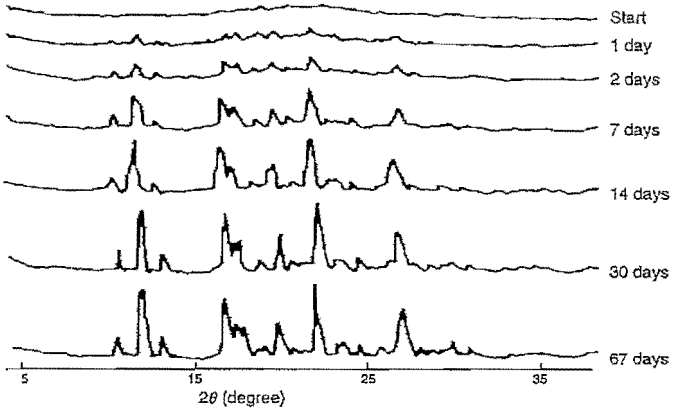

Figure 1.31 Crystallisation of pulverised amorphous indomethacin at ambient conditions (Byrn *et al.*, 1999:254).

Nucleation and growth of new crystalline phases from amorphous solids may be accelerated by the sorption of moisture (exposed to high humidity) or upon exposure of the amorphous form to increased temperatures (Byrn *et al.*, 1999:249-252). The crystallisation of amorphous cephalexin stored at 35°C and high humidity for two weeks is illustrated in Figure 1.32 (Byrn *et al.*, 1999:252-253). Due to the fact that amorphous solids tend to be metastable, their preparation and stability-control during pharmaceutical manufacturing remains a challenging task (Bernstein, 2002:253-255).

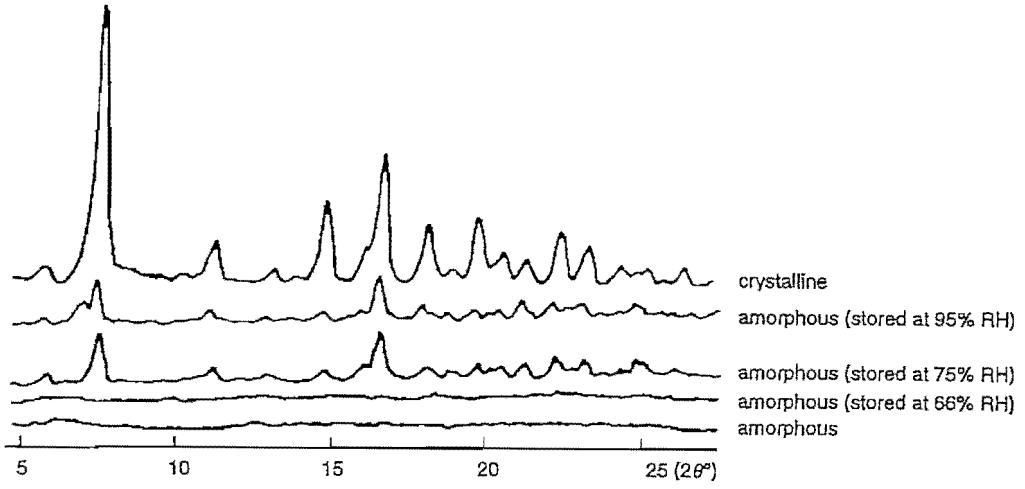

Figure 1.32 X-ray powder diffraction patterns of amorphous cephalexin stored at 35°C and different humidities for two weeks (Byrn *et al.*, 1999:253).

The above mentioned example revealed that the storage conditions and packaging of pharmaceutical substances is of great importance, since it may cause dramatic changes in the stability of the product. It is therefore critical to conform to the correct storage conditions of a product, to ensure the therapeutic efficacy.

1.7.5.3 Polymorphic stability and solid-state kinetics

An understanding of the solid-state kinetics not only provide a means to determine the stability of polymorphs and pseudo-polymorphs, but also gives insight on the mechanisms followed during phase transitions (i.e. desolvation, phase transitions, etc) (Zhou *et al.*, 2003:1780). Thermodynamic stability studies of polymorphic and pseudo-polymorphic forms are therefore important, since the stability thereof may be influenced during manufacturing of dosage forms by initiating phase transformations such as: solvation, desolvation, formation of amorphous solids phases or the crystallisation of amorphous phases (Khawam, 2008:2160- 2161). Chapter

6 and 7 will discuss the kinetic principles in more detail, based on the analysis performed on the pseudo-polymorphic forms identified and prepared in this study.

Conclusion

Polymorphism is the ability of an API to crystallise in more than one distinct crystalline form. It is possible for an API to crystallise in a variety of crystal forms, such as: polymorphs, pseudopolymorphs (solvate and hydrates), co-crystals, and amorphous solids. These different polymorphic forms of an API exhibit different physico-chemical properties, i.e. melting point, solubility, bioavailability, crystal habit, etc. due to their differences in internal packing arrangements and subsequent differences in thermodynamic stability. As a result solid-state studies of APIs form a cornerstone in the research and development of all APIs by pharmaceutical manufacturers.

Through the understanding of the principles of polymorphism and the physico-chemical properties of the different polymorphs, innovator companies and researchers can ensure the development of APIs with suitable pharmaceutical and pharmacological properties for registration and marketing.

Polymorphic and pseudo-polymorphic stability are influenced by a variety of factors, the most common being: humidity, temperature and compression.

Several techniques are used to investigate the solid-state properties of APIs. These techniques will be discussed in Chapter 3.

CHAPTER 2

Physico-chemical and pharmacological properties of mebendazole and various crystalline forms thereof

Introduction

Mebendazole, (methyl 5-benzoyl-2-benzimidizolecarbamate), is a synthetic benzimidazole used as a broad-spectrum anthelmintic against cestodal and nematodal helmintic species (Buys, 2003:22). Mebendazole was first introduced into veterinary medicine in 1971 and has since been used as an anthelmintic in modern medicine. Three polymorphic forms of mebendazole have been identified: Forms A, B and C (Himmelreich, 1977:123). Another pseudo-polymorphic form of mebendazole has been identified by Caira *et al.* (1998:11-12): a 1:1 complex formed between mebendazole and propionic acid when recrystallised from propionic acid. The focus of this chapter will be the physico-chemical and pharmacological properties of the mebendazole polymorphic forms. The information provided in this chapter will be used as a reference in the chapters to follow.

2.1 Physico-chemical properties

2.1.1 Structural formula and chemical name

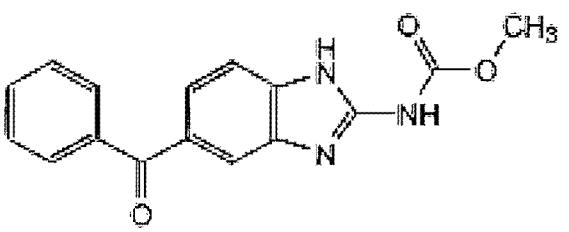

Figure 2.1 The structural formula of mebendazole (Caira *et al.*, 1998:11).

The chemical name of mebendazole is methyl 5-benzoyl-2-benzimidizolecarbamate, 5-benzoyl-2-benzimidazolecarbamic acid methyl ester, (5-benzoyl-1H-benzimidazole-2-yl)-carbamic acid methyl ester (O'Niel, 2006:5766). The structural formula of mebendazole is illustrated in Figure 2.1.

2.1.2 Molecular formula

The molecular formula for mebendazole is $C_{16}H_{13}N_3O_3$ (BP, 2007).

2.1.3 Molecular weight

The molecular weight of mebendazole is 295.30 g/mol (BP, 2007).

2.1.4 Appearance and colour

The BP described mebendazole as a white or almost white (slightly yellow) powder with no odour or taste (BP, 2007). The USP 29 described mebendazole as a white to slightly yellow, almost odourless powder (USP, 2007).

2.1.5 Melting point

The melting point for mebendazole is 288.5°C (BP, 2007).

2.1.6 Solubility, stability and storage conditions

Mebendazole is practically insoluble in water, diluted mineral acid solutions, alcohol, chloroform, ether, methylene chloride, and freely soluble in formic acid (Sweetman, 2007:1).

Mebendazole should be stored in an airtight container, protected from moisture and light at room temperature (25°C) (BP, 2007; USP, 2007). When exposed to high temperatures and humidity the pharmaceutical preferred polymorph, Form C converts to the stable polymorph, Form A (Brits, 2008:223). The metastable Form C is used during pharmaceutical manufacturing, due to its preferred therapeutic activity and physico-chemical properties (Agatonovic-Kustrin *et al.*, 2008:1-6; Swanepoel *et al.*, 2003:345-349).

To ensure that mebendazole formulations contain the pharmaceutical preferred polymorph, qualitative identification techniques were utilised by Liebenberg *et al.* (1998:486). De Villiers *et al.* (2005:435-441) investigated the transformation of Form C when subjected to increased temperatures by means of variable-temperature x-ray powder diffraction (VT-XRPD). Liebenberg *et al.* (1998:485-488) identified the mebendazole polymorphs present in the pharmaceutical products and raw materials available in South Africa.

The dissolution profile of the mebendazole polymorphs in 0.1 N HCl has been reported as (from most soluble to less soluble): Form B > Form C > Form A (Swanepoel *et al.*, 2003:345-349).

2.1.7 Preparation and identification of mebendazole polymorphs

Pioneer polymorph identification studies on mebendazole were performed by Himmelreich *et al.* (1977:123-125). Since then, numerous scientists have performed studies on the identification, solubility and bioavailability of mebendazole especially on that of the pharmaceutical preferred polymorph, Form C (Himmelreich *et al.*, 1977:123-125; De Villiers *et al.*, 2005:435-441; Liebenberg *et al.*, 1998:485-488 and Swanepoel *et al.*, 2003:345-349). The recrystallisation of Form A is done using acetic acid, Form B using chloroform and Form C using methanol as recrystallisation solvents (De Villiers *et al.*, 2005:436; Swanepoel *et al.*, 2003:346).

A mebendazole propionic acid 1:1 complex was prepared and identified by Caira *et al.* (1998:11-15) using propionic acid as solvent. Unfortunately no IR, DSC, or XRPD data have been published by Caira *et al.* (1998:11-15) for the propionic acid complex.

Mebendazole hydrochloride salt was prepared by recrystallisation of mebendazole using a pure organic solvent with the addition of concentrated hydrochloric acid to the solution (Brusau *et al.*, 2007:543).

2.1.7.1 Infrared spectroscopy analysis

Himmelreich *et al.* (1977:123-125) identified the three polymorphic forms of mebendazole (i.e. Forms A, B and C) by means of IR absorption. The major absorption bands used for the identification include the >C=O (carbonyl) stretching frequency (1700 - 1730 cm^{-1}) and –NH stretching frequency (3340 – 3410 cm^{-1}) (Himmelreich *et al.*, 1977:123). The characteristics peaks used to distinguish between the polymorphs are listed in Table 2.1 and illustrated in Figure 2.2.

Table 2.1 Main characteristic peaks (cm^{-1}) used to identify the mebendazole polymorphs (Himmelreich *et al.*, 1977:123)

Form	-NH (cm^{-1})	>C=O (cm^{-1})
A	3370	1730
B	3340	1700
C	3410	1720

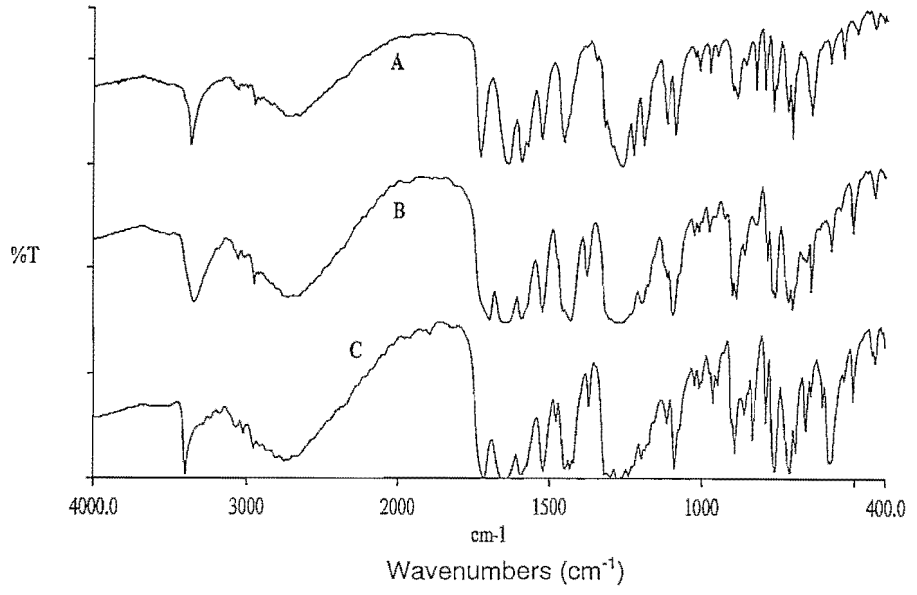

Figure 2.2 FT-IR transmittance spectra of the mebendazole polymorphs (Banaciu *et al.*, 2001:527-536).

2.1.7.2 Thermal and decomposition behaviour of mebendazole

Himmelreich *et al.* (1977:123-124) observed that mebendazole Forms A, B and C exhibited different DSC thermograms. The three polymorphic forms showed two common endotherms at 235°C and 320°C, where the latter can be considered as the melting point of mebendazole followed by thermal decomposition. In the study performed by Himmelreich *et al.* (1977:124) it was illustrated that mebendazole underwent pyrolysis. When mebendazole Forms B and C were heated above 210°C, but below 235°C and allowed to cool down, the samples were found to consist entirely out of Form A. It was documented that when mebendazole was heated above 270°C and allowed to cool down, no mebendazole traces were detected in the sample. The endotherm at 320°C therefore represents the thermal decomposition of mebendazole resulting in the formation of a mixture of decomposition compounds (II, III and IV) as illustrated in Figure 2.3 (Himmelreich *et al.*, 1977:124).

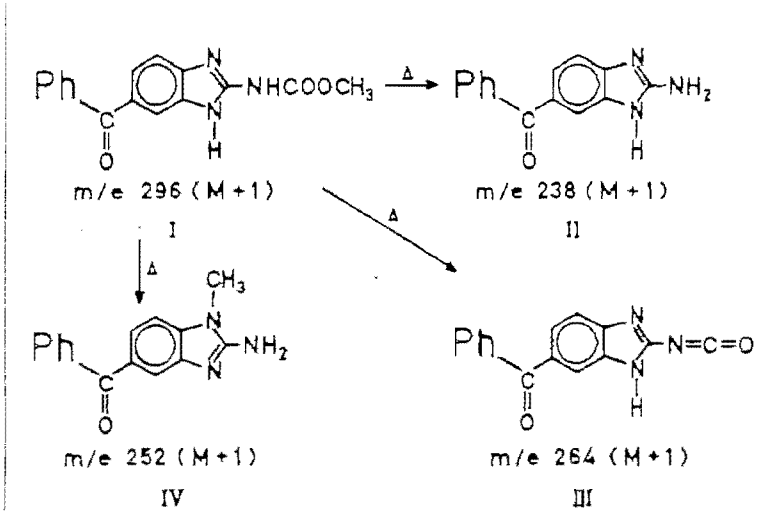

Figure 2.3 Thermal decomposition products of mebendazole (II, III & IV) when heated above 270 °C and allowed to cool down (Himmelreich *et al.*, 1977:124).

The characteristic DSC thermal events for the mebendazole polymorphs are listed in Table 2.2 and illustrated in Figure 2.4.

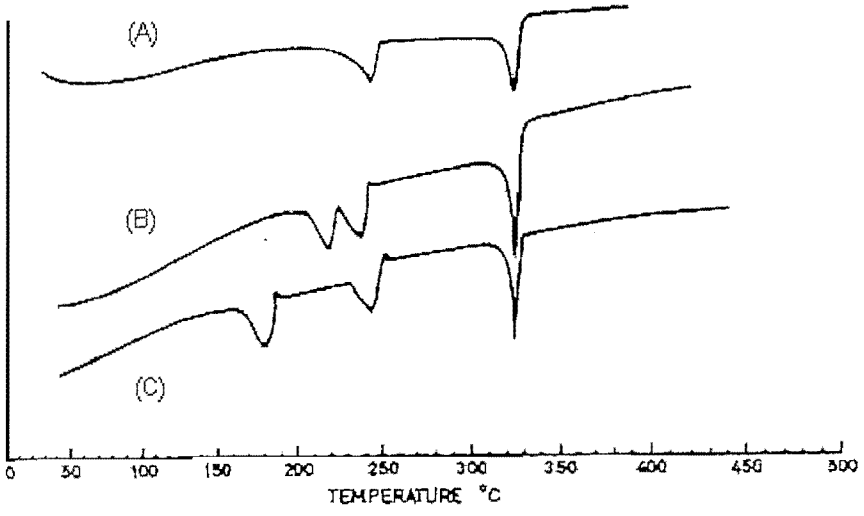

Figure 2.4 DSC thermograms of mebendazole polymorphs (Himmelreich *et al.*, 1977:124).

Table 2.2 Summary of the characteristic thermal events of mebendazole polymorphs (Himmelreich *et al.*, 1977:124)

Form	Thermal events			
A			235°C	320°C
B		210°C	235°C	320°C
C	170°C		235°C	320°C

In a more recent study, De Villiers *et al.* (2005:436-438) reported DSC thermograms for the three polymorphs of mebendazole (Figure 2.5) that indicated differences from those reported by Himmelreich *et al.* (1977:124). The thermal events observed by De Villiers *et al.* (2005:438) are listed in Table 2.3.

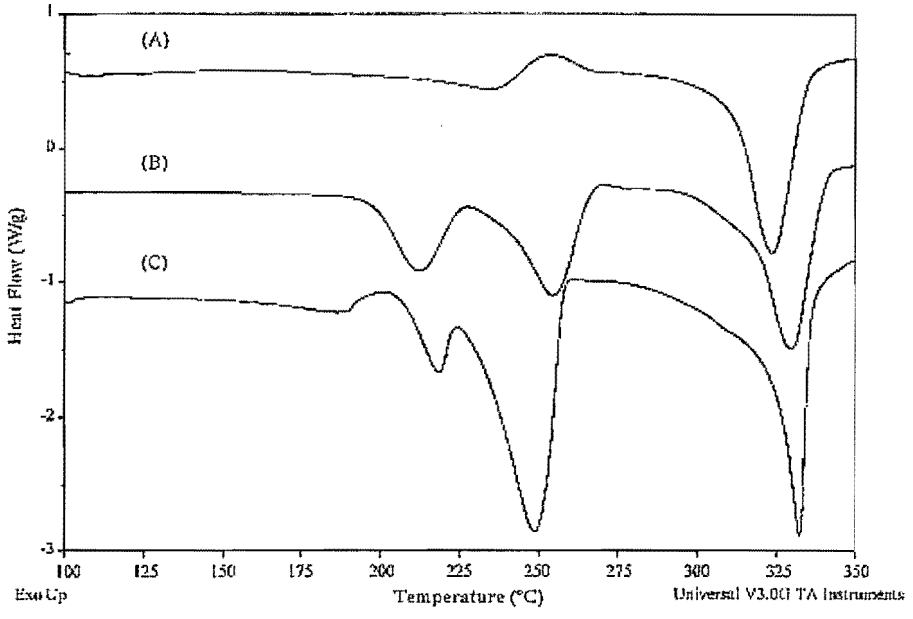

Figure 2.5 Mebendazole polymorph DSC thermograms (De Villiers *et al.*, 2005:436).

The inconsistencies in the thermal behaviour will be discussed in Chapter 3 (Section 3.3).

Table 2.3 Summary of characteristic thermal events of mebendazole polymorphs reported by De Villiers *et al.* (2005:438)

Form	Thermal events			
A			250-255°C	330°C
B		220°C	263°C	330°C
C	195°C	225°C	253°C	330°C

2.1.7.3 X-ray powder diffraction

X-ray powder diffraction is a powerful identification tool utilised by Brits (2008:71), De Villiers *et al.* (2005:435-441), Rodriques-Caabeiro *et al.* (1987:266-271) and Swanepoel *et al.* (2003:345-349) for the identification of the mebendazole polymorphs. The XRPD patterns and main peak relative intensity values (I/I_0) of mebendazole Forms A, B and C are illustrated in Figure 2.6 and listed in Table 2.4.

Table 2.4 Main characteristics peaks and intensity ratios of mebendazole polymorphs (De Villiers *et al.*, 2005:437)

Main peaks	Form A		Form B		Form C	
	d (Å)	I/I_0 (%)	d (Å)	I/I_0 (%)	d (Å)	I/I_0 (%)
1	11.52	100	4.65	100	4.48	100
2	6.13	25	9.34	85	3.34	73
3	5.13	70	3.64	68	17.91	72
4	4.87	19	4.13	61	3.60	56
5	4.49	13	14.62	60	5.45	51
6	4.35	11	3.54	51	3.09	36
7	3.84	38	7.09	49	4.59	32
8	3.78	47	4.22	47	4.89	30
9	3.61	34	3.94	46	4.16	28
10	3.53	23	3.09	43	7.19	28

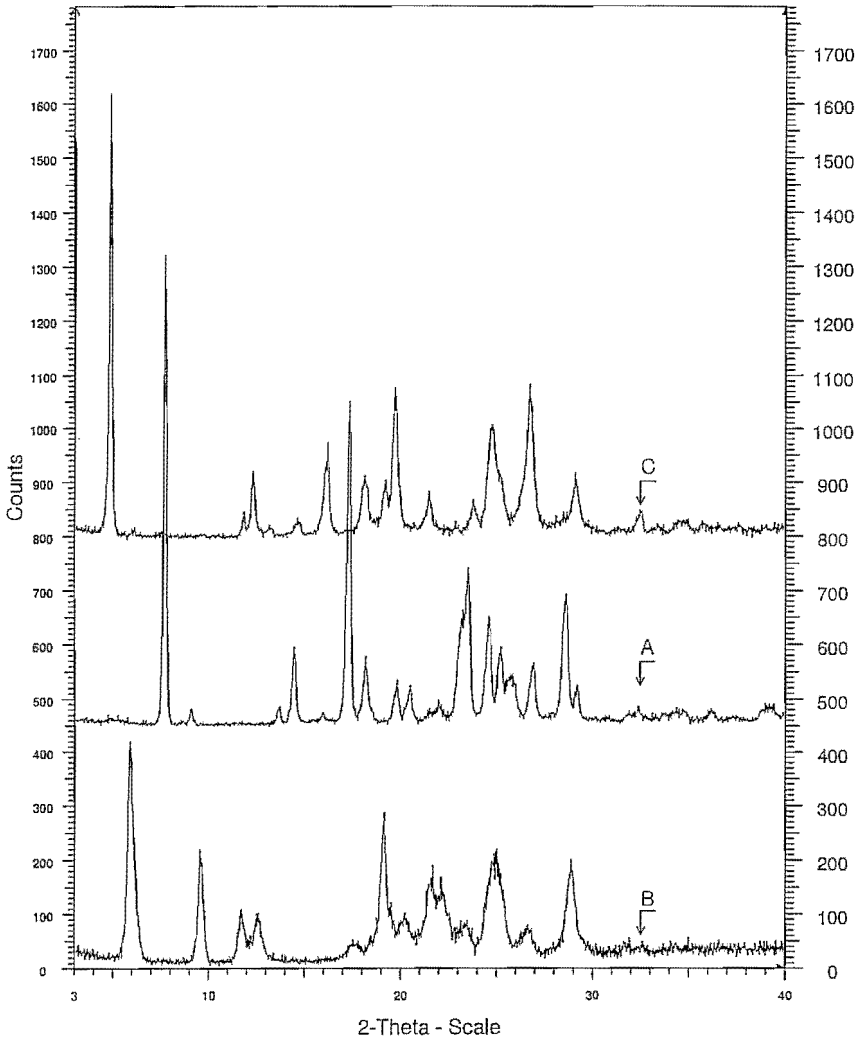

Figure 2.6 X-ray powder diffraction patterns of mebendazole Forms A, B and C (Brits, 2008:71).

The mebendazole propionic acid complex was reported to crystallise as white to slightly yellow needles (Caira *et al.,* 1998:12). Single crystal x-ray data has been published for the mebendazole propionic acid complex by Caira *et al.* (1998:11-15), however no x-ray powder diffraction data have been published.

Single-crystal crystallographic data of the mebendazole propionic-acid complex was requested from the Cambridge Crystallographic Data Centre, CCDC-1003/5265 (CCDC, 12 Union Road, Cambridge CB2 1EZ, UK). Figure 2.7 illustrates the XRPD pattern and illustration of the unit-cell packing of the propionic-acid complex, computed from the x-ray crystallographic data obtained using Mercury® software.

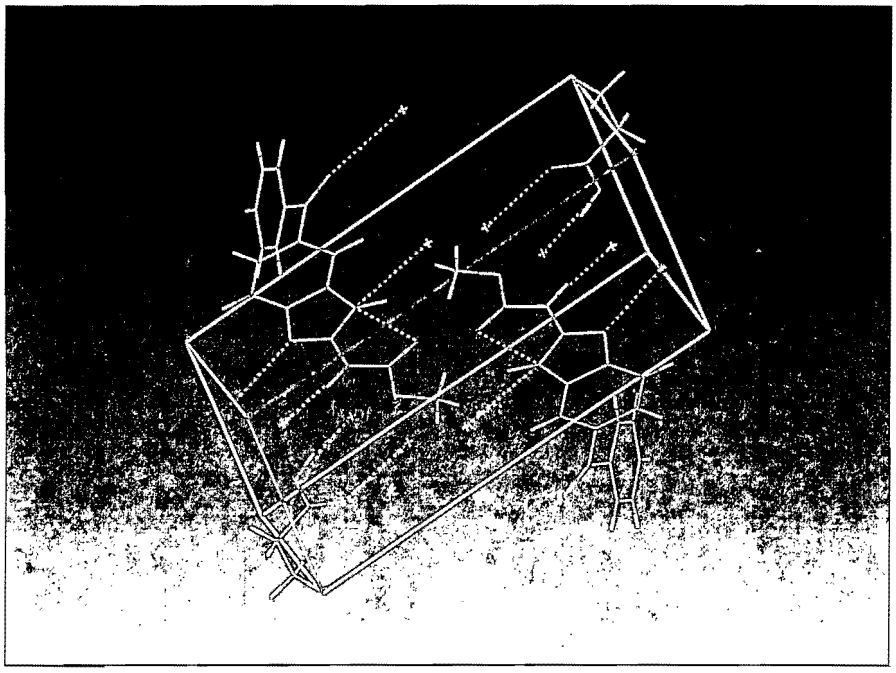

(a)

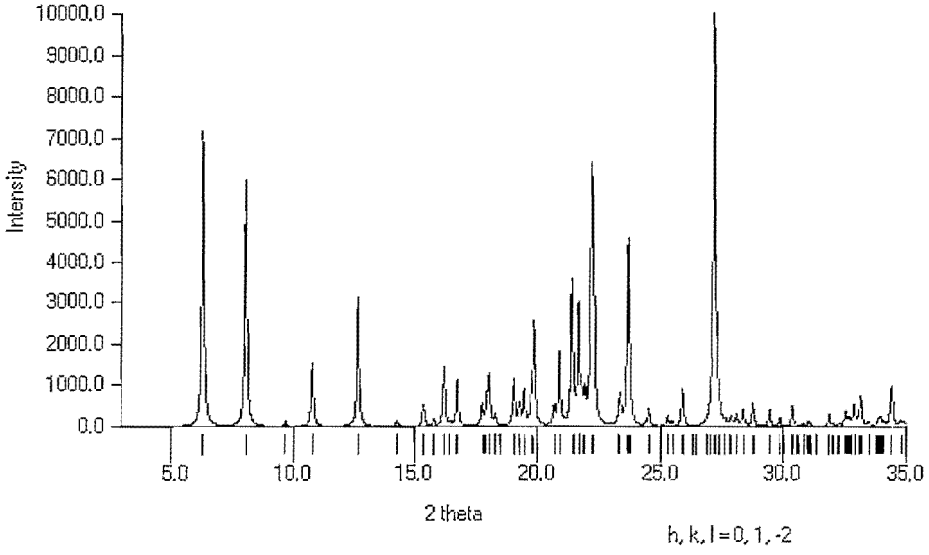

(b)

Figure 2.7 (a) Unit-cell packing of the mebendazole propionic complex illustrating the hydrogen bonding properties and (b) calculated XRPD pattern thereof using x-ray crystallographic data obtained from the Cambridge Crystallographic Data Center (CCDC-1003/5265).

2.2 Pharmacological properties of mebendazole

2.2.1 Indication of use

Mebendazole is indicated for the treatment of patients with single or mixed helminth infestations including: roundworms (*Ascaris lumbricoides*), hookworm (*Ancyclostoma duodenale, Necator americanus*), pinworm (*Enterobius vermicularis*) and whipworm (*Trichuris trichiura*) (Tierney *et al.*, 2004:1451-1470; Anon, 1995:1-8).

2.2.2 Mechanism of action

Mebendazole causes degeneration of the cytoplasmic microtubules and inhibits the microtubule synthesis of the parasite. Mebendazole has a high affinity for tubulin binding, inhibiting the transformation of tubulin into microtubules. By selectively inhibiting the microtubule synthesis, mebendazole irreversibly blocks glucose uptake and eventually decrease the main energy source of the parasite. The inhibition of the glucose uptake results in a depletion of the parasite glycogen stores and reduces the formation of adenosine tri-phosphate (ATP) required for it's survival and reproduction. Ultimately, the inhibition of ATP production causes immobility, leading to the death and excretion of the helminth (Frayha *et al.*, 1997:273-299; Katzung, 2001:910; Anon, 1995:2).

Verheyen *et al.* (1978:411-425) illustrated the effect of mebendazole on the microtriches of *Cysticerus fasciolaris* in mice after a 14 day treatment. Figure 2.8 (a) illustrated the microtubules on the scolex of *C. fasciolaris* prior to the treatment with mebendazole. The microtriches on the scolex as illustrated in Figure 2.8 (a) are conical in form and assume an anterior-posterior orientation. After 72 hours of treatment with mebendazole the microtriches on the scolex were significantly reduced (Figure 2.8 (b)) and after 7 days of treatment, crater-like structures were observed on the scolex of the parasite (Figure 2.8 (c)). This study revealed that treatment with mebendazole caused a drastic time-related change on the topography of the parasite, leading to a gradual decrease and disappearance of microtriches. This resulted in the formation of crater-like structures, holes and grooves on the parasite, followed by death (Verheyen *et al.*, 1978:411-425).

(a)

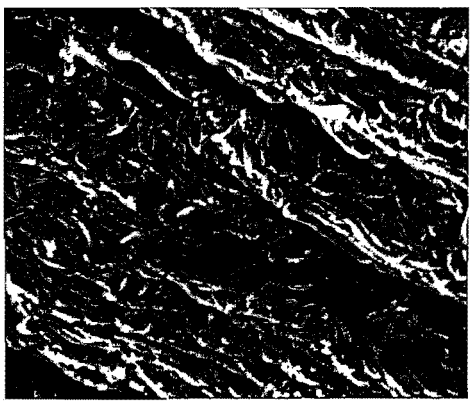

(b)

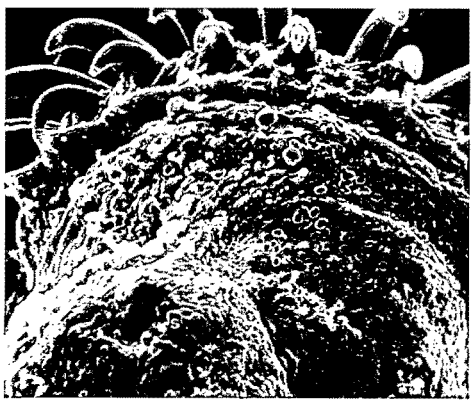

(c)

Figure 2.8 SEM photomicrographs of the microtriches on the (a) scolex of *C. fasciolaris*. (b) Decrease in microtriches on the scolex, 72 hours after treatment with mebendazole and (c) the formation of crater-like structures on the scolex after 7 days of treatment with mebendazole (Vereyen *et al.*, 1978:411-425).

2.3 Pharmacokinetics and pharmaceutical considerations

2.3.1 Absorption, distribution and metabolism

Mebendazole is poorly absorbed from the gastrointestinal tract after oral administration and less than 10% of the absorbed drug reaches the bloodstream (Münst *et al.*, 1980:375-378). Mebendazole is mostly protein-bound (more than 90%) and is rapidly converted to inactive metabolites following first-pass elimination by the liver. Mebendazole has a half-life of 2-9 hours in healthy patients. The half-life is increased up to 35 hours in patients suffering from impaired hepatic function, metabolism and biliary elimination (Janssen-Ortho, 2004:1-10; Münst *et al.*, 1980:375-378).

Patients diagnosed with hepatic impairment will therefore require a reduced dosage of mebendazole to minimize the possibility of toxicity (Gibbon, 2008:499). The bioavailability of mebendazole is influenced by food intake and may be increased when taken with fatty meals (Janssen-Ortho, 2004:1-10; Münst *et al.*, 1980:375-378).

The poor bioavailability of mebendazole (after oral administration) achieved in the clinical trail study using 5 volunteers (Table 2.5) can be attributed to the poor solubility of mebendazole and the subsequent difficulty to achieve and maintain effective blood levels (Dawson *et al.*, 1982:453-455; Dawson *et al.*, 1985:78-86).

Table 2.5 Pharmacokinetic data for mebendazole following oral and intravenous administration to 5 volunteers (Dawson *et al.*, 1985:81)

	Patient code and mass (kg)					
	DW (53)	LB (74)	LB (65)	JA (60)	JT (108)	Mean ± s.d.
Intravenous administration						
$AUC_{i.v.}$ (pg ml/h)	30.14	18.93	30.12	23.49	10.27	22.68 ± 8.18
$t_{½\ i.v.}$ (h)	0.23	0.25	0.20	0.18	0.13	0.20 ± 0.05
$t_{½\ i.v.}$ (h)	1.07	0.83	1.35	0.98	1.36	1.12 ± 0.24
$Vd_{i.v}$ (l/kg)	1.142	0.998	1.176	1.186	1.998	1.230 ± 0.40
$CL_{i.v.}$ (l/min)	0.654	1.040	0.645	0.831	1.831	1.063 ± 0.45
Oral administration						
$AUC_{po.}$ (pg ml/h)	3.75	62.64	6.69	6.37	3.73	4.63 ± 1.79
$t_{½\ po.}$ (h)	0.88	0.65	1.22	0.73	1.14	0.93 ± 0.25
$T_{max\ po.}$ (h)	0.50	0.52	0.52	0.28	0.30	0.42 ± 0.12
$CL_{po.}$ (l/min)	0.533	0.833	0.548	0.706	1.563	0.846 ± 0.424
F*	0.12	0.14	0.22	0.27	0.35	0.22 ± 0.09

*F= Bioavailability after oral administration. Other abbreviations are discussed in Section 2.3.2.

2.3.2 Elimination

Mebendazole is mainly excreted after 24-48 hours in the faeces as the unchanged drug or as the primary metabolite, following large doses. Less than 5% of the oral dose is excreted in the urine as decarboxylated derivates of mebendazole (Gibbon, 2008:499; Katzung, 2001:910-911).

In a study performed by Dawson *et al.* (1985:79-86) the pharmacokinetic parameters of mebendazole (i.e. half-life ($t_{½}$), volume of distribution (Vd), clearance (CL) and area under curve (AUC)) were calculated after intravenous and oral administration to 5 volunteers (aged: 37 - 64 years) who had been previously treated for cystic hydatid disease. The results of the study are summarised in Table 2.5 (Dawson *et al.*, 1985:79-86).

Dawson *et al.* (1982:454) also indicated that mebendazole underwent extensive first pass metabolism and elimination. The results indicated that mebendazole was rapidly absorbed with a distribution volume of 2.03l/Kg and an elimination half-life of 1.16 hours following intravenous administration of mebendazole. Oral administration of mebendazole to a volunteer revealed no absorption and the elimination half-life of mebendazole was calculated to be 0.74 hours (Dawson *et al.*, 1982:454).

Dawson *et al.* (1985:80) indicated that the mebendazole metabolites exhibited a lack in anti-parasitic activity in humans and animals. These four metabolites as documented by Dawson *et al.* (1985:80) are 2-amino-5(6)-benzoylbenzimidazole ([I] Figure 2.9), 2-amino-5-(6)-benzoylbenzimidazole ([II] Figure 2.9), methyl-5(6)-[α-hydroxybenzyl] benzamidazole carbamate ([III], Figure 2.9) and 2-amino-5(6) [α-hydroxybenzyl] benzimidazole ([IV], Figure 2.9).

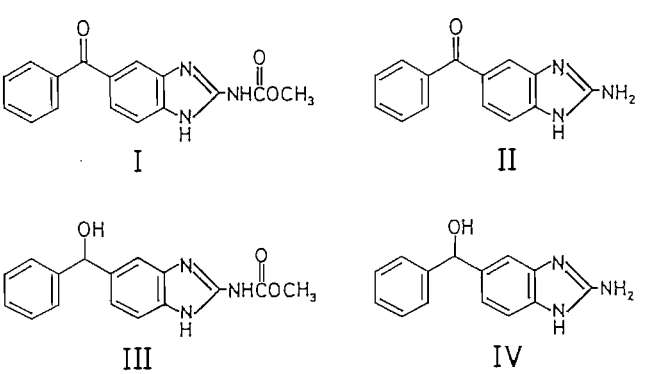

Figure 2.9 Known metabolites of mebendazole (Dawson *et al.*, 1985:80).

2.3.3 Efficacy of mebendazole polymorphs

Rodriquez-Caabeiro *et al.* (1987:266-271) investigated the toxicity of the mebendazole polymorphs by determining the LD_{50} for each polymorph in mice. The results of their studies indicated that Forms B and C both showed anthelmintic activity when administered orally at the experimental doses, but that Form B was more toxic in comparison to Form C. Their studies also revealed that Form A was ineffective during treatment, with limited toxicity. Rodriquez-Caabeiro *et al.* (1987:266-271) recommended that Form C be used in anthelmintic treatment. The preference for the use of Form C was supported by Costa *et al.* (1991:415-426) and Swanepoel *et al.* (2003:345-349) following the determination of the solubility and dissolution behaviour of the mebendazole polymorphs. It was reported that Form C had a significantly higher solubility profile compared to Forms A and B in 0.1 N HCl at 37°C (Swanepoel *et al.*, 2003:345-349).

2.3.4 Dosage and administration

Mebendazole is administered orally as a single- or multiple-dose in the form of a tablet or suspension. Section 2.5 provides more information on the commercially available products. Patients with hepatic impairment require a reduction in the dose to prevent toxicity and adverse effects as mentioned in Sections 2.3.1 & 2.3.2. The dosage and administration of mebendazole in children under the age of 1 year have not been fully determined as of yet. The dosage requirements for children over the age of 2 years are the same as that of adults (Anon, 1978:3; Gibbon, 2008:499; Dawson *et al.* 1982:453-455). Table 2.6 summarises the indications and dosages for mebendazole administration.

Table 2.6 Indications and dosage regimens for mebendazole (Gibbon, 2008:499)

Indication	Adult dose	Paediatric dose
Roundworm	Oral, 100 mg twice daily for 3 days or 500 mg as a single dose. Repeat after 3-4 weeks.	Oral, 100 mg twice daily for 3 days or 500 mg as a single dose. Repeat after 3-4 weeks.
Pinworm	Oral, 100 mg as a single dose, repeated after 2 weeks.	Oral, 100 mg as a single dose, repeated after 2 weeks.
Whipworm	Oral, 100 mg twice daily for 3 days or 500 mg as a single dose. Repeat after 3-4 weeks.	Oral, 100 mg twice daily for 3 days or 500 mg as a single dose. Repeat after 3-4 weeks.
Tapeworm	Oral, 100 mg twice a day for 6 days or 200 mg twice a day for 4 days or 300 mg twice a day for 3 days. Repeat after 3-4 weeks.	Oral, 100 mg twice a day for 6 days.
Hookworm	Oral, 100 mg twice daily for 3 days or 500 mg as a single dose. Repeat after 3-4 weeks.	Oral, 100 mg twice daily for 3 days or 500 mg as a single dose. Repeat after 3-4 weeks.

2.4 Side-effects, contra-indications, drug interactions and precautions of mebendazole

2.4.1 Side effects and precautions

Treatment of intestinal, nematodal and cestodal infestations with low doses of mebendazole for a period less than or equal to three days is mostly free from any adverse effects. Patients may experience mild nausea; vomiting, diarrhoea and abdominal pain during treatment of severe infestations. In rare cases patients experienced itching, dizziness, drowsiness and headaches with the use of low doses of mebendazole (Anon, 1978:2). Administration of high doses of mebendazole may lead to bone marrow depression, hepatoxicity, allergic reactions and alopecia. Adverse effects may differ from patients depending on the type and severity of infestation, age, culture, dosage and period of treatment. The occurrence of these side effects are rare, but there are documented reports of the occurrence thereof in patients (Anon, 1978:2; Gibbon, 2008:499; Janssen-Ortho, 2004:1-10). A summary of the possible adverse effects of mebendazole are listed in Table 2.7.

As a precaution, mebendazole has been contra-indicated for patients diagnosed with Chron's disease, ulcerative colitis, porphyria and hepatic impairment (Gibbon, 2008:499). Mebendazole is also known to cross the placenta and has therefore been categorised as a Category C drug and must be avoided during the first trimester due to its embryotoxic and teratogenic effects in humans and animals (Dayan, 2003:141-159; Janssen-Ortho, 2004:1-10).

Table 2.7 · Summary of the adverse reactions of mebendazole (Janssen-Ortho, 2004:4; Anon, 1995:1-8; Anon, 1978:1-5; Gibbon, 2008:499)

System affected	Adverse reaction(s) observed
Cardiovascular system	Angioedema.
Central nervous system	Fever, dizziness, headaches, seizures and convulsions in infants.
Dermatologic system	Rash, itching, alopecia (with high doses), epidermal necrolysis and Stevens-Johnson syndrome.
Gastro-intestinal system	Abdominal pain, diarrhoea nausea, vomiting, hepatitis, abnormal liver function tests and glomerulonephritis.
Haematologic system	Neutropenia (sore throat and unusual fatigue associated with high doses and prolonged treatment).
Neuromuscular and skeletal system	Unusual weakness.
Immune system	Hypersensitivety reactions including anaphylactic shock and anaphylactoid reactions.

2.4.2 Drug interactions

It has been documented that mebendazole interacted with numerous pharmaceuticals (Table 2.8) that may lead to decreased or increased levels of mebendazole. These drug interactions are based on the mechanisms and effects that the contra-indicated pharmaceuticals have on the hepatic microsomal enzymes (Gibbon, 2008:499; Janssen-Ortho, 2004:1-10).

Table 2.8 Drug interactions and the effects on mebendazole serum concentrations (Gibbon, 2008:499; Anon, 1995:1-8; Anon, 1978:1-5; Janssen-Ortho, 2004:1-10)

Drug	Interaction
Aminoquinolines (Anti-malarial)	Decreased serum concentration of mebendazole.
Carbamazepine	Decreased serum concentration of mebendazole.
Phenytoin	Decreased serum concentration of mebendazole.
Cimetidine	Increased serum levels of mebendazole.
Metronidazole	Possible relationship between Stevens-Johnson syndrome / toxic epidermal necrolysis with concominent use.
Ethanol	Increased serum levels of mebendazole.
Nutrition and food	Increased serum levels of mebendazole.

2.5 Registered pharmaceutical preparations of mebendazole

The first FDA (Food and Drug Administration) registered dosage form containing mebendazole (i.e. the innovator product) for the treatment of nematodal and cestodal infestations was Vermox® (Gibbon, 2008:499). Vermox® is available in 100 mg and 500 mg tablets and in 100 mg/5 ml and 500 mg/10 ml suspensions. Mebendazole preparations in South Africa are registered as schedule 1 preparations and can be bought over-the-counter at any pharmacy without a prescription (Gibbon, 2008:499). Table 2.9 provides a list of generic mebendazole products available in South Africa.

Table 2.9 Mebendazole preparations available in South Africa (Gibbon, 2008:500)

Registered Product	Manufacturer	Available preparations
Vermox® **	Janssen-Cilaq	Tablets: 100 mg, 500 mg Suspensions: 100 mg /5 ml and 500 mg/10 ml.
Adco-Wormex®	Adco-Generic	Tablets: 100 mg, 500 mg Suspensions: 100 mg/5 ml.
Cipex®	Cipla Medpro	Tablets: 100 mg, Suspensions: 100 mg/5 ml.
D-Worm®	Aspen Pharmacare	Tablets: 100 mg, 500 mg.
Adco-Rioworm®	Adcock Ingram Pharmaceuticals	Tablets: 100 mg, Suspensions: 100 mg/5 ml.
Wormgo®	Aspen Pharmacare	Tablets: 100 mg, Suspensions: 100 mg/5 ml.
Wormstop®	Be-Tabs	Tablets: 100 mg, 500 mg Suspensions: 100 mg/5 ml.

** Innovator product

Conclusion

Mebendazole is used for the treatment of helminth infestations. Three distinct polymorphic forms and one pseudo-polymorphic form (1:1 mebendazole propionic acid complex) have been identified for mebendazole. The preferred use of Form C in pharmaceutical products is based on the superior anthelmintic activity, lowered toxicity and higher solubility in comparison with that of the other forms. Form C proved to be equally efficient and less toxic than Form B. Form A showed little to none anthelmintic activity and toxicity. Dissolution studies indicated the rate of dissolution for the polymorphs of mebendazole were in the order: C > B > A (in 0.1 N HCl at 37°C). These three forms can be identified using XRPD and DRIFT-IR.

From the literature study on mebendazole it was evident that there were some inconsistencies regarding the thermal behaviour of the polymorphic forms. Further investigation was required to ascertain a valid conclusion, especially when comparing the results of this study to those found in the literature. These inconsistencies will be addressed in Chapter 3 (Section 3.3).

The next chapter will discuss the techniques and methods utilised in the investigation of the mebendazole polymorphic forms in more detail.

CHAPTER 3

Preparation and characterisation techniques utilised in the study of the mebendazole polymorphs and pseudo-polymorphs

Introduction

A variety of methods and techniques exist to aid in the preparation and characterisation of crystal forms. The microscope was one of the first instruments to play a crucial role in the study of polymorphism and became a more sophisticated analytical tool during the nineteenth century (Bernstein, 2002:21). With the turn of the twentieth century more analytical techniques and theoretical models were introduced for the investigation of crystal studies. These experimental techniques included hot-stage microscopy (McCrone, 1969:918), dilatometry, precise vapor and solubility measurements, infrared spectrometry, x-ray powder diffraction, thermo-kinetic and thermodynamic methods (heat capacity, melting point, degradation and stability studies) (Bernstein, 2002:23-24). The above mentioned analytical techniques aid in the identification and classification of different crystal forms by detecting differences in the crystal structure or molecular structure of the API (Bernstein, 2002:94).

The purpose of this chapter is to describe the methods and experimental techniques utilised during the characterisation of the mebendazole crystal forms in the chapters to follow, and to address the inconsistencies in the thermal behaviour of the polymorphic forms as identified in Chapter 2.

3.1 Characterisation techniques in polymorph screening

This section provides a general overview of the experimental techniques utilised in the study to identify and characterise the mebendazole crystal forms. These methods are tabulated in Table 3.1.

Table 3.1 Characterisation methods used in the investigation of different polymorphic forms (adapted from Yu *et al.*, 1998:124)

Type of polymorphic form	DRIFT-IR	Thermal methods	XRPD	Microscopy	Karl-Fischer
True polymorph	Characteristic spectra. Sensitive to H-bonding.	Unique melting point, heat capacity, heats of fusion/transition, solubility. Useful for determining relative stability of forms.	Unique diffraction peaks. Useful for the determination of phase purity and % crystallinity.	Characteristic indices of refraction, birefringence, dispersion color and crystal habits.	N/A
Solvates	Unique solvent bands. Shifted drug bands. Sensitive to H-bonding.	Low-temperature transitions due to desolvation (TGA moisture loss).	Same as true polymorphs.	Same as true polymorphs. Desolvation observable by HSM.	Moisture (water) content can be determined.
Isomorphic desolvates	Solvent bands disappear. Drug bands shifted.	Low-temperature desolvation absent. Events due to crystallization or lattice relaxation.	Diffraction pattern only slightly changed from parent solvates.	Birefringent microcrystalline domains, with cracks and fissures.	N/A
Amorphous solids	Broadened spectra.	Glass transition seen. Often followed by crystallization and melting. "Fragility" related to width of T_g.	No diffraction peaks.	No birefringence, irregular particle shape.	N/A
Polymorphic mixtures	Composite spectrum of all components.	Thermal behaviour indicative of phase diagram (e.g. melting point depression, eutectic melting, dissolution).	Composite pattern of crystalline compounds.	Composite of distinct crystalline and amorphous particles.	Moisture (water) content can be determined.

3.1.1 X-ray crystallography

3.1.1.1 X-ray powder diffraction (XRPD)

X-radiation (x-rays) or electromagnetic radiation found between gamma- and ultraviolet rays on an electromagnetic spectrum, has a wavelength between 0.01 nm and 10 nm and is about the same size as that of an atom (Doitpoms, 2007). With the discovery of x-rays by Wilhelm Roentgen in 1895, scientists gained the ability to probe crystalline structures on an atomic level even though they where not sure if x-rays consisted out of particles or electromagnetic waves (Sands, 1993:88; Whittingham, 1989:1). Since then, x-ray diffraction has been used in two main focus areas, i.e. fingerprint characterisation of crystalline substances and the determination of crystalline structures. Each crystalline solid exhibits a unique distinguishable x-ray diffraction pattern which can be used as a "fingerprint" for identification. X-ray crystallography can also be implemented to determine the structure of the crystalline solid (i.e. the packing of atoms in the crystalline state and the interatomic distances and angles). Using x-ray diffraction the size and shape of the unit cell for any crystalline API can be determined (Whittingham, 1989).

In 1912, Max von Laue proved that x-rays are diffracted by a crystal structure if the typical spacing of adjacent atoms in a crystal structure is the same as that of x-rays (Doitpoms, 2007). This led to the formulation of Bragg's law in 1912 by W.L. Bragg. Bragg's law formed the cornerstone of x-ray analysis and was used to prove that crystals only reflect x-rays at certain angles of incidence. Bragg's law also produced a simple geometrical interpretation, making it easy to relate the angle of diffraction to the interplanar spacing between atoms in a crystalline structure (Doitpoms, 2007).

All x-ray diffraction techniques are ultimately based on Bragg's law, which described the diffraction of a monochromatic x-ray beam impinging on a plane of atoms. According to this theory, parallel incident rays strike the crystal at an angle of θ and are also diffracted by the same angle of θ, hence the 2θ angle (Brittain, 1999:231; Sands, 1993:92-94). The physical process involved the scattering of the x-rays by the electron clouds of the atoms in the crystal, creating the observed diffraction pattern as a result of the constructive and destructive interference of the x-rays scattered by all the atoms in the atomic arrangement of the crystal (Sands, 1993:93). For these x-rays to be reinforced by each other, the path difference of the impacting beam on the distance between two molecular planes of the crystal must be equal to the number of wavelengths (Brittain, 1999:229-235).

Bragg's law is illustrated in Figure 3.1. This figure illustrates the diffraction of the x-ray beam by the different interplanar spacings (*hkl*) of a crystalline structure.

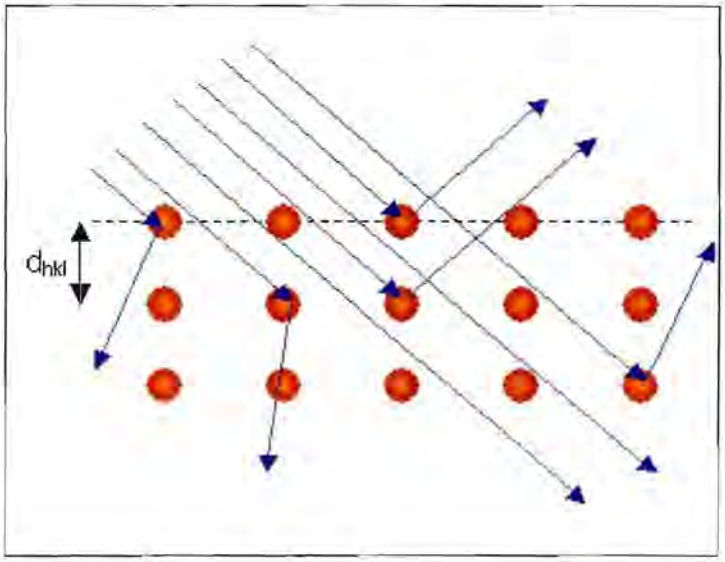

Figure 3.1. An illustration of Bragg's law (Doitpoms, 2007).

The scattering angles are therefore accordant to the spacings between the planes of molecules in the lattice by means of Bragg's law (Equation 3.1) (Brittain, 1999:229-235)

$$n\lambda = 2d \sin \theta \tag{3.1}$$

Where: n = order of diffraction pattern

λ = wavelength of the incident beam

d = distance between the planes in the crystal

θ = angle of beam diffraction

λ and d are measured in the same units, usually angstroms.

The application of x-ray diffraction is mainly divided into two disciplines, s*ingle crystal x-ray diffraction* and x-*ray powder diffraction*. X-ray powder diffraction is mainly used for qualitative identification of individual API polymorphic forms or mixtures of polymorphs (Bernstein, 2002:111). Single crystal x-ray diffraction is used for the detailed investigation and determination of the molecular and crystal structure of an API (bond lengths, bond angles, intermolecular interactions, etc.) and provide some of the most precise data on the structural features of a crystal (Bernstein, 2002:112).

Bragg's law is illustrated in Figure 3.1. This figure illustrates the diffraction of the x-ray beam by the different interplanar spacings (*hkl*) of a crystalline structure.

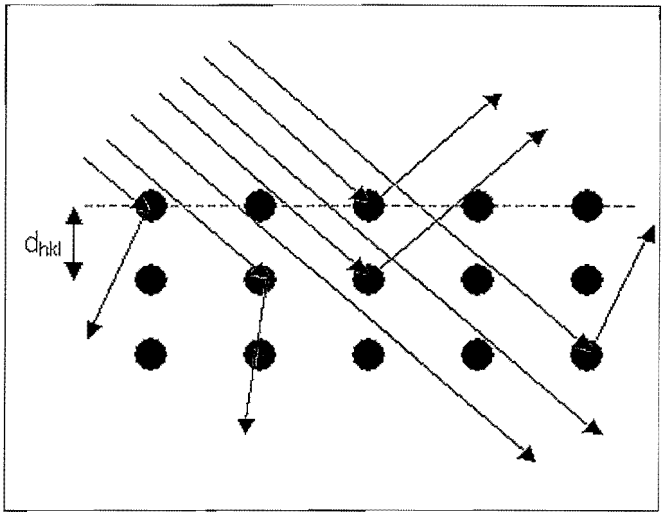

Figure 3.1. An illustration of Bragg's law (Doitpoms, 2007).

The scattering angles are therefore accordant to the spacings between the planes of molecules in the lattice by means of Bragg's law (Equation 3.1) (Brittain, 1999:229-235)

$$n\lambda = 2d \sin \theta \qquad (3.1)$$

Where: n = order of diffraction pattern

λ = wavelength of the incident beam

d = distance between the planes in the crystal

θ = angle of beam diffraction

λ and d are measured in the same units, usually angstroms.

The application of x-ray diffraction is mainly divided into two disciplines, s*ingle crystal x-ray diffraction* and x-*ray powder diffraction*. X-ray powder diffraction is mainly used for qualitative identification of individual API polymorphic forms or mixtures of polymorphs (Bernstein, 2002:111). Single crystal x-ray diffraction is used for the detailed investigation and determination of the molecular and crystal structure of an API (bond lengths, bond angles, intermolecular interactions, etc.) and provide some of the most precise data on the structural features of a crystal (Bernstein, 2002:112).

A typical comparison of two polymorphic forms would traditionally be done by simple visual comparison of their diffractograms, with emphasis being given to the 2-theta peak position over the 2-theta peak intensity. If all peak positions of the two diffractograms agree within some tolerance (± 0.2°2θ as a typical rule-of-thumb value) the polymorphic forms of the two samples are considered to be the same (USP, 2007). If one or more of the peak positions disagree then the level of confidence in a positive comparison is lower. If one or more peaks from a sample are not observed in a second sample, but a number of major peaks agree, then it is possible that the second sample is a different polymorph or a mixture of two polymorphic forms (Runger *et al.*, 2005:1).

X-ray powder diffraction patterns (XRPD patterns) were recorded using a Bruker D8 Advance diffractometer (Bruker, Germany). The experimental conditions were: target, Cu; voltage, 40kV; current, 30mA; divergence slit, 2 mm; anti-scatter slit, 0.6 mm; detector slit, 0.2 mm; monochromator; scan speed, 2°/min with an increment of 0.025° and a increment time of 1.0 seconds. Samples were prepared by packing the lightly ground powder into an aluminium sample holder. The aluminium sample holder was then placed into the XRPD sample accessory and rotated at 15 revolutions per minute to reduce potential preferred orientation effects of crystals. The peak positions and intensities where extracted from the diffractograms using the Eva® software (version 10.0 revision 1) which is part of the Diffrac^{plus} 2004 software package (Bruker, Germany).

3.1.1.2 Variable temperature x-ray powder diffraction (VT-XRPD)

Variable temperature x-ray powder diffraction (VT-XRPD) is an analytical method used in the characterisation of pharmaceutical solid-state phase reactions, including crystal transformations, dehydration and desolvation, when samples are exposed to increased temperatures (Karjalainen *et al.*, 2005:28; Byrn *et al.*, 1999:64).

Samples for VT-XRPD analysis were prepared and analysed using the diffractometer setup mentioned in section 3.1.1.1. Diffraction data were recorded after heating the samples to different temperatures, using an Anton Paar TTK 450 low temperature camera (Anton Paar, Austria) at a heating rate of 10°C/step (3 – 40 °2θ).

3.1.2 Diffuse reflectance infrared Fourier transform spectroscopy (DRIFTS)

Infrared (IR) spectroscopy is a useful analytical technique used in the analysis of APIs in the pharmaceutical industry. This method is based on the measurement of the vibrational modes of chemical compounds (generally bonded atoms) within the range of 400 – 4000 cm^{-1}, where they can be directly observed with their absorbance in the infrared region of the light spectrum (Brittain, 1999:256; Bernstein, 2002:125). The infrared spectrum is extremely sensitive to the structure, conformation and environment of the API and can therefore be implemented as a powerful tool in the characterisation and identification of polymorphs and pseudo-polymorphs (Byrn *et al.*, 1999:111; Brittain, 1999:258). As different polymorphic forms of a specific API have different arrangements of molecules in the solid-state and differ in physico-chemical properties, variations of the intermolecular forces in the crystalline state results in variations in the vibrational modes of the molecules. These differences can be detected via the absorption in the infrared region resulting in the characterisation of the different polymorphic forms (Bernstein, 2002:125).

Distinctly different from other techniques used in the characterisation of polymorphic forms, infrared spectroscopy may be implemented in both qualitative (polymorph identification) and quantitative (polymorph purity control) analysis (Bernstein, 2002:129-130). Bugay (referenced by Bernstein, 2002:129-130) gave an example of cefepime dihydrochloride where the amount of dehydrate was determined in the marketed monohydrate form (Figure 3.2).

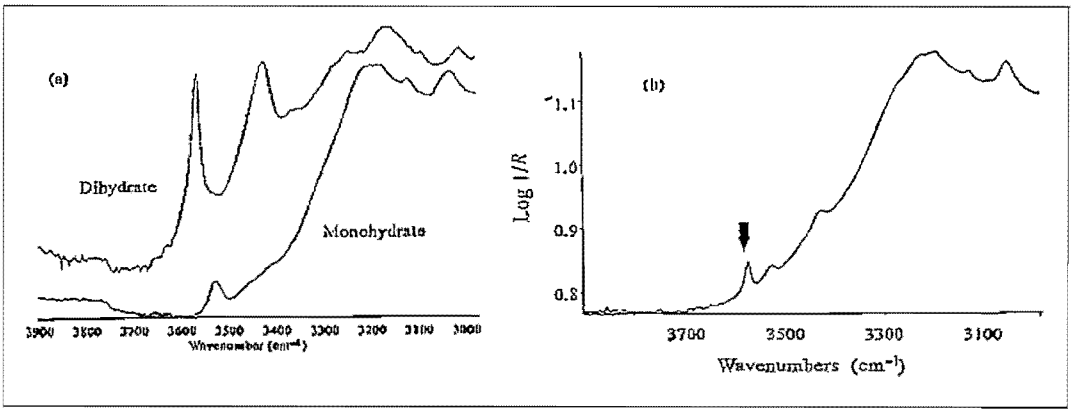

Figure 3.2 (a) IR spectra of the monohydrate and dehydrate form of cefepime dihydrochloride. (b) The arrow indicates the distinct dehydrate absorption used for quantitative analysis in a 5:95 (w/w) mixture of the dehydrate and monohydrate (Bernstein, 2002:131).

In the method of *diffuse reflectance infrared fourier transform spectroscopy* (DRIFTS) a minimum amount of sample is prepared for infrared absorption by dispersing the sample in a matrix of powdered alkali halide salt (KBr) to decrease the probability of polymorphic transformations or solvent loss usually associated with grinding or preparation of a pellet using pressure (Bernstein, 2002:129).

The infrared spectra of the samples were recorded on a Nicolet Nexus™ 470 Spectrophotometer (Nicolet Instrument Corporation, Madison WI, USA) over a range of 4000 – 400 cm^{-1} with the samples placed in an Avatar Diffuse Reflectance Smart accessory after being mixed and lightly ground with dried KBr (Merck, Darmstadt, Germany). The peak positions and intensities of the spectra recorded were determined using version 7.3 of the OMNIC© software package (Thermo Electron Corporation).

3.1.3 Thermal methods of analysis

Thermal analyses involve methods used in the determination and measurement of changes or reactions in the physico-chemical properties of a sample when exposed to increased temperatures (Byrn *et al.*, 1999:81; Brittain, 1999:245). These thermal reactions measured can be endothermic (melting, boiling, sublimation, vaporisation, desolvation, solid-solid phase transitions, chemical degradation, etc.) or exothermic (crystallisation, oxidative decomposition, etc.) (Brittain, 1999:245). The two most important thermal methods used in this study were *differential scanning calorimetry* (DSC) and *thermogravimetric analysis* (TGA).

3.1.3.1 Differential scanning calorimetry (DSC)

Differential scanning calorimetry (DSC) is probably one of the most commonly used methods for polymorph screening. The method incorporates the measurement of differences in energy (heat flow) absorbed or released between a reference standard (R) and an experimental sample (S) as a function of temperature. The result obtained by the DSC analysis is a thermogram where the differences in heat flow (ΔT) between the sample (T_S) and reference (T_R) are plotted as a function of temperature (Craig, 2007:43-48; Brittain, 1999:252-253). The energy associated with the transition of the sample is calculated by Equation 3.2 (Craig, 2007:43-48).

$$dQ/d = \Delta T/R \tag{3.2}$$

Where: dQ/d = heat flow

ΔT = temperature difference between the reference and experimental samples

R = thermal resistance of the heat path between crucible and furnace

Figure 3.3 illustrates the typical features that can be observed in the DSC thermogram of a polymorphic system of sulphapyridine (Bernstein, 20002:105).

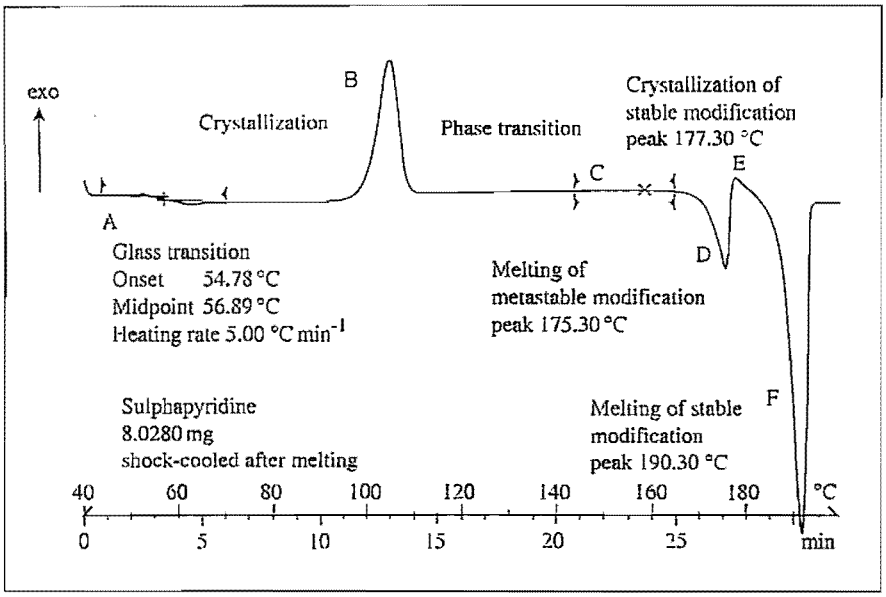

Figure 3.3 Typical features detected for the polymorphic system of sulphapyridine using DSC. The reactions are described as follow: (A) second-order glass transition to a supercooled liquid, (B) crystallisation of supercooled liquid, (C) exothermic solid-solid transition resulting in a metastable phase, (D) melting, (E) recrystallisation to stable modification and (F) melting and / or degradation (Bernstein, 20002:105).

For the purpose of this study 2-5 mg of each sample was placed in a 40 µl aluminium sample pan (Mettler Toledo, Switzerland), crimp sealed with a pierced aluminium lid. The lid was pierced to relieve possible pressure build up which could cause a variation in results. Samples were analysed using a Mettler Toledo DSC823^e (Greifensee, Switzerland) that was calibrated using an indium reference standard (Mettler Toledo, Switzerland). Samples were analysed at temperatures ranging between 25 - 350°C at a heating rate of 10°C/min and a nitrogen gas purge flow rate of 80 ml/min. The thermal events in the thermograms were evaluated using the STAR^e Software programme (version 9.0*x*) (Mettler Toledo, Switzerland).

3.1.3.2 Thermogravimetric analysis (TGA)

Thermogravimetric analysis (TGA) is used to measure the weight loss of a material as a function of temperature (Brittain, 1999:246). TGA is not utilised in the study of polymorphic transitions, as the transition in polymorphs do not involve a change in mass, however TGA analysis plays a vital role in the characterisation of the dehydration / desolvation behaviour of hydrates and solvates (Craig, 2007:67). TGA is useful in the measurement of transitions that involve a weight loss or gain, desolvation processes and API decomposition. In adjunct with Karl Fischer titration the TGA can be used in quantitative determination of the total volatile content of the API and type of moisture loss (Brittain, 1999:246).

During thermogravimetric analysis the sample is heated in a furnace while a microbalance measures and records changes in sample mass. The balance chamber is constructed so that the atmosphere inside may be controlled by a flowing gas stream (normally nitrogen = dry atmosphere) (Byrn *et al.*, 1999:81). The key weakness of the TGA is that it only measures the change in mass, but not the nature of the substance being lost. Alternative techniques may be implemented to determine the type and nature of the substances lost during the characterisation of APIs (solvates and hydrates) by connecting the TGA to a mass spectrometer or infrared spectrophotometer (Craig, 2007:68).

Determination of the theoretical weight loss of a solvated sample in this study was calculated using Equation 3.3 (Brits, 2008:50). The experimental weight loss recorded by the TG-Analyser was compared with the calculated theoretical weight loss for a solvate.

$$\%\ Weight\ loss = \frac{Molecular\ weight\ (solvent)}{Molecular\ weight\quad (solvent) + Molecular\ weight\ (API)} \times 100\% \qquad (3.3)$$

For the purpose of this study 10-15 mg of each sample was placed in a 100 µl aluminium pan and covered with a pierced lid (not crimped sealed). Samples were analysed using a calibrated Mettler Toledo TGA/SDTA851^e (Greifensee, Switzerland), with the samples heated between 25 - 200°C at a heating rate of 10°C/min and a nitrogen gas flow rate of 80 ml/min. The weight loss of the sample was calculated using the STAR^e Software programme (version 9.0*x*) (Mettler Toledo, Switzerland).

3.1.4 Microscopy

Microscopy plays a vital role in the characterisation of polymorphs and solvates with regards to the habits, desolvation behaviour and crystal growth (Brittain, 1999:238). The identified variations in the size, shape, colour or behaviour of the API may indicate the possibility towards polymorphism (Bernstein, 2002:94). Two types of microscopy techniques have been used in the characterisation of crystal forms: optical (i.e. polarising and hot-stage) and electron (i.e. scanning electron) microscopy. Both techniques are complementary to other characterisation techniques (Brittain, 1999:238-239).

3.1.4.1 Polarising optical and hot stage microscopy (HSM)

A polarising light microscope is essentially a light microscope that has been modified and fitted with a polarising filter (the polariser) below the specimen and a second polarising filter (the analyser) above the specimen (Nichols, 2007:169). A schematic diagram of the basic components of a polarising light microscope is illustrated in Figure 3.4.

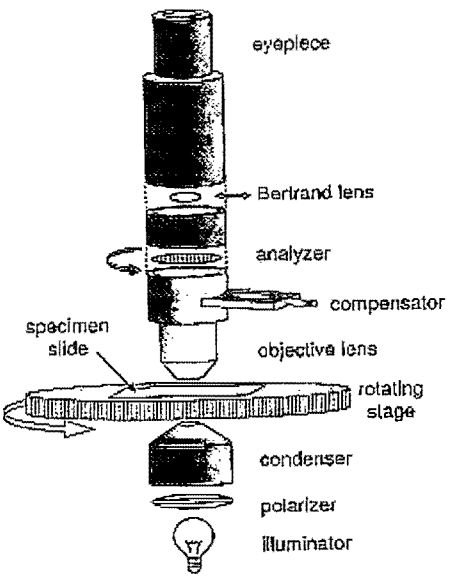

Figure 3.4 Illustration of the basic components of a polarising light microscope (Nichols, 2007:169).

Crystalline solids will either change colour or intensity as the stage of the polarising microscope is rotated, due to the anisotropic nature of light refraction in the crystals (Byrn *et al.*, 1999:71). *Anisotropic behaviour* is described as the observed property that varies in different directions in or on a crystal (i.e. changes in crystal faces) (Byrn *et al.*,1999:12,505). The observed changes in appearance (colour refraction) of the crystalline substances occur when the crystal separates the light beam by refracting the light beam into two unequal polarised light beams. The two beams occur as a result of differences in the velocity of the light beam dispersed through the crystal on impact. Nichols (2007:177) described the interference in colours within crystals (observed between crossed polarisers) as the resultant of constructive and deconstructive interference of white light. Figure 3.5 illustrates an example of a wedge-shaped crystal of lactose monohydrate showing interference in colour bands, where the latter corresponds to changes in the thickness of the crystal (Nichols, 2007:178). No physical changes in colour or refraction of light is observed in isotropic non-crystalline solids or APIs with cubic symmetry (Byrn *et al.*, 1999:71).

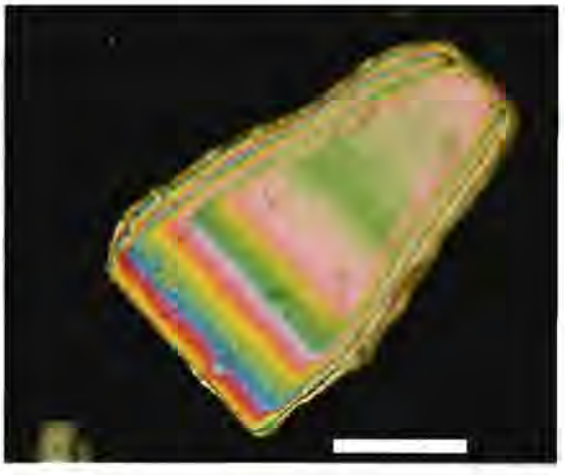

Figure 3.5 A wedge-shaped crystal of lactose monohydrate showing interference in colour bands, where the latter corresponds to changes in the thickness of the crystal (Nichols, 2007:178).

Thermal microscopy (hot-stage microscopy) is a rapid and effective method used in the screening of pseudo-polymorphs and provides insight on the thermal transitions of polymorphs (Bernstein, 2002:94; Craig, 2007:68). HSM involves the heating of a small amount of sample on a microscope slide, while observing changes in the sample upon heating and cooling (Brittain, 1999:244). Hot-stage microscopy (HSM) can be used to resolve thermal events in DSC thermograms for example: identify the existence of solvates (bubbles forming in silicon oil –

Figure 3.6), evaluate changes in crystal structure or habit, witness polymorphic transition (Figure 3.7) and confirm melting point temperatures (Byrn *et al.*, 1999:73).

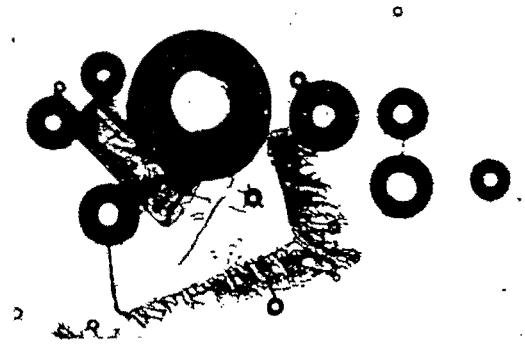

Figure 3.6 Bubble formation indicates the desolvation of a solvated form when heated in silicone oil (Bernstein, 2002:101).

For the purpose of this study a small amount of sample was placed on a microscope slide and either covered with silicon oil (Fluka Chemika, Switzerland) and a cover slide (in the case of solvates), or only a cover slide for non-solvated forms. A Nikon Eclipse E400 thermo-microscope (Tokyo, Japan) with a Leitz 350 heating unit (Leitz – now known as Leica Microsystems – Wetzlar, Germany) and a Metratherm 1200d thermostat were used for the hot-stage microscopy. A Nikon Simple Polarizing Attachment (Tokyo, Japan) was used on the microscope for the polarising optical microscopy. Photographs were taken using a Nikon Coolpix 5400 digital camera (Tokyo, Japan) which was attached to the microscope.

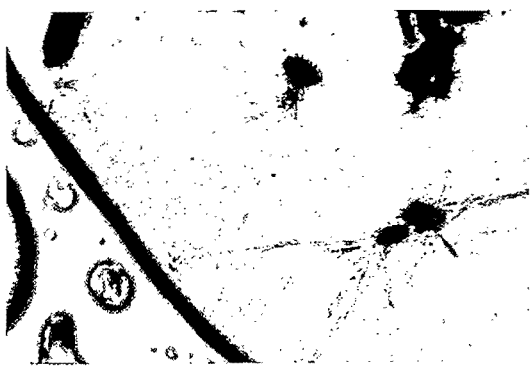

Figure 3.7 Polymorphic transition of caffeine (Form 2) to the metastable enantiotropic form when heated to 50°C. The formation of needle-shaped crystals indicated the formation of the metastable form (Craig, 2007:68).

3.1.4.2 Scanning electron microscopy (SEM)

Scanning electron microscopy provides photomicrographs with higher magnification and resolution compared to light microscopy. Scanning electron microscopy (SEM) is a useful technique for the study of polymorphism (Bernstein, 2002:144; Yu *et al.*, 1998:121). This method involves the placement of a sample in a vacuum, where the sample is then bombarded with electron beams. The electron bombardment and conditions may unfortunately alter the nature and properties of the sample (Yu *et al.*, 1998:121). However SEM remains a valuable technique for the characterisation of the morphology of different polymorphs. An example of where SEM was used in the study of different polymorphic forms is in that of ranitidine hydrochloride as illustrated in Figures 3.8 (a) and (b).

Samples for SEM analysis were prepared by covering the SEM pin with carbon tape and sample, mounted onto a metal disc and coated with gold-palladium film (Eiko engineering ion coater IB-2, Japan) in a vacuum. The samples were placed in the microscope sample holder and analysed using a FEI Quanta 200 ESEM & Oxford INCA 400 EDS microscope system (FEI Corporation, Hillsboro OR, USA).

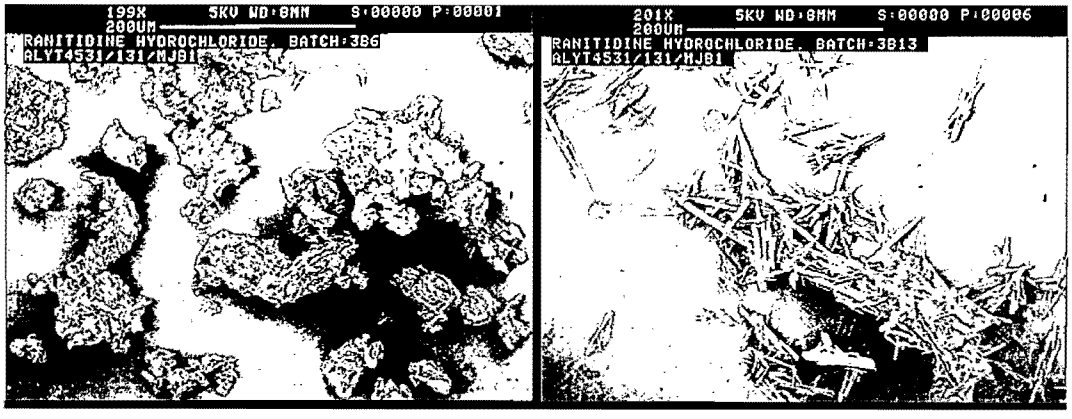

(a) (b)

Figure 3.8 SEM photomicrographs of the two polymorphic forms of ranitidine hydrochloride. (a) From 1 and (b) Form 2 (Bernstein, 2002:145).

3.1.5 Karl Fischer analysis (KF)

Karl Fischer titration is a method used for quantifying the water content in samples. The method is based on the Bunsen reaction between iodine and sulphur dioxide in a water medium (EMD Chemicals Inc, 2008). The Karl Fischer reaction is illustrated in Equation 3.4.

$$\underset{\text{[alcohol]}}{ROH} + SO_2 + \underset{\text{[base]}}{R'N} \longrightarrow \underset{\text{[alkylsulfite salt]}}{[R'NH]SO_3R} + \underset{\text{[water]}}{H_2O} + \; + 2R'N \longrightarrow \underset{\text{[hydroiodic acid salt]}}{2[R'NH]I} + \underset{\text{[alkylsulfate salt]}}{[R'NH]SO_4R}$$

(3.4)

The reactive alcohol is usually methanol or 2-(2-Ethoxyethoxy) ethanol. The Karl Fischer reagent (base) is pyridine. During the reaction, water and iodine are consumed in a 1:1 ratio in the Bunsen reaction, and once all the water is consumed, the excess iodine is detected by an indicator electrode. The amount of water present in the sample is calculated based on the concentration of the excess iodine in the Karl Fischer titrating reagent and the amount of Karl Fischer reagent used in the titration (EMD Chemicals Inc, 2008).

During this study a Metrohm 701 KF Titrino (Herisau, Switzerland) was utilised. The instrument was calibrated with distilled water and validated using sodium tartrate dihydrate (Riedel-de Haën, Germany).

3.2 The solid state forms of mebendazole

The following section summarises the preparation of the known polymorphic and pseudo-polymorphic forms of mebendazole as described in the literature. The goal of the investigation was to determine the possibility for the preparation of a new polymorphic form of mebendazole. The known mebendazole polymorphs can be recrystallised from various solvents. Figure 3.10 provides a schematic summary with reference to the literature and solvents used for the preparation of the known mebendazole crystalline forms.

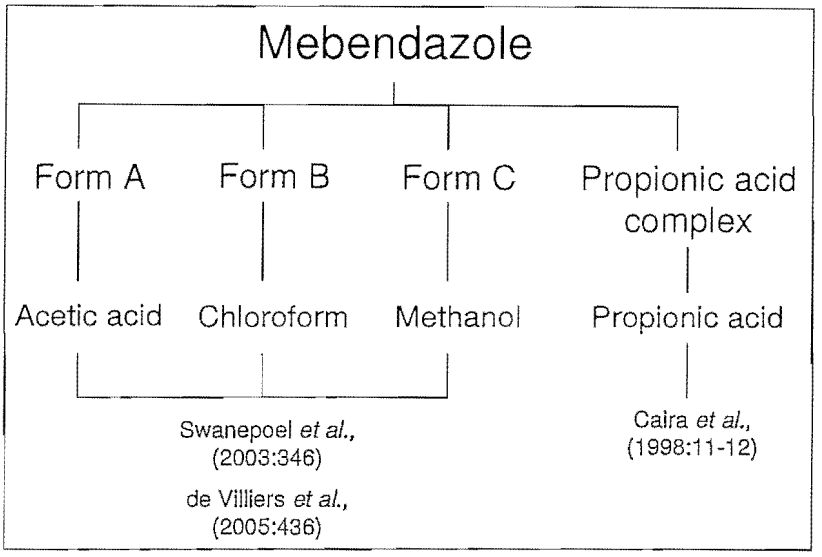

Figure 3.10 Schematic illustration of the known crystal forms of mebendazole and the corresponding solvents used for recrystallisation.

3.2.1 Recrystallisation of polymorphic forms

Mebendazole polymorphic forms (Forms A, B and C) may be prepared by evaporation of supersaturated solutions of mebendazole. Form A is obtained by recrystallisation using glacial acetic acid as solvent, Form B from chloroform and Form C from methanol (De Villiers *et al.*, 2005:436). The mebendazole propionic acid complex is recrystallised from propionic acid (Caira *et al.*, 1998:11-12). The physico-chemical properties of these crystal forms have been described in the literature as discussed in Chapter 2.

Form B and C raw materials were procured for use in this study (section 3.2.2), whilst Form A was obtained from the desolvation of the solvated forms of mebendazole (Chapter 4) using the method described by Himmelreich *et al.* (1977:124).

3.2.2 Mebendazole raw materials

Mebendazole Forms B and C raw materials where used during the study. Mebendazole USP-Form B (Batch number: MWB/M-007/2006) was purchased from Exim-Pharm International (Santacruz, Mumbai). The properties of the batch used are summarised in Table 3.2.

Table 3.2 Certificate of analysis (CoA) of mebendazole USP (Form B) used in this study

Tests	Specifications (USP30[1])	Results
Description	White to slightly yellowish powder, almost odorless	Complies
Identification	IR[2]	Complies
Heavy metals	NMT 0.002%	≤ 0.002%
Melting range	290°C	288 - 290°C
Loss of drying	NMT 0.5%	0.28%
Residue of ignition	NMT 0.1%	0.056%
Solubility	Practically insoluble in water, diluted solution of mineral acid, alcohol, ether and chloroform. Freely soluble in formic acid.	Complies
Chromatographic purity by TLC[3]	No spot other than the principle spot in the chromatogram of the test solution is larger or more intense than the principle spot obtained from the diluted standard solution	Complies
Assay (on dried basis)	98.0 – 102.0% ($C_{16}H_{13}N_3O_3$)	99.52%

[1] United States Pharmacopeia 30 – National Formulary 25

[2] Infrared spectroscopy

[3] Thin layer chromatography

Mebendazole BP - Form C (Batch number: F10958) was purchased from Rolab (South Africa). The properties of the batch used are summarised in Table 3.3.

Table 3.3 Certificate of analysis (CoA) of mebendazole BP (Form C)

Tests	Specifications (USP30[1])	Results
Description	White to slightly yellowish powder, almost odorless	Complies
Identification	IR[2]	Complies
Heavy metals	NMT 0.002%	NMT 0.002%
Loss of drying	NMT 0.5%	Complies
Residue of ignition	NMT 0.1%	Complies
Solubility	Practically insoluble in water, diluted solution of mineral acid, alcohol, ether and chloroform. Freely soluble in formic acid.	Complies
Chromatographic purity by TLC[3]	No spot other than the principle spot in the chromatogram of the test solution is larger or more intense than the principle spot obtained from the diluted standard solution	Complies
Assay (on dried basis)	98.0 – 102.0% ($C_{16}H_{13}N_3O_3$)	101.0%

[1] United States Pharmacopoeia 30 – National Formulary 25

[2] Infrared spectroscopy

3.3 Characterisation and verification of mebendazole polymorph properties

In Chapter 2 (Section 2.1.7.2) it was noted that there were inconsistencies in the literature with regards to the thermal behaviour of the polymorphic forms of mebendazole (Forms A, B and C).

Form A was prepared by heating Form C to 230°C and allowing the sample to cool down to ambient temperature as described by Himmelreich *et al.* (1977:124). Infrared analysis was performed on the sample to confirm the conversion of Form C to Form A. The presence of the main absorption bands at 3369 cm^{-1} and 1730 cm^{-1} confirmed the sample to be Form A (Figure 3.11). The XRPD pattern of the sample (Figure 3.12) was found to be concurrent with that of the data reported in the literature [Brits (2008:71) and Brusau *et al.* (2007:549)]. Thus, XRPD confirmed the DRIFT-IR data.

The XRPD patterns of mebendazole Forms A, B and C are shown in Figure 3.12.

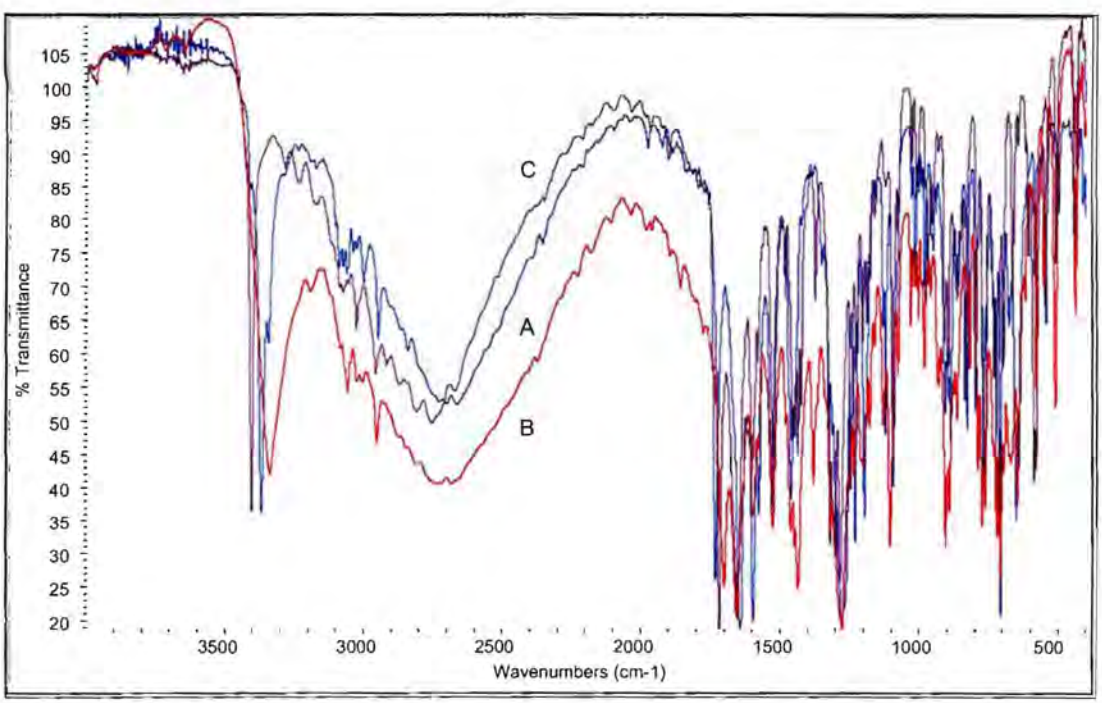

Figure 3.11 Overlay of mebendazole Form A, Form B and Form C.

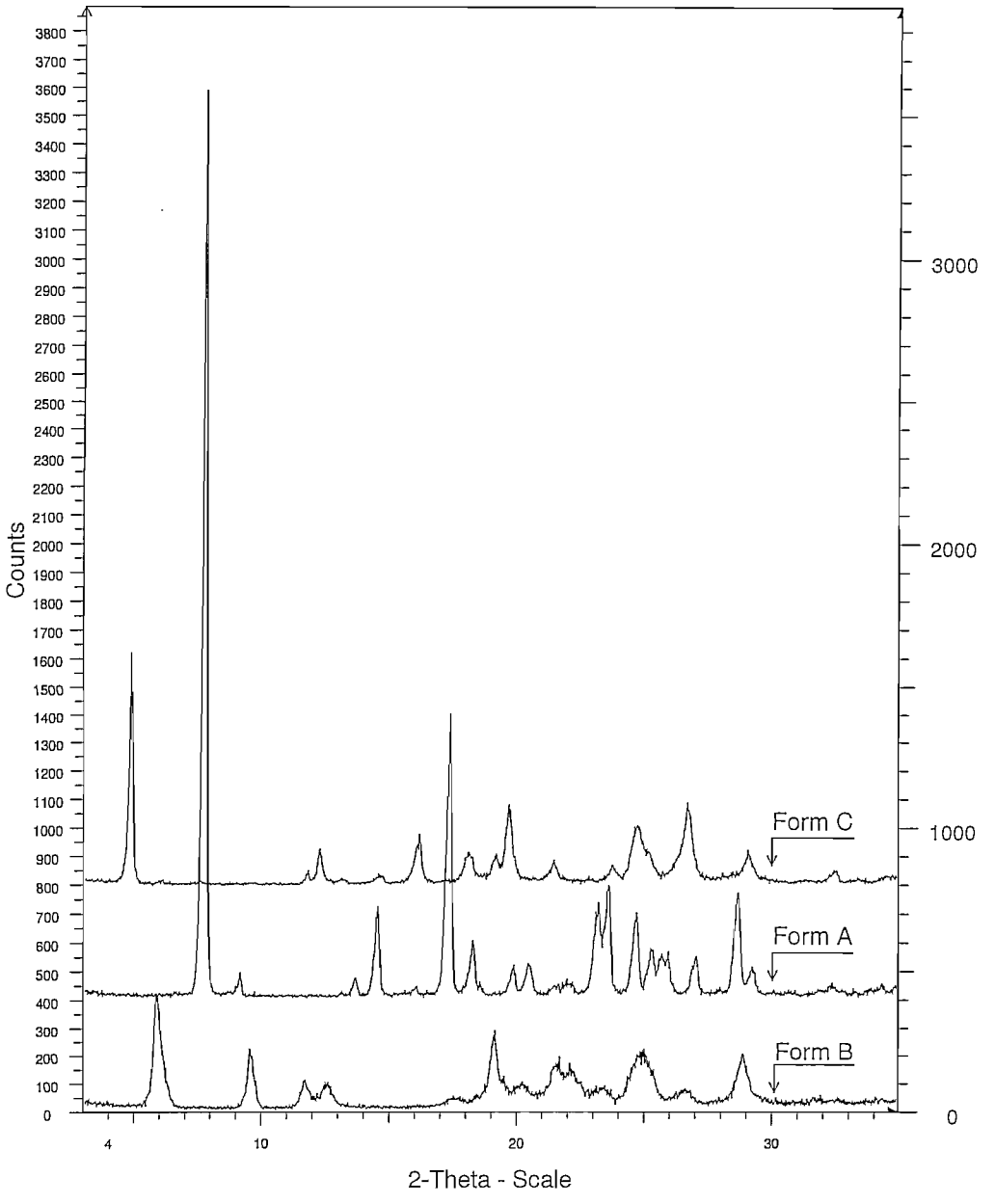

Figure 3.12 XRPD overlay of the mebendazole polymorphs.

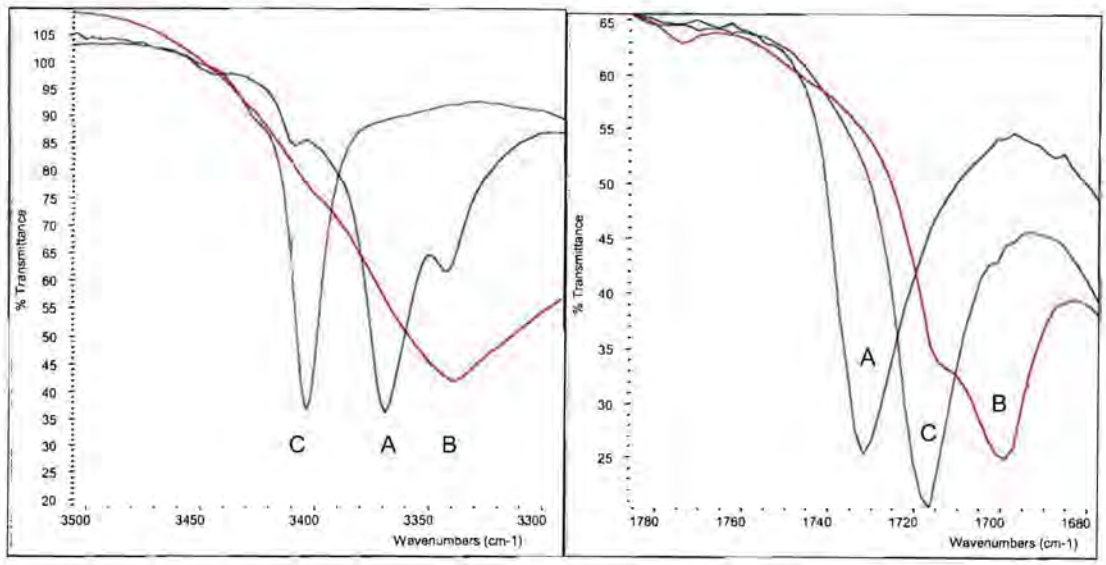

(a) (b)

Figure 3.13 Superimposed spectra of mebendazole Forms A, B and C: (a) –NH and (b) >C=O stretching frequencies of the mebendazole polymorphs.

Closer investigation of the 3370 cm^{-1} and 1730 cm^{-1} absorption bands (Figure 3.13 (a) and (b)) revealed that the spectrum of Form A contained two small shoulder peaks that could be associated with traces of Form B and C. No traces of Forms B & C were detected in the XRPD diffractograms (Figure 3.12) or in the >C=O stretch of the DRIFT-IR spectrum for Form A (Figure 3.13 (b)). The IR-absorbance of these shoulder peaks were found to be less than 0.020 and could therefore be regarded as insignificant, or as characteristic to the maxima of Form A (at 3370 cm^{-1}).

In 1977 Himmelreich *et al.* published an article on the polymorphic forms of mebendazole. According to the thermogram and related endotherms Form A consisted of two sharp endothermic events, where as Form C consisted out of three sharp endothermic events (refer to Chapter 2, Figure 2.4 and Table 2.2). De Villiers *et al.* (2005:436) later published an article containing the characterisation of the thermal behaviour of the mebendazole polymorphs (Chapter 2, section 2.1.7.2). Thus, the two sets of thermograms published showed differences.

The DSC thermograms of mebendazole Forms A, B and C were collected using the instrumental setup as described in Section 3.1.3.1. The thermal events are listed in Table 3.4 and the DSC thermograms of the polymorphic forms are shown in Figure 3.14.

Table 3.4 Thermal events characteristic to the polymorphic forms of mebendazole as determined from the DSC thermograms in this study

Forms	Thermal events (°C)			
A			253	330
B		223	249	330
C	186	235	253	330

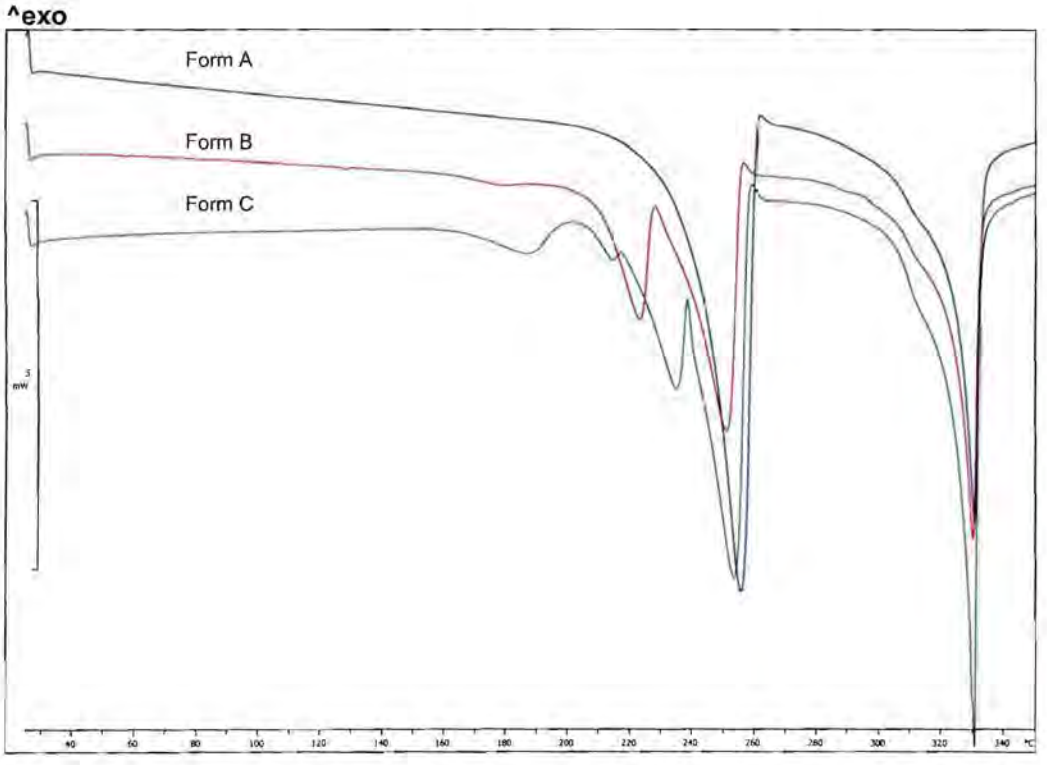

Figure 3.14 DSC thermograms of the mebendazole Forms A, B and C.

The DSC data reported in Figure 3.14 was found to be comparable to the DSC thermograms in an article recently published by Kumar *et al.* (2008:138) on the thermal behaviour of mebendazole polymorphs.

Byrn *et al.* (1999:84) stated that there are a number of factors that may influence the DSC data and cause differences in DSC thermograms of the same sample: heating rate, atmosphere, sample holder, particle size, sample packing etc. The conditions at which the DSC

thermograms of Forms A, B and C were recorded by Kumar *et al.* (2008:142) was similar to the conditions in this study.

Conclusion

The methods discussed in this chapter play an integral role in the characterisation, differentiation and ultimately the understanding of the solid-state chemistry of APIs. These techniques assist the pharmaceutical industry in the synthesis and manufacturing of APIs by providing relevant information with regards to the physico-chemical properties of the crystal forms.

From the literature study on mebendazole it was evident that there were some inconsistencies regarding the thermal behaviour of the polymorphic forms. This study revealed that those inconsistencies might have been due to the fact that the conditions (during the DSC analysis) differed. The DSC data reported for the mebendazole polymorphs was found to be comparable to the DSC thermograms in an article recently published by Kumar *et al.* (2008:138) on the thermal behaviour of mebendazole polymorphs.

The techniques and equipment discussed in this chapter were used in the chapters to follow, to investigate the solid-state properties of the solvated crystal forms of mebendazole.

CHAPTER 4

Characterisation of mebendazole solvated forms

Introduction

During the manufacturing of an API and the specific dosage forms thereof, it is important to ensure that the desired crystal form is obtained and maintained to prevent undesired polymorphic conversions. For the validation of the manufacturing process it is important to understand the physico-chemical properties and crystalline behaviour of the API (Hilfiker, 2007:3). During the manufacturing process of dosage forms, APIs are exposed to solvents or solvent vapors, either through precipitation, wet granulation, spray-drying, lyophilisation, crystallisation or recrystallisation from a suitable solvent or mixture of solvents, that may cause solvent inclusion or phase transformations of the crystalline solid. Solvents may be associated with the API in different ways, i.e. (1) binding of solvent molecules to the surface of the API by weak interactions (van der Waals, hydrogen bonding, etc.), (2) entrapped in growing crystals (solvent inclusion), (3) absorbed in disordered regions of the crystalline solid or (4) dissolved into the highly energetic metastable areas of the crystalline solid (Griesser, 2007:211). Figure 4.1 illustrates the potential mechanisms of solvent association with crystalline solids.

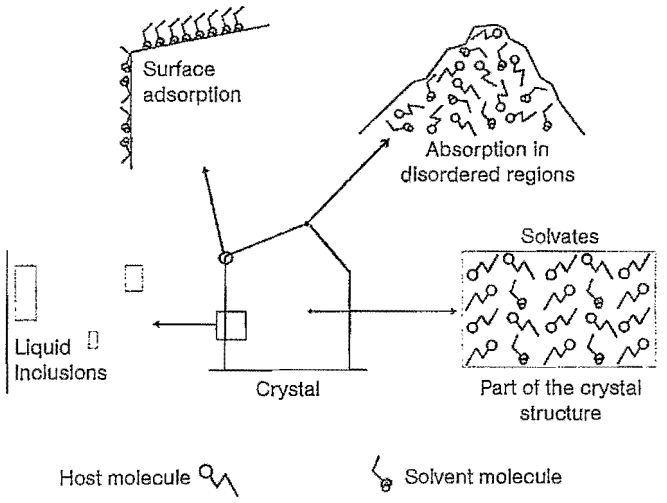

Figure 4.1 Illustration of the different mechanisms by which a solvent may associate with crystalline solids (Griesser, 2007:212).

4.1 New pseudo-polymorph (solvate) of mebendazole

During the study of the solid-state properties of mebendazole, a new pseudopolymorph (Acetic acid solvate – Form D) was recrystallised and characterised using the techniques and methods discussed in Chapter 3. The mebendazole propionic acid complex (hereafter referred to as Form E) discovered by Caira *et al.* (1998:11-15) was also further characterised. Dissolution-, stability- and kinetic studies performed on Forms D and E are discussed in the following chapters.

4.2 Preparation of mebendazole solvated forms

The acetic acid solvate (Form D) was prepared by recrystallisation of mebendazole raw material in a glass beaker using glacial acetic acid (analytical grade) as solvent. The solution was heated to approximately 110°C in a fume hood under continues stirring, using a Heidolph MR300K (Heidolph, Germany) magnetic stirrer. Small quantities of solvent were added to the solution to ensure that all the raw material had dissolved, resulting in a supersaturated solution. The supersaturated solution was then removed from the heat source and covered using Parafilm® (Pechiney® plastic packing, Chicago IL, USA). Small holes were pierced in the Parafilm® (Pechiney® plastic packing, Chicago IL, USA) to allow the solvent to evaporate from the solution. Rapid recrystallisation was then induced by cooling the solution in an ice bath. Small quantities of acetone were poured over the ice to allow the temperature to decrease. The sample was kept in the ice bath for at least 12 hours before it was removed and filtered. The crystals were then carefully spread out over filtration paper, to allow residual solvent to evaporate at ambient conditions.

The mebendazole propionic acid solvate (Form E) was prepared using the same method as described for the acetic acid solvate (Form D). The only difference being propionic acid was used as the recrystallisation solvent. Caira *et al.* (1998:12) initially prepared a solution of the mebendazole propionic solvate by dissolving 50 mg of mebendazole in 8 ml of propionic acid, stirred for 25 minutes at 56°C and left to crystallize for 6 months. Contrary to the method described in the literature for the preparation of Form E (slow and low yield), this method provided a fast means for the preparation of Form E that provided a greater yield.

4.3 Characterisation of the solvated forms of mebendazole

The solvated forms prepared (i.e. Form D and Form E) were characterised using the following techniques: DRIFT-IR, XRPD, DSC, TGA, HSM, SEM and KF. The thermodynamic stability of the solvated forms were also investigated using VT-XRPD.

4.3.1 Diffuse reflectance infrared Fourier transform spectroscopy (DRIFTS)

The infrared (DRIFT-IR) spectra of the two solvates are shown in Figure 4.2 and Figure 4.3 respectively. The two spectra showed similarities (Figure 4.4). A closer investigation of the -NH stretching frequency and >C=O stretching frequency revealed remarkable differences between the two solvated forms (Figure 4.4 (b) and (c)). The acetic acid solvate (Form D) showed unique absorption bands at 3352 cm^{-1} and 1737 cm^{-1}, where as the propionic acid solvate (Form E) showed unique absorption bands at 3364 cm^{-1} and 1735 cm^{-1}. No traces of Forms A, B or C were detected (refer to Figure 4.5). The absorption peaks of the solvated forms of mebendazole are listed in Table 4.1.

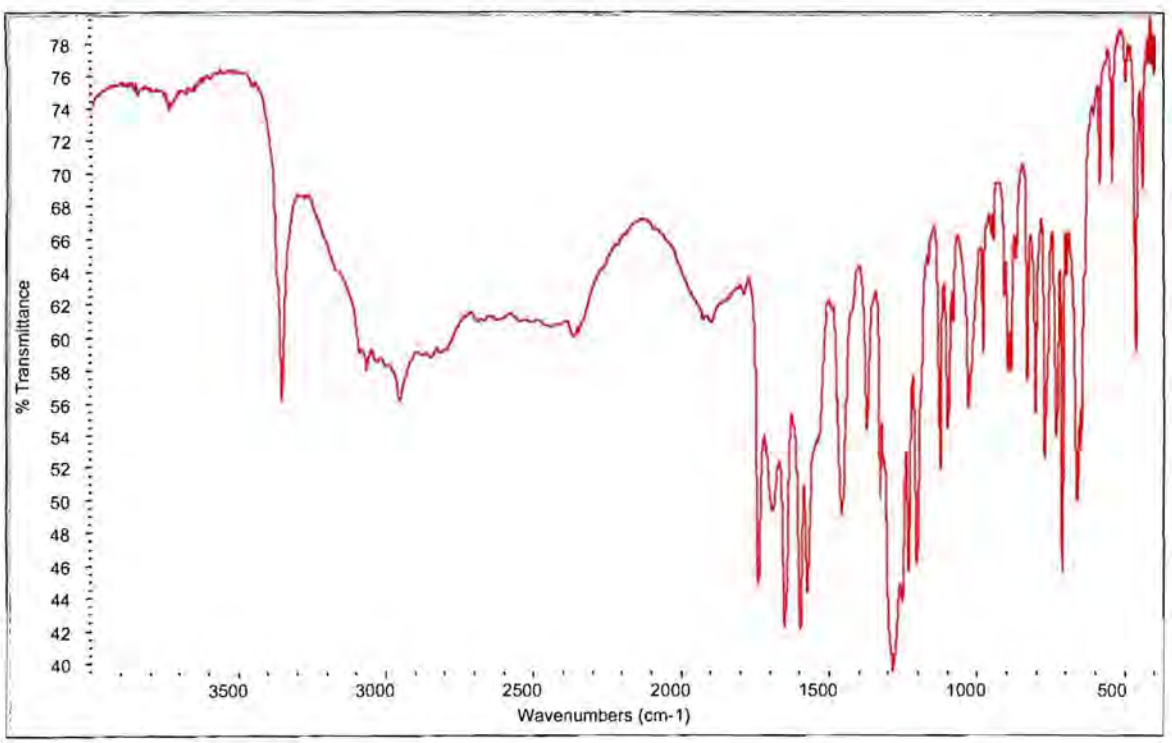

Figure 4.2 IR spectrum of the mebendazole acetic acid solvate (Form D).

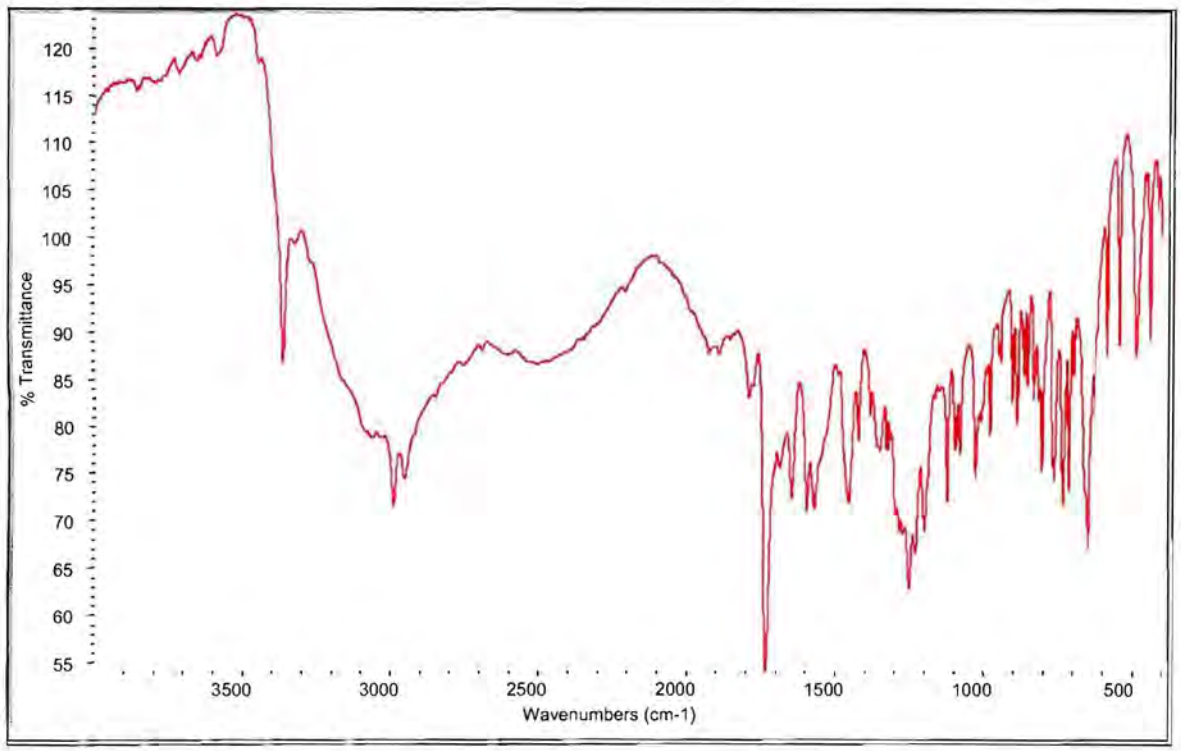

Figure 4.3 IR spectrum of the mebendazole propionic acid solvate (Form E).

A comparative investigation of the DRIFT-IR spectra of Form D and Form E with that of the polymorphic forms of mebendazole (Forms A, B and C), revealed that the absorption bands of Form D and Form E differed from the –NH stretching and >C=O stretching frequencies (Figure 4.5) of the known polymorphic forms, as reported in Chapter 2.

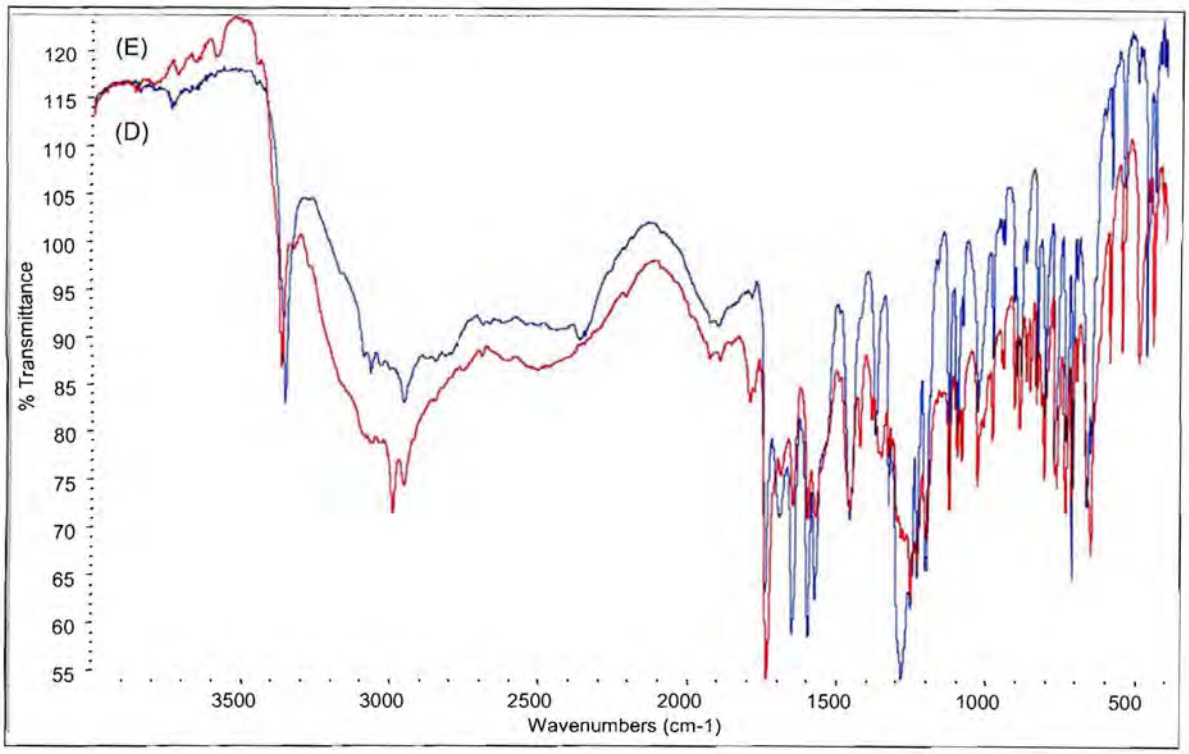

(a)

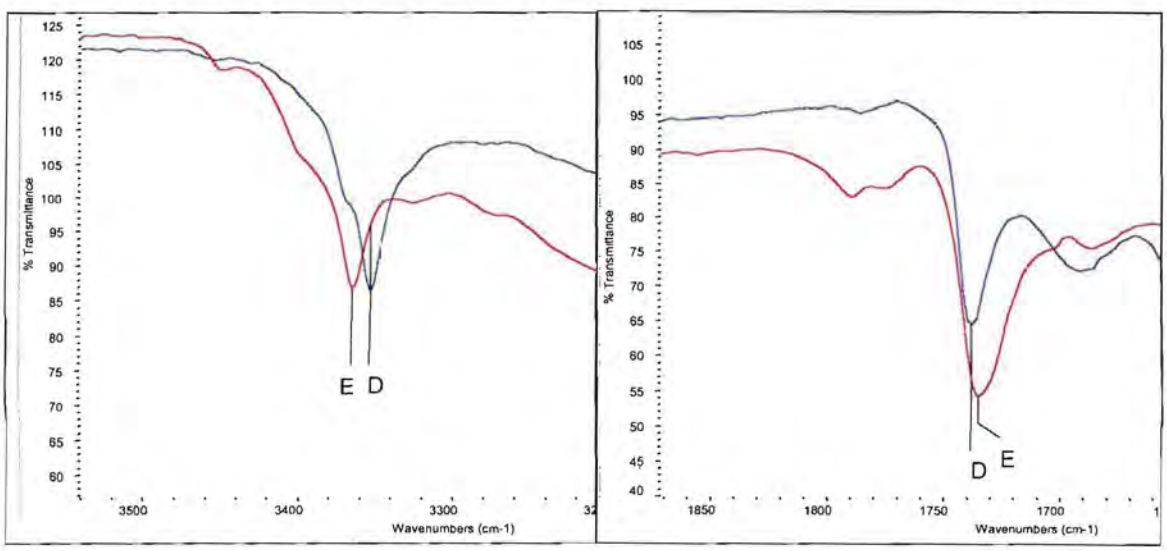

(b) (c)

Figure 4.4 (a) Overlay of mebendazole solvated forms (Form D and Form E) (b) –NH and (c) >C=O stretching frequencies of the mebendazole Form D and Form E.

Table 4.1 Main absorption peaks in the infrared spectra of the two solvated forms of mebendazole

Mebendazole acetic acid solvate (Form D)	Mebendazole propionic acid solvate (Form E)
Wavenumbers (cm^{-1})	Wavenumbers (cm^{-1})
3353 *	3364 *
2953	2989
2362	2953
1898	2503
1738 *	1892
1691	1789
1648	1735 *
1596	1686
1571	1645
1455	1595
1369	1570
1325	1452
1282 *	1420
1228	1381
1200	1348
1121	1326
1095	1249
1077	1228
1025	1198
977	1121
942	1093
904 *	1078
892	1024
882	977
827	942
801	902 *
768	884
728	863
708	850
693	829
659	802
646 *	759
584	729
540	710
495	694
461	646 *
439	585
418	542
407	486
-	440
-	413

* Main identification peaks

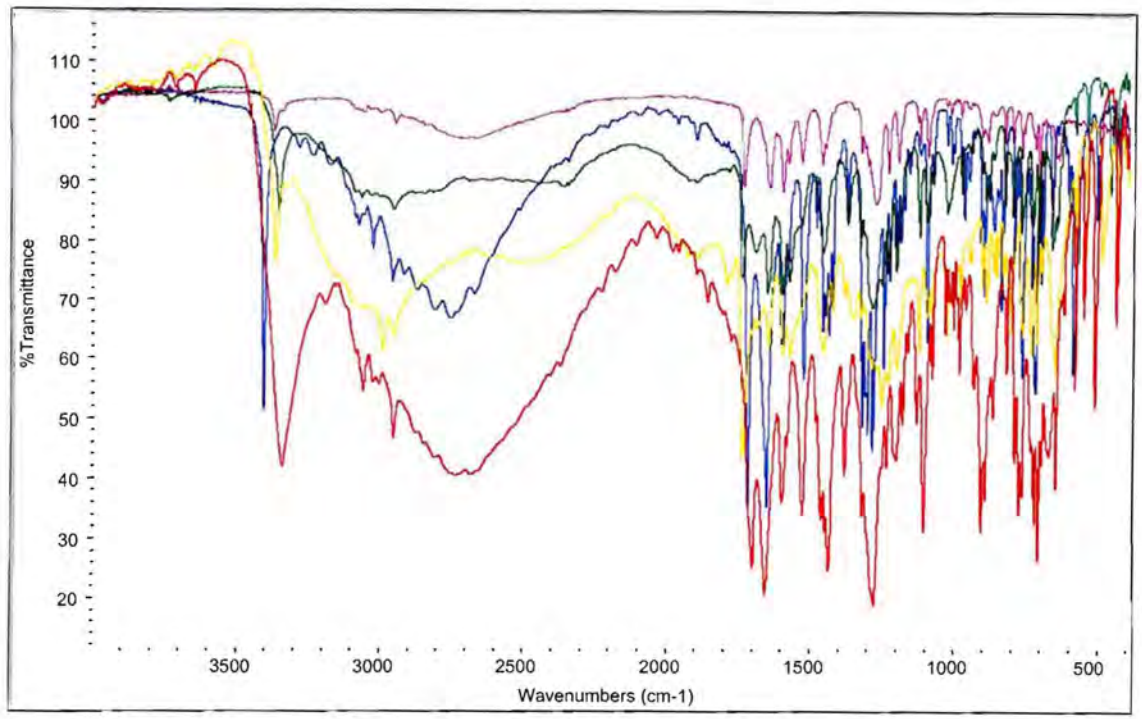

(a)

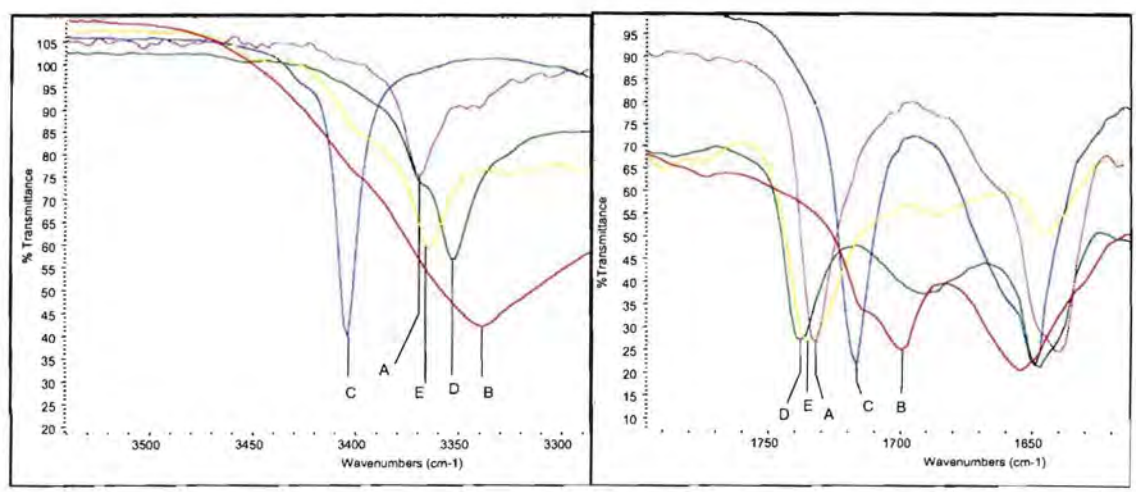

(b) (c)

Figure 4.5 (a) IR overlay spectra of the solid states of mebendazole (Forms A, B, C, D and E). (b) –NH and (c) >C=O stretching frequencies illustrating the differences between the absorption peaks of the mebendazole solid states.

4.3.2 X-ray powder diffraction (XRPD)

The XRPD patterns of the two solvated forms of mebendazole are shown in Figure 4.6 and Figure 4.7 respectively.

In an overlay of the diffractograms of Form D and Form E (Figure 4.8), similarities and small differences in diffraction patterns became visible. The main diffraction peaks used in the identification of mebendazole acetic acid solvate (Form D) and propionic acid solvate (Form E) are listed in Table 4.2 together with the characteristic (°2θ) diffraction angles of the known polymorphic forms. The diffraction angles (°2θ) and corresponding relative intensities (I/I_0) from the XRPD patterns of the two solvates are listed in Table 4.3.

Single electron microscopy (SEM) revealed that both solvated forms exhibited needle-like crystal habits that could lead to preferred orientation of the crystals during XRPD analysis (refer to section 4.3.5). Preferred orientation is one of the most pervasive problems in crystallography that influences the intensity values of powder diffraction peaks due to the tendency of non-spherical crystalline habits to become orientated and to occupy only a minimum volume (Bernstein, 2002:117). To limit the effect of preferred orientation, the size of the crystals were reduced by careful grinding and rotation of the samples during the collection of the XRPD patterns (Byrn *et al.*, 1999:63).

Table 4.2 Main diffraction peaks (°2θ) used in the identification of the mebendazole polymorphic and pseudo-polymorphic forms (adapted from Brits, 2008:70)

Polymorph A	Polymorph B	Polymorph C	Polymorph D	Polymorph E
7.6	5.8	4.9	6.6 7.9 13.2	6.3 8.0 12.6

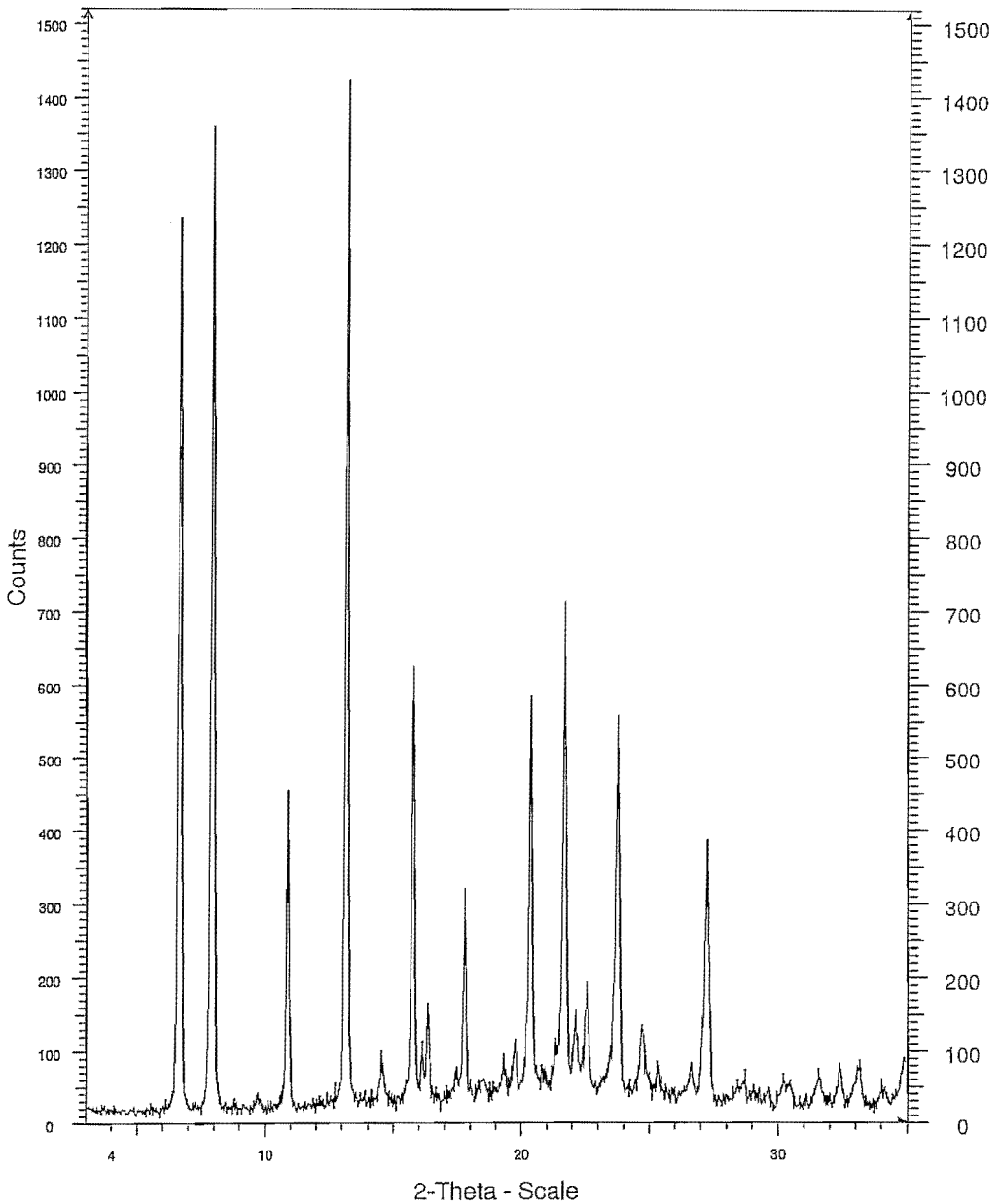

Figure 4.6 XRP diffractogram of the mebendazole acetic acid solvate (Form D).

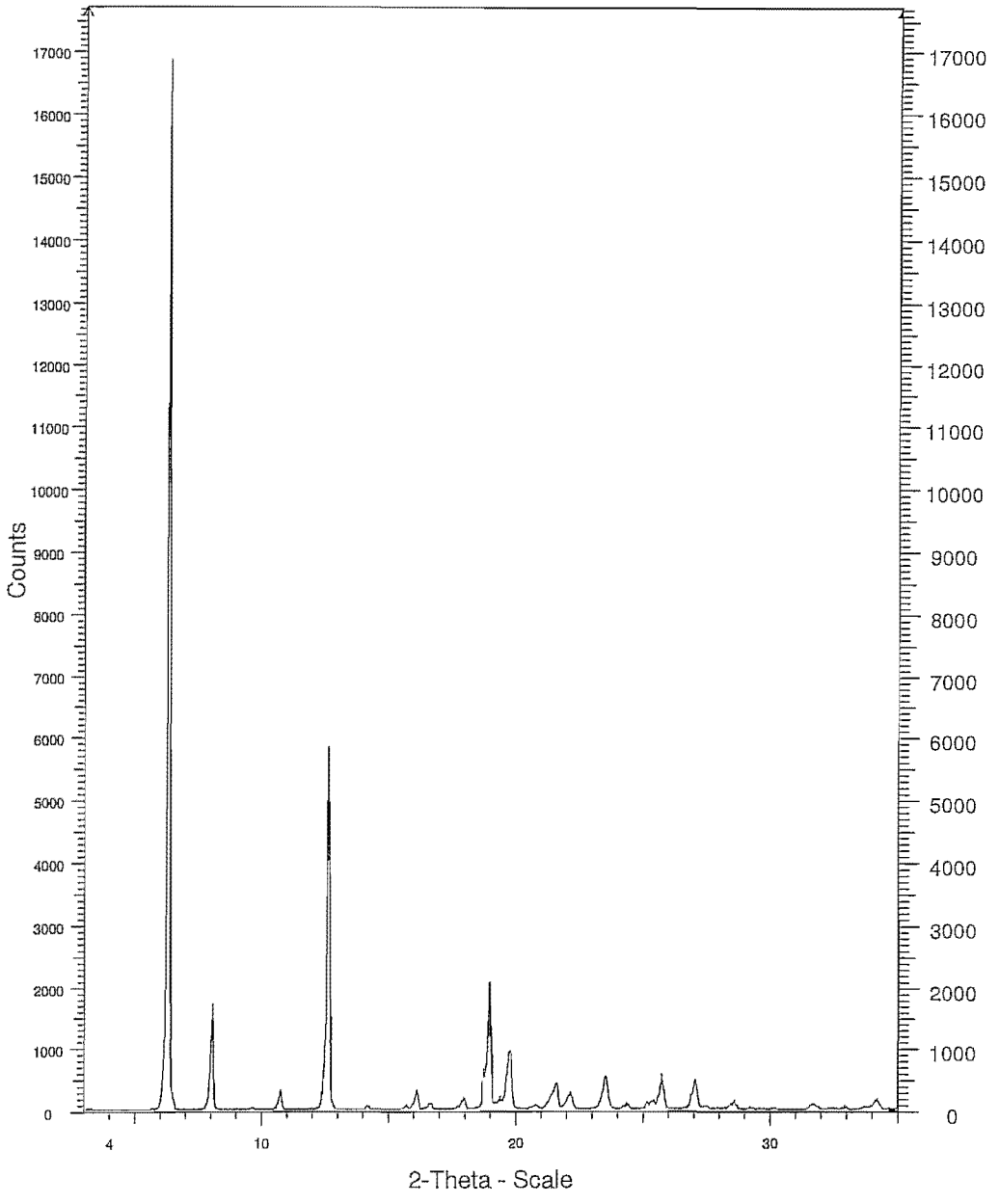

Figure 4.7 XRP diffractogram of the mebendazole propionic acid solvate (Form E).

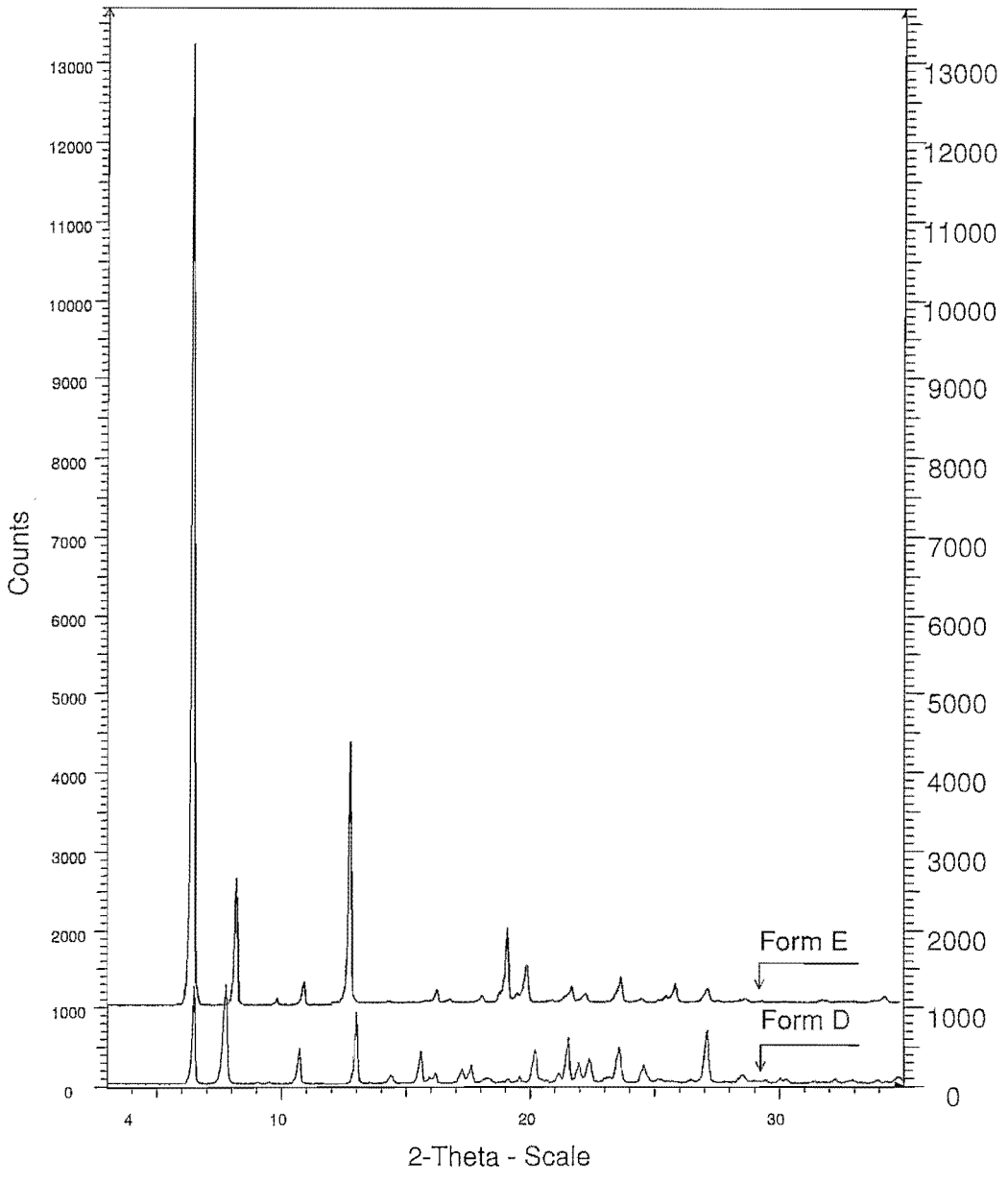

Figure 4.8 XRPD overlay of the mebendazole Form D and Form E.

Table 4.3 Diffraction angles (°2θ) and corresponding relative intensities (I/I_0) of the XRPD peaks of mebendazole Form D and Form E

Mebendazole acetic acid solvate (Form D)		Mebendazole propionic acid solvate (Form E)	
Position (°2θ)	Intensity (I/I_0)	Position (°2θ)	Intensity (I/I_0)
6.62*	86.7	6.27*	100.0
7.93*	95.4	8.00*	10.1
9.70	2.8	9.62	0.2
10.86	31.8	10.71	1.9
-	-	12.59*	34.6
13.17*	100.0	-	-
14.54	6.9	14.15	0.4
15.76	43.7	15.70	0.5
16.12	7.9	16.10	1.8
16.35	11.4	16.63	0.7
17.47	5.3	-	
17.78	22.3	17.73	3.9
18.51	4.1	18.95	12.2
19.32	6.5	-	-
19.77	8.0	19.76	5.5
20.39	40.9	20.78	0.5
21.72	49.9	21.59	2.5
22.14	10.7	22.14	1.7
22.57	13.4	-	-
23.79	39.0	23.54	3.2
24.75	9.3	24.38	0.7
-	-	25.20	0.8
25.34	5.8	25.38	0.9
-	-	25.77	3.3
26.67	5.7	-	-
-	-	27.07	2..8
27.29	26.9	27.50	0.4
28.73	3.9	28.61	0.9
29.65	3.3	29.26	0.3
30.27	4.6	30.20	0.2
30.50	3.9	-	-
31.64	5.1	31.72	0.6
32.45	5.6	32.47	0.2
33.17	5.1	33.01	0.4
-	-	33.80	0.3
34.11	4.1	34.22	1.1

* Main characteristic peaks

An overlay of the mebendazole polymorphs (Forms A, B and C) and pseudo-polymorphs (Form D and Form E) are shown in Figure 4.9 to illustrate the differences between the polymorphic and pseudo-polymorphic forms.

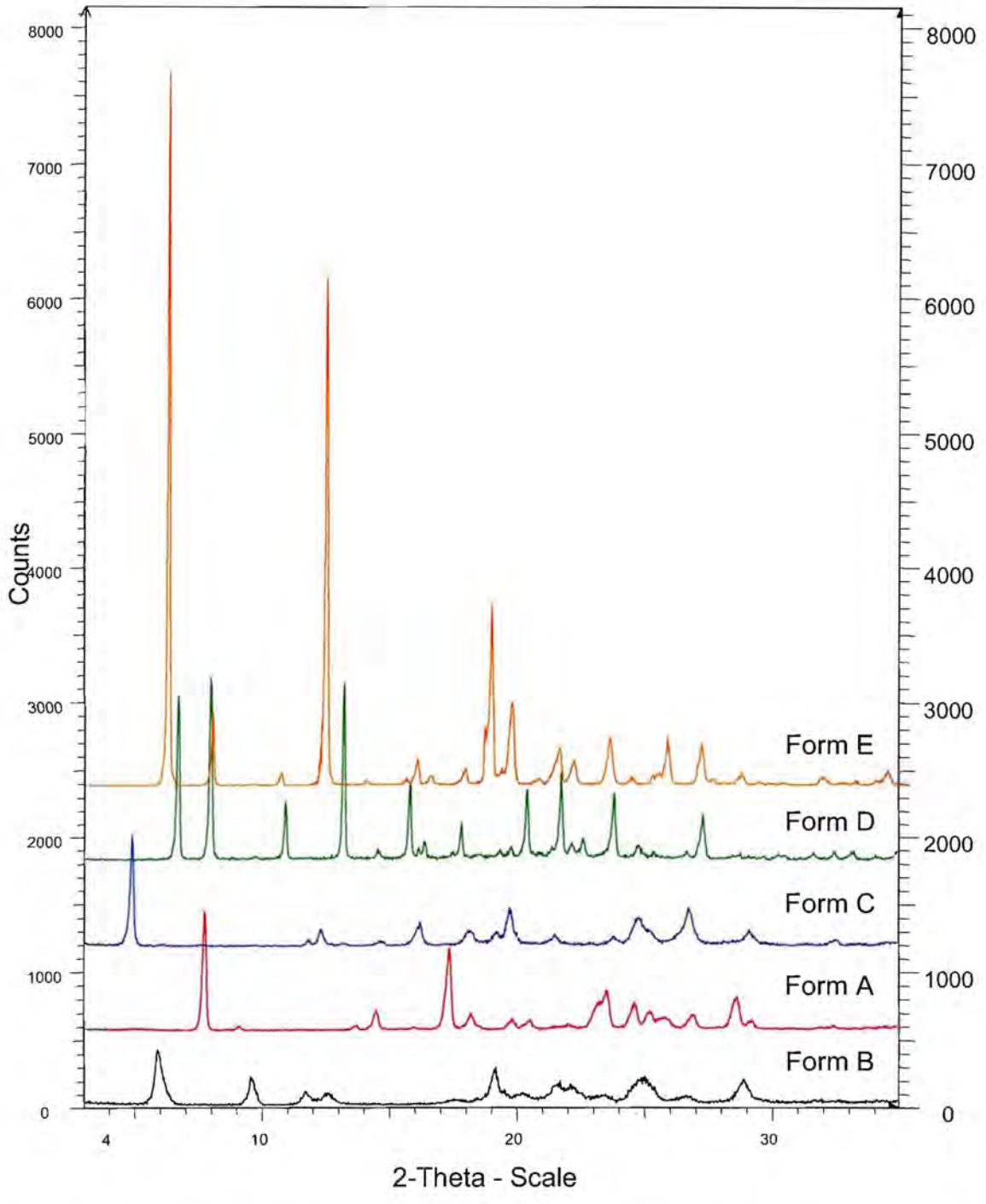

Figure 4.9 XRPD overlay of mebendazole polymorphs (Forms A, B and C) and pseudo-polymorphs (Forms D and E).

When comparing the XRPD patterns of the two solvated forms of mebendazole (Figure 4.10) it was observed that the peaks were very similar as far as the main peak positions, but that there were discrepancies between the weaker peaks of the two XRPD patterns. The acetic acid solvate (Form D) showed a slight shift in the peaks between the regions of 5-9±0.1 °2θ with the addition of extra peaks at 16.3±0.1 °2θ, 17-18±0.1 °2θ and 22.1±0.1 °2θ and the absence of peaks at 9.6±0.1 °2θ, 19.0±0.1 °2θ and 25.8±0.1 °2θ when compared to the XRPD pattern of the propionic acid solvate (Form E). Although the two solvated forms did show resemblances in the main peak patterns, they can not be considered as the same iso-structural pseudo-polymorphs.

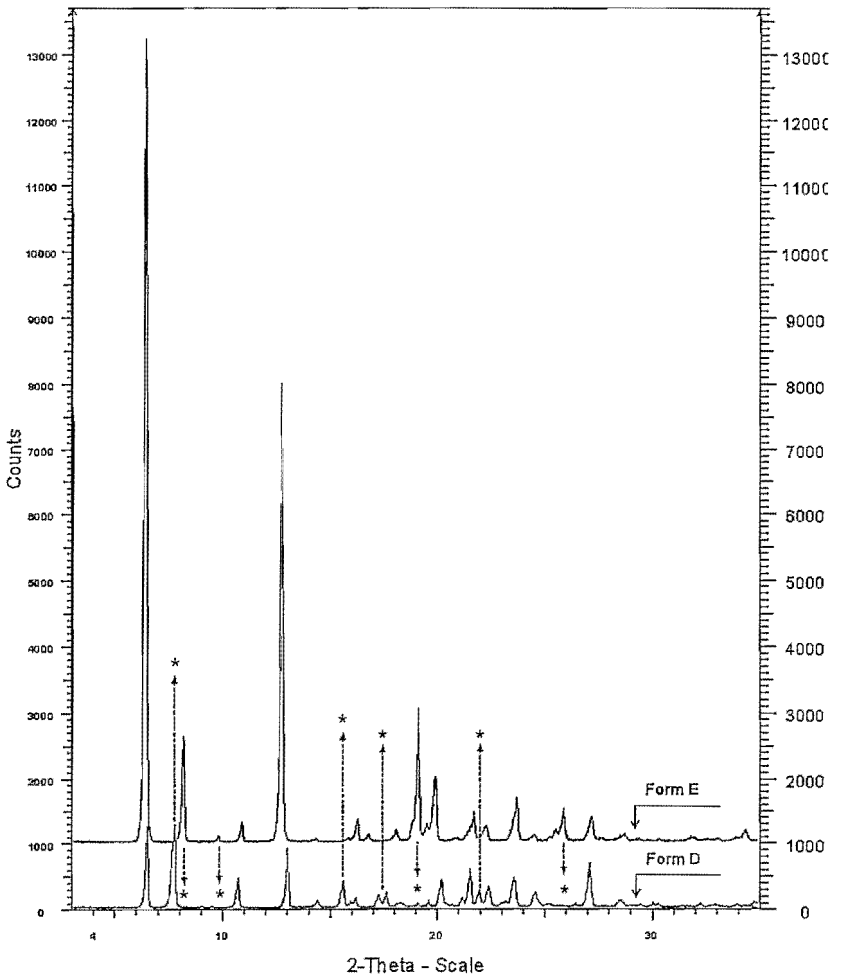

(* - indicates significant differences in peak angular positions between the two solvates)

Figure 4.10 XRPD overlay of Form D and Form E.

The XRPD pattern of the mebendazole propionic acid solvate (Form E) prepared in this study was found to be comparable to the theoretically derived XRD pattern from the single crystal x-ray data reported and produced by Caira *et al.* (1998:14), as illustrated in Figure 4.11 (refer to Chapter 2, section 2.1.7.3). Differences between the two patterns are observed in terms of relative intensity values of the unique characteristic peaks. These differences in resolution and relative intensity values may be attributed to preferred orientation of the crystals and to the fact that the theoretically derived pattern was derived from single-crystal data which provided more information with regards to all crystal planes in the crystal structure.

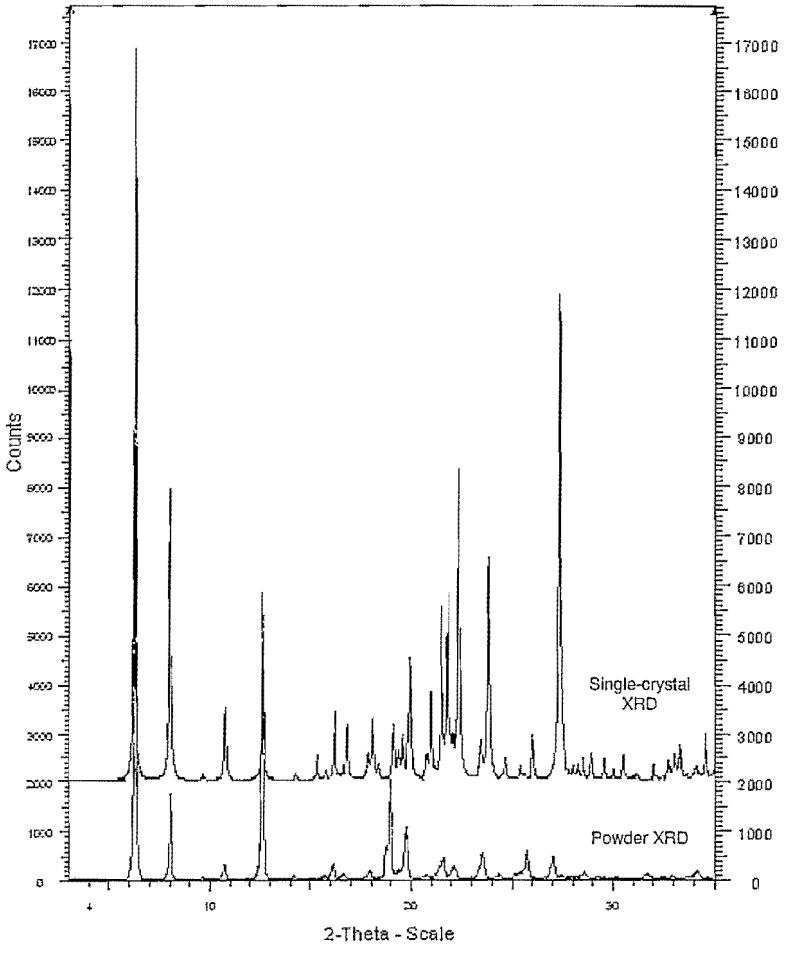

Figure 4.11 Overlay of the theoretical XRD pattern derived from the single-crystal data published by Caira *et al.* (1998:14) and x-ray powder diffractogram of the mebendazole propionic acid solvate (Form E). Crystallographic data of the mebendazole propionic complex was requested from the Cambridge Crystallographic Data Centre, CCDC-1003/5265 (CCDC, 12 Union Road, Cambridge CB2 1EZ, UK).

4.3.3 Thermal analysis

The thermal properties of the two solvated forms where investigated using differential scanning calorimetry (DSC), thermogravimetric analysis (TGA) and hot-stage microscopy (HSM).

The DSC thermogram (Figure 4.12) of the mebendazole acetic acid solvate (Form D) exhibited three sharply defined endothermic events at 109°C, 256°C and 331°C. Himmelreich *et al.* (1977:123-124) reported mebendazole to melt at a temperature above 270°C, followed by decomposition of the sample (refer to section 2.1.7.2). The decomposition of mebendazole above 320°C was verified by TLC (section 4.3.7). The endothermic event at 109°C was evident of desolvation (boiling point of acetic acid is 118°C).

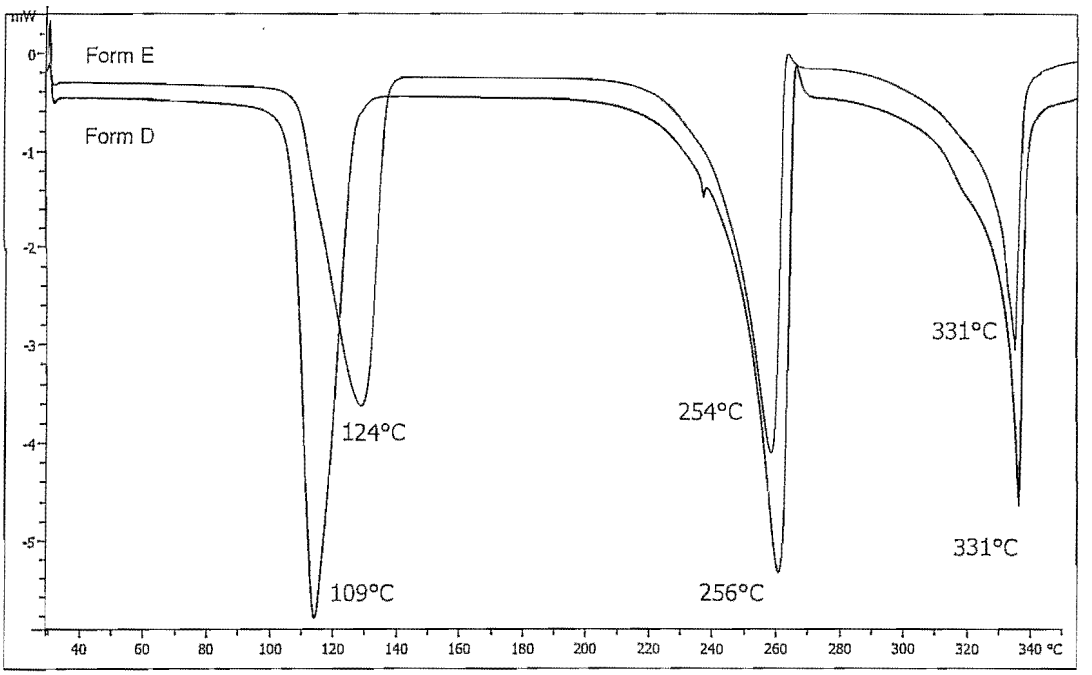

Figure 4.12 DSC thermograms of mebendazole acetic acid solvate (Form D) and propionic acid solvate (Form E).

The DSC thermogram (Figure 4.12) of the mebendazole propionic acid solvate (Form E) also exhibited three sharply defined endothermic events at 124°C, 254°C and 331°C. The endothermic event at 124°C was evident of desolvation (boiling point of propionic acid is 141°C). The desolvation of both solvated forms were verified by hot-stage microscopy (HSM) (Section 4.3.4) and TGA analysis. The thermal events in the two DSC thermograms of the solvated forms of mebendazole are summarised in Table 4.4

Table 4.4 Summary of the thermal events of the two solvated forms of mebendazole

Solvated form	Desolvation endotherm (°C)	Thermal endotherm (°C)	Thermal endotherm (°C)
Form D	109	256	331
Form E	124	254	331

The TGA thermogram (Figure 4.13) of the mebendazole acetic acid solvate (Form D) showed a one-step mass loss of 15.40% in the temperature range 100-150°C (theoretical mass loss of 17.00%, calculated using Equation 4.1) confirming the possibility of a 1:1 mebendazole-acetic acid complex. The TGA thermogram (Figure 4.13) of the mebendazole propionic acid solvate (Form E) showed a two-step mass loss of 10.01% and 20.76% respectively. The theoretical mass loss calculated for the propionic acid solvate was 20.05% using Equation 4.1.

$$\%\ Weight\ loss = \frac{Molecular\ weight\ (solvent)}{Molecular\ weight\quad (solvent) + Molecular\ weight\ (API)} \times 100\% \quad (4.1)$$

Caira *et al.* (1998:12) reported the mass loss of the mebendazole-propionic complex (Form E) to be a one-step process of 19.85% in the temperature range of 100-150°C. Unfortunately no data was published on the composition and nature of the mass loss detected by TGA analysis in the temperature range of 25-100°C. The TGA thermogram for the mebendazole propionic acid solvate (Form E) showed a significant mass loss of 10.01% in the temperature range of 25-100°C. Karl Fischer (KF) analysis using the techniques described in Chapter 3 (section 3.1.5) was utilised to determine if the % mass loss in the temperature range of 25-100°C was due to water absorption by the sample or solvent adsorbed onto the surface of the crystal structure (refer to Figure 4.1). The KF results indicated that the sample contained 0.40% (m/m) water which was too low for the % mass loss (determined as 10.01%) detected in the 25-100°C temperature region of Form E, hence the change in mass in this region may be attributed to solvent adsorbed onto the surface of the crystals.

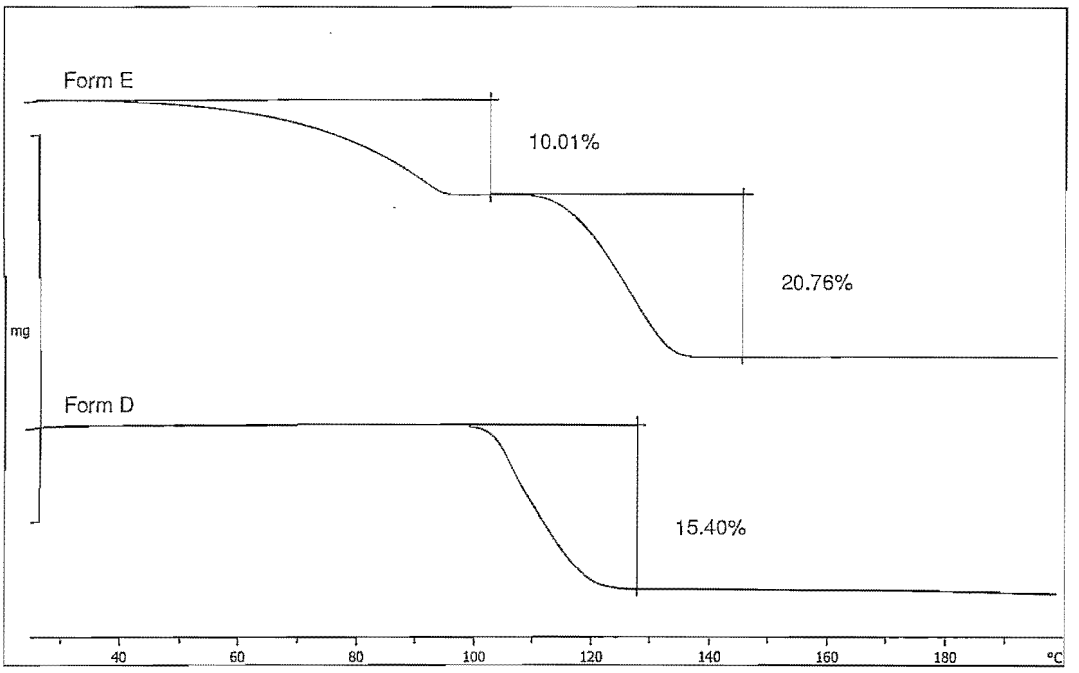

Figure 4.13 TGA thermograms of Form D and Form E.

It was noted that the first-step on the TGA of Form E varied in % mass loss throughout this study (individual sample preparations), indicating possible adsorbed solvent on the external crystal structure or changes in sample vapour pressure. The onset and end set temperatures for the desolvation endotherm of Form E was found to be at 100-150°C, which were concurrent to the onset and end set temperatures of the TGA thermogram. No thermal events were detected in the DSC thermogram of Form E (Figure 4.12) in the range 40-100°C, therefore supporting the observation that the first mass-loss step was due to surface adsorbed solvent.

4.3.4 Polarising optical and hot-stage microscopy (HSM)

Polarising optical microscopy revealed the needle-like crystal habits of both solvated forms of mebendazole. Changes were observed in the birefringes of the crystals (Table 4.5 and Table 4.6). Hot-stage microscopy (HSM) confirmed the desolvation process (as identified in the DSC and TGA results) of the crystals when submerged in silicon oil and subjected to increased temperatures. According to Bernstein (2002:98), the initial turbidity appearance within the crystals or formation of bubbles (sample covered with silicon oil) upon heating of the API could be considered a sign of desolvation and the entrapped solvent being forced out of the crystalline structure. Table 4.5 and Table 4.6 illustrate the desolvation process of the two solvated forms of mebendazole using HSM.

Table 4.5 Photomicrographs obtained with polarising optical and hot-stage microscopy of the mebendazole acetic acid solvate (Form D)

Mebendazole acetic acid solvate (Form D)		
Photomicrograph	**Technique and temperature**	**Remarks**
	Optical microscopy (25°C)	Initial photomicrograph showed a dense dark mass, but on closer examination a small change in the birefringence of polarised light was visible.
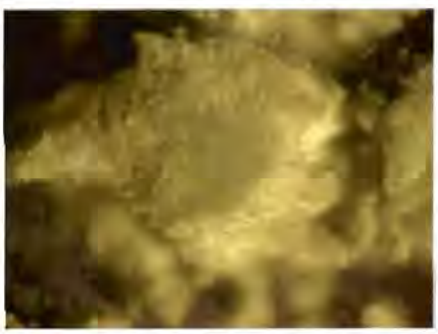	Optical microscopy (25°C) with external lighting	Fine needle-like crystalline habits were observed in the sample. Crystals appeared yellow due to external lighting.
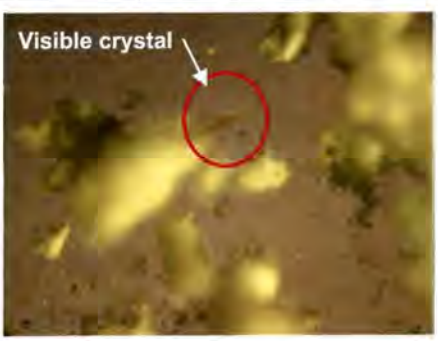	Optical microscopy (25°C) with external lighting	Differences in crystal sizes were observed in the sample mass. Changes in the birefringence of light were observed in the larger crystals.
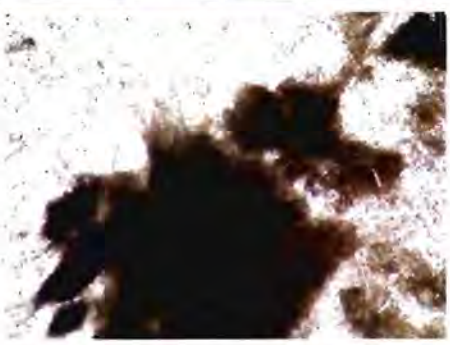	Hot-stage microscopy (23°C) (with silicon oil)	A dark sample mass was observed under the microscope.

Table 4.5 (continued)

Mebendazole acetic acid solvate (Form D)		
Photomicrograph	**Technique and temperature**	**Remarks**
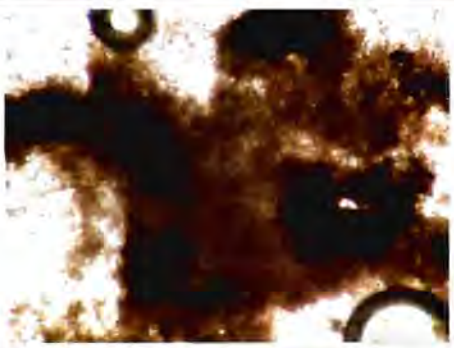	Hot-stage microscopy (100-154°C) (with silicon oil)	Bubbles started to appear, indicative of desolvation. Desolvation of the sample continued. No visible change in the appearance of the sample was detected.

Table 4.6 Photomicrographs obtained with polarising optical and hot-stage microscopy of the mebendazole propionic acid solvate (Form E)

Mebendazole propionic acid solvate (Form E)		
Photomicrograph	**Technique and temperature**	**Remarks**
	Optical microscopy (25°C)	Crystals appeared dark and had needle-like crystal habits.
	Polarising optical microscopy (25°C)	Visible changes in the crystal colour were detected (due to birefringence of polarised light).
	Hot-stage microscopy (19°C) combined with optical microscopy	Crystals appeared colourless to dark and had definite needle-like crystalline habits.

Table 4.6 (continued)

Mebendazole propionic acid solvate (Form E)		
Photomicrograph	**Technique and temperature**	**Remarks**
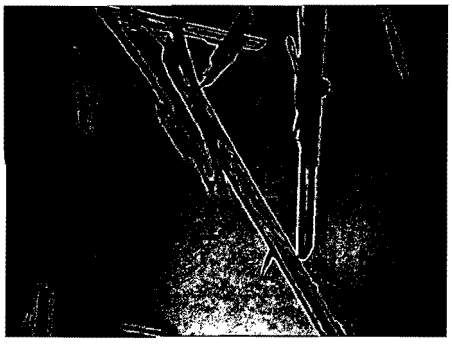	Hot-stage microscopy (127°C) combined with optical microscopy	No desolvation was detected in the crystals between 40° - 100°C. Crystals became darker as desolvation occurred.
	Hot-stage microscopy (131°C) combined with optical microscopy	Desolvation of crystals continued.
	Hot-stage microscopy (135°C) combined with optical microscopy	Desolvation was almost complete. Crystals appeared dark.
	Hot-stage microscopy (138°C) combined with optical microscopy	Crystals were black. Desolvation process complete.

Table 4.6 (continued)

Mebendazole propionic acid solvate (Form E)		
Photomicrograph	**Technique and temperature**	**Remarks**
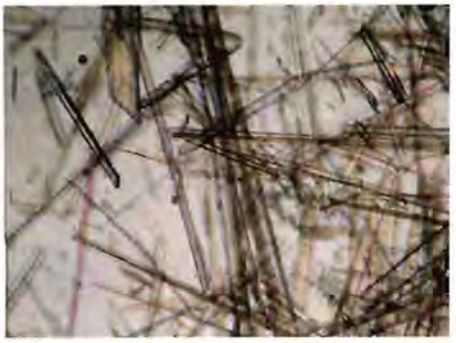	Hot-stage microscopy (16°C) combined with optical microscopy (With silicon oil)	Crystals had a needle-like crystalline habit. Visible changes in crystal colour were detected (due to birefringence of polarised light).
	Hot-stage microscopy (120°C) combined with optical microscopy (With silicon oil)	Desolvation bubbles appeared.
	Hot-stage microscopy (132°C) combined with optical microscopy (With silicon oil)	Desolvation bubbles almost covering whole area.
	Hot-stage microscopy (159°C) combined with optical microscopy (With silicon oil)	Desolvation process complete. Crystals appeared dark. No further changes in the crystalline sample were visible.

4.3.5 Scanning electron microscopy (SEM)

Scanning electron microscopy (SEM) was used to investigate and compare the morphology of the two solvated forms of mebendazole (Table 4.7). Both the mebendazole acetic acid solvate (Form D) and mebendazole propionic acid solvate (Form E) exhibited needle-like shapes with acicular crystalline habits. SEM photomicrographs were also taken for mebendazole Forms A, B and C. No SEM photomicrographs of the mebendazole polymorphs were available in the literature.

Table 4.7 Scanning electron microscopy photomicrographs of the mebendazole polymorphs and pseudo-polymorphs

SEM photomicrograph	Crystal form
	Form A Form A exhibited non-uniform dispersed crystals with larger needle-like crystals.
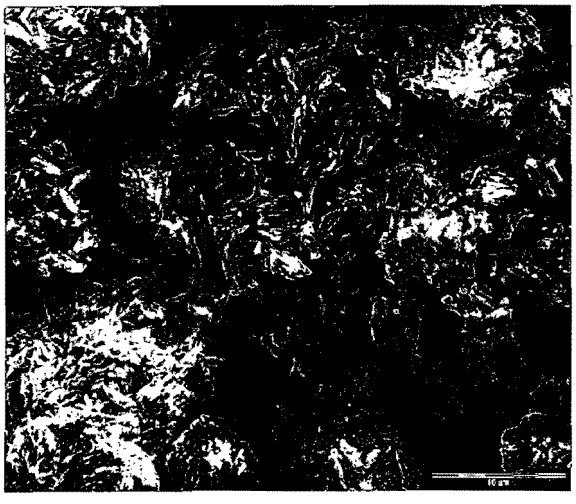	Form B Form B exhibited non-uniform needle-like crystals which agglomerated.

Table 4.7 (continued)

SEM photomicrograph	Crystals form
	Form C Form C exhibited non-uniform shapeless crystals which agglomerated.
	Form D (Acetic acid solvate) Form D exhibited non-uniform needle-like crystals.
	Form E (Propionic acid solvate) Form E exhibited non-uniform needle-like crystals.

4.3.6 Variable temperature x-ray powder diffraction (VT-XRPD)

VT-XRPD analysis was performed on the two solvated forms in order to investigate the desolvation behaviour of Form D and Form E when subjected to increased temperatures. The results of these studies are illustrated in Figure 4.14 and Figure 4.15, respectively.

Variable-temperature XRPD analysis showed that the mebendazole acetic acid solvate (Form D) was stable between 25-75°C with no crystal transitions detected in the temperature range. Desolvation was detected from the decrease in the intensity of the 6.6±0.1°2θ peak, characteristic to Form D (Figure 4.14) after 85°C. At 100°C the diffractogram of Form D showed the transition to the stable Form A with the appearance of the 7.6±0.1°2θ peak (characteristic to Form A). As the temperature increased, the peaks at 7.6±0.1°2θ and 17.3±0.1°2θ increased in intensity while the characteristic peaks of Form D at 6.3±0.1°2θ and 13.2±0.1°2θ disappeared after 100°C. The transition of the Form D to the stable crystal form (Form A) was completed at temperatures above 110°C with no further transitions detected in the sample. The sharp endotherm detected on the DSC at 109°C (section 4.3.3) indicated the temperature of desolvation. The VT-XRPD results confirmed DSC findings.

The variable-temperature XRPD analysis of Form E showed that the mebendazole propionic acid solvate (Form E) was stable between 25-85°C with no significant changes in the XRPD patterns (Figure 4.15). At 95°C the diffractogram of Form E indicated the transition to the stable Form A with the appearance of the 7.6±0.1°2θ and 17.3±0.1°2θ peaks (characteristic to Form A). As the temperature was increased the peak at 7.6±0.1°2θ and 17.3±0.1°2θ increased in intensity while the characteristic peak of Form E at 6.3±0.1°2θ decreased. The transition of Form E to the stable crystal form (Form A) was completed at temperatures above 130°C with no further transitions detected in the sample. The sharp endotherm detected on the DSC at 124°C (section 4.3.3) indicated the temperature of desolvation. The VT-XRPD results confirmed DSC findings.

From the VT-XRPD analysis it was clear that at some point during the desolvation process, a mixture of the relevant solvated form (Form D or Form E) and Form A was present in the sample. The reason for the observation may be due to the fact that the observed desolvation process was not an instantaneous process. The mechanism of desolvation of Form D and Form E will be discussed in Chapters 6 and 7. The XRPD patterns of Form D and Form E after heating of the sample to ±130°C were comparable with the XRPD pattern of mebendazole Form A, indicating complete transition to the most stable polymorphic form (i.e. Form A).

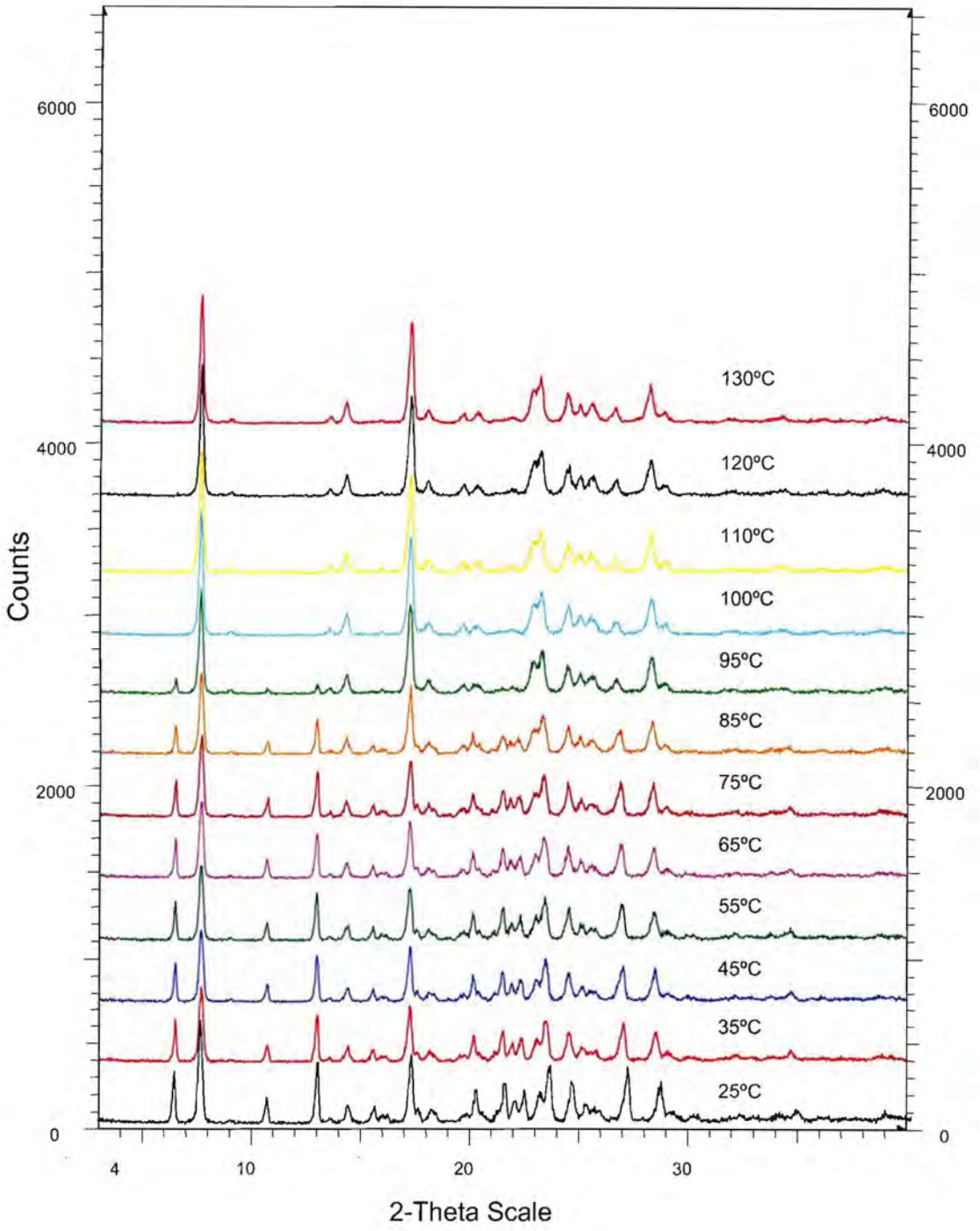

Figure 4.14 VT-XRPD diffractograms of mebendazole Form D.

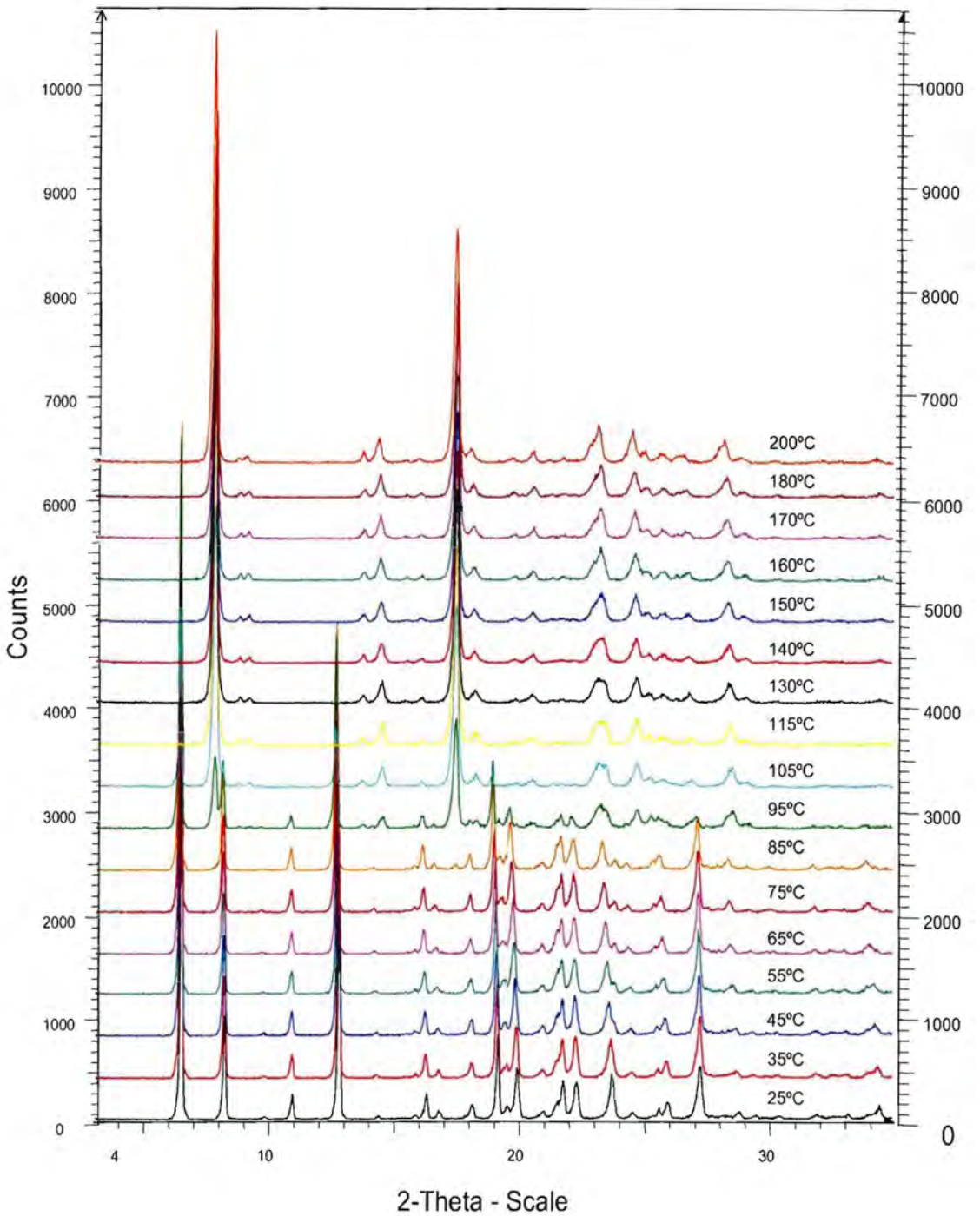

Figure 4.15 VT-XRPD diffractograms of mebendazole Form E.

Conclusion

A new pseudo-polymorphic form of mebendazole (acetic acid solvate, Form D) was prepared by means of a rapid recrystallisation method. The same method was used to recrystallise the mebendazole propionic acid complex (Form E) over a short period with high yield.

Form D and Form E were characterised by DRIFT-IR, XRPD, DSC, TGA, HSM and VTXRPD.

Form D and Form E exhibited needle-like crystalline habits, which were verified by polarised light microscopy and SEM. Upon heating of the solvates the solvent entrapped within the crystalline structures were released, which led to the transition to the stable Form A.

VT-XRPD analysis of Form D and Form E revealed that desolvation of Form D started at 85°C and Form E at 95°C, suggesting that Form D was thermodynamically less stable than Form E.

A summary of the physico-chemical properties of the polymorphic and pseudo-polymorphic forms of mebendazole are tabulated in Table 4.8. The following chapters will focus on the dissolution behaviour, stability and kinetics of desolvation of the two pseudo-polymorphic forms (Form D and Form E) of mebendazole.

Table 4.8 Summary of the characteristic physico-chemical properties of the polymorphic and pseudo-polymorphic forms of mebendazole

Technique	Form A	Form B	Form C	Form D	Form E
DRIFT-IR (-NH) (cm^{-1})	3370 [1]	3340 [1]	3410 [1]	3353	3364
DRIFT-IR (>C=O) (cm^{-1})	1730 [1]	1700 [1]	1720 [1]	1738	1735
XRPD (°2θ)	7.6 [2] 17.3 *	5.8 [2]	4.9 [2]	6.6 7.9 13.2	6.3 8.0 12.6
DSC (°C)	250-255 [3,4] 330 [3,4]	220 [3] 263 [3] 330 [3]	195 [3] 225 [3] 253 [3] 330 [3]	109 256 331	124 254 331
TGA Range 100 - 200°C	N/A	N/A	N/A	15.40%	20.76%

(*) The 17.3°2θ peak did not show any peak overlapping with peaks associated with Form D and / or Form E, and was thus identified as a characteristic peak of Form A. The 17.3°2θ peak was utilised in the stability study of Form D and Form E to determine the presence of polymorphic conversion.

[1] Himmelreich *et al.* (1977:123)

[2] Brits (2008:70)

[3] De villiers *et al.*(2005:438)

[4] Chapter 3, section 3.3

CHAPTER 5

Dissolution behaviour of the mebendazole solvates

Introduction

The dissolution and solubility behaviour of polymorphic forms play a crucial role in the selection of the most favoured crystal form suitable for the manufacturing of pharmaceuticals. Different crystal forms (including solvates, hydrates and amorphous solids) exhibit different dissolution rates and solubility profiles that may affect the bioavailability of the API in the final dosage form (Byrn *et al.*, 1999:91). The physiological absorption of an API after oral administration usually involves the dissolution of the API in the gastro-intestinal tract, where the rate and extent of dissolution influences the rate of absorption and bioavailability of the API (Bernstein, 2002:243; Hilfiker, 2007:6). The purpose of this chapter was to investigate the dissolution behaviour of Form D and Form E.

5.1 Theory of dissolution

Dissolution is defined as the transfer of molecules or ions from the solid-state into solution, where the extent of dissolution is governed under a given set of experimental conditions that are proportional to the solubility of the API in the solvent (Aulton, 2002:16). In polymorphism, higher dissolution rates are obtained for metastable polymorphic forms compared to the thermodynamically stable polymorphic forms (Aulton, 2002:9).

Three theories exist for the mechanism by which an API dissolves. The first theory assumes that there is a diffusion layer or a static liquid film on the surface of the API. The second theory states that there is an interfacial barrier between the solid surface and the solution where the concentration of the API varies significantly over the barrier and the concentration being higher adjacent to the particle than near the solution. The third theory states that dissolution occurres when a group of solvent molecules reaches the surface of the solid by diffusion, dissolving the API. The third theory is based on the Danckwert model for dissolution (Byrn *et al.*, 1999:93). Aulton (2002:18-19) described the dissolution process as a two step process The first step involves a phase change, resulting in the liberation of the solid molecules into a solute phase, where the solution become saturated with the API (the concentration of the saturated solution was donated C_s). The second step involves the migration of the solute molecules through the boundary layers surrounding the crystal to the main solution at which time the concentration will be C. These boundary layers around the crystal are static or slow moving layers of liquid affecting the dissolution of the API. The rate of dissolution is determined by the rate of the

slowest step (Aulton, 2002:18-19). Figure 5.1 illustrates the boundary layers and concentration change in a dissolving API particle.

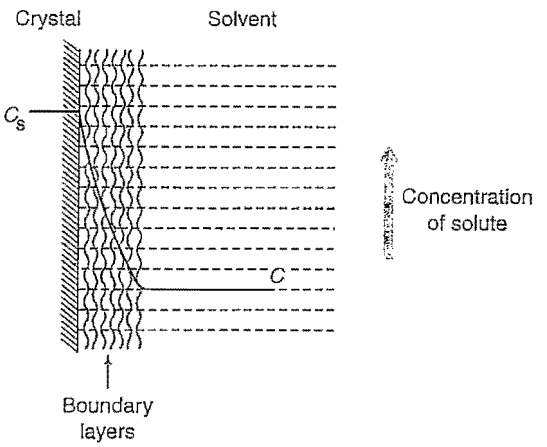

Figure 5.1 Illustration of the dissolution of an API particle (Aulton, 2002:19).

The diffusion layer model is used to describe transport-controlled dissolution, where the dissolution rate is controlled by the diffusion of the solute molecules across a thin diffusion layer in a non-linear manner. This model is described by the Noyes-Whitney equation (Equation 5.1) (Brittain, 1999:309).

$$\frac{dm}{dt} = \frac{kA\,(C_s - C)}{h} \qquad (5.1)$$

Where: dm/dt = dissolution rate

A = surface area of the dissolving API particle

C_s = saturation concentration of the API

C = concentration of the bulk solution with the API

k = diffusion coefficient and

h = thickness of boundary layer

The factors that may influence the rate of dissolution in terms of the Noyes-Whitney equation are summarised in Table 5.1 (Brittain, 1999:310; Aulton, 2002:20).

Table 5.1 Summary of the factors that may influence the dissolution rates of APIs (adapted from Aulton, 2002:20)

Term in Noyes-Whitney equation	Affecting factors in dissolution	Influence on dissolution rate
Surface area of undissolved API (*A*)	Particle size	Particle size will change during dissolution. The smaller the particle size, the faster the rate of dissolution. *A* $\propto$ *1/ particle size.*
	Dispersibility of powdered API	Formation of coherent powder masses in the dissolution medium results in a decrease in the rate of dissolution.
	Porosity of API particles	API's with large pores will allow access of the dissolution medium and increase the rate of dissolution.
Solubility of API in dissolution medium (C_s)	Temperature	Dissolution may be an endothermic or exothermic process.
	Nature of dissolution medium	The pH and buffer concentration and the pK_a values of the dissolving solid and or buffer may increase or decrease the rate of dissolution (Brittain, 1999:310).
	Molecular structure of solute	Polar solutes dissolve in polar solvents and non-polar solutes dissolve in non-polar solvents (Aulton, 2002:23).
	Crystalline form of API	The different polymorphs vary in their solubility and stability (Aulton, 2002:9).
	Presence of other compounds	The addition of compounds like SLS may increase or decrease the rate of dissolution.

Table 5.1 (continued)

Term in Noyes-Whitney equation	Affecting factors in dissolution	Influence on dissolution rate
Concentration of solute in solution at time t (C)	Volume of dissolution medium	The larger the volume of the dissolution medium, the lower the concentration of the solute in the bulk solution, the faster the rate of dissolution.
	Processes removing dissolved solute from the dissolution medium	Adsorption onto insoluble substances will lower the bulk concentration and increase the rate of dissolution.
Dissolution rate constant (diffusion coefficient) (k)	Thickness of boundary layer	The thicker the boundary layer the slower the rate diffusion of API particles into the bulk concentration, the lower the dissolution rate.
	Diffusion coefficient of solute in the dissolution medium	High viscosity decreases the rate of diffusion and large molecules decrease the rate of diffusion.

5.2 Particle size

Particle size may affect the dissolution of an API (Table 5.1). The smaller the particle size, the more rapidly the process of dissolution, due to the increased surface area of the API exposed to the dissolution medium. The morphology of the crystalline solid may also affect the particle size (Brittain, 1999:163). Most often the particle size distribution of a sample can be attributed to differences in the morphology of the particles in the sample. To characterise and compare the particles of two or more powders it is often advised to break down the particle size distribution into different size ranges by sieving the particles using at least 5-6 different mesh sizes. The percentage of each particle size on each sieve can then be plotted in a histogram against particle size, representing the particle size distribution in the powder (Byrn *et al.*, 1999:104; Staniforth, 2002:154-155). Figure 5.2 illustrates three types of particle size distribution profiles.

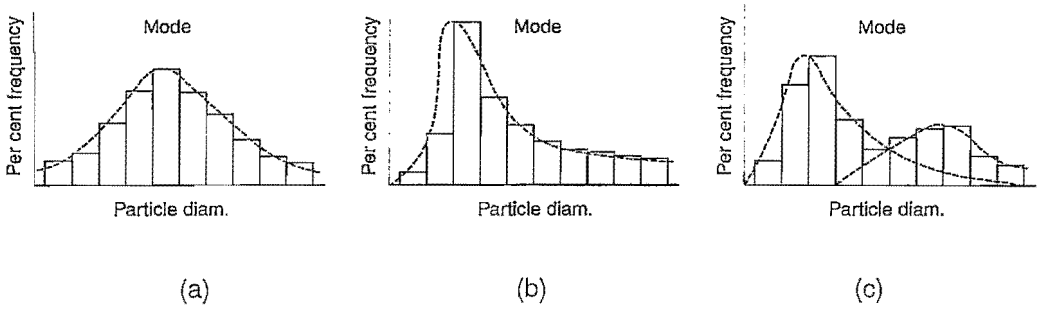

Figure 5.2 Illustration of three particle size distribution profiles: (a) normal distribution, (b) positively skewed distribution and (c) a bimodal distribution (Staniforth, 2002:154).

Scanning electron microscopy (SEM) indicated the morphology of both solvated forms (i.e. Form D and Form E) to be needle-like (refer to Chapter 4, section 4.3.5) with differences in particle sizes. Figure 5.3 illustrates the SEM photomicrographs of the two solvated forms of mebendazole (prior to sieving of the samples).

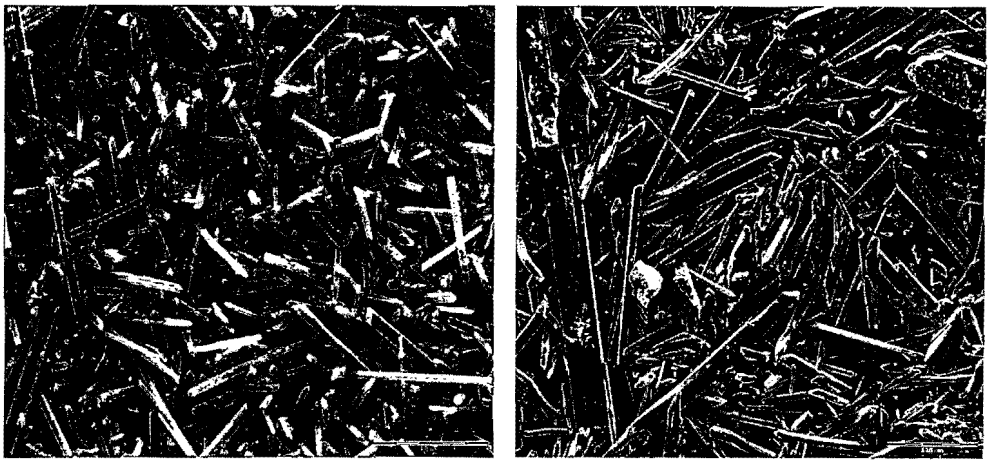

(a) (b)

Figure 5.3 SEM photomicrographs of (a) Form D and (b) Form E.

Form D and Form E crystals were sieved using 106 µm and 250 µm Madison test sieves (Madison Filter Solutions, Madison Filter SA Pty (Ltd), Johannesburg, South Africa). The fraction between the 106 and 250 µm sieves was used for the dissolution studies.

Particle size distributions were measured using a Malvern Mastersizer 2000 (Malvern Instruments Ltd, Malvern, UK) fitted with a Hydro 2000SM dispersion unit. The particle sizer uses laser light scattering for the determination of the particle size distributions. The samples intended for particle size analysis were dispersed in the sample suspension unit containing deionized water with Polysorbate 80 (Tween® 80). A cell stirrer prevented sedimentation of the dispersed particles and the dispersed particles were circulated through the sample cell via a sample pump. The acquired data was used to compute means, medians and standard deviations based on the total particle population.

Small particles of both solvated forms (Form D and Form E) appeared to be static and agglomerated during the sieving process. During the particles size analysis, the agglomerated particles were dispersed and the smaller particles (< 106 µm) were clearly detected.

Particle size analysis performed on Form D and Form E revealed a bimodal particle size distribution. A summary of the particle size distribution results are tabulated in Table 5.2.

Table 5.2 Summary of the particle sizes of Form D and Form E used for dissolution testing

Particle size distribution	Form D	Form E
	(µm)	(µm)
d(0.1)	2.55	7.22
d(0.5)	10.22	26.14
d(0.9)	127.90	105.89

The particle size distribution profiles of Form D and Form E are illustrated in the histograms in Table 5.3. The particle size distributions (d(0.9)) of Form D and Form E could be considered similar (Table 5.2 and Table 5.3).

Table 5.3 Particle size histograms of the two solvated forms of mebendazole used during the dissolution testing

Particle size analysis	Remarks
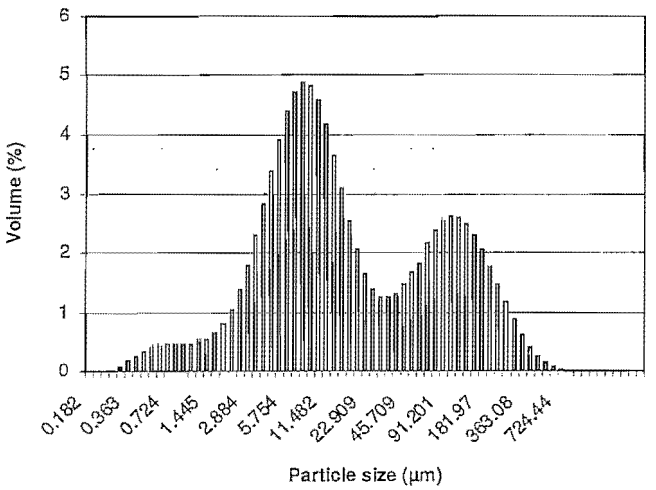	**Form D** Particle size distribution: bimodal d(0.1) = 2.55 d(0.5) = 10.22 d(0.9) = 127.90
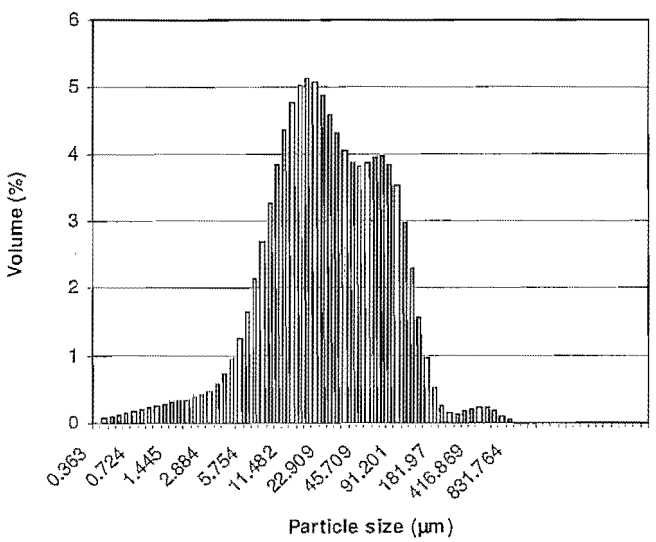	**Form E** Particle size distribution: bimodal d(0.1) = 7.22 d(0.5) = 26.14 d(0.9) = 105.89

5.3 Dissolution method

Dissolution tests were performed on Form D and Form E using the method proposed by Swanepoel *et al.* (2003:346). The dissolution conditions were:

Apparatus: USP Paddle assembly (Apparatus 2) – 75 rpm.

The dissolution tests were performed using a Vankel VK7000 dissolution tester (Varian Inc., Palo Alto, CA, USA) and the withdrawn samples were analysed spectrophotometrically using a Shimadzu UV-2400PC spectrophotometer (Schimadzu Inc., Palo Alto, CA, USA).

Medium: 900 ml 0.1 N HCl preheated and maintained at 37 °C.

Approximately 50 mg of the powdered samples were weighed into 10 ml glass test tubes. Glass beads (approximately 50 mg) with a mean size of 0.1 mm and 2 ml of dissolution medium were added to each glass test tube. These mixtures were agitated for 20 seconds (using a vortex mixer) before the contents thereof were transferred into the individual dissolution vessels. Samples (7 ml) were withdrawn from the dissolution vessels after 7.5, 15.0, 22.5, 30.0, 45.0, 60.0, 90.0 and 120.0 minutes. 5 ml of the individually withdrawn samples were then diluted to a final volume of 25 ml using the dissolution medium (Swanepoel *et al.*, 2003:346). The concentration of the dissolved mebendazole was calculated from the UV-absorbance obtained at 288 nm.

A standard solution was prepared by dissolving approximately 11.11 mg of mebendazole RS in 2.5 ml formic acid and making it up to a final volume of 500 ml with 0.1 N HCl (Solution A). 5ml of Solution A was diluted to a final volume of 10 ml using 0.1 N HCl. The concentrations (%) of the dissolution samples were determined using Equation 5.2 and the derivatives thereof. The mathematical derivates of Equation 5.2 were used to compensate for the reduction in the volume of dissolution medium (in the vessels), due to the withdrawal of 7 ml of the medium at each time interval.

KP1:

$$= \frac{A_{SAMPLE} \times mgSTD \times C \times 5 \times 900 \times 25 \times 100}{A_{STD} \times 100 \times \left(\frac{mgSAMPLE \times (100 - TGA)}{100} \right) \times 500 \times 10 \times 5} \qquad (5.2)$$

KP2 (7.5 min):

$$= K_{P1}$$

KP3 (15 min):

$$= K_{P1} \times \frac{893}{900} + \frac{7}{900 \times K_{P2}}$$

KP4 (22.5 min):

$$= K_{P1} \times \frac{886}{900} + \frac{7}{900 \times K_{P2}} + \frac{7}{893 \times K_{P3}}$$

KP5 (30 min):

$$= K_{P1} \times \frac{879}{900} + \frac{7}{900 \times K_{P2}} + \frac{7}{893 \times K_{P3}} + \frac{7}{886 \times K_{P4}}$$

KP6 (45 min):

$$= K_{P1} \times \frac{872}{900} + \frac{7}{900 \times K_{P2}} + \frac{7}{893 \times K_{P3}} + \frac{7}{886 \times K_{P4}} + \frac{7}{879 \times K_{P5}}$$

KP7 (60 min):

$$= K_{P1} \times \frac{865}{900} + \frac{7}{900 \times K_{P2}} + \frac{7}{893 \times K_{P3}} + \frac{7}{886 \times K_{P4}} + \frac{7}{879 \times K_{P5}} + \frac{7}{872 \times K_{P6}}$$

KP8 (90 min):

$$= K_{P1} \times \frac{858}{900} + \frac{7}{900 \times K_{P2}} + \frac{7}{893 \times K_{P3}} + \frac{7}{886 \times K_{P4}} + \frac{7}{879 \times K_{P5}} + \frac{7}{872 \times K_{P6}} + \frac{7}{865 \times K_{P7}}$$

KP9 (120 min):

$$= K_{P1} \times \frac{851}{900} + \frac{7}{900 \times K_{P2}} + \frac{7}{893 \times K_{P3}} + \frac{7}{886 \times K_{P4}} + \frac{7}{879 \times K_{P5}} + \frac{7}{872 \times K_{P6}} + \frac{7}{865 \times K_{P7}} + \frac{7}{858 \times K_{P8}}$$

Where:

K_{PX} = the % sample dissoluted at the specific time interval

A_{SAMPLE} = Absorbance of the diluted sample at the specific time interval

A_{STD} = Absorbance of the diluted standard solution

$mgSTD$ = the mass of mebendazole RS used to prepare the standard solution

$mgSAMPLE$ = the mass of mebendazole Form D or Form E sample transferred into the dissolution vessel

TGA = the mass loss (expressed as a percentage) of the mebendazole sample (Form D or Form E) obtained from TGA data, to compensate for the mass of solvent molecules present in the solvated crystal lattice

C = potency of the mebendazole RS (expressed as a percentage)

Swanepoel *et al.* (2003:346) stated that the absorption of mebendazole should be measured at 254 nm. However, Himmelreich *et al.* (1977:123) measured the absorption of mebendazole at 288 nm during solubility measurements.

A method transfer was performed on the analytical technique to ensure the efficacy of the method used to determine the % mebendazole dissolved at the various intervals. The method transfer included the following tests: *specificity*, *linearity & range* and finally *accuracy*.

5.3.1 Specificity

Specificity has been defined as the ability of the analytical method to assess unequivocally the analyte in the presence of components, which may cause potential interference (ICH-Q2(R1), 2005:4).

The spectrophotometer used for the analysis of the samples was auto-zeroed using the 0.1 N HCl (dissolution medium) as blank solution, to ensure that the dissolution medium did not interfere with the absorbance of mebendazole in the range: 200-500 nm. A full range UV-spectrum of mebendazole in 0.1 N HCl was collected over the range: 200-500 nm and the main absorption peaks were identified (Figure 5.4 (a)). From the wavelength spectrum analysis it was observed that the mebendazole absorption spectrum showed multiple absorbance peaks with the strongest absorption peaks at 235 and 288 nm (Figure 5.4 (a)). The 254 nm

wavelength (suggested to be used by Swanepoel *et al.*, 2003:346) was identified on the slope of the 235 nm peak (Figure 5.4 (a)).

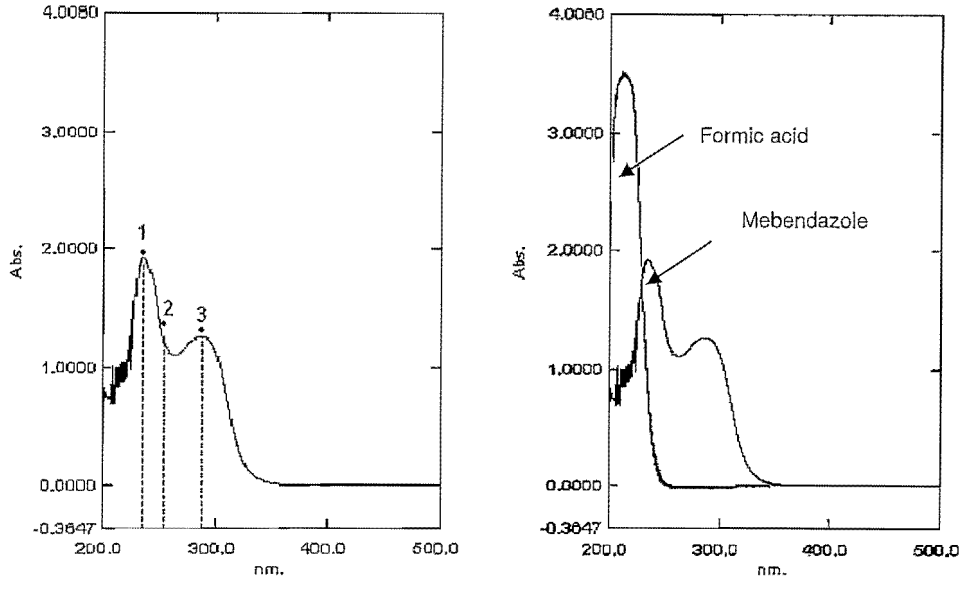

(a) (b)

Figure 5.4 UV spectra for (a) mebendazole in a 0.1 N hydrochloric acid showing the positions of the various wavelengths: ([1] = 235 nm, [2] = 254 nm and [3] = 288 nm). (b) An overlay of the obtained mebendazole and formic acid absorption spectra.

To effectively rule out the interference of formic acid (used for the preparation of standard solutions) on the UV absorption spectrum, an UV absorption spectrum was collected for a formic acid in 0.1 N HCl mixture and overlaid with that of mebendazole in 0.1 N HCl (Figure 5.4(b)). The spectrum indicated a single strong absorption peak for the formic acid at approximately 217 nm. Therefore the formic acid used in the dissolution studies did not indicate any interference with the UV absorption of mebendazole at 288 nm.

To exclude the potential interference of acetic acid and propionic acid (that may be released from the solvated crystal lattices of Form D and Form E respectively) on the detection of mebendazole, the UV absorption spectra of diluted acetic acid and propionic acid in dissolution medium were collected (Figure 5.5).

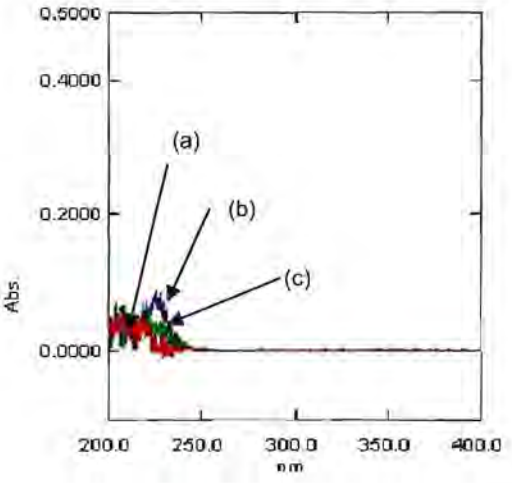

Figure 5.5 UV absorption spectra for the (a) dissolution medium (0.1 N hydrochloric acid), (b) acetic acid and (c) propionic acid (diluted in 0.1 N hydrochloric acid).

From the UV absorption spectra of the diluted acetic acid and propionic acid solutions it was evident that the acetic acid and propionic acid did not influence the sensitivity for the detection of mebendazole at 288 nm.

Based on the above mentioned observations it was concluded that UV spectrophotometry (at 288 nm) to be effective in determining the traces of mebendazole present in 0.1 N HCl unequivocally.

5.3.2 Linearity and range

The linearity of an analytical procedure is defined as its ability (within a given range) to obtain test results which are directly proportional to the concentration (amount) of analyte in the sample (ICH-Q2(R1), 2005:4).

A calibration curve of absorbance (A) versus concentration (c) was plotted in order to determine whether a linear relationship existed between the absorbance and concentration of the mebendazole solutions. The calibration curve was produced by preparing a series of mebendazole solutions with concentrations representing: 60% [6.66 µg/ml], 80% [8.88 µg/ml], 100% [11.11 µg/ml] & 120% [13.33 µg/ml] of the target concentration for the dissolution. The UV-absorbancies of these samples were determined at 288 nm. The correlation between the measured absorbance (A) and the concentrations are illustrated in Figure 5.6.

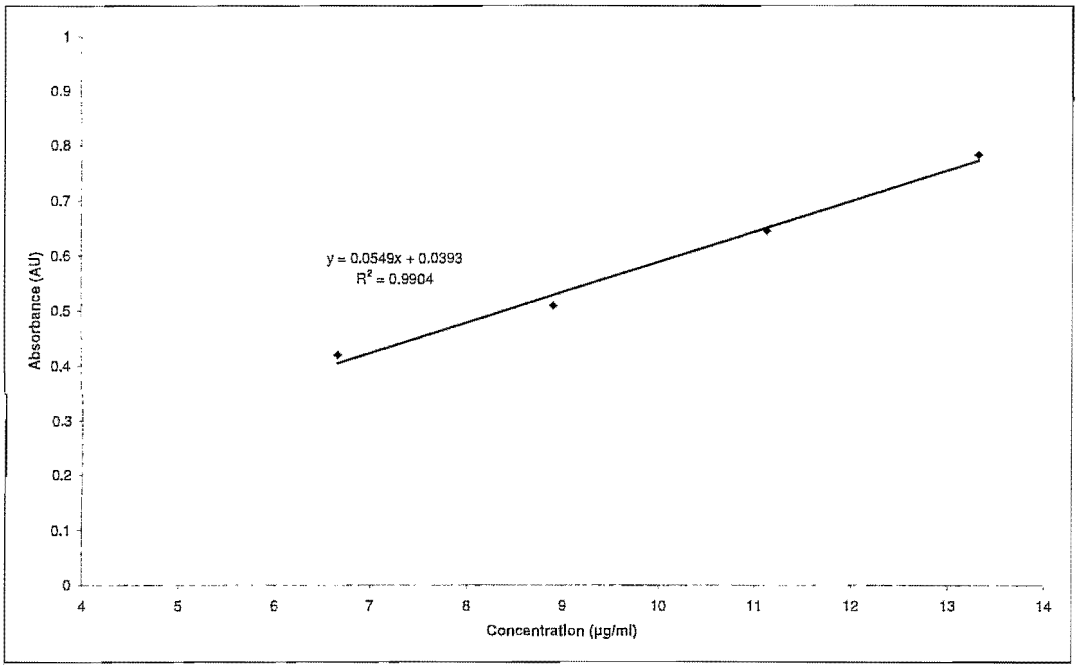

Figure 5.6 Linear correlation between the measured absorbance (*A*) and the concentrations of mebendazole standard solutions in 0.1 N HCl.

Linear regression analysis should yield a regression coefficient (r^2) of ≥ 0.99 (ICH-Q2(R1), 2005:4). From the data presented in Figure 5.6 it was evident that the method was linear (r^2=0.9904) over the concentration range of 6.66 - 13.33 µg/ml.

5.3.3 Accuracy

The ICH guideline on method validation defined the accuracy of an analytical procedure as the ability of the analytical procedure to expresses the closeness of agreement between the value which is accepted either as a conventional true value or an accepted reference value and the value found (ICH-Q2(R1), 2005:4).

Spiked solutions (i.e. solutions with known concentrations) of mebendazole were prepared. The three spiked solutions with concentrations of approximately 80, 100 & 120% of the target concentration (11.11 µg/ml) were prepared. The concentrations of the spiked solutions were determined from the UV-absorbance at 288 nm and using the linear formula reported in Figure 5.6. Table 5.4 provides a summary of the results obtained. According to the ICH guideline the % recovery should be between 98-102% (ICH-Q2(R1), 2005:4).

Table 5.4 Accuracy results obtained for spiked solutions

Solution no	Known concentration (µg/ml)	Experimental determined concentration (µg/ml)	% Recovery
1	8.90	8.93	100.34
2	11.10	11.03	99.37
3	13.30	13.54	101.80

The % recovery for the spiked solutions ranged between 99.37-101.80%, and thus confirmed the accuracy of the analytical procedure.

5.4 Results and discussion

The results (Q = average percentage of mebendazole dissolved at a specific time interval (n=6)) of the dissolution study on the solvated forms of mebendazole are summarised in Table 5.5.

Table 5.5 Dissolution results of mebendazole Form D and Form E in 0.1 N HCl at 37±2°C

Time (min)	Form D		Form E	
	Q	% RSD	Q	% RSD
7.5	44	5	88	2
15.0	46	5	94	2
22.5	47	5	95	2
30.0	48	5	96	2
45.0	49	4	96	2
60.0	49	4	96	2
90.0	49	4	98	2
120.0	51	4	97	2

The powder dissolution profile of Form D (Figure 5.7) indicated that approximately 51% of the sample dissolved after 120 minutes. The powder dissolution profile of Form E indicated that approximately 97% of the sample dissolved after 120 minutes.

The similarity factor (f_2) as first described by Moore and Flanner was used to compare the dissolution profiles of Form D and Form E, using Equation 5.3 (Freitag, 2001:867; Costa, 2001:77).

$$f_2 = 50 \log \left\{ \left[1 + \frac{1}{n} \sum_{t=1}^{n} (R_t - T_t)^2 \right]^{-0.5} \times 100 \right\} \qquad (5.3)$$

Where: Rt = % of reference sample dissolved

Tt = % of test sample dissolved

n = number of dissolution time points

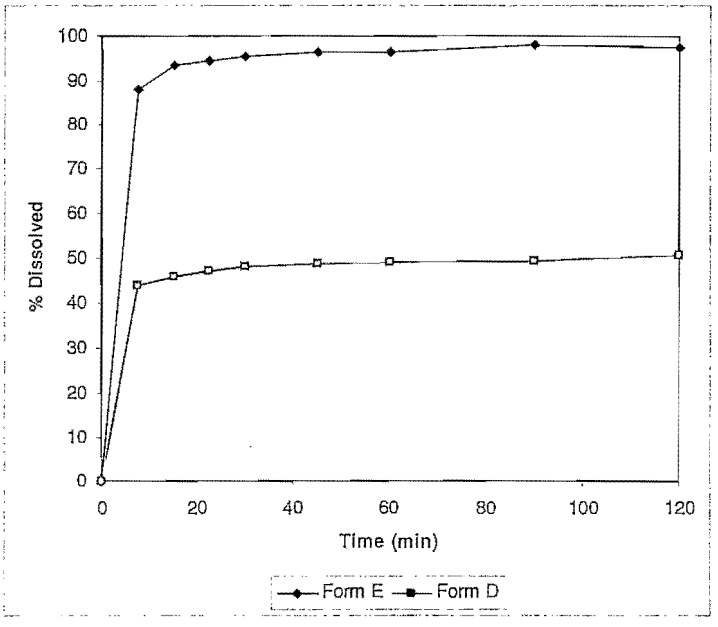

Figure 5.7 Dissolution profiles of Form D and Form E in 0.1 N HCl at 37±2°C.

If the f_2-value = 100, then the dissolution profiles of the reference and test sample are considered to be identical. If the f_2-value ranges between 50 and 100, then it is assumed that a similarity exists between the dissolution profiles of the reference and test sample. If the f_2-value ranges between 0 and 50, it is considered that no similarity exists between the dissolution profiles of the reference and test sample. The degree of dissimilarity between dissolution profiles increases as the f_2-value approaches 0 (Costa, 2001:77; O'Hare *et al.*, 1998:216).

A comparison of the dissolution profiles of Form D and Form E revealed that the profiles differed significantly (f_2 = 16).

The Q_{120}-values for the dissolution profiles of Form D and Form E (Figure 5.7) were compared to the Q_{120}-values of mebendazole polymorphs A, B and C as reported by Swanepoel *et al.* (2003:346-348). The order of the dissolution rate (based on Q_{120}-values) for the mebendazole polymorphic and pseudo-polymorphic forms in 0.1 N HCl is thus: A < B < D< C < E.

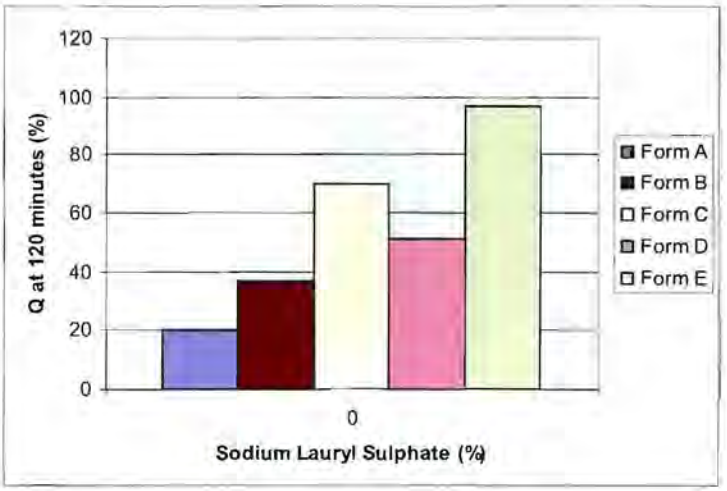

Figure 5.8 Comparison of the dissolution profiles (Q at 120 min) of the polymorphic and pseudo-polymorphic forms of mebendazole (0.1 N HCl at 37°C) - adapted from Swanepoel *et al.* (2003:348).

An important observation was made during the dissolution testing. After approximately 15 minutes, no traces of the mebendazole Form E were visible in the various dissolution vessels. However, suspended particles (mebendazole) were detected in the dissolution vessels of Form D after 120 minutes, confirming the UV-spectrophotometric results that only a limited fraction of the Form D sample dissolved in the dissolution medium.

At the end of the dissolution test the suspended particles were filtered from the dissolution medium and allowed to dry at ambient conditions. A DRIFT-IR spectrum was collected of the dried particles (see Figure 5.9).

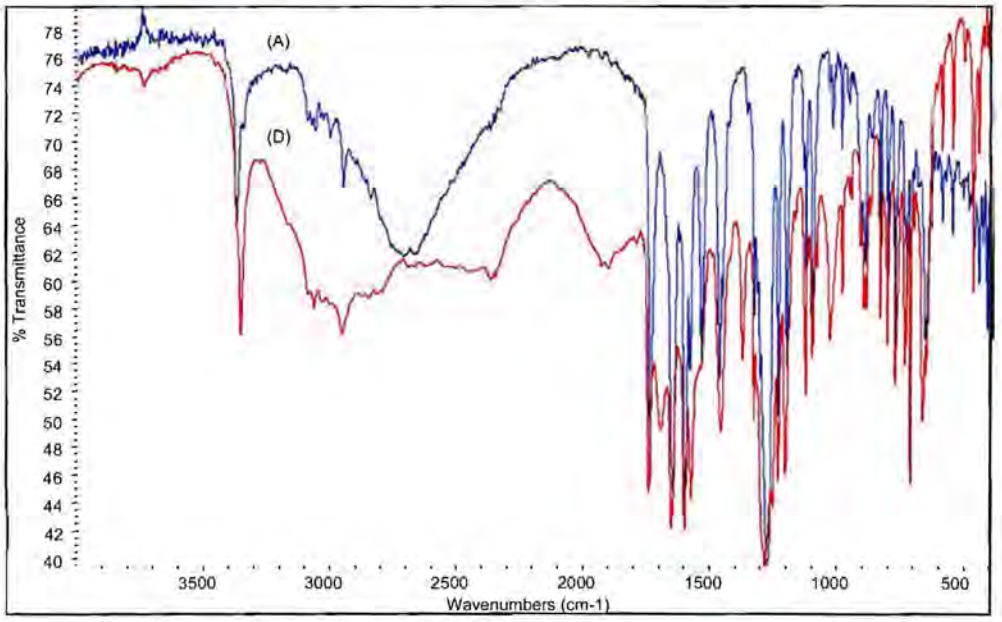

Figure 5.9 Overlay of the IR absorption spectra of Form D before and after dissolution test.

The IR spectrum of the suspended particles was found to be concurrent with the IR spectrum of mebendazole Form A. Figure 5.9 shows a comparison of the IR spectra of the mebendazole acetic acid solvate before and after dissolution (the suspended particles). It can therefore be concluded that a potential reason for the poor Q_{120}-value of mebendazole Form D could be attributed to the fact that a fraction of Form D underwent a solvent mediated phase transition and was transformed to the poorly soluble Form A.

The release of the solvent molecules from the lattices of Form D and Form E (i.e. desolvation) during the dissolution testing, was investigated by determining the potential influence of the released solvent molecules on the pH of the dissolution medium. The pH of the dissolution medium was measured prior to and at the end of the dissolution tests. Dissolution of mebendazole (Form C) in 0.1 N HCl did not have any influence on the pH of the 0.1 N HCl solution (dissolution medium). The pH measurements are tabulated in Table 5.6.

Table 5.6 Effect of the released solvent molecules (Form D = acetic acid, Form E = propionic acid) on the pH of the dissolution medium (0.1 N HCl)

Form	pH of dissolution medium	
	Before dissolution	After dissolution
Form D	1.27	1.25
Form E	1.27	1.23

From the results obtained (Table 5.6) it was evident that the release of the solvent molecules from the solvated crystal lattices, caused a decrease in the pH of the dissolution medium. Shehatta (2002:1239) indicated that the solubility of mebendazole is influenced by the pH of the medium. The increase in acidity of the dissolution medium might therefore have facilitated the dissolution (increased the dissolution rate and extend) of Form D and Form E.

Conclusion

This chapter revealed that the dissolution profiles of Form D and Form E differed significantly (f_2 = 16). The powder dissolution profiles of Form D (Figure 5.7) indicated that approximately 51% of the sample dissolved after 120 minutes, whereas 97% of Form E dissolved after 120 minutes in 0.1 N HCl.

Particle size analysis indicated that the particle size distribution of Form D and Form E was comparable, thus the differences in the dissolution profiles could not be attributed to differences in particle size.

Upon further investigation, it was observed that the differences in the dissolution profiles of Form D and Form E could be attributed to the fact that a fraction of Form D underwent a solvent mediated phase transition (in the dissolution medium) and was transformed to the poorly soluble Form A.

Comparison of the dissolution profiles of the Forms A, B, C, D and E revealed that Form E was the most soluble in 0.1 N HCl (at 37ºC) and Form A the least soluble. Form D was found to be more soluble in 0.1 N HCl (at 37ºC) than Forms A and B (see Figure 5.8).

The differences in the dissolution profiles of the solvated forms (Forms D and E) and non-solvated forms (Forms A, B and C) of mebendazole could also be attributed to the decrease in the pH of the dissolution medium caused by the release of solvent molecules from the solvated lattices which facilitated the dissolution (increased the dissolution rate and extend) of Form D and Form E.

The results presented in this chapter revealed that it is advised that quantitative UV-analysis of mebendazole should be performed at 288 nm.

CHAPTER 6

Thermal behaviour of mebendazole pseudo-polymorphic forms

Introduction

Desolvation is defined as the process where the lattice entrapped solvent is removed by external factors (i.e. temperature, humidity, changes in atmospheric pressure, grinding, etc.). The desolvation process may induce phase transformations in the crystalline solid (Byrn *et al.*, 1999:507). One of the major concerns in the pharmaceutical industry regarding the use of solvated APIs is the physical stability (desolvation behaviour) thereof, since this may affect the development and performance of pharmaceutical dosage forms (Khawam & Flanagan, 2008:2160-2161). An understanding of the solid-state kinetics not only provide a means to determine the stability of polymorphs and pseudo-polymorphs, but also gives insight into the mechanisms followed during phase transitions (Zhou *et al.*, 2003:1780).

According to Wang *et al.* (2006:1220) the most popular methods used in the investigation of the thermal behaviour of APIs (i.e. desolvation / dehydration / decomposition) are DSC and TGA. The process of desolvation in solvates may occur during or after the melting of the solvated API, depending on the physico-chemical properties of the solvent trapped within the crystal lattice (Giron, 1995:21-22). HSM was be used in conjunction with DSC and TGA analysis to confirm and study the desolvation behaviour of solvated forms (Chapter 4, section 4.3.4).

Desolvation may affect the crystal lattice in two ways. The crystal lattice may collapse upon desolvation and transform into a polymorphic form; in the event where the desolvated lattice remains intact, the crystal form is known as a desolvated solvate. Factors that may affect the desolvation (removal of solvents) of a solvate are: (1) the tunnel size and number of tunnels per unit area, (2) the compactness of the crystal packing, (3) the number and strength of hydrogen bonds between the solvent and API or the (4) citation coordinates of the solvent (Byrn *et al.*, 1999:294).

In Chapter 4, two solvated forms of mebendazole (Forms D and E) were prepared and characterised. VT-XRPD (section 4.3.6) and thermal analysis (section 4.3.3) performed on the two solvated forms, confirmed the desolvation of the samples at different temperatures, which suggested that Form E was thermodynamically more stable compared to Form D.

The purpose of this chapter was to determine the desolvation activation energy, mechanism and rate of desolvation of Forms D and E by means of isothermal and non-isothermal kinetic analysis.

6.1 Transition kinetics of polymorphs and pseudo-polymorphs

Investigation of the phase transitions of polymorphs and pseudo-polymorphs involve a heterogeneous kinetic approach, where there are at least two modifications or two phases present that may be influenced by particle size, temperature gradient, activation energy, nucleus and diffusion of the different phases (Giron, 1995:45).

The rate of a reaction in the solid-state (*dc/dt*) is defined as the rate by which the concentration of a specific phase increases or decreases over a period of time (Martin, 1993:284). The process of desolvation involves the removal of a solvent from the crystal lattice at a specific temperature below the melting point of the host crystal lattice (Khawam & Flanagan, 2008:2160; Khawam & Flanagan, 2005:104) as illustrated in Equation 6.1.

$$A_{(s)} \rightarrow B_{(s)} + C_{(g)} \tag{6.1}$$

Where: $A_{(s)}$ = Solvated crystal form (Metastable pseudo-polymorph)

$B_{(s)}$ = Desolvated crystal form (Stable polymorph)

$C_{(g)}$ = Evaporated solvent as a gas

The rate of the desolvation reaction is expressed in Equation 6.2, where n represents the reaction order and k the rate constant (Martin, 1993:286; Khawam, 2007:4).

$$\text{Reaction rate} = \frac{d[A]}{dt} = -\frac{d[B]}{dt} = -\frac{d[C]}{dt} = -k[A]^n \tag{6.2}$$

In general, the rate of solid-state reactions is expressed as (Equation 6.3) (Khawam & Flanagan, 2005:101; Giron, 1995:45):

$$\frac{d\alpha}{dt} = k(T)f(\alpha) \tag{6.3}$$

Where: $d\alpha/dt$ is defined as a function of temperature (T), k is the rate of the reaction, $f(\alpha)$ the reaction model and α is the converted fraction. Integration of Equation 6.3 provides the integral rate law as expressed in Equation 6.4 (Khawam & Flanagan, 2005:101):

$$g(\alpha) = kt \tag{6.4}$$

Where: $g(\alpha)$ is the integral reaction model (Khawam & Flanagan, 2005:101; Tanaka, 1995:32; Giron, 1995:45). The rate constant (k) is assumed to be governed by the different temperatures as described by the Arrhenius equation (Equation 6.5) (Giron, 1995:45):

$$k = Ae^{-Ea/RT} \tag{6.5}$$

Where: A is the pre-exponential factor, E_a is the activation energy, T the absolute temperature and R the gas constant (8.3143 J K^{-1} $mole^{-1}$) (Giron, 1995:45).

Polymorphic and pseudo-polymorphic phase transitions can be investigated by *isothermal* and *non-isothermal* kinetic methods. *Non-isothermal methods* were developed to reduce experimental testing periods by implementing kinetic parameters to determine and obtain information on API concentrations, stability, desolvation and degradation over a specific period of time. During non-isothermal methods the temperature to which the sample is exposed is changed periodically (Oliva *et al.*, 2006:2595). In comparison, *isothermal methods* are considered to be more reliable in the determination of phase stability and degradation, due to the fact that the one variable, temperature (T), is maintained throughout the study (Oliva *et al.*, 2006:2595):

Isothermal kinetic studies are based on Equation 6.6. Non-isothermal kinetic studies incorporate the heating rate ($d\alpha/dT$) as a function of temperature ($T = T_0 + \beta t$) to produce a linear increase in temperature (Equation 6.7) (Khawam & Flanagan, 2005:102).

$$g(\alpha) = Ae^{\frac{Ea}{RT}}t \tag{6.6}$$

$$\frac{d\alpha}{dT} = \frac{d\alpha}{dt}\frac{dt}{dT} \tag{6.7}$$

Where: $d\alpha/dT$ is defined as the non-isothermal reaction rate, $d\alpha/dt$ as the isothermal reaction rate and dt/dT as the inverse heating rate ($1/\beta$). The differential form of the non-isothermal rate law is produced by substituting the Arrhenius equation (Equation 6.5) into Equation 6.7, giving rise to Equation 6.8 (Khawam & Flanagan, 2005:102).

$$\frac{d\alpha}{dT} = \frac{A}{\beta}e^{-Ea/RT}dT \tag{6.8}$$

Two different kinetic approaches have been applied in the study of isothermal and non-isothermal kinetic data, i.e. model-fitting and model-free methods. Traditionally, the *model-fitting* method has been defined as a single-step reaction represented by the kinetic triplet (A, E_a and $f(\alpha)$) and is used by fitting the data obtained to various models at different temperatures. The model is based on Equation 6.3 or an integral of Equation 6.3 and the data that best fit in the model is assumed to describe the process under investigation (Zhou *et al.*, 2003:1780-1781; Rodante *et al.*, 2002:1031).

The *model-free* method used in isothermal and non-isothermal studies can be evaluated by means of a minor manipulation of Equation 6.3 to produce Equation 6.9. The model-free method is represented by different activation energies that affect the rate of phase conversion. Model-free methods are based on the assumption that the reaction model $f(\alpha)$ is identical at a given conversion fraction (α) for a given reaction investigated under different conditions (Zhou *et al.*, 2003:1780-1781; Rodante *et al.*, 2002:1031).

$$\ln\left(\frac{dx}{dt}\right)_\alpha = \ln\left[Af(\alpha)\right]_\alpha - \frac{Ea_\alpha}{RT_\alpha} \tag{6.9}$$

During the isothermal and non-isothermal kinetic studies on the desolvation behaviour of the mebendazole solvated forms (Forms D and E), model-fitting methods were applied.

6.2 Model-fitting methods

6.2.1 Isothermal model-fitting method

The model-fitting method is facilitated by fitting the degree of conversion (α) to a specific model (Table 6.1) that best describes the determined reaction rate constant (k), activation energy (E_a) and frequency factor (A), using Equation 6.5. The degree of conversion (α) is expressed in Equation 6.10. The reaction rate constant (k) is determined from the slope when plotting the specific model $g(\alpha)$ for each (temperature) as a function of time (t) (Khawam, 2007:13-14).

$$\alpha(t) = \frac{m_i - m_t}{m_i - m_f} \tag{6.10}$$

Where: m_i is the initial mass of the sample used at the onset of the study, m_t is the mass of the sample at a specific time (t) and m_f is the final mass of the sample determined from isothermal TGA cycles (Rodante *et al.*, 2002:10).

6.2.2 Non-isothermal model-fitting method

Non-isothermal methods contain a single heating rate *($d\alpha/dT$)* in the determination of kinetic data. The methods also extract the kinetic triplet data *(A, E_a* and *$f(\alpha)$)* from the slope of the α-temperature curve plotted for each model (Rodante *et al.*, 2002:11; Khawam & Flanagan, 2008:2161).

Table 6.1 Algebraic expressions of functions g(α) and corresponding mechanism (Turmanova *et al.*, 2008:137)

No.	Sym.	Model	$g(\alpha)$	Rate-determining mechanism
1. Chemical process or mechanism non-invoking equations				
1.	F1/3	One-third order	$1 - (1 - \alpha)^{2/3}$	Chemical reaction
2.	F3/4	Three-quarters order	$1 - (1 - \alpha)^{1/4}$	Chemical reaction
3.	F3/2	One and a half order	$(1 - \alpha)^{-1/2}-1$	Chemical reaction
4.	F2	Second order	$(1 - \alpha)^{-1}-1$	Chemical reaction
5.	F3	Third order	$(1 - \alpha)^{-2}-1$	Chemical reaction
2. Acceleratory rate equations				
6.	P3/2	Mampel power law	$\alpha^{3/2}$	Nucleation
7.	P1/2	Mampel power law	$\alpha^{½}$	Nucleation
8.	P1/3	Mampel power law	$\alpha^{1/3}$	Nucleation
9.	P1/4	Mampel power law	$\alpha^{¼}$	Nucleation
10.	E1	Exponential law	$\ln \alpha$	Nucleation
3. Sigmoidal rate equations or random nucleation and subsequent growth				
11.	A1,F1	Avrami-Erofeev equation	$-\ln(1 - \alpha)$	Assumed random nucleation and its subsequent growth, $n = 1$
12.	A3/2	Avrami-Erofeev equation	$[-\ln(1 - \alpha)]^{2/3}$	Assumed random nucleation and its subsequent growth, $n = 1.5$
13.	A2	Avrami-Erofeev equation	$[-\ln(1 - \alpha)]^{1/2}$	Assumed random nucleation and its subsequent growth, $n = 2$
14.	A3	Avrami-Erofeev equation	$[-\ln(1 - \alpha)]^{1/3}$	Assumed random nucleation and its subsequent growth, $n = 3$
15.	A4	Avrami-Erofeev equation	$[-\ln(1 - \alpha)]^{1/4}$	Assumed random nucleation and its subsequent growth, $n = 4$
16.	Au,B1	Prout-Tompkins equation	$\ln[\alpha/(1 - \alpha)]$	Branching nuclei

Table 6.1 (Continued)

4. Deceleratory rate equations				
4.1 Phase boundary reactions				
17.	R1,F0,P1	Power law	α	Contracting disk
18.	R2,F1/2	Power law	$1-(1-\alpha)^{1/2}$	Contracting cylinder (Cylindrical symmetry)
19.	R3,F2/3	Power law	$1-(1-\alpha)^{1/3}$	Contracting sphere (Spherical symmetry)
4.2 Based on the diffusion mechanism				
20.	D1	Parabola law	α^2	One-dimensional diffusion
21.	D2	Valensi equation	$\alpha + (1-\alpha)\ln(1-\alpha)$	Two-dimensional diffusion
22.	D3	Jander equation	$[1-(1-\alpha)^{1/3}]^2$	Three-dimensional diffusion, spherical symmetry
23.	D4	Ginstling-Brounstein equation	$1-\frac{2}{3}\alpha-(1-\alpha)^{2/3}$	Three-dimensional diffusion, cylindrical symmetry
24.	D5	Zhuravlev, Lesokin, Tempelman equation	$[(1-\alpha)^{-1/3}-1]^2$	Three-dimensional diffusion
25.	D6	Anti-Jander equation	$[(1+\alpha)^{1/3}-1]^2$	Three-dimensional diffusion
26.	-	Anti-Ginstling-Brounstein equation	$1+\frac{2}{3}\alpha-(1+\alpha)^{2/3}$	Three-dimensional diffusion
27.	-	Anti-Zhuravlev, Lesokin, Tempelman equation	$[(1+\alpha)^{-1/3}-1]^2$	Three-dimensional diffusion

6.3 Results and discussion

6.3.1 Isothermal kinetic analysis of Form D and Form E

Isothermal studies were performed on Form D and Form E individually by heating the samples isothermally at 80, 90 and 100°C respectively, using a Mettler Toledo DSC823^e (Greifensee, Switzerland) for a period of 210 minutes. The mass losses of the samples at predetermined intervals were determined.

The TGA thermogram of Form D is characterised by a single (one-step) desolvation process (Chapter 4, section 4.3.3). However, the TGA thermogram of Form E was characterised by a two-step mass loss process (Chapter 4, section 4.3.3), where the first step was associated with the evaporisation of surface adsorbed propionic-acid and the second step represented desolvation. To exclude the potential influence of the surface-bound solvent on the isothermal

desolvation of Form E, the samples were preheated from 25°C - 100°C (at a heating rate of 20°C /min) in the TGA furnace to evaporate the surface bound solvent. The samples were then allowed to cool down to 25°C prior to the initiation of the isothermal studies. The desolvated fractions (α) of Form D and Form E were calculated for each temperature using Equation 6.10 and plotted as a function of time (t) - Figure 6.1 and Figure 6.2.

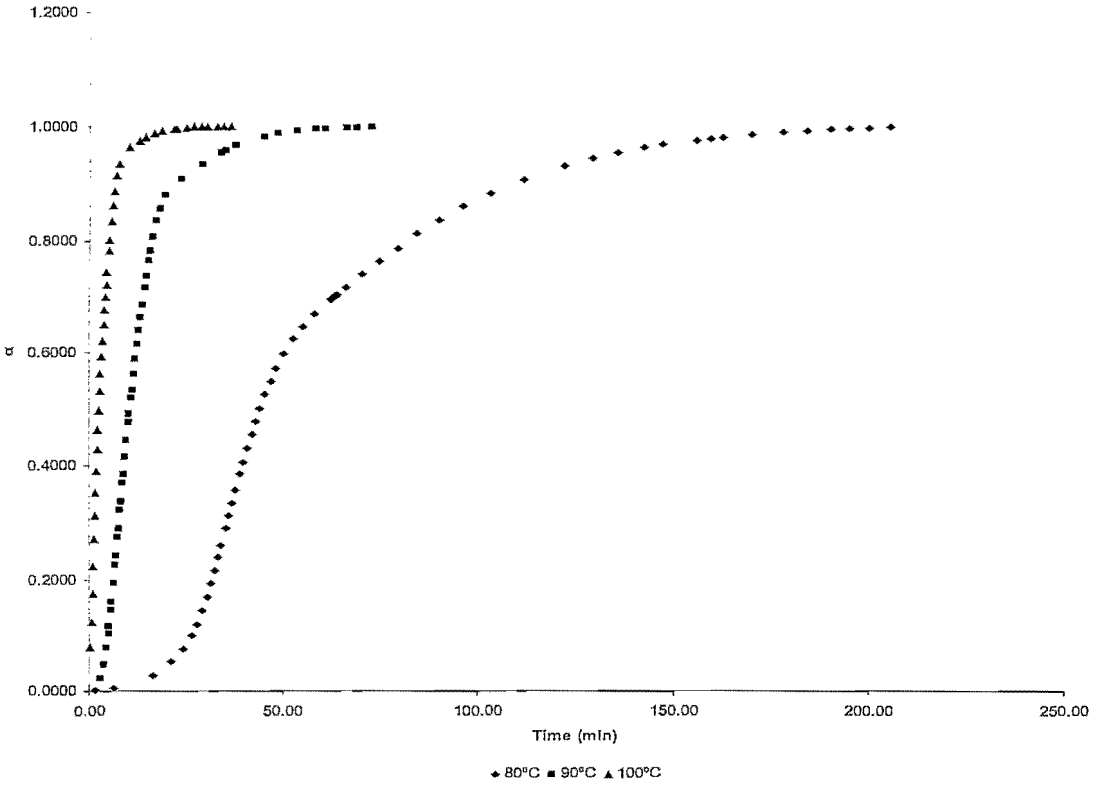

Figure 6.1 Desolvated fractions (α) of Form D plotted as a function of time (t).

From Figure 6.1 and Figure 6.2 it was evident that the rates of desolvation of Form D and Form E were temperature dependent. The rate of desolvation (for Form D and Form E) increased at higher temperatures.

The desolvated fractions (α) vs. time plots of Form D and Form E at 80°C revealed a lag-time, which produced sigmoidal curves. No lag-time was identified in the desolvated fractions (α) vs. time plots of Form D and Form E at 90°C and 100°C, which suggested that the mechanism of desolvation (i.e. kinetic mechanism) might differ at the different isothermal temperatures. Taylor & York (1998:215) confirmed that the mechanism of desolvation may be influenced by the temperature. Changes in the temperatures of desolvation induce changes in the mechanism of desolvation (Taylor & York, 1998:221).

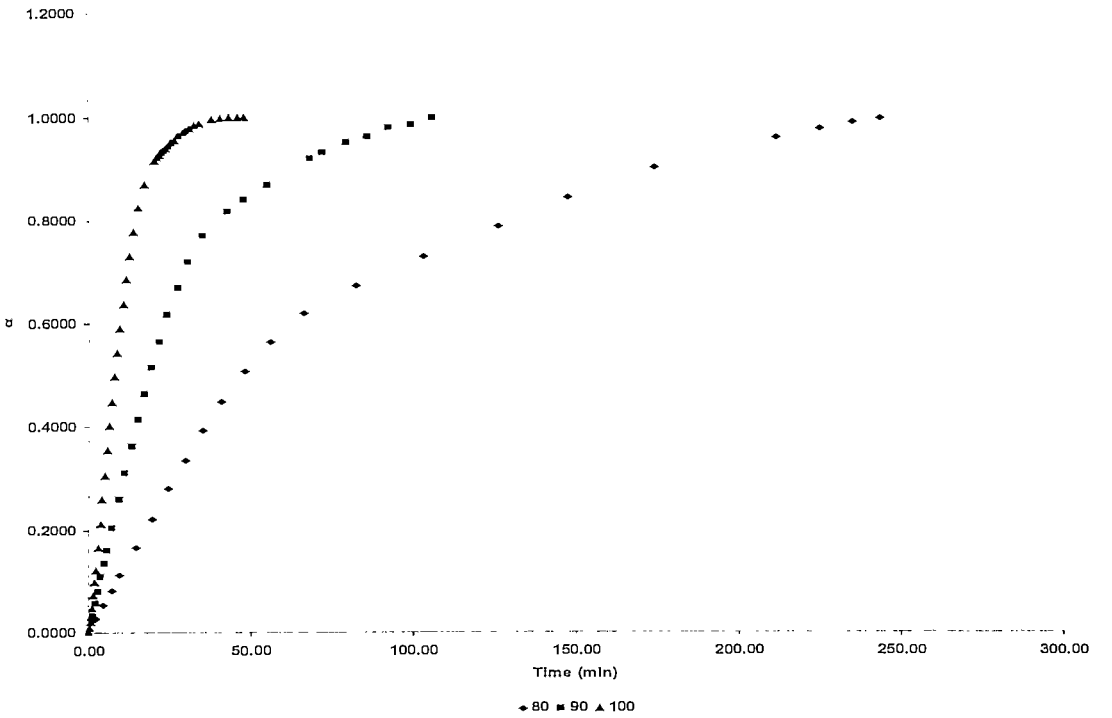

Figure 6.2 Desolvated fractions (α) of Form E plotted as a function of time (t).

The desolvated fraction values (α) at the predetermined intervals (t) were substituted into the mathematical integrated expressions (Table 6.1) to determine the model that best described the mechanism ($r^2 \approx 1.00$) for desolvation of Form D and Form E. From the plots made for each model, the regression values (r^2) were calculated and are tabulated in Table 6.2 and Table 6.3.

From the results in Table 6.2 and Table 6.3 it was concluded that the three-quarters order (F3/4) reaction described the desolvation of Form D at 80°C, while the Avrami-Erofeev reaction (A1,F1) described the desolvation reactions at 90 & 100°C (illustrated in Figure 6.5). An overview of the Avrami-Erofeev model is discussed in Chapter 7.

The Valensi reaction (D2) described the desolvation of Form E at 80°C, while the three-quarters order (F3/4) reaction described the desolvation at 90°C and the Avrami Erofeev reaction (A3/2) the desolvation reaction of Form E at 100°C (illustrated in Figure 6.6). It can therefore be concluded that the mechanism of desolvation of the solvated forms of mebendazole was affected by the desolvation temperatures.

Table 6.2 Regression values (r^2) calculated from the model-fitting of the desolvation of Form D

			r^2		
Sym.	**Model**	$g(\alpha)$	**80°C**	**90°C**	**100°C**
F1/3	One-third order	$1-(1-\alpha)^{2/3}$	0.8818	0.7509	0.6788
F3/4	Three-quarters order	$1-(1-\alpha)^{1/4}$	0.9871	0.9310	0.8861
F3/2	One and a half order	$(1-\alpha)^{-1/2}-1$	0.5683	0.8630	0.9226
F2	Second order	$(1-\alpha)^{-1}-1$	0.2404	0.6392	0.7602
F3	Third order	$(1-\alpha)^{-2}-1$	0.1090	0.3981	0.5703
P3/2	Mampel power law	$\alpha^{3/2}$	0.8492	0.6999	0.6096
P1/2	Mampel power law	$\alpha^{1/2}$	0.6452	0.5229	0.4677
P1/3	Mampel power law	$\alpha^{1/3}$	0.5799	0.4797	0.4363
P1/4	Mampel power law	$\alpha^{1/4}$	0.5411	0.4563	0.4199
E1	Exponential law	$\ln \alpha$	0.3998	0.3802	0.3680
A1,F1	Avrami-Erofeev equation	$-\ln(1-\alpha)$	0.9648	0.9933	0.9794
A3/2	Avrami-Erofeev equation	$[-\ln(1-\alpha)]^{2/3}$	0.9831	0.9566	0.9385
A2	Avrami-Erofeev equation	$[-\ln(1-\alpha)]^{1/2}$	0.9643	0.9154	0.9027
A3	Avrami-Erofeev equation	$[-\ln(1-\alpha)]^{1/3}$	0.9132	0.8536	0.8532
A4	Avrami-Erofeev equation	$[-\ln(1-\alpha)]^{1/4}$	0.8708	0.8141	0.8227
Au	Prout-Tompkins equation	$\ln[\alpha/(1-\alpha)]$	0.8970	0.9087	0.9319
R1,F0,P1	Power law	α	0.7739	0.6267	0.5482
R2,F1/2	Power law	$1-(1-\alpha)^{1/2}$	0.9336	0.8238	0.7589
R3,F2/3	Power law	$1-(1-\alpha)^{1/3}$	0.9746	0.8974	0.8445
D1	Parabola law	α^2	0.8969	0.7528	0.6562
D2	Valensi equation	$\alpha+(1-\alpha)\ln(1-\alpha)$	0.9625	0.8547	0.7615
D3	Jander equation	$[1-(1-\alpha)^{1/3}]^2$	0.9786	0.9859	0.9427
D4	Ginstling-Brounstein equation	$1-\frac{2}{3}\alpha-(1-\alpha)^{2/3}$	0.5250	0.3660	0.2311
D5	Zhuravlev, Lesokin, Tempelman equation	$[(1-\alpha)^{-1/3}-1]^2$	0.3510	0.7297	0.8373
D6	Anti-Jander equation	$[(1+\alpha)^{1/3}-1]^2$	0.8634	0.7145	0.6211
-	Anti-Ginstling-Brounstein equation	$1+\frac{2}{3}\alpha-(1+\alpha)^{2/3}$	0.8750	0.7274	0.6329
-	Anti-Zhuravlev, Lesokin, Tempelman equation	$[(1+\alpha)^{-1/3}-1]^2$	0.8291	0.6796	0.5857

Table 6.3 Regression values (r^2) calculated from the model-fitting of the desolvation of Form E

			r^2		
Sym.	**Model**	$g(\alpha)$	**80°C**	**90°C**	**100°C**
F1/3	One-third order	$1 - (1-\alpha)^{2/3}$	0.9531	0.9112	0.8694
F3/4	Three-quarters order	$1 - (1-\alpha)^{1/4}$	0.9889	0.9856	0.9861
F3/2	One and a half order	$(1-\alpha)^{-1/2}-1$	0.7079	0.5587	0.6240
F2	Second order	$(1-\alpha)^{-1}-1$	0.4652	0.2814	0.3882
F3	Third order	$(1-\alpha)^{-2}-1$	0.2588	0.1804	0.2254
P3/2	Mampel power law	$\alpha^{3/2}$	0.9469	0.8916	0.8349
P1/2	Mampel power law	$\alpha^{1/2}$	0.7610	0.7229	0.6857
P1/3	Mampel power law	$\alpha^{1/3}$	0.7072	0.6780	0.6326
P1/4	Mampel power law	$\alpha^{1/4}$	0.6777	0.6537	0.6007
E1	Exponential law	$\ln \alpha$	0.5811	0.5736	0.4798
A1,F1	Avrami-Erofeev equation	$-\ln(1-\alpha)$	0.9450	0.9463	0.9770
A3/2	Avrami-Erofeev equation	$[-\ln(1-\alpha)]^{2/3}$	0.9772	0.9728	0.9959
A2	Avrami-Erofeev equation	$[-\ln(1-\alpha)]^{1/2}$	0.9691	0.9590	0.9772
A3	Avrami-Erofeev equation	$[-\ln(1-\alpha)]^{1/3}$	0.9365	0.9224	0.9288
A4	Avrami-Erofeev equation	$[-\ln(1-\alpha)]^{1/4}$	0.9093	0.8949	0.8902
Au	Prout-Tompkins equation	$\ln[\alpha/(1-\alpha)]$	0.9236	0.9219	0.9282
R1,F0,P1	Power law	α	0.8802	0.8263	0.7843
R2,F1/2	Power law	$1-(1-\alpha)^{1/2}$	0.9792	0.9505	0.9191
R3,F2/3	Power law	$1-(1-\alpha)^{1/3}$	0.9907	0.9791	0.9674
D1	Parabola law	α^2	0.9802	0.9318	0.8641
D2	Valensi equation	$\alpha + (1-\alpha)\ln(1-\alpha)$	0.9984	0.9818	0.9234
D3	Jander equation	$[1-(1-\alpha)^{1/3}]^2$	0.9298	0.9608	0.9841
D4	Ginstling-Brounstein equation	$1 - \frac{2}{3}\alpha - (1-\alpha)^{2/3}$	0.6977	0.6371	0.5856
D5	Zhuravlev, Lesokin, Tempelman equation	$[(1-\alpha)^{-1/3}-1]^2$	0.5182	0.3453	0.4703
D6	Anti-Jander equation	$[(1+\alpha)^{1/3}-1]^2$	0.9594	0.9045	0.8437
-	Anti-Ginstling-Brounstein equation	$1 + \frac{2}{3}\alpha - (1+\alpha)^{2/3}$	0.9671	0.9140	0.8508
-	Anti-Zhuravlev, Lesokin, Tempelman equation	$[(1+\alpha)^{-1/3}-1]^2$	0.9323	0.8757	0.8256

6.3.1.1 Diffusion models and process of diffusion

The motion and rate by which the solvated molecules exit the crystal lattice during desolvation may be restricted, depending on the properties of the lattice. During diffusion controlled reactions the rate of desolvation is influenced by the thickness of the product-diffusion barrier layer, in other words the effort of solvent molecules to be released from the solvated-lattice (decrease in rate propotional to the thickness of the barrier) (Khawam, 2007:91).

The morphology of the desolvating particles also influences the diffusion model describing a specific reaction (Figure 6.3). Reactions containing flat plane particles are described by the one-dimensional (D1) model, spherical particles by the three-dimensional (D3) model and cylindrical particles by the two-dimensional (D2) model (Khawam, 2007:65-.67).

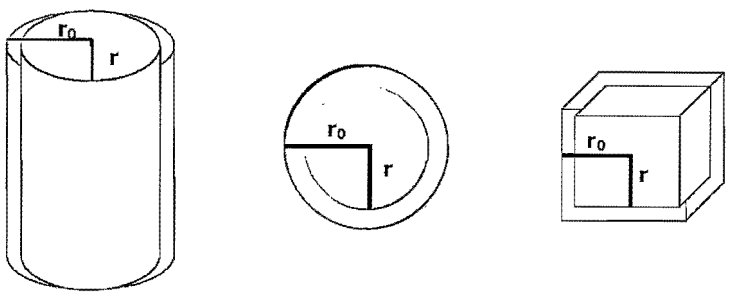

(a) (b) (c)

Figure 6.3 Geometrical crystal shapes. (a) Cylindrical, (b) Spherical and (c) cube (Khawam, 2007:79).

The two-dimensional model (D2) describes the diffusion of the molecules through a cylindrical shell with an increasing reaction zone (Khawam, 2007:67). The model is defined by Equation 6.11:

$$x = R(1-(1-\alpha)^{1/2}) \tag{6.11}$$

By incorporating the Jander approach ($k=k/R^2$), Equation 6.11 can be defined as Equation 6.12 (Khawam, 2007:68):

$$(1-(1-\alpha)^{1/2})^2 = kt \tag{6.12}$$

Fick's first law of diffusion is defined by Equation 6.13. If it is assumed that the diffusion rate at the interface of a cylindrical particle is faster ($C_1 \approx 0$) than the diffusion rate at the interface of a spherical particle, Equation 6.14 is utilised to determine the concentration of the reactant (Khawam, 2007:68).

$$C_r = \frac{C_1 \ln(b/r) + C_2 \ln(r/a)}{\ln(b/a)} \tag{6.13}$$

$$C_r = \frac{C_2 \ln(b/r)}{\ln(b/a)} \tag{6.14}$$

Where: C_r is the concentration of the reactant at a specific particle volume ($a<r<b$), and C_1 & C_2 the concentrations of the diffusing sample at the surface of the particle ($r=a$) and ($r=b$), respectively (Khawam, 2007:68).

The derivative of Equation 6.14 ($r=a$) provides Equation 6.15:

$$\frac{dC}{dr}\Big|_{r=a} = \frac{C_2}{a \ln(b/a)} \tag{6.15}$$

Where: dC/dr is the the diffusion rate.

The application of Equation 6.14 (in Figure 6.4) provides Equation 6.16 that illustrates the diffusion reaction from a cylindrical particle (Khawam, 2007:68):

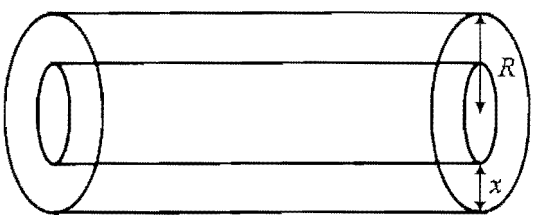

Figure 6.4 Schematic presentation of the reaction in a cylindrical particle (Khawam, 2007:81).

$$\frac{dC}{dr} = \frac{C_2}{(R-x)\ln(R/(R-x))} \tag{6.16}$$

Where: dC/dr is the diffusion rate, $a=(R-x)$ and $b=R$ (Khawam, 2007:68).

6.3.1.2 Order-based reaction models

For desolvation reactions that follow order-based models, the rate of the desolvation is proportional to the concentration of the remaining solvated fraction, raised to a particular power which is defined as the reaction order (n) and where n=0, 1, 2 or 3. Order-reaction models are described by Equation 6.17 (Khawam, 2007:70):

$$\frac{d\alpha}{dt} = k(1-\alpha)^n \tag{6.17}$$

Where: $d\alpha/dt$ is the reaction rate, α is the fraction of sample, k the rate constant and n the reaction order (Khawam, 2007:70).

6.3.1.3 Determination of rate of desolvation (i.e. rate constants (k)) of Form D and Form E

The rate constants (k) of Form D and Form E following desolvation at the various temperatures were determined from the slopes of the linear equations (based on Equation 6.4) reported in Figure 6.5 and Figure 6.6.

The rate constants confirmed that the order for the desolvation of Form D was: 100°C > 90°C > 80°C. The rate for the desolvation of Form D at 80°C was approximately 54 times lower compared to the rate of desolvation of Form D at 100°C.

The rate constants also confirmed that the order for the desolvation of Form E was: 100°C > 90°C > 80°C. The rate of desolvation of Form E at 80°C was approximately 19 times lower compared to the rate of desolvation of Form E at 100°C.

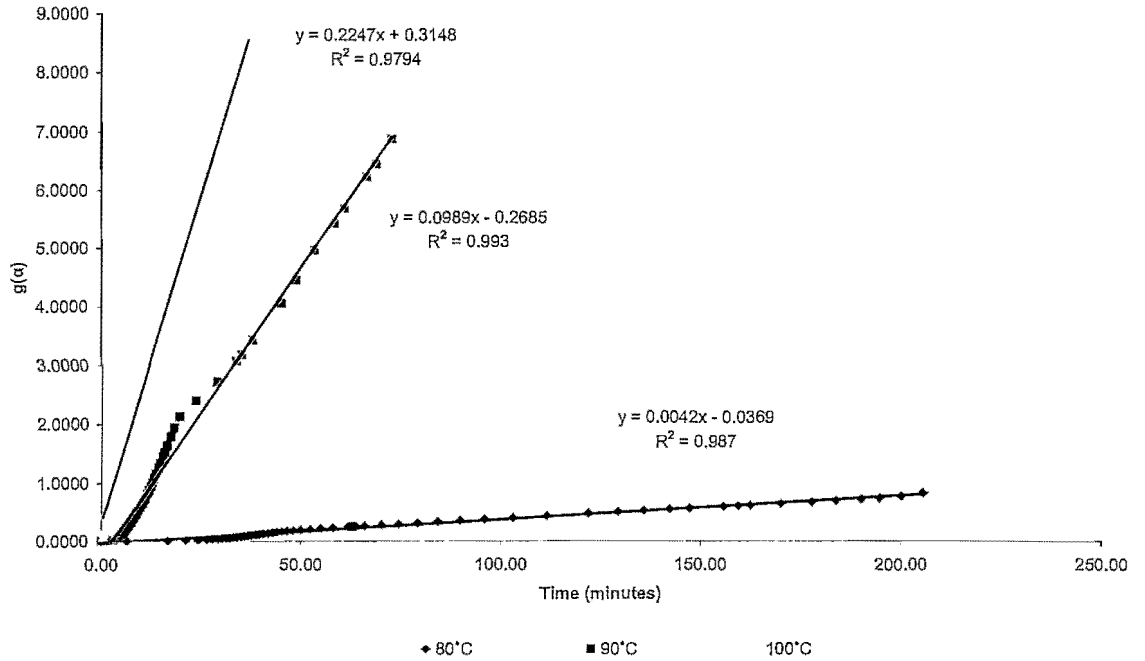

Figure 6.5 *g(α)* versus time plots for Form D when heated isothermally at: 80, 90 and 100°C.

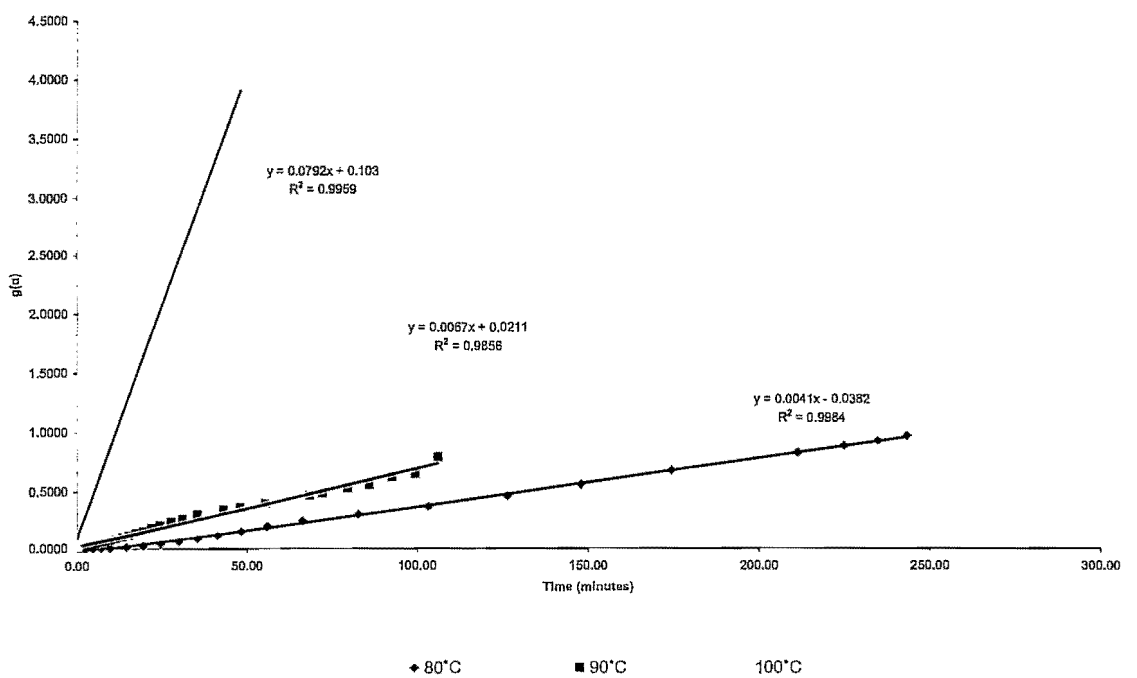

Figure 6.6 *g(α)* versus time plots for Form E when heated isothermally at: 80, 90 and 100°C.

In Chapter 4 (section 4.3.6) it was indicated that the desolvation of Form D was completed at 110°C and that of Form E at 130°C, which suggested that Form D was thermodynamically less stable compared to Form E, when exposed to increased temperatures. This observation was substantiated by indicating that the rate of desolvation of Form D at 80, 90 and 100°C was higher when compared to Form E (thus indicating that Form D was less stable at the mentioned temperatures).

Figure 6.7 illustrates that the rates of desolvation (rate constants) of Form D was significantly higher compared to that of Form E at 80, 90 and 100°C.

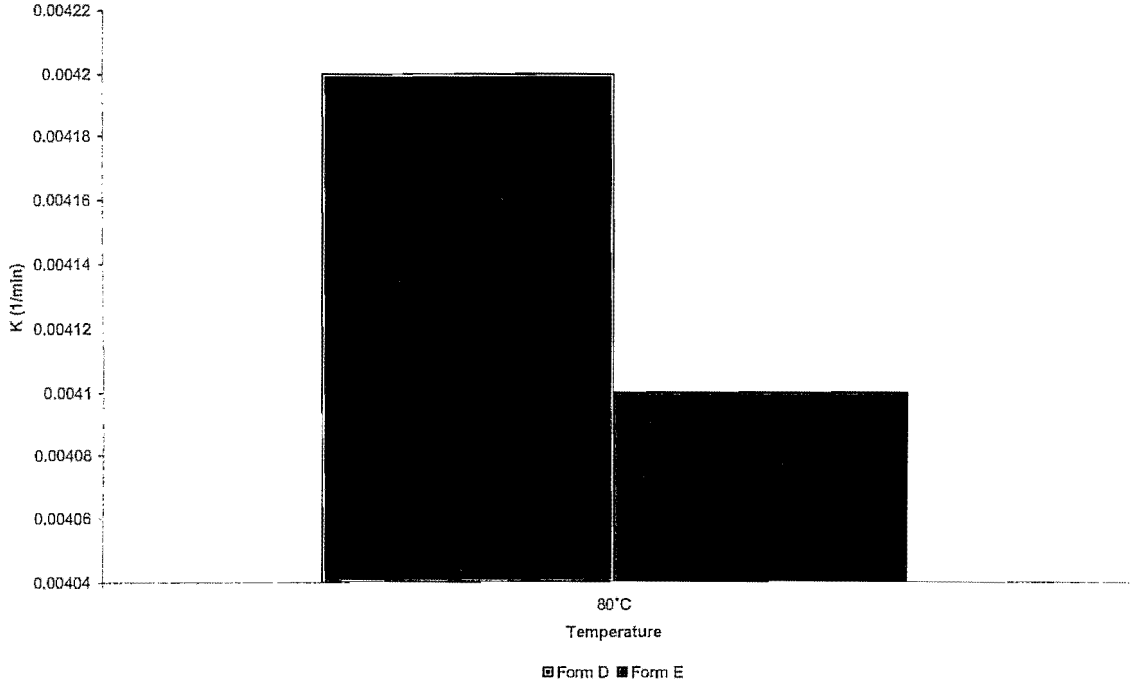

(a)

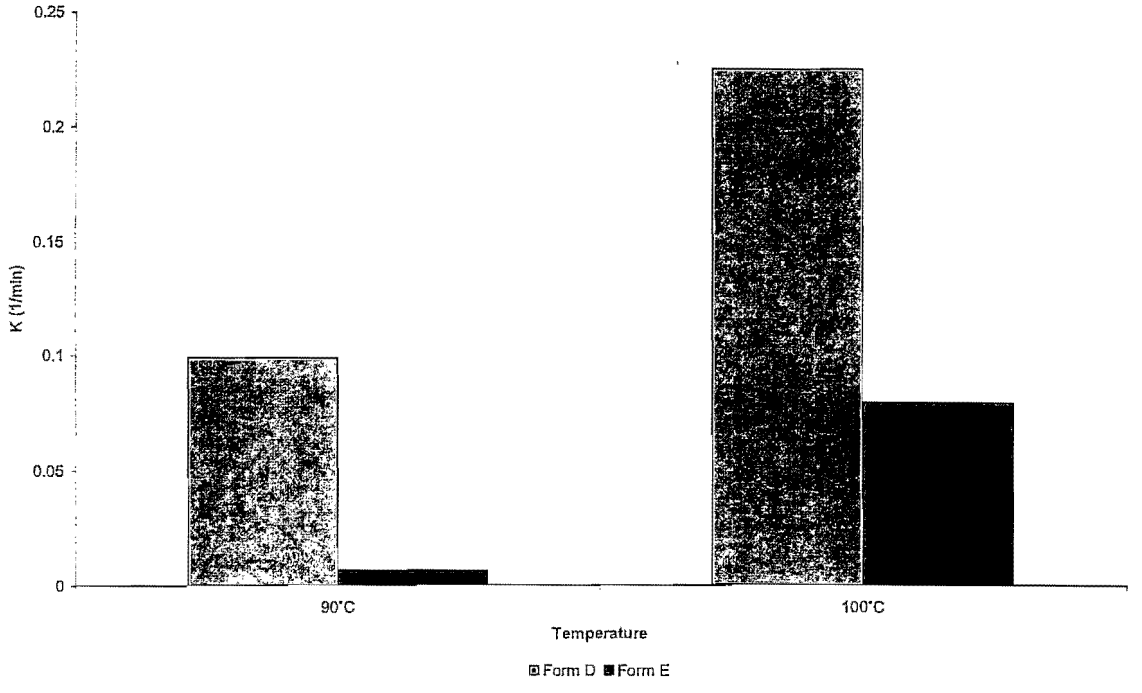

(b)

Figure 6.7 Rate constants (k) of Form D and Form E at: (a) 80°C, and (b) 90 and 100°C, indicating that Form E desolvated at lower rates compared to Form D.

6.3.2 Non-isothermal kinetic analysis of Form D and Form E

The activation energy (E_a) for the desolvation of Form D and Form E was calculated from the TGA data, utilising the method described by Flynn and Wall (1966:323-328). The method involved the analysis of the weight loss (mg) versus temperature (T) thermograms at the different heating rates (β), to determine the corresponding temperatures (in Kelvin) at constant weight losses.

The TGA thermograms of Form D and Form E at the various heating rates (β = 2, 3, 5, 7, 10°C/min) are depicted in Figure 6.8 and Figure 6.9.

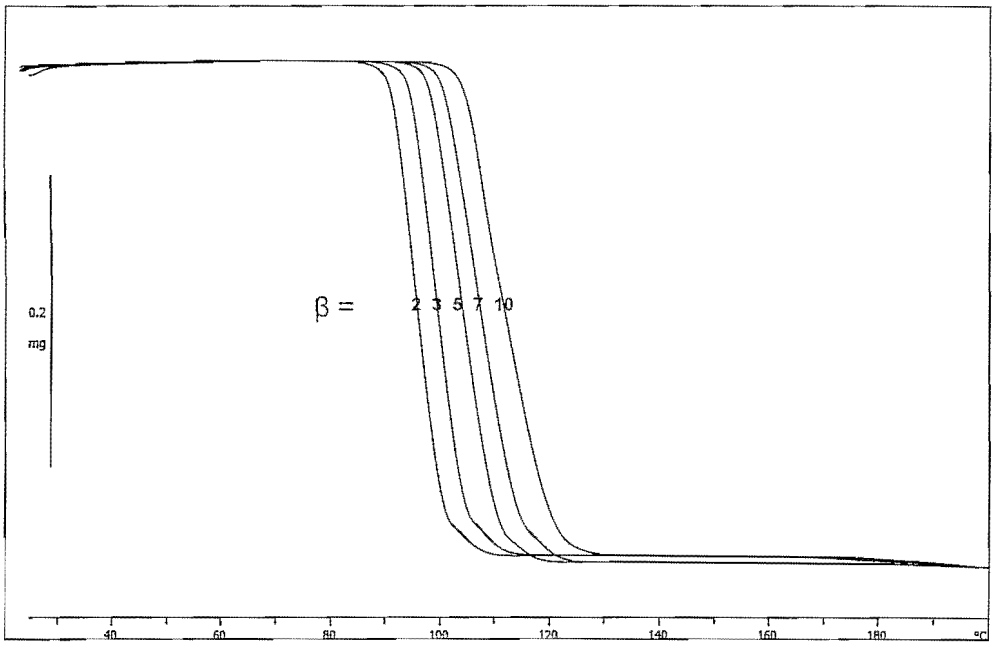

Figure 6.8 TGA thermograms of mebendazole Form D at heating rates (β) of 2, 3, 5, 7 and 10°C/min.

From the TGA thermograms of Form D it was evident that only one desolvation (mass loss) reaction occurred in the temperature range of 25-200°C.

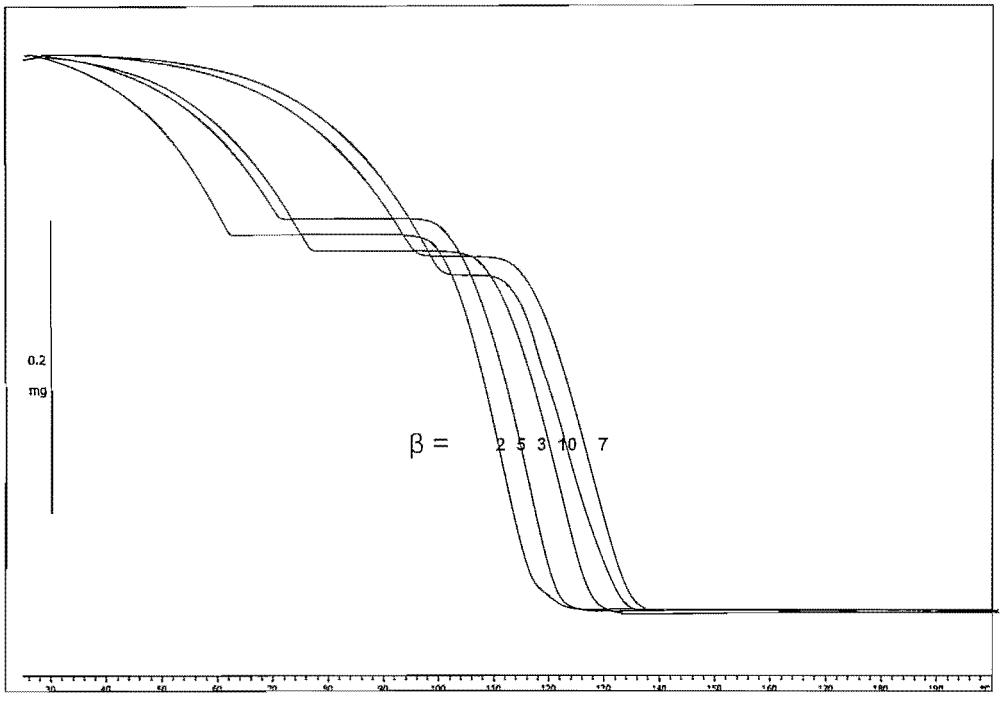

(a)

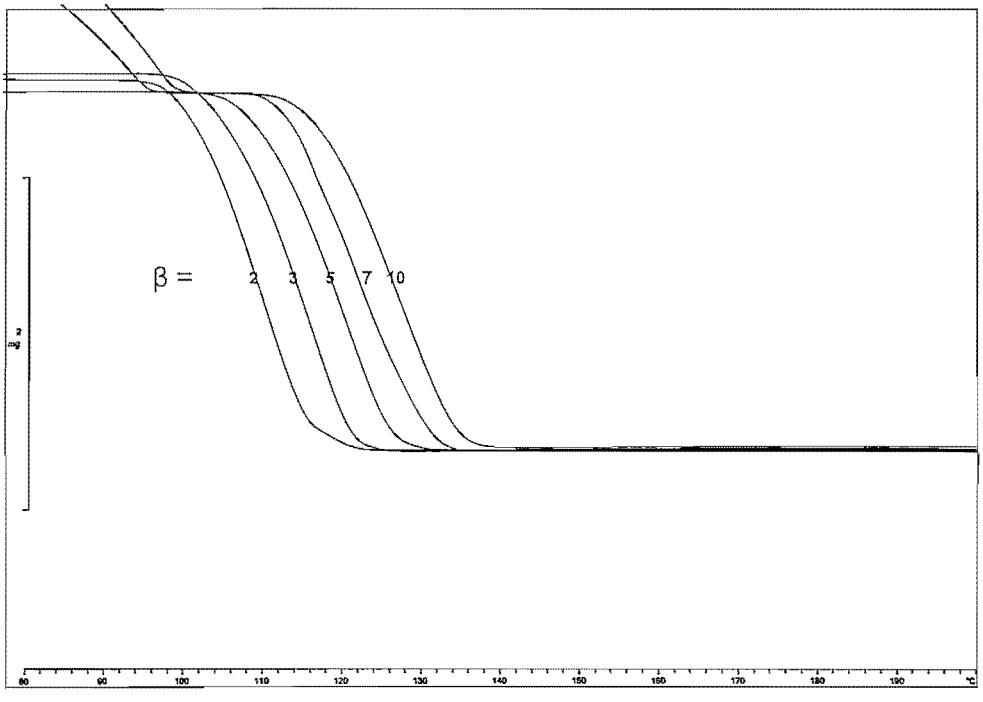

(b)

Figure 6.9 TGA thermograms of mebendazole Form E at heating rates (β) of 2, 3, 5, 7 and 10°C/min between (a) 25-200°C and (b) 100-200°C.

The TGA thermograms of Form E showed two desolvation steps (section 4.3.3) in the range of 25-100°C and 100-200°C respectively. The solvent loss at 25-100°C (Figure 6.9 (a)) was attributed to the loss of adsorbed solvent molecules on the crystal surface (Chapter 4, Section 4.3.3). Caira *et al* (1998:12) reported the main desolvation process of Form E to occur between the temperature regions of 100-200°C. The focus of this study was on the desolvation step which occurred in the 100-200°C regions (Figure 6.9 (b)).

The desolvation activation energies (E_a) for both Form D and Form E were determined using the Ozawa-Flynn-Wall equation (Equation 6.18) (Rodante *et al.*, 2002:1036):

$$\log\beta = -0.4567(E_a / RT) - 2.3115 + \log(AE_a / R) - \log[g(\alpha)] \qquad (6.18)$$

Where: β is the heating rate (°C/min) of the sample, A is the pre-exponential factor (min^{-1}) and R is the universal gas constant (8.314 $J.K^{-1}.mol^{-1}$).

The desolvated fractions (α) were calculated using Equation 6.10 and were plotted against the absolute temperature (T) for both Form D and Form E, at the various heating rates (β) (Figure 6.10 and Figure 6.11).

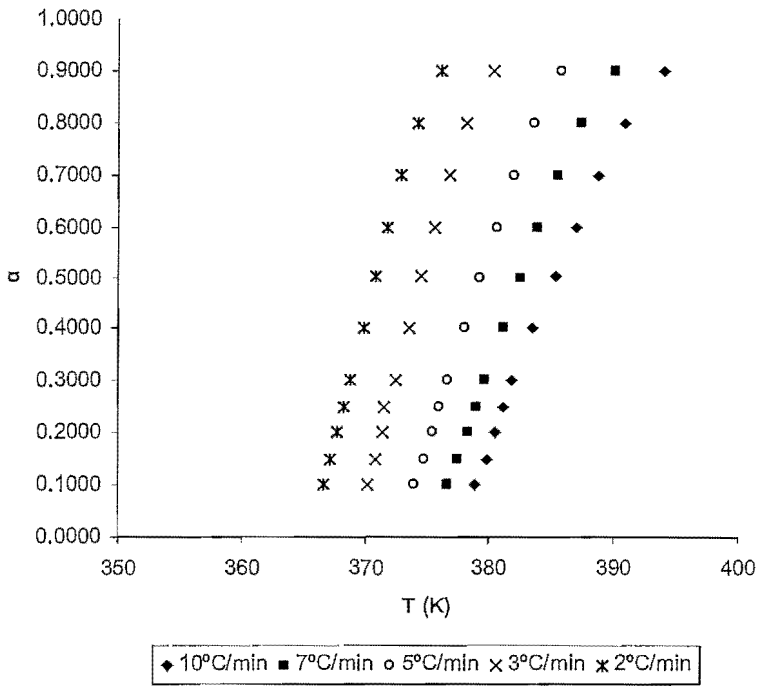

Figure 6.10 Desolvated fraction (α) plotted against the absolute temperature (T) for mebendazole Form D at various heating rates (2, 3, 5, 7, and 10°C/min).

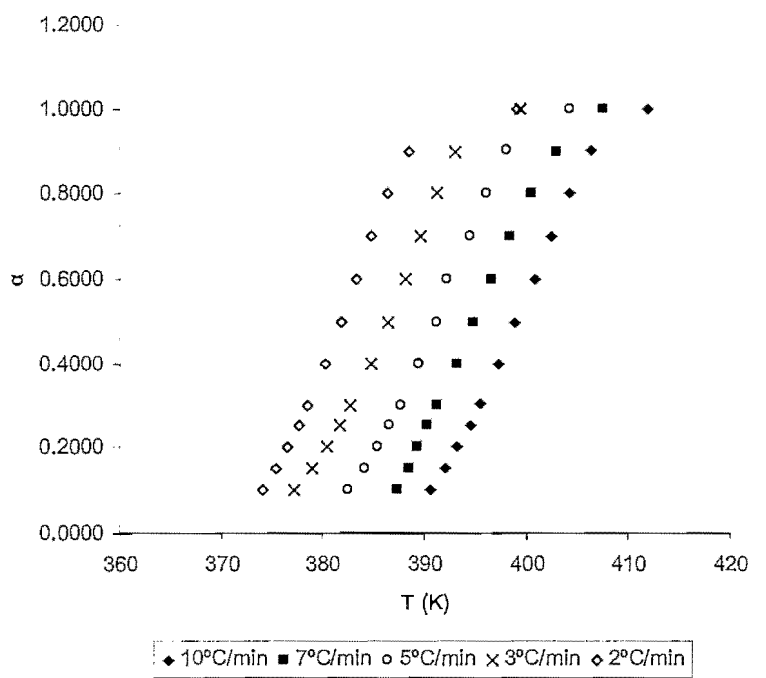

Figure 6.11 Desolvated fraction (α) plotted against the absolute temperature (T) for mebendazole Form E at various heating rates (2, 3, 5, 7, and 10°C/min).

The natural logarithm of the heating rates ($log\ \beta$) was plotted against $1/T$ for both Form D and Form E (Figure 6.12 and Figure 6.13). The desolvation energies (E_a) were determined for both solvated forms from the slopes (m) of the parallel lines (in Figure 6.12 and Figure 6.13) using Equation 6.19.

$$m = \frac{-0.4567E_a}{R} \tag{6.19}$$

Where: m is the slope of the parallel line, E_a the activation energy and R the universal gas constant (8.314 $J.K^{-1}.mol^{-1}$) (Brits, 2008:393).

The desolvation activation energy of Form D and Form E are listed in Table 6.4. The desolvation activation energy (E_a) of Form E was found to be 0.3 $kJ.mole^{-1}$ (3.03%) higher than that of Form D, confirming that Form E may be considered to be the thermodynamically more stable pseudo-polymorph of mebendazole.

Table 6.4 Desolvation activation energy (E_a) of mebendazole Form D and Form E calculated using the Ozawa-Flynn-Wall method

Form D	Form E
9.6 kJ/mol	9.9 kJ/mol

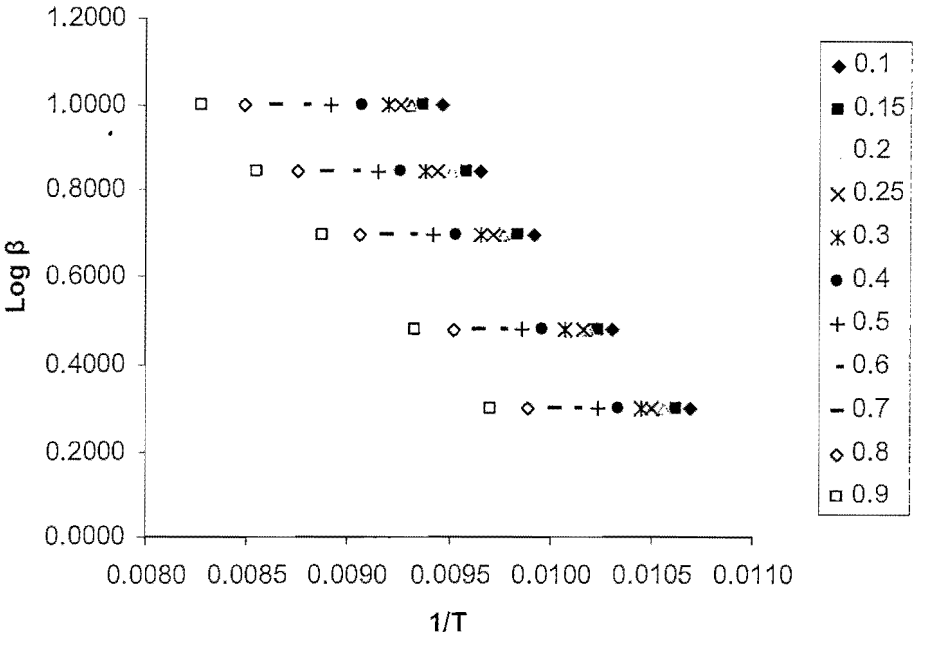

Figure 6.12 Log β plotted against $1/T$ for mebendazole Form D for the α values ranging between 0.10-0.90.

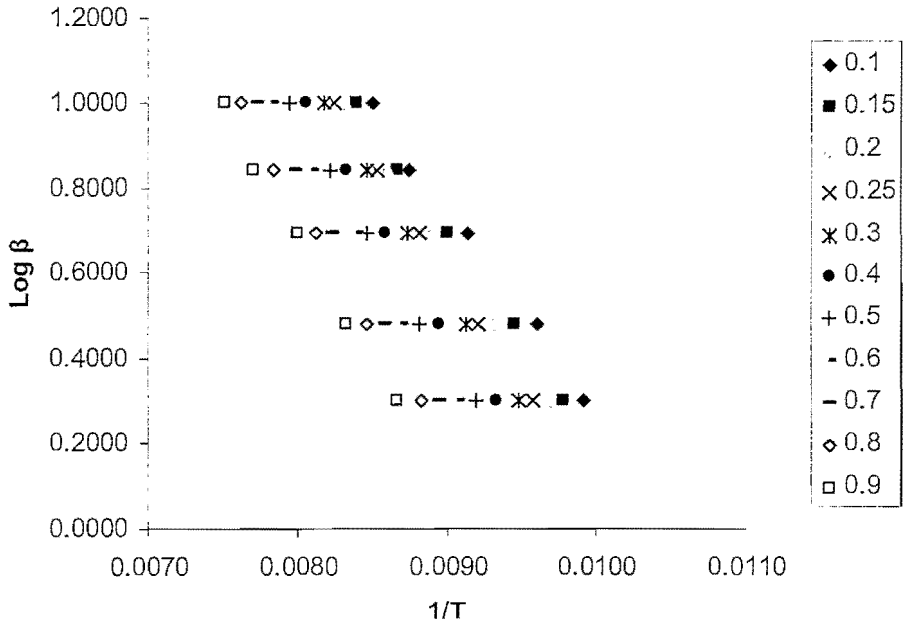

Figure 6.13 Log β plotted against $1/T$ for mebendazole Form E for the α values ranging between 0.10-0.90.

Conclusion

When Form D and Form E are desolvated, the desolvated lattices are transformed into the thermodynamically stable form, Form A. Isothermal and non-isothermal kinetic analysis were used to evaluate the stability and mechanism of desolvation for Form D and Form E.

The results obtained in this study revealed that Form E could be considered more stable than Form D by virtue of the higher (0.3 k.J.mol-1) activation energy needed for the desolvation of Form E. The mechanism (or model) of desolvation for the solvated forms of mebendazole (Table 6.5) was found to be temperature dependant at isothermal conditions.

Table 6.5 Model of desolvation for mebendazole Form D and Form E at different temperatures

Form	Temperature	Desolvation model
Form D	80°C	Three-quarters order
Form E	80°C	Valensi diffusion model
Form D	90°C	Avrami-Erofeev model
Form E	90°C	Three-quarters order
Form D	100°C	Avrami-Erofeev model
Form E	100°C	Avrami-Erofeev model

The rate constants (k) confirmed that the order of desolvation of Form D was: 100°C > 90°C > 80°C. The rate of desolvation of Form D (at 80°C) was approximately 54 times lower compared to the rate of desolvation of Form D at 100°C.

The rate constants (k) revealed that the order of desolvation of Form D was: 100°C > 90°C > 80°C. The rate of desolvation of Form E (at 80°C) was approximately 19 times lower compared to the rate of desolvation of Form E at 100°C.

The effect of increased temperatures and humidity on the stability of the solvated forms (i.e. Form D and Form E) will be discussed in Chapter 7.

CHAPTER 7

Thermodynamic stability of the mebendazole pseudo-polymorphic forms

Introduction

APIs can be classified as: crystalline, amorphous, solvated, hydrated or as hydrated-solvates (refer to Chapter 1). The physico-chemical properties (i.e. solubility, thermodynamic stability, dissolution profiles, etc.) of these different types of solids may differ significantly and influence the efficacy of the pharmaceutical dosage form (Stephenson *et al.*, 2001:67). One of the most important challenges in drug development is to ensure that the crystal form present in the pharmaceutical dosage form remains unchanged during the manufacturing and shelf-life of the product (Byrn *et al.*, 1999:516; Waterman *et al.*, 2005:101).

Physical stability, refers to the stability of the crystal form with respect to polymorphic or phase transformations i.e. transition to another polymorphic or crystal form, desolvation, etc. (Byrn *et al.*, 1999:513; Phipps *et al.*, 2000:9). The stability rules of polymorphic forms were discussed in Chapter 1 (Section 1.7).

Chapter 6 revealed that Form E was more stable than Form D at increased temperatures, due to the lower activation energy needed for desolvation.

The purpose of this chapter was to investigate the physical stability of the two pseudo-polymorphic forms of mebendazole (Forms D and E) by means of accelerated stability testing.

7.1 Apparatus

Binder KBF720 Climatic chambers (Apollo Scientific, Northriding, South Africa) were used during the stability study. Two individually programmed incubators were used to simulate the following conditions: 25±2℃ & 60±5 % RH and 40±2℃ & 75±5 % RH.

The temperature and humidity control of the two chambers were maintained and monitored with the APT-Com (version 3.0) software (Binder GmbH, Tuttingen, Germany).

7.2 Stability study protocol

The physical stability of the acetic acid solvate (Form D) and propionic acid solvate (Form E) was investigated after the mentioned forms were exposed to the following conditions: (1) 25±2 ℃ & 60±5 % RH, (2) 40±2 ℃ & 75±5 % RH, (3) 25±2 ℃ & 0 % RH and (4) 40±2 ℃ & 0 % RH.

The two solvated forms of mebendazole were prepared as discussed in Chapter 4 (section 4.2). For each of the solvated forms approximately 200 mg of sample were weighed into weighing boats and ampoules. The air in the ampoules was replaced with nitrogen gas to create a "dry" environment (≈ 0 % RH) and sealed thereafter. The samples were then stored in stability chambers at 25±2℃ & 60±5 % RH and 40±2℃ & 75±5 % RH respectively.

Figure 7.1 provides a stability matrix and illustrates the storage of the samples in the stability chambers. Samples were withdrawn after 3, 7, 14, 21 and 28 days respectively and analysed.

Table 7.1 summarises the characteristic differences of the polymorphic forms of mebendazole as determined from the literature (also refer to Chapter 3, section 3.3), with the addition of the characteristic properties of Forms D and E, as determined in Chapter 4.

Relative humidity	Temperature: 25±2 °C	40±2 °C
0±5 %	√	√
60±5 %	√	
75±5 %		√

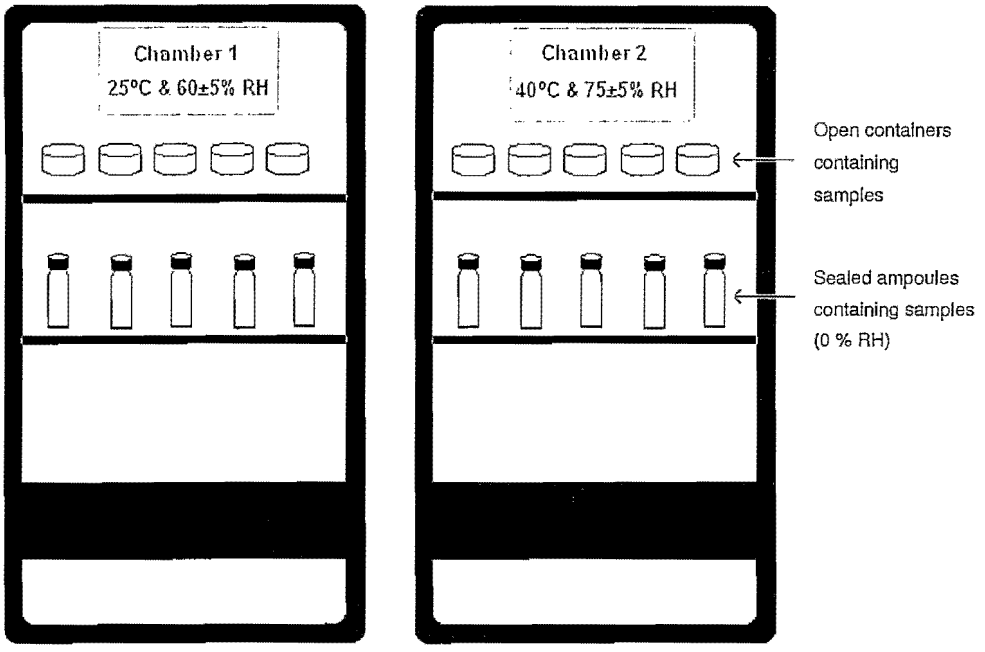

Figure 7.1 Stability matrix and schematic presentation of the storage conditions for the samples during the stability trial.

Table 7.1 Summary of the characteristic physico-chemical properties of the polymorphic and pseudo-polymorphic forms of mebendazole

Technique	Form A	Form B	Form C	Form D	Form E
DRIFT IR (-NH) (cm^{-1})	3370 [1]	3340 [1]	3410 [1]	3353	3364
DRIFT IR (>C=O) (cm^{-1})	1730 [1]	1700 [1]	1720 [1]	1738	1735
XRPD (°2θ)	7.6 [2] 17.3 *	5.8 [2]	4.9 [2]	6.6 7.9 13.2	6.3 8.0 12.6
DSC (°C)	250-255 [3] 330 [3]	220 [3] 263 [3] 330 [3]	195 [3] 225 [3] 253 [3] 330 [3]	109 256 331	124 254 331
TGA Range 100-200 °C	N/A	N/A	N/A	15.40%	20.76%

(*) The 17.3°2θ peak did not show any peak overlapping with peaks associated with Form D and / or Form E, and was thus identified as a characteristic peak of Form A. The 17.3°2θ peak was utilised in the stability study of Form D and Form E to determine the presence of polymorphic conversion.

[1] Himmelreich *et al.* (1977:123)

[2] Brits (2008:70)

[3] De Villiers *et al.*(2005:438)

7.3 Physical stability determination of Form D and Form E when exposed to elevated temperatures and humidities

The rate and extent of polymorphic conversion in the samples at the mentioned intervals were investigated using DRIFT-IR, XRPD, DSC and TGA as described in Chapter 3.

The main IR identification peaks (-NH and >C=O stretching frequency) used for the determination of the polymorphic form of mebendazole as described and used by Himmelreich *et al.* (1977:123) were used to identify the polymorphic form present in the samples at the specific time intervals. Table 7.2 summarises the polymorphic forms present in the samples as derived from the DRIFT-IR data.

The XRPD analysis was based on the main identification peaks as described by Brits (2008:70). Table 7.3 summarises the polymorphic forms present in the samples as derived from the XRPD data. The DSC and TGA observations are summarised in Table 7.4 and Table 7.5.

7.3.1 Calculation of desolvation factor (D_f)

The extent to which desolvation occurred in the solvated systems were investigated by means of a desolvation factor, which was calculated from the DSC and TGA results. The desolvation factor (D_{f1}) calculated from the DSC data indicated the changes in the desolvation enthalpy (ΔH_{Di}) using the initial desolvation enthalpy (ΔH_{Do}) as the point of reference (Equation 7.1).

$$D_{f1} = \frac{\Delta H_{Di}}{\Delta H_{Do}} \tag{7.1}$$

Where: D_{f1} is the desolvation factor, ΔH_{Di} the desolvation enthalpy at interval i and ΔH_{Do} the desolvation enthalpy of the solvated sample at interval 0.

The desolvation factor (D_{f2}) calculated from the TGA data indicated the changes in the desolvation mass loss (m_i) (associated with desolvation), using the initial desolvation mass loss (m_o) as the point of reference (Equation 7.2).

$$D_{f2} = \frac{m_i}{m_o} \tag{7.2}$$

Where: D_{f2} is the desolvation factor, m_i the mass loss at interval i (associated with desolvation) and m_o the mass loss of the solvated sample at interval 0.

A decrease in the desolvation factor (D_f) indicates a decrease in the solvated fraction present in the sample.

Table 7.3 Mebendazole polymorphic forms present in the samples derived from the XRPD data for the stability study

Form	Interval (days)	Solvate (°2θ)	*i*	Polymorphic form	Solvate (°2θ)	*i*	Polymorphic from
		25±2°C & 0 % RH			40±2°C & 0 % RH		
Form D	Initial	6.62 13.17	1236 1425	D	6.62 13.17	1236 1425	D
	3	6.50 7.79	855 763	D	7.71 17.32	3539 623	A
	7	6.56 7.84 17.35	801 751 115	D with traces of A	7.71 17.31	2897 442	A
	14	6.53 7.76 17.33	661 812 284	D with traces of A	7.71 17.32	3085 430	A
	21	6.52 7.72 17.32	299 1656 699	D with traces of A	7.71 17.34	4270 547	A
	28	6.50 7.70 17.30	269 1127 547	D with traces of A	7.80 17.42	2555 693	A
		25±2°C & 60±5 % RH			40±2°C & 75±5 % RH		
Form D	Initial	6.62 13.17	1236 1425	D	6.62 13.17	1236 1425	D
	3	6.51 17.33	1503 151	D with traces of A	7.66 17.33	2441 959	A
	7	6.59 7.76 17.40	401 1568 675	D with traces of A	7.76 17.41	2404 960	A
	14	6.57 7.70 17.36	56 1551 669	D with traces of A	7.70 17.35	2602 1039	A
	21	7.72 17.39	2320 905	A	7.68 17.36	2423 992	A
	28	7.69 17.35	2061 827	A	7.73 17.40	2657 1034	A

Table 7.3 (Continued)

Form	Interval (days)	Solvate (°2θ)	i	Polymorphic form	Solvate (°2θ)	i	Polymorphic form
		25±2°C & 0 % RH			40±2°C & 0 % RH		
Form E	Initial	6.27 8.00 12.59	16891 1714 5836	E	6.27 8.00 12.59	16891 1714 5836	E
	3	6.31 8.07 12.63	6717 1003 4419	E	6.32 8.03 12.65	12416 1018 7271	E
	7	6.33 8.08 12.66	9776 1051 6911	E	6.34 8.05 12.66	7715 1157 6023	E
	14	6.34 8.06 12.65	10230 1120 8143	E	6.34 7.75 8.09 12.66 17.34	4401 184 827 2506 69	E with traces of A
	21	6.30 8.03 12.64	3197 693 3873	E	6.34 7.72 8.08 12.65 17.33	11559 1003 1188 6391 196	E with traces of A
	28	6.37 8.12 12.68	5024 1552 3885	E	6.32 7.72 8.05 12.65 17.35	6237 1252 1249 4768 295	E with traces of A

Table 7.3 (Continued)

Form	Interval (days)	Solvate (°2θ)	*i*	Polymorphic form	Solvate (°2θ)	*i*	Polymorphic form
		25±2°C & 60±5 % RH			40±2°C & 75±5 % RH		
Form E	Initial	6.27 8.00 12.59	16891 1714 5836	E	6.27 8.00 12.59	16891 1714 5836	E
	3	6.33 8.05 12.59 17.40	7669 1111 3579 45	E with traces of A	6.38 7.74 8.10 12.67 17.41	1260 1840 138 682 3080	E with traces of A
	7	6.33 7.76 8.09 12.59 17.40	4663 113 700 1973 153	E with traces of A	7.66 8.61 17.30	1147 84 2815	A
	14	6.32 7.69 8.05 12.65 17.34	3294 6201 734 2626 366	E with traces of A	7.65 8.60 17.28	1888 81 2943	A
	21	6.30 7.67 8.04 12.60 17.32	3141 325 545 2665 646	E with traces of A	7.66 8.61 17.30	1466 76 2905	A
	28	6.30 7.67 8.03 12.62 17.31	2930 407 477 1713 967	E with traces of A	7.65 8.62 17.29	1547 84 2410	A

Table 7.4 DSC data of Form D and Form E during the stability study

Form	Interval (days)	Solvate peak (°C)	Enthalpy (ΔH) ($J.g^{-1}$)	Solvate peak (°C)	Enthalpy (ΔH) ($J.g^{-1}$)
		25±2°C & 0 % RH		40±2°C & 0 % RH	
Form D	Initial	109.26	162.44	109.26	162.44
	3	109.92	149.89	-	-
	7	108.73	139.08	-	-
	14	109.99	99.90	-	-
	21	111.39	33.07	-	-
	28	110.35	63.28	-	-
		25±2°C & 60±5 % RH		40±2°C & 75±5 % RH	
Form D	Initial	109.26	162.44	109.26	162.44
	3	103.66	144.11	-	-
	7	97.95	39.05	-	-
	14	112.80	2.25	-	-
	21	-	-	-	-
	28	-	-	-	-
		25±2°C & 0 % RH		40±2°C & 0 % RH	
Form E	Initial	127.82	178.47	127.82	178.47
	3	124.95	169.51	119.98	172.87
	7	118.75 130.56	176.86	128.86	178.00
	14	118.45 130.28	165.10	117.45 127.34	156.80
	21	129.26	165.58	120.68	135.84
	28	129.08	175.16	120.02	128.63
		25±2°C & 60±5 % RH		40±2°C & 75±5 % RH	
Form E	Initial	127.82	178.47	127.82	178.47
	3	125.32	174.86	122.77	38.08
	7	127.14	168.36	-	-
	14	125.98	145.15	-	-
	21	125.54	94.43	-	-
	28	123.33	99.43	-	-

Table 7.5 TGA data of Form D and Form E during the stability study

Form	Interval (days)	% mass loss	% mass loss
		25±2°C & 0 % RH	40±2°C & 0 % RH
Form D	Initial	15.40	15.40
	3	15.07	33.45
	7	13.09	37.20
	14	9.58	35.11
	21	2.55	39.91
	28	5.59	32.70
		25±2°C & 60±5 % RH	40±2°C & 75±5 % RH
Form D	Initial	15.40	15.40
	3	13.90	-
	7	3.23	-
	14	-	-
	21	-	-
	28	-	-
		25±2°C & 0 % RH	40±2°C & 0% RH
Form E	Initial	20.76	20.76
	3	22.04	19.13
	7	19.61	21.49
	14	19.32	18.45
	21	19.72	16.65
	28	19.72	14.50
		25±2°C & 60±5 % RH	40±2°C & 75±5 % RH
Form E	Initial	20.76	20.76
	3	19.52	4.10
	7	17.12	-
	14	14.11	-
	21	11.57	-
	28	12.32	-

7.3.2 Mebendazole acetic acid solvate (Form D) stored at 25±2°C & 0 % RH

The DRIFT-IR spectra of Form D stored at 25±2°C & 0 % RH are shown in Figure 7.2 and the peaks are listed in Table 7.2. From the DRIFT-IR spectra it was clear that the decrease in the intensity of the 3353 cm^{-1} and 1738 cm^{-1} bands (characteristic of Form D) and the increase of the 3369 cm^{-1} and 1730 cm^{-1} bands (characteristic of Form A), indicated that the onset of desolvation occurred after 3 days. The sample did not desolvate entirely. Traces of Form D were still detected after 28 days.

The XRPD patterns of Form D stored at 25±2°C & 0 % RH are shown in Figure 7.3 and the main diffraction angles (°2θ) and corresponding peak intensities (*i*) are listed in Table 7.3. The disappearance of the characteristic peak of Form D (6.6±0.1°2θ) and the appearance of the characteristic peak of Form A (17.3±0.1°2θ) after 7 days confirmed the DRIFT-IR desolvation results.

Various authors (Bunaciu *et al.*, 2002:647, Brits, 2008:114 and Liebenberg *et al.*, 1998:487) revealed that the detection of Form A (using XRPD) was delayed due to the amorphous-like behaviour of mebendazole and that infrared spectroscopy has emerged as the preferred method for the identification of mebendazole polymorphic forms.

The DSC thermograms depicted in Figure 7.4 and data listed in Table 7.4 showed a decrease in the integrated intensity of the desolvation endotherm (162.44 – 63.28 $J.mol^{-1}$) of Form D. The percentage (%) mass loss of the sample (Table 7.5) decreased from 15.40 - 5.59 % during the 28 days, confirming the desolvation process.

The desolvation factor (D_{f2}) calculated from the TGA data decreased as a function of time and revealed a minimum after 21 days, confirming the presence of solvated fractions in the sample (as observed with XRPD and DRIFT-IR data). A slight increase in the desolvation factor (D_{f2}) (+0.19) was observed on day 28, indicating that a greater solvated fraction was present in the sample tested on day 28 (Figure 7.5).

The desolvation factor (D_{f1}) calculated from the DSC data was concurrent with that calculated from the TGA data. The decrease in the D_{f1} values indicated that the energy needed for desolvation decreased as a function of the solvated fraction present in the samples, due to the fact that Form D underwent desolvation when stored at 25±2°C & 0 % RH. The slight increase in the desolvation factor D_{f2} was verified by a similar increase (+0.19) in the D_{f1} value on day 28 (Figure 7.5) and the fact that the percentage (%) weight loss was 2.19% higher on day 28 compared to that on day 21.

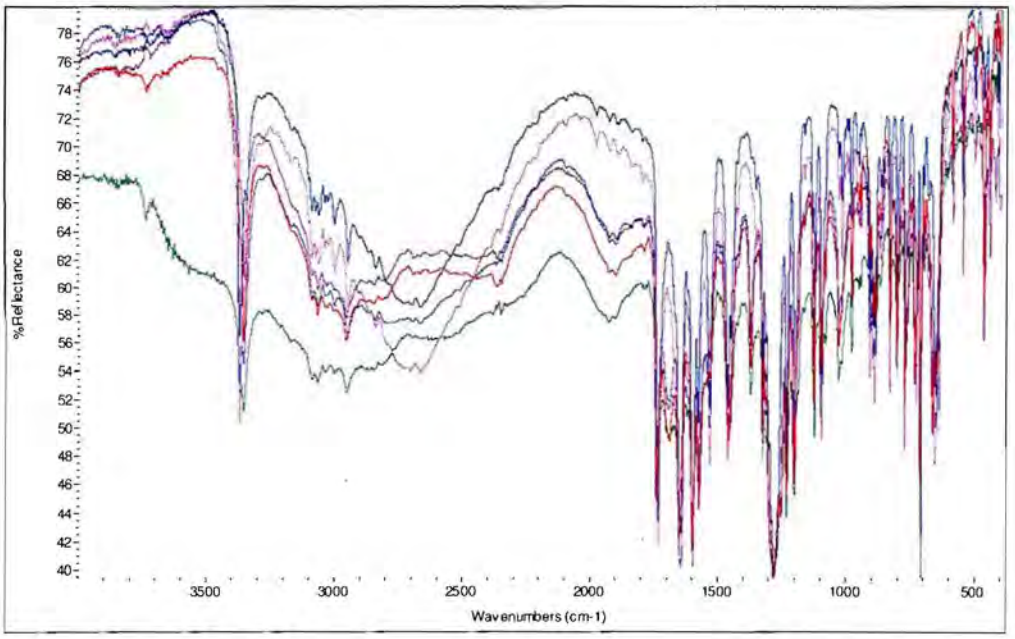

(a)

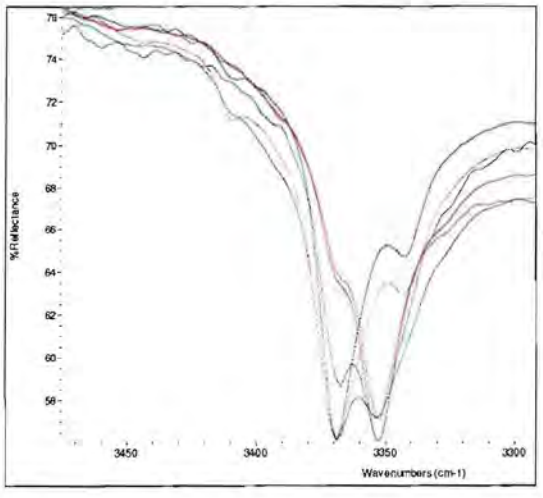

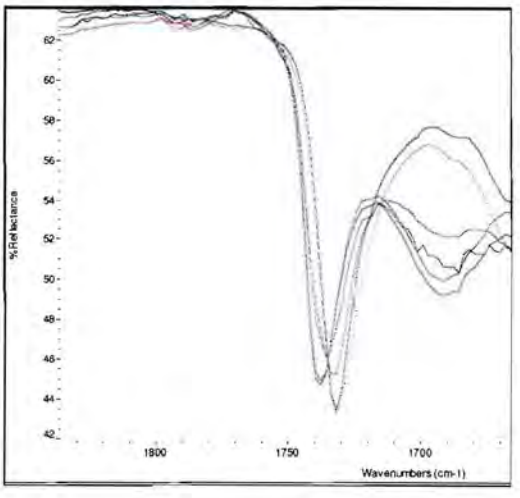

(b) (c)

Figure 7.2 (a) IR overlay spectra of the mebendazole acetic acid solvate (Form D) stored at 25±2℃ & 0 % RH for twenty-eight days. (b and c) Superimposed DRIFT-IR spectra of the main absorptions at the –NH and >C=O stretching frequencies showing polymorphic transition in the sample (initial, 3, 7, 14, 21 and 28 days).

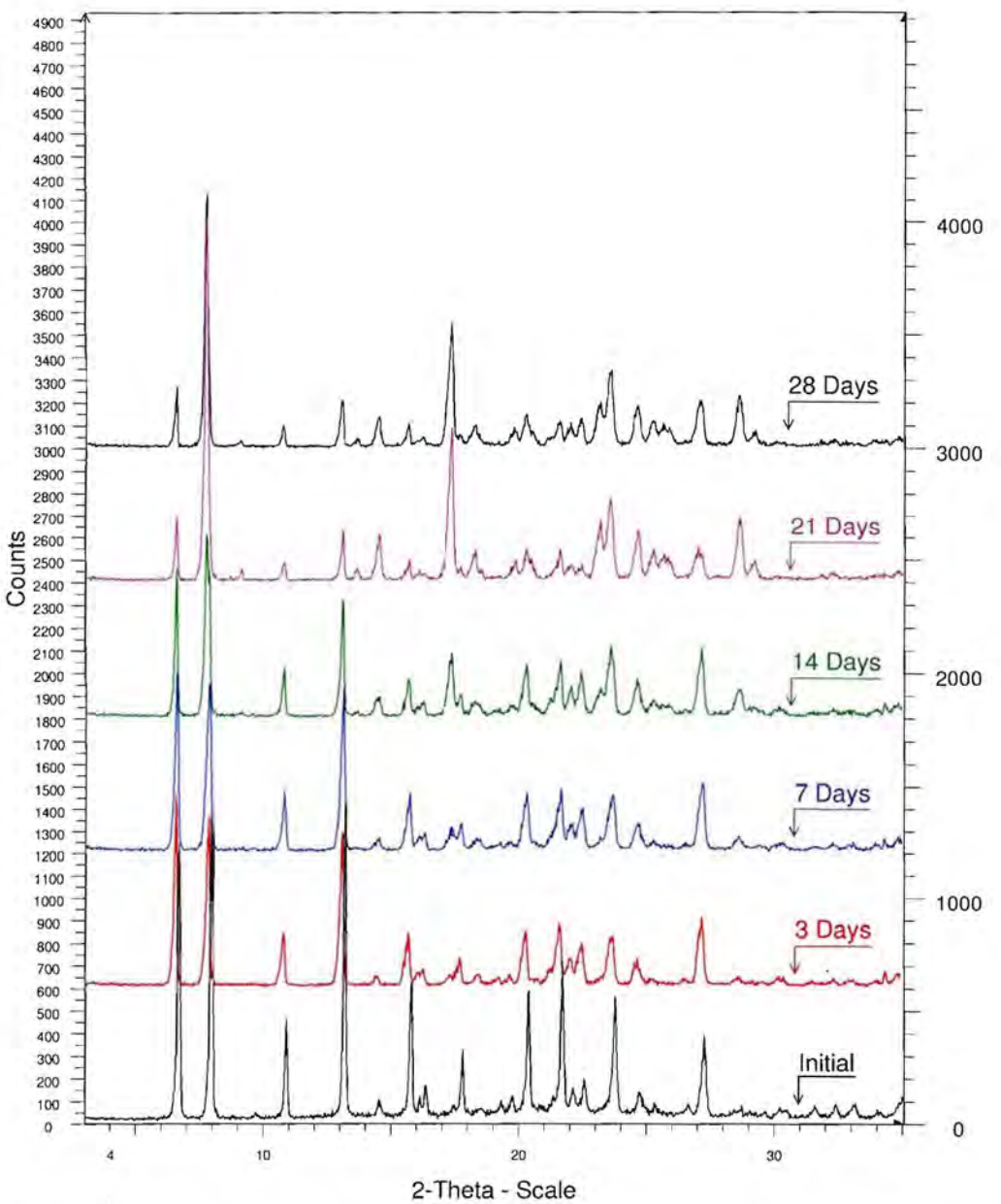

Figure 7.3 XRPD overlay of mebendazole acetic acid solvate (Form D) stored at 25±2℃ & 0 % RH for twenty-eight days.

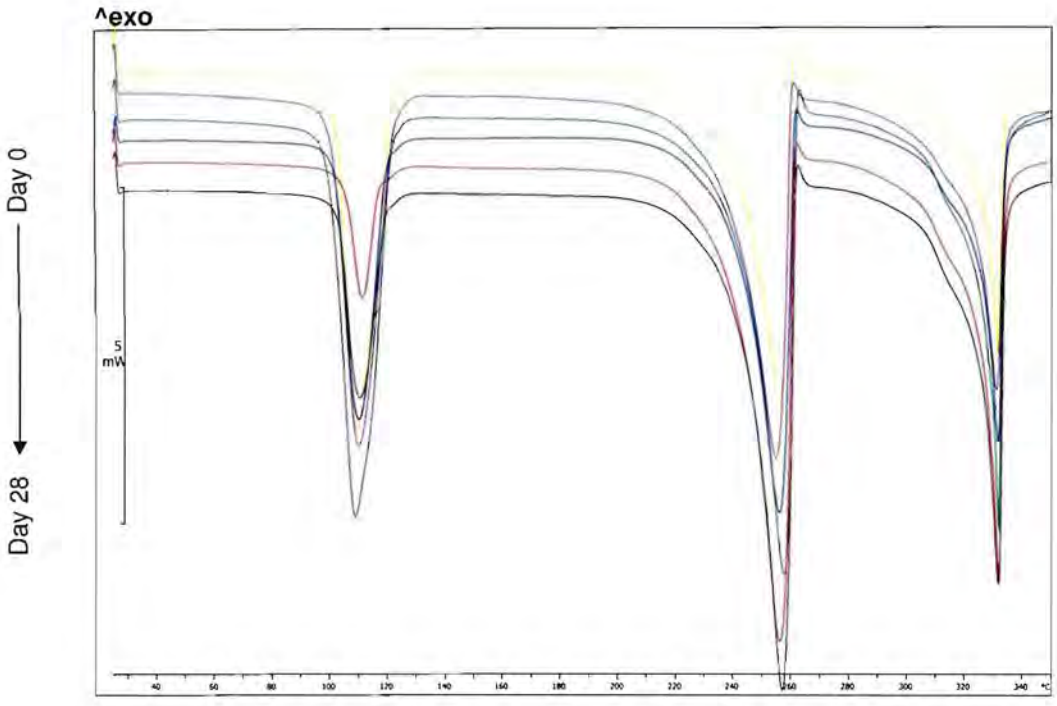

Figure 7.4 DSC thermogram overlay of mebendazole acetic acid solvate (Form D) stored at 25±2℃ & 0 % RH for twenty-eight days.

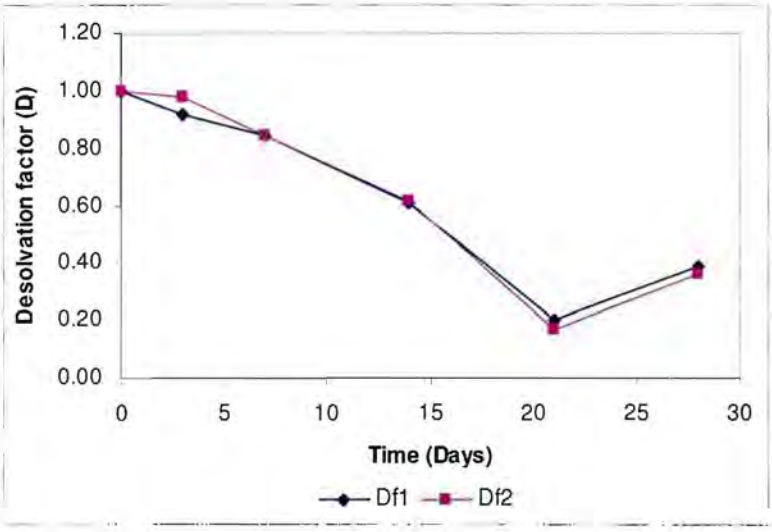

Figure 7.5 Desolvation factors for both DSC and TGA of Form D (25±2℃ & 0 % RH) plotted as a function of time (days).

7.3.3 Mebendazole acetic acid solvate (Form D) stored at 25±2°C & 60±5 % RH

The DRIFT-IR spectra of From D stored at 25±2°C & 60±5 % RH are shown in Figure 7.6 and the peaks are listed in Table 7.2. The DRIFT-IR spectra indicated traces of Form A (shoulder formation at 3370 cm^{-1} and shift in bands at 1730 cm^{-1}) after 3 days with the conclusion of the desolvation process after 14 days.

The XRPD patterns of Form D (Figure 7.7 and Table 7.3) showed a decrease in the intensity of the characteristic peak of Form D (6.6±0.1°2θ) and the appearance of the characteristic peak of Form A (17.3±0.1°2θ) after 3 days. The XRPD data confirmed the complete desolvation of Form D after 14 days.

The DSC thermograms (Figure 7.8) and data listed in Table 7.4 showed a decrease in the integrated intensity of the desolvation endotherm (162.44 – 0 $J.mol^{-1}$) of Form D. The visible shift in the position of the desolvation endotherm between days 0 to 7 may be due to changes in the vapour pressure during desolvation of the sample (Han & Suryanarayanan, 1997:209-210). A small endotherm (2.25 $J.mole^{-1}$) was detected on day 14 that may be due / could be attributed to energy uptake to stabilise the lattice when desolvated, compared to the lack of mass loss of the corresponding TGA. The % mass loss of the sample (Table 7.5) decreased from 15.40 – 0.00 % after 14 days.

The desolvation factor (D_{fl}) reached 0.00 at 21 days verifying complete desolvation of the sample. The energy needed for the desolvation of the sample decreased as a function of the solvated fraction present, confirming the presence of solvated fractions in the sample up to day 14 (Figure 7.9) and the absence of Form D after day 21-28.

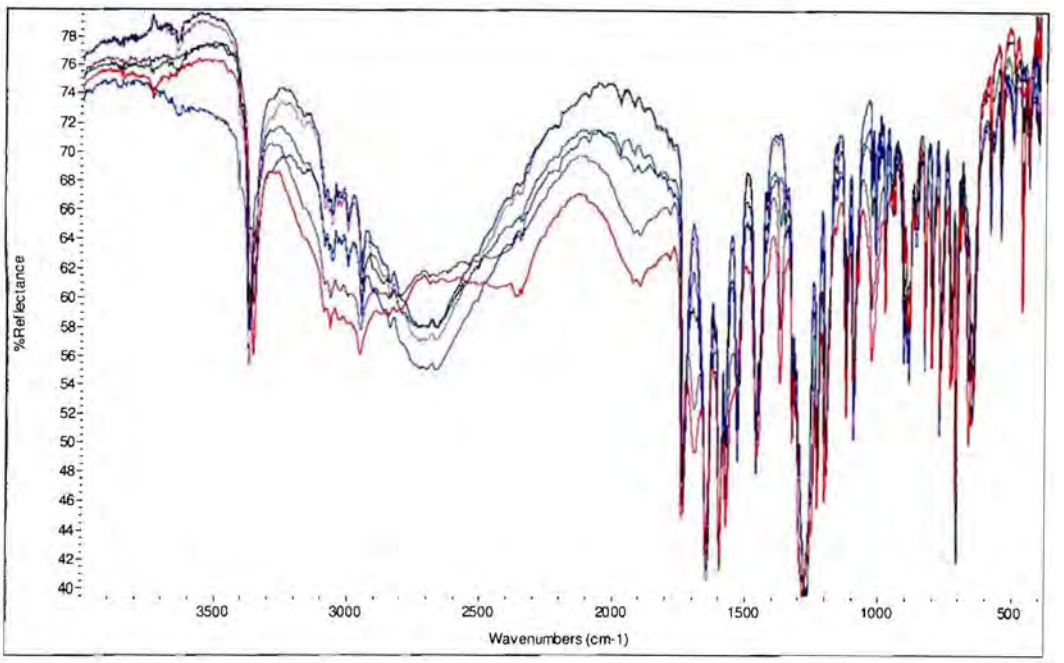

(a)

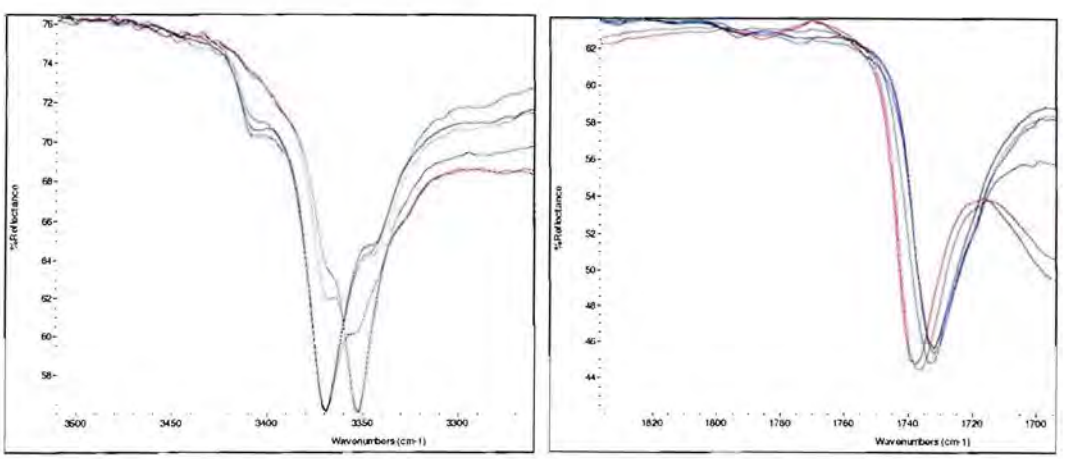

(b) (c)

Figure 7.6 (a) Overlay spectra of the mebendazole acetic acid solvate (Form D) stored at 25±2℃ & 60±5 % RH for twenty-eight days. (b and c) Superimposed DRIFT-IR spectra of the main absorptions at the –NH and >C=O stretching frequencies showing polymorphic transition in the sample (initial, 3, 7, 14, 21 and 28 days).

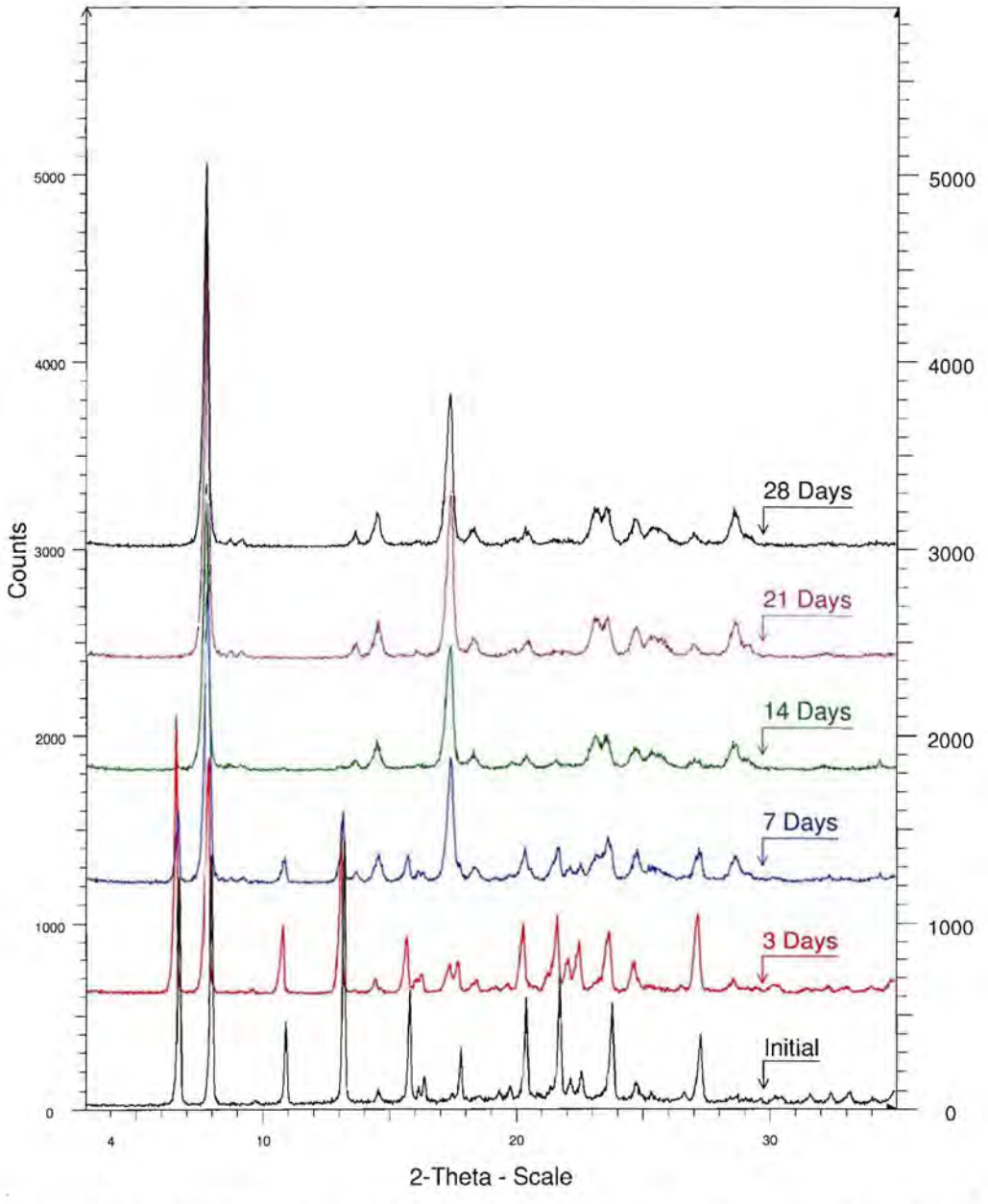

Figure 7.7 XRPD Overlay of the mebendazole acetic acid solvate (Form D) stored at 25±2℃ & 60±5 % RH for twenty-eight days.

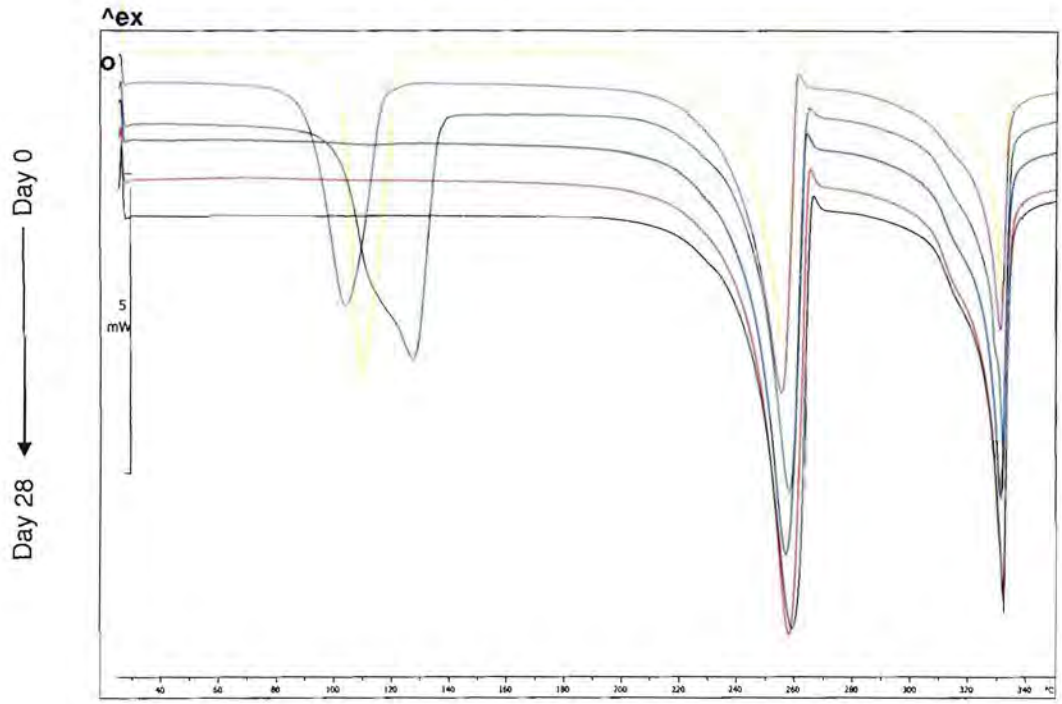

Figure 7.8 DSC thermogram overlay of mebendazole acetic acid solvate (Form D) stored at 25±2℃ & 60±5 % RH for twenty-eight days.

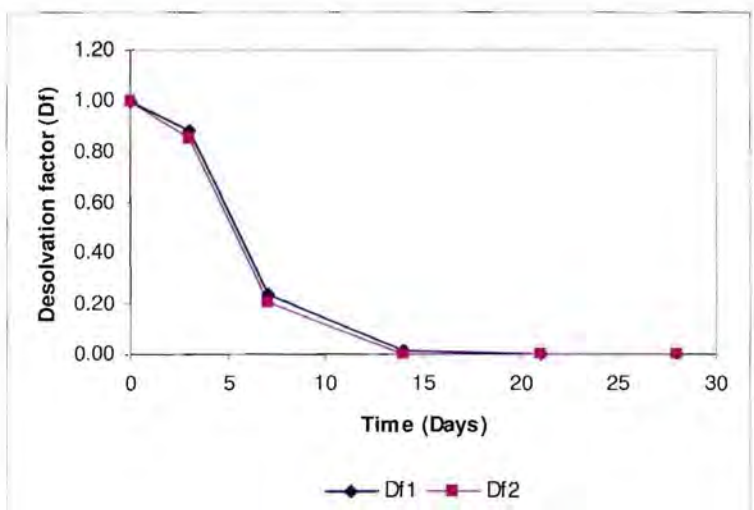

Figure 7.9 Desolvation factors for both DSC and TGA of Form D (25±2℃ & 60±5 % RH) plotted as a function of time (days).

7.3.4 Mebendazole acetic acid solvate (Form D) stored at 40±2°C & 0 % RH

The DRIFT-IR spectra (Figure 7.10 and Table 7.2) indicated that Form D underwent complete desolvation after only 3 days when stored at 40±2°C & 0 % RH, due to the disappearance of the 3353 cm^{-1} and 1738 cm^{-1} bands and the appearance of strong 3369 cm^{-1} and 1730 cm^{-1} bands, characteristic of Form A.

The XRPD patterns of Form D are shown in Figure 7.11 and the main diffraction angles (°2θ) and corresponding peak intensities (i) are listed in Table 7.3. The XRPD patterns of the samples after 3 days were found to be concurrent with that of Form A (Figure 2.7) and did not reveal any traces of Form D (6.6±0.1 °2θ).

The DSC thermograms (Figure 7.12) and data listed in Table 7.4 revealed no desolvation endotherms after 3 days when stored at 40±2°C & 0 % RH. The TGA data revealed a significant increase in the % mass loss of the sample. This increase may be the result of adsorbed solvent onto the crystal surface after the desolvation of Form D followed by the condensation of the solvent from the atmosphere inside the closed system (Figure 7.14). Visual inspection of the samples after 3 days revealed that the samples had a slurry appearance. The complete desolvation of the sample after 3 days was verified by the absence of desolvation endotherms in the DSC thermograms (Table 7.4).

The desolvation factor (D_{f1}) confirmed the complete desolvation of Form D after 3 days (Figure 7.13), while the D_{f2} revealed a significant mass loss in the sample during TGA analysis. This increase in the D_{f2} was attributed to the adsorbed solvent being removed from the surface of the crystalline mass and not desolvation of the samples.

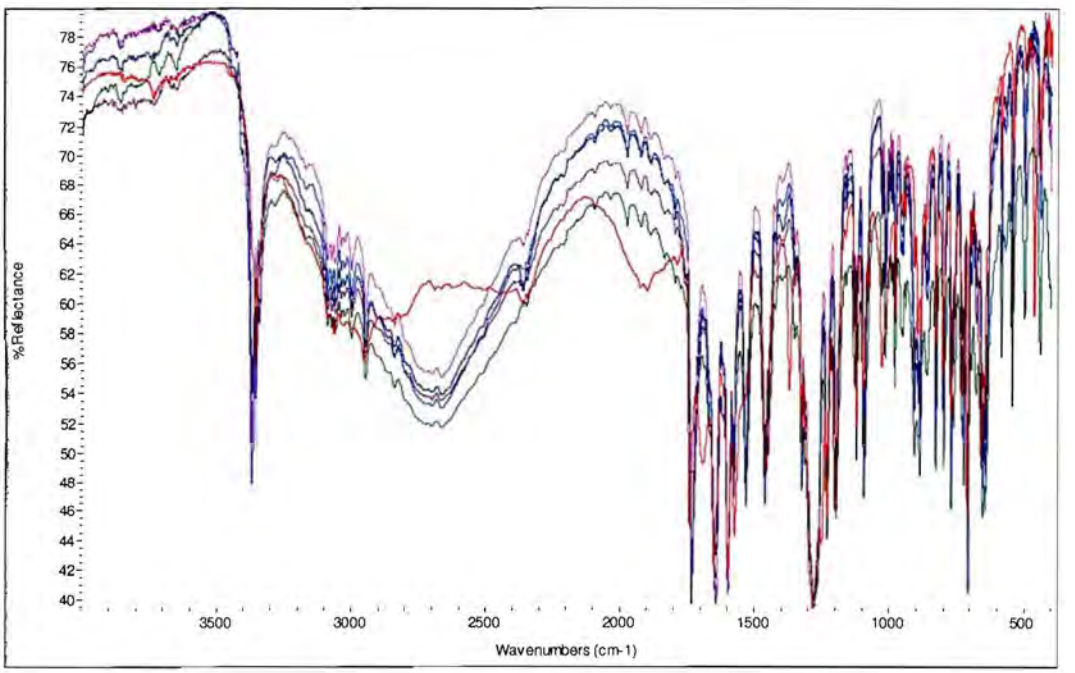

(a)

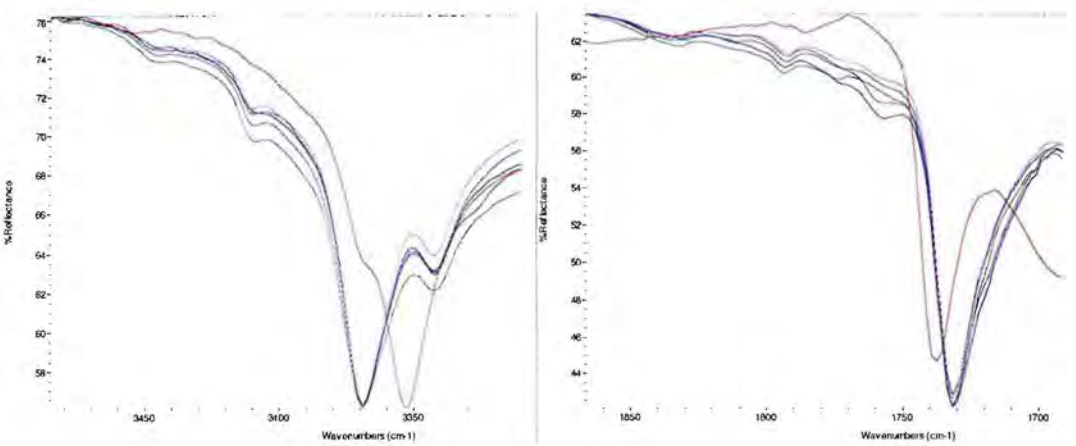

(b) (c)

Figure 7.10 (a) Overlay spectra of the mebendazole acetic acid solvate (Form D) stored at 40±2℃ & 0 % RH for twenty-eight days. (b and c) Superimposed DRIFT-IR spectra of the main absorptions at the –NH and >C=O stretching frequencies showing polymorphic transition in the sample (initial, 3, 7, 14, 21 and 28 days).

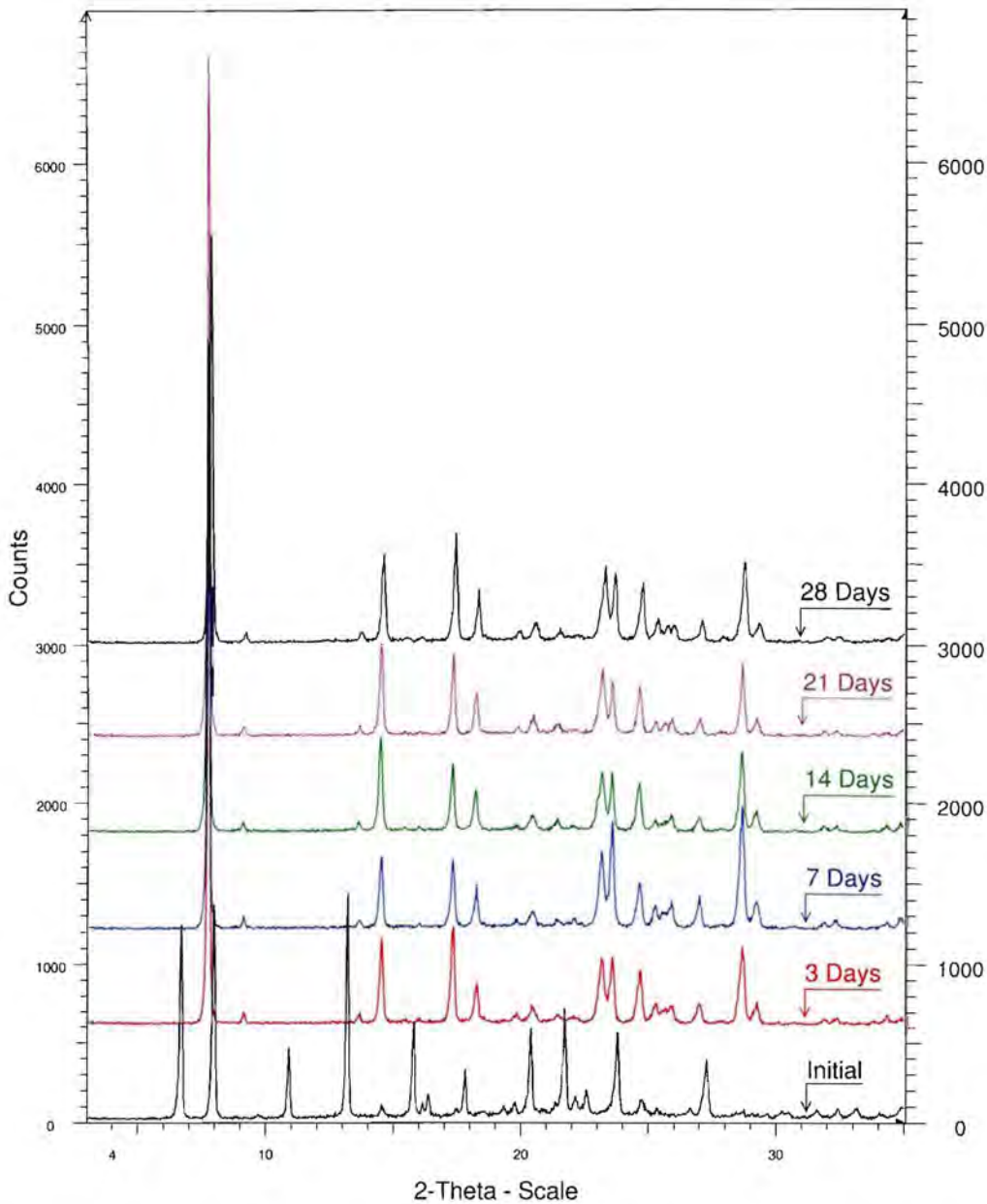

Figure 7.11 XRPD Overlay of the mebendazole acetic acid solvate (Form D) stored at 40±2℃ & 0 % RH for twenty-eight days.

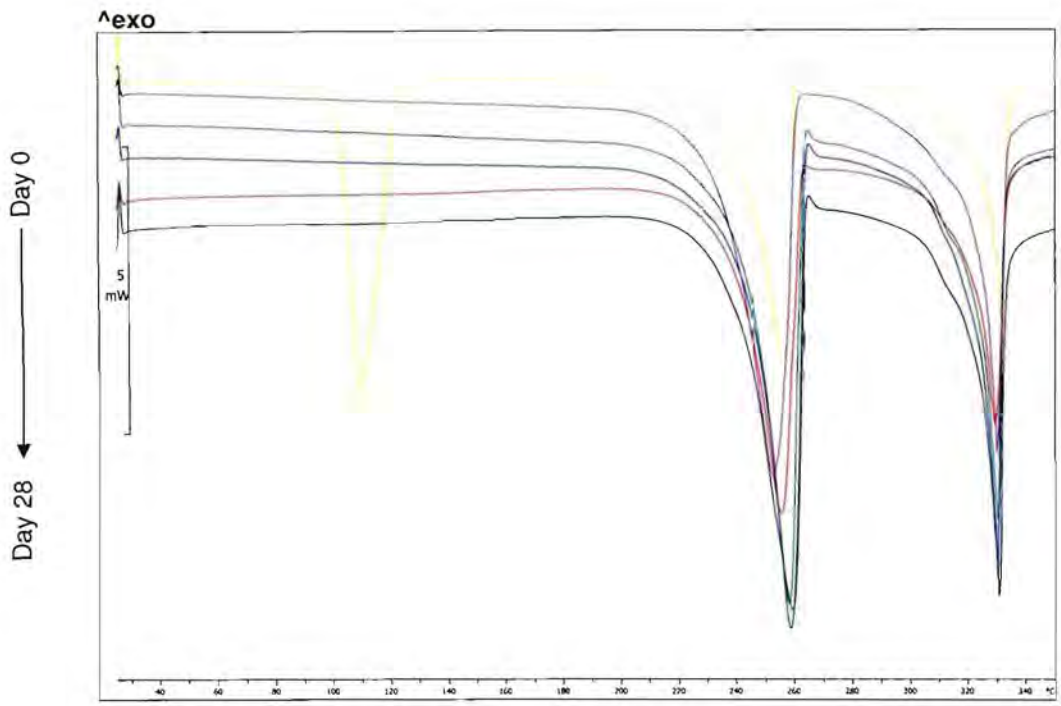

Figure 7.12 DSC thermogram overlay of mebendazole acetic acid solvate (Form D) stored at 40±2℃ & 0 % RH for twenty-eight days.

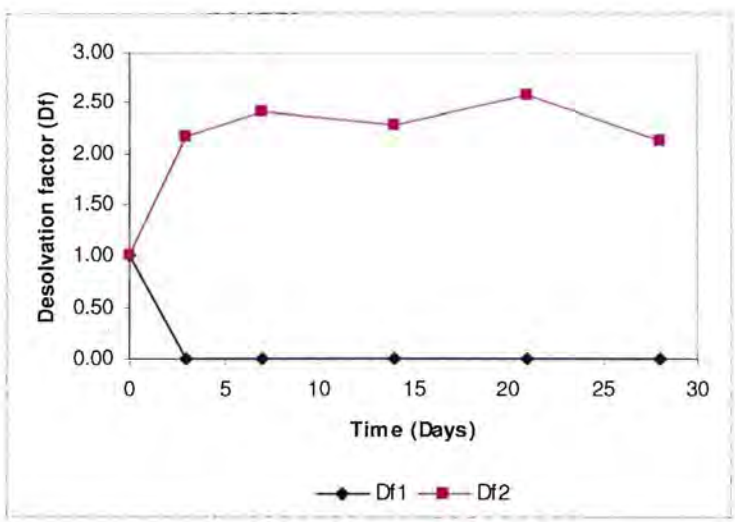

Figure 7.13 Desolvation factors for both DSC and TGA of Form D (40±2℃ & 0 % RH) plotted as a function of time (days).

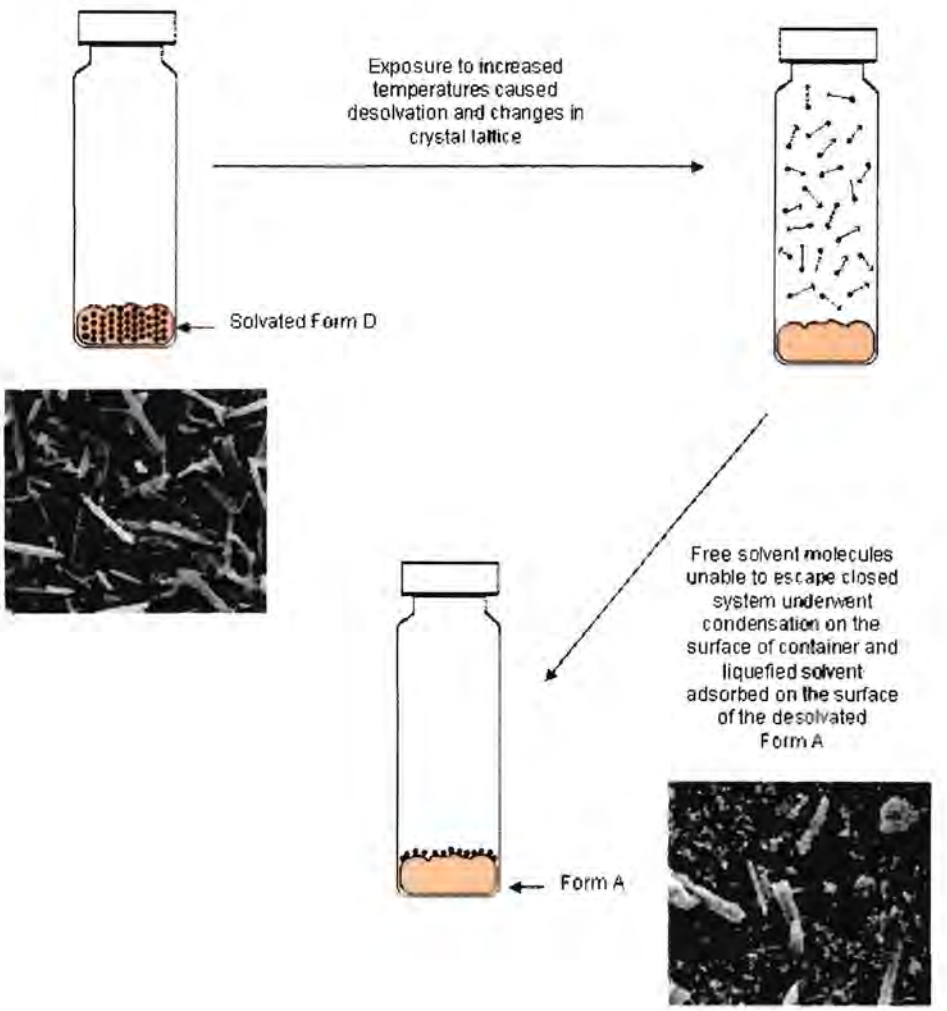

Figure 7.14 Schematic illustration of the desolvation behaviour of Form D when stored at 40±2℃ & 0 % RH.

7.3.5 Mebendazole acetic acid solvate (Form D) stored at 40±2 °C & 75±5 % RH

The DRIFT-IR spectra of Form D are shown in Figure 7.15 and the peaks are listed in Table 7.2. The DRIFT-spectra indicated the presence of Form A (bands detected at 3370 cm^{-1} and 1730 cm^{-1}) with no traces of Form D after 3 days when the samples were stored at 40±2 °C & 75±5 % RH.

The XRPD patterns of Form D (Figure 7.16) and the main diffraction angles (°2θ) and corresponding peak intensities (i) in Table 7.3 confirmed the complete desolvation of Form D, due to the absence of the peak at (6.6±0.1 °2θ) and the fact that the XRPD patterns were concurrent with that of Form A after 3 days, when stored at 40±2 °C & 75±5 % RH.

The absence of the desolvation endotherms in the DSC thermograms (Figure 7.17 and Table 7.4) and no mass loss detected by TGA analysis (Table 7.5), verified the complete desolvation of Form D after 3 days.

The calculated desolvation factors (D_{f1} and D_{f2}) of the sample reached 0.00 after 3 days, indicating that Form D completely desolvated (Figure 7.18).

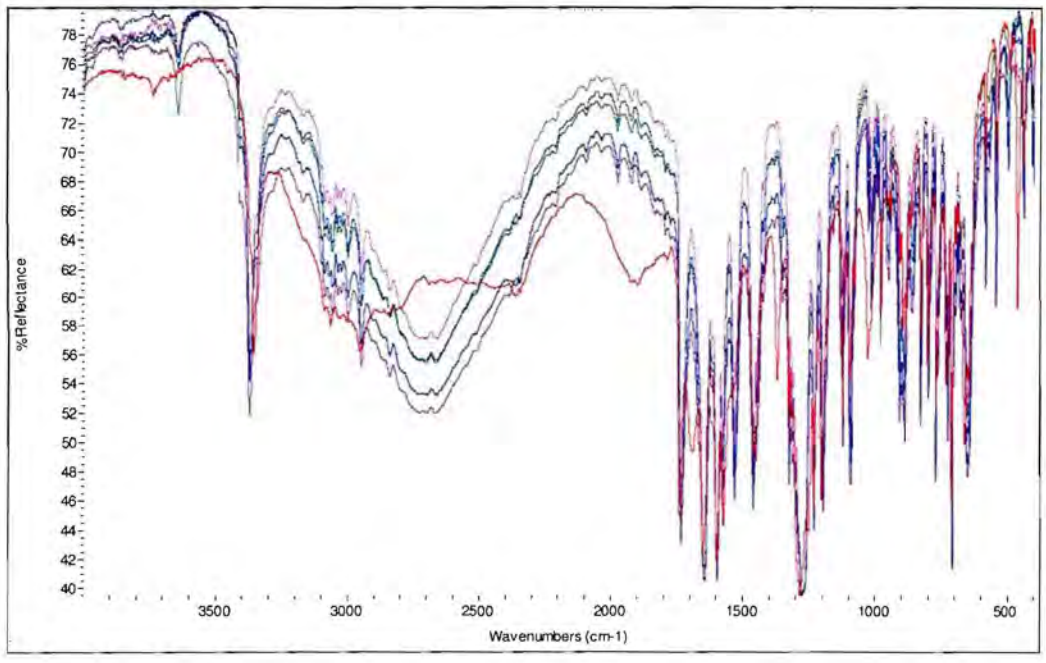

(a)

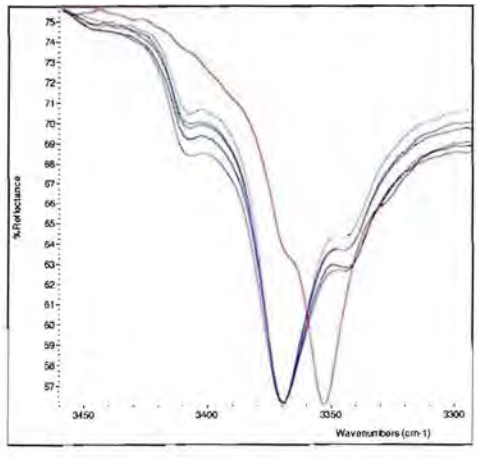

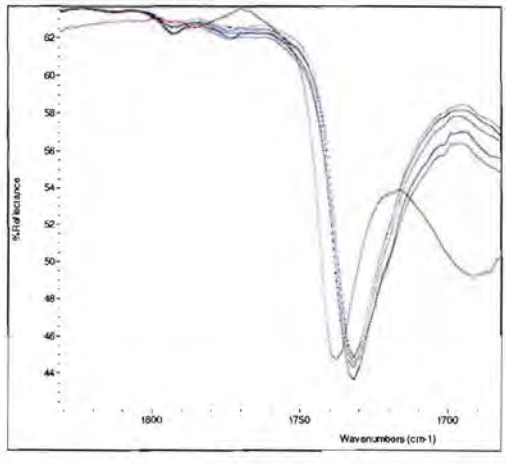

(b) (c)

Figure 7.15 (a) Overlay spectra of the mebendazole acetic acid solvate (Form D) stored at 40±2℃ & 75±5 % RH for twenty-eight days. (b and c) Superimposed DRIFT-IR spectra of the main absorptions at the –NH and >C=O stretching frequencies showing polymorphic transition in the sample (initial, 3, 7, 14, 21 and 28 days).

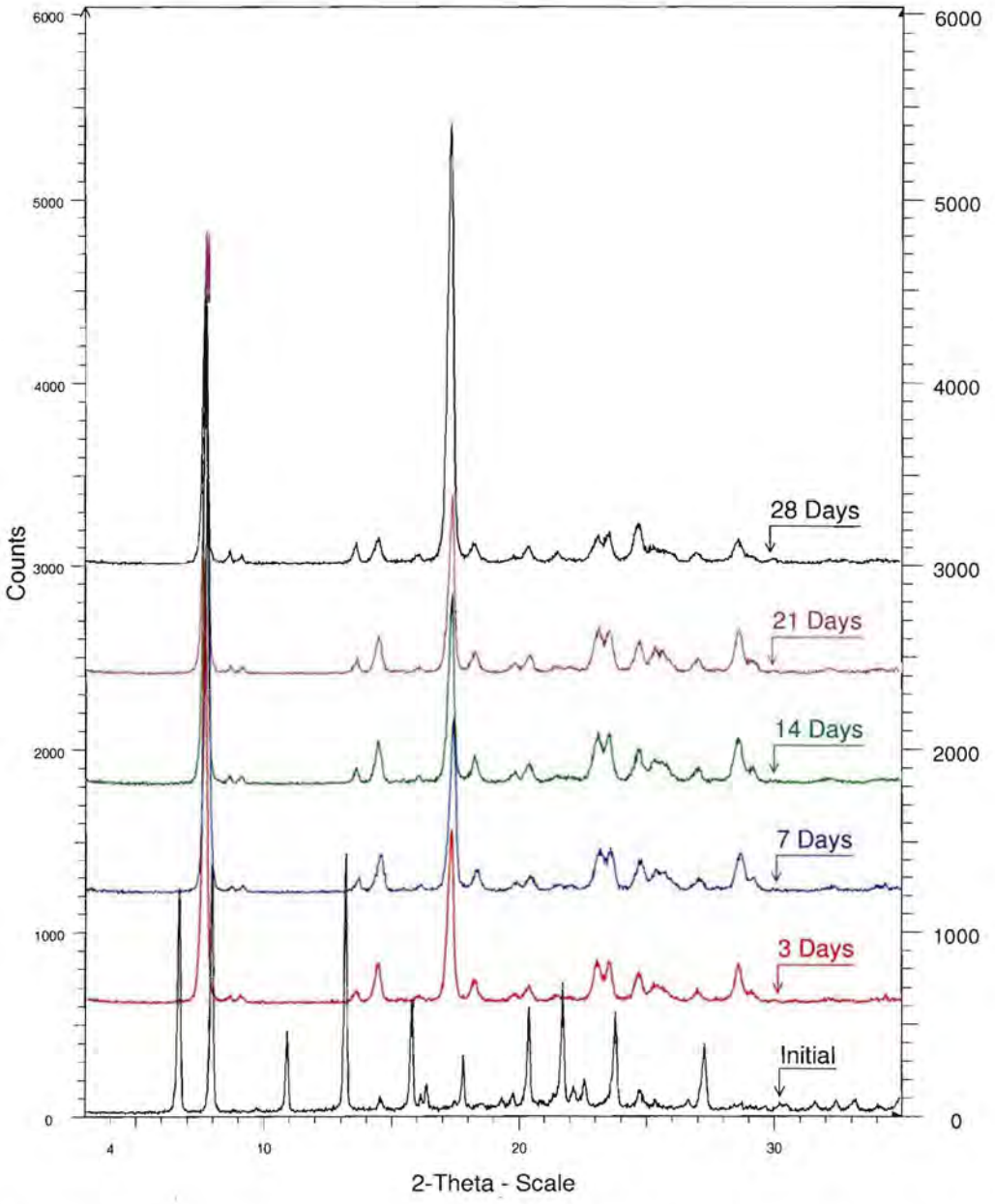

Figure 7.16 XRPD Overlay of the mebendazole acetic acid solvate (Form D) stored at 40±2℃ & 75±5 % RH for twenty-eight days.

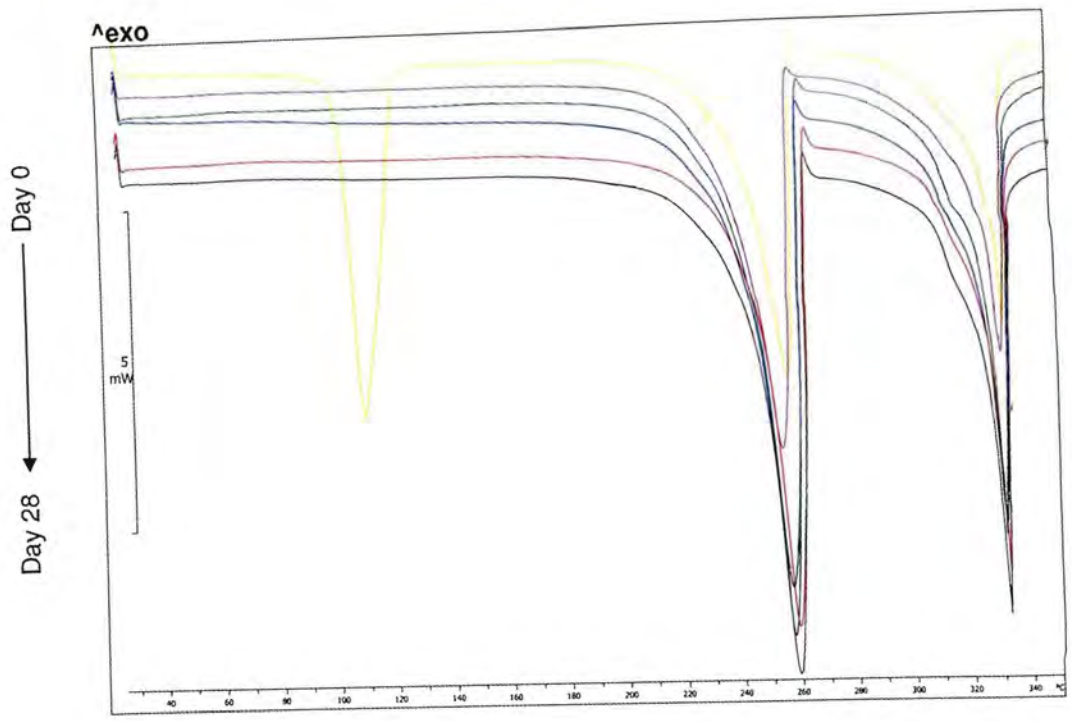

Figure 7.17 DSC thermogram overlay of mebendazole acetic acid solvate (Form D) stored at 40±2℃ & 75±5 % RH for twenty-eight days.

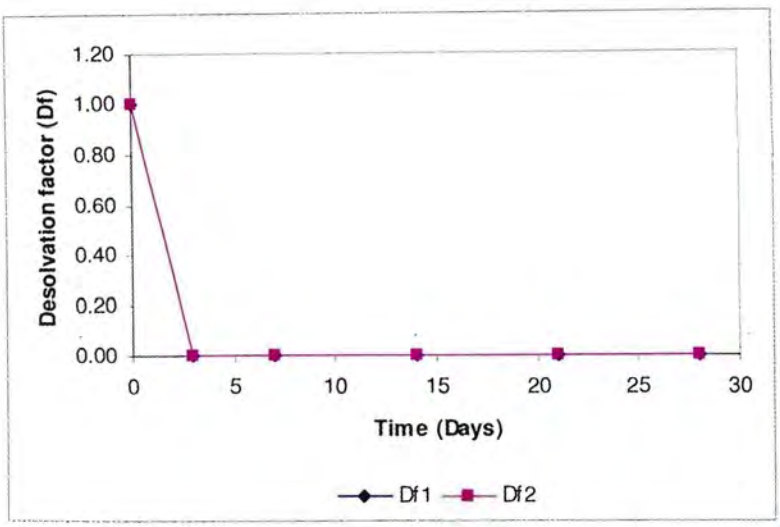

Figure 7.18 Desolvation factors for both DSC and TGA of Form D (40±2℃ plotted as a function of time (days).

7.3.6 Mebendazole propionic acid solvate (Form E) stored at 25±2°C & 0 % RH

The DRIFT-IR spectra and peak data of Form E are shown in Figure 7.19 and in Table 7.2. The spectra revealed strong bands at 3364 cm^{-1} and 1735 cm^{-1} which are characteristic of Form E. These bands remained unchanged for the duration of the study, indicating that Form E remained stable when exposed to 25±2°C & 0 % RH for 28 days.

The XRPD patterns of Form E are shown in Figure 7.20 and the main diffraction angles (°2θ) and corresponding peak intensities (*i*) are listed in Table 7.3. The XRPD patterns confirmed the presence of Form E with no traces of Form A (17.3±0.1°2θ) for the duration of the study.

The DSC thermograms depicted in Figure 7.21 and data listed in Table 7.4 indicated Form E to be relatively stable, with minor changes detected in the integrated intensity values of the desolvation endotherms (%RSD = 3.4). The appearance of the two overlapping endotherms in the desolvation region may be attributed to the desolvation and vaporisation (Han & Suryanarayanan, 1997:209-210). Based on the model proposed by Han & Suryanarayanan (1997:210), the different steps in the desolvation of a solvated form is described by Equation 7.3:

$$API \cdot nSO_{(s)} \xrightarrow{\Delta} API_{(s)} + nSO_{(v)} \qquad (7.3)$$

Where: *SO* is the solvent, *s* the solid-state, *l* the liquid-state and *v* the vapour phase.

The enthalpy of desolvation (ΔH_s) can be described as follow (step 1, Equation 7.4):

$$API_{(s)} + nSO_{(l)} \rightarrow API_{(s)} + nSO_{(v)} \qquad (7.4)$$

The enthalpy of vaporisation of the solvent can be described as follow (step 2, Equation 7.5):

$$API \cdot nSO_{(s)} \rightarrow API_{(s)} + nSO_{(v)} \qquad (7.5)$$

Thus the enthalpy of the overall transition (ΔH_t) is defined as (Equation 7.6):

$$\Delta H_t = \Delta H_d + \Delta H_v \qquad (7.6)$$

Han & Suryanarayanan (1997:210) indicated that the desolvation and vaporisation endotherms in DSC may overlap, and depending on the pressure in the sample crucible the desolvation endotherm may separated to produce two individual or partly overlapping endotherms.

The percentage (%) mass loss of the sample (Table 7.5) remained relatively unchanged (%RSD = 1.4) during the 28 days, confirming the DSC data and the stability of Form E.

The desolvation factor (D_{f2}) remained relatively unchanged during the 28 days, confirming the presence of the solvated fractions in the sample (as observed with XRPD and DRIFT-IR data). A slight increase in the desolvation factor (D_{f2}) was observed on day 3 (+0.10) and day 21 (+0.02), indicating that a greater solvated fraction was present in the samples analysed (Figure 7.22).

The desolvation factor (D_{f1}) was concurrent with that calculated from the TGA data (D_{f2}) indicating that Form E remained stable. A slight increase in the desolvation factor D_{f2} was detected on day 3 (+0.06) and 28 (+0.05), indicating that a greater solvated fraction was present in the samples tested (Figure 7.22). The appearance of the overlapping desolvation endotherms (in the DSC thermogram) complicated the calculation of the desolvation enthalpy (ΔH_{Di}) and could thus have attributed to the slight differences observed in the D_{f1} and D_{f2} values in Figure 7.22.

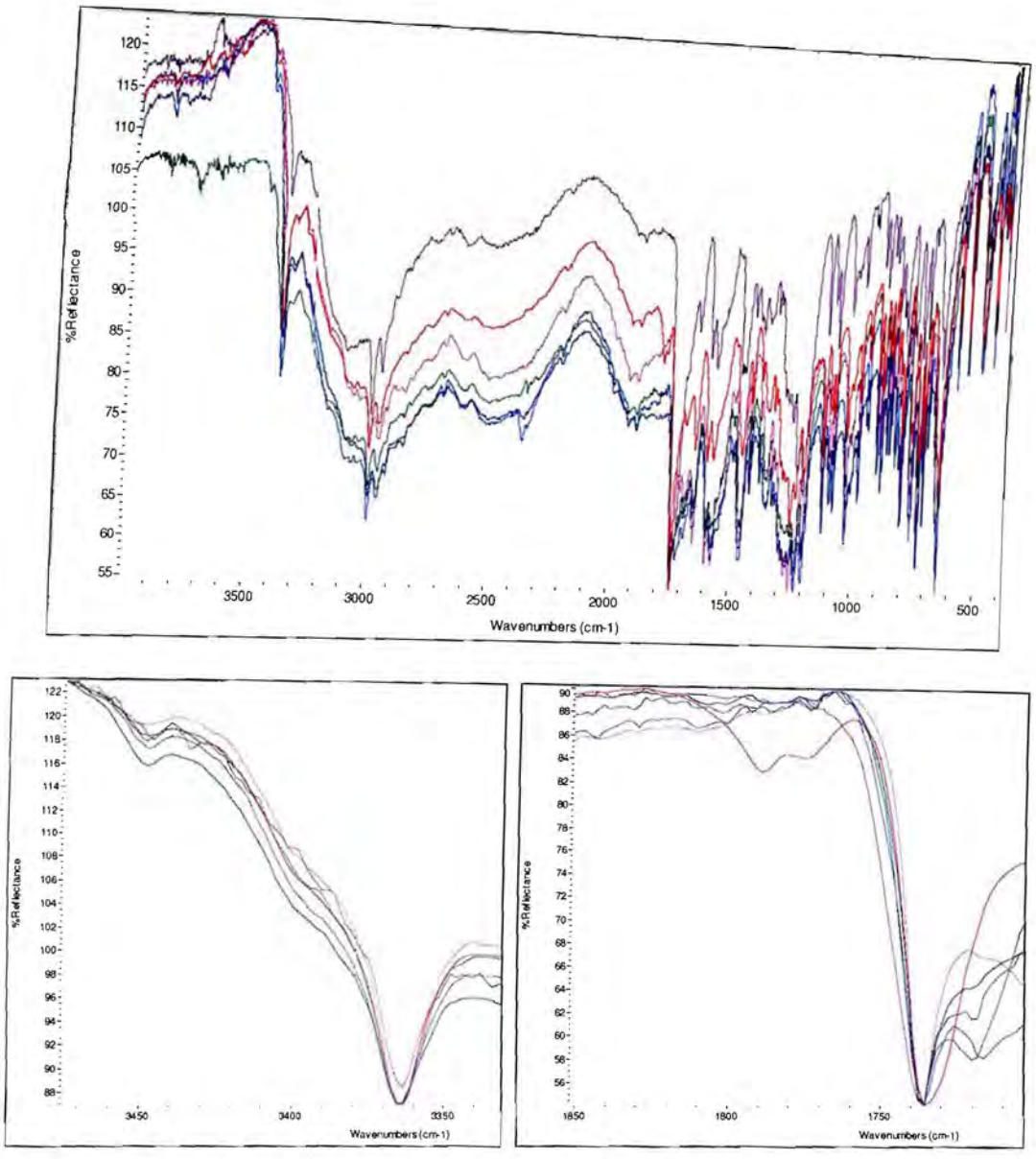

Figure 7.19 (a) Overlay spectra of the mebendazole propionic acid solvate (Form E) stored at 25±2℃ & 0 % RH for twenty-eight days. (b and c) Superimposed DRIFT-IR spectra of the main absorptions at the –NH and >C=O stretching frequencies in the sample (initial, 3, 7, 14, 21 and 28 days).

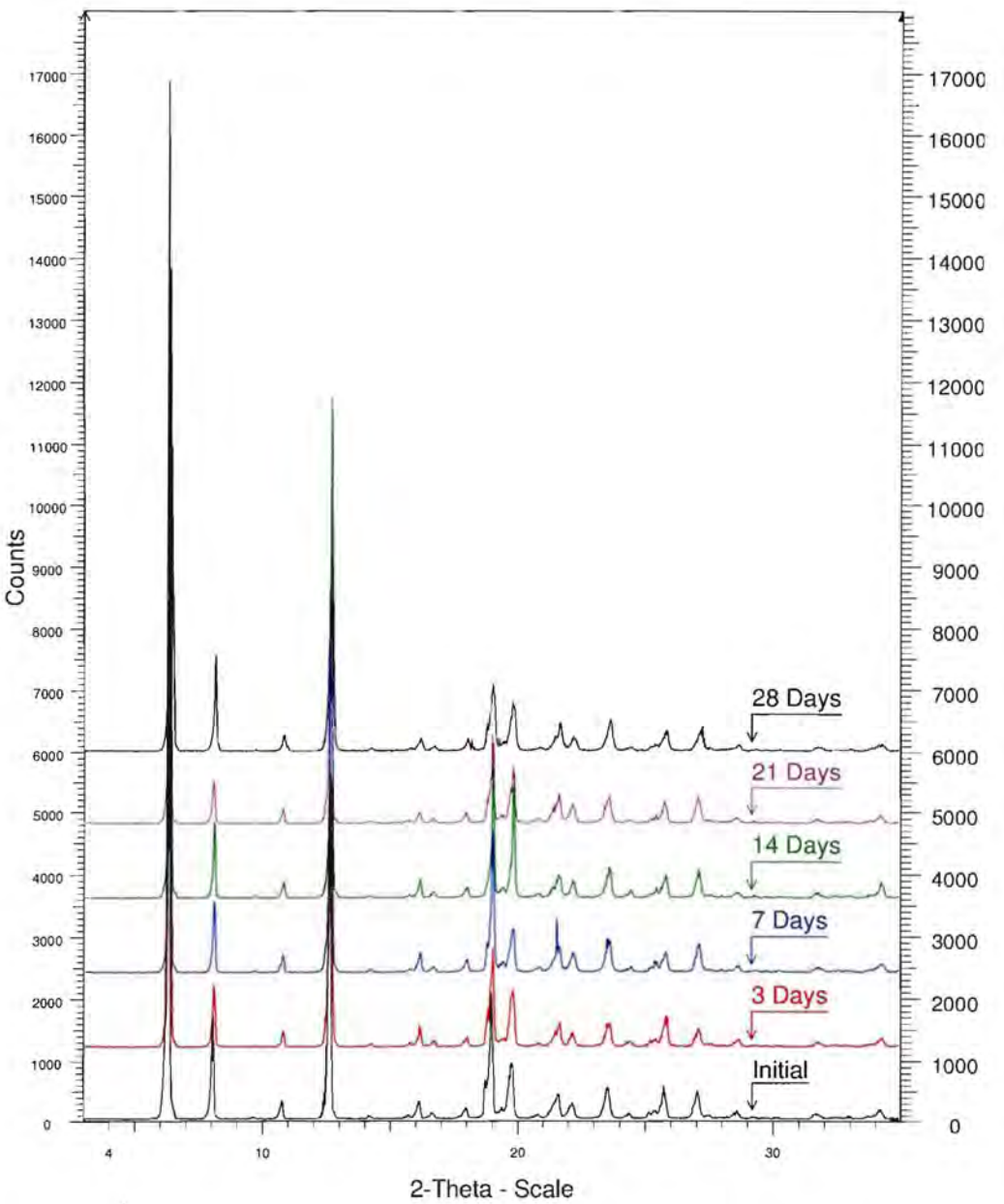

Figure 7.20 XRPD Overlay of the mebendazole propionic acid solvate (Form E) stored at 25±2℃ & 0 % RH for twenty-eight days.

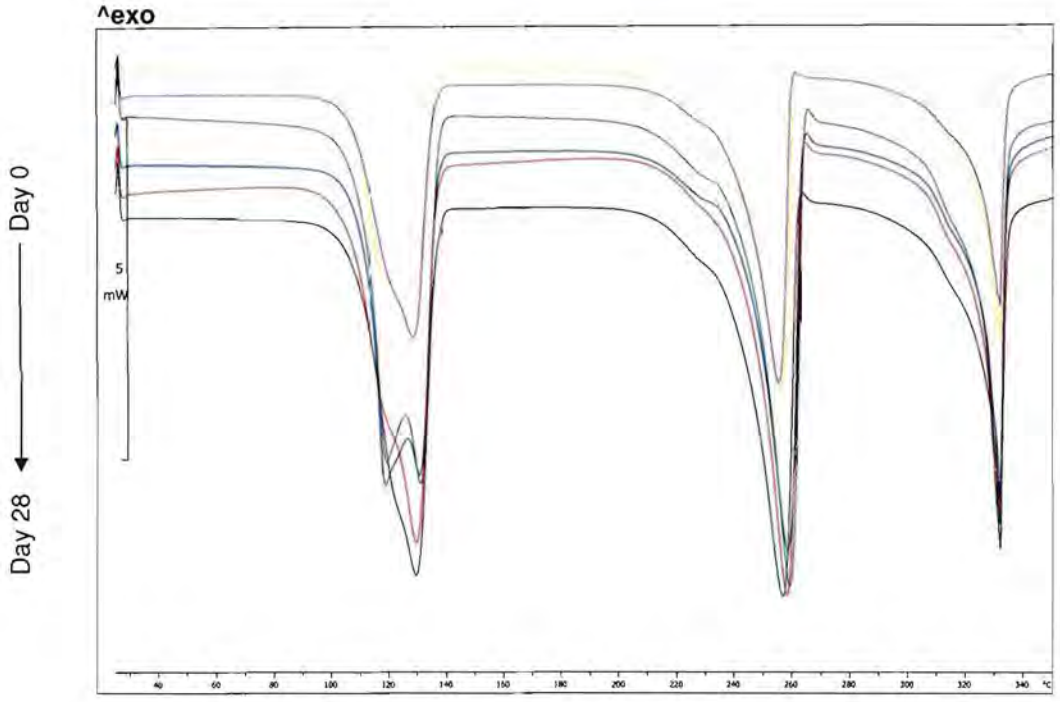

Figure 7.21 DSC thermogram overlay of mebendazole propionic acid solvate (Form E) stored at 25±2℃ & 0 % RH for twenty-eight days.

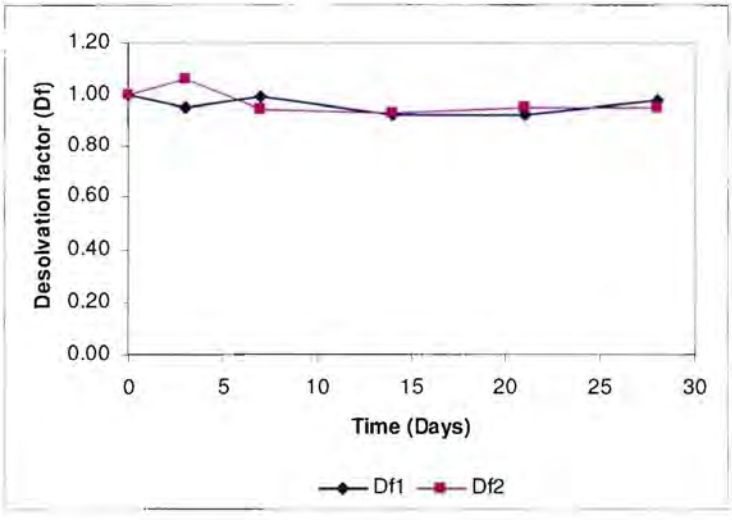

Figure 7.22 Desolvation factors for both DSC and TGA of Form E (25±2℃ & 0 % RH) plotted as a function of time (days).

7.3.7 Mebendazole propionic acid solvate (Form E) stored at 25±2°C & 60±5 % RH

The DRIFT-IR spectra of Form E stored at 25±2°C & 60±5 % RH are shown in Figure 7.23 and the peaks are listed in Table 7.2. The presence of absorption bands at 3364 cm^{-1} and 1735 cm^{-1} in the DRIFT-IR spectra suggested that Form E remained stable when exposed to 25±2°C & 60±5 % RH for 28 days. Upon closer inspection of the DRIFT-IR spectra (Figure 7.23) it became clear that shoulder formation occurred in the 3370 cm^{-1} region (characteristic of Form A) after 3 days and that the 1735 cm^{-1} band shifted to the 1730 cm^{-1} region. As mentioned in Chapter 4 (Figure 4.5) the –NH and >C=O bands of Form E and Form A are closely related (Table 7.1) and therefore complicated the detection of Form A from the desolvation product of Form E.

The XRPD patterns of Form E are shown in Figure 7.24 and the main diffraction angles (°2θ) and corresponding peak intensities (*i*) are listed in Table 7.3. The decrease in the intensity of the characteristic peak of Form E (6.3±0.1 °2θ) and the appearance of the characteristic peaks of Form A (7.6±0.1 °2θ and 17.3±0.1 °2θ) after 3 days indicated that Form E started to desolvate and confirmed the peak shift and shoulder formation observed in the DRIFT-IR data.

The DSC thermograms depicted in Figure 7.25 and data listed in Table 7.4 indicated a decrease in the integrated intensity of the desolvation endotherm (178.47 – 99.43 $J.mol^{-1}$) of Form E. The % mass loss of the sample (Table 7.5) decreased from 20.76 - 11.57 % during the 28 days, confirming the progressive desolvation of Form E upon storage at 25±2°C & 60±5 % RH.

The desolvation factors (D_{f2}) decreased during day 0 – 21, supporting the gradual desolvation of Form E (as observed with XRPD and DRIFT-IR data). A slight increase in the desolvation factor (D_{f2}) was observed on day 28 (+0.04), indicating that a slightly greater solvated fraction might have been present in the samples tested (Figure 7.26).

The behaviour of the desolvation factors (D_{f1}) calculated from the DSC data was concurrent with that of D_{f2}. The decrease in the D_{f1} values indicated that the energy required for desolvation decreased as a function of the solvated fraction present in the samples. A similar increase in the desolvation factor D_{f2} was verified (+0.03) in the D_{f1} value on day 28 (Figure 7.26). The appearance of the overlapping desolvation endotherms (in the DSC thermogram) complicated the calculation of the desolvation enthalpy (ΔH_{Di}) and could thus have attributed to the slight differences observed in the D_{f1} and D_{f2} values in Figure 7.26.

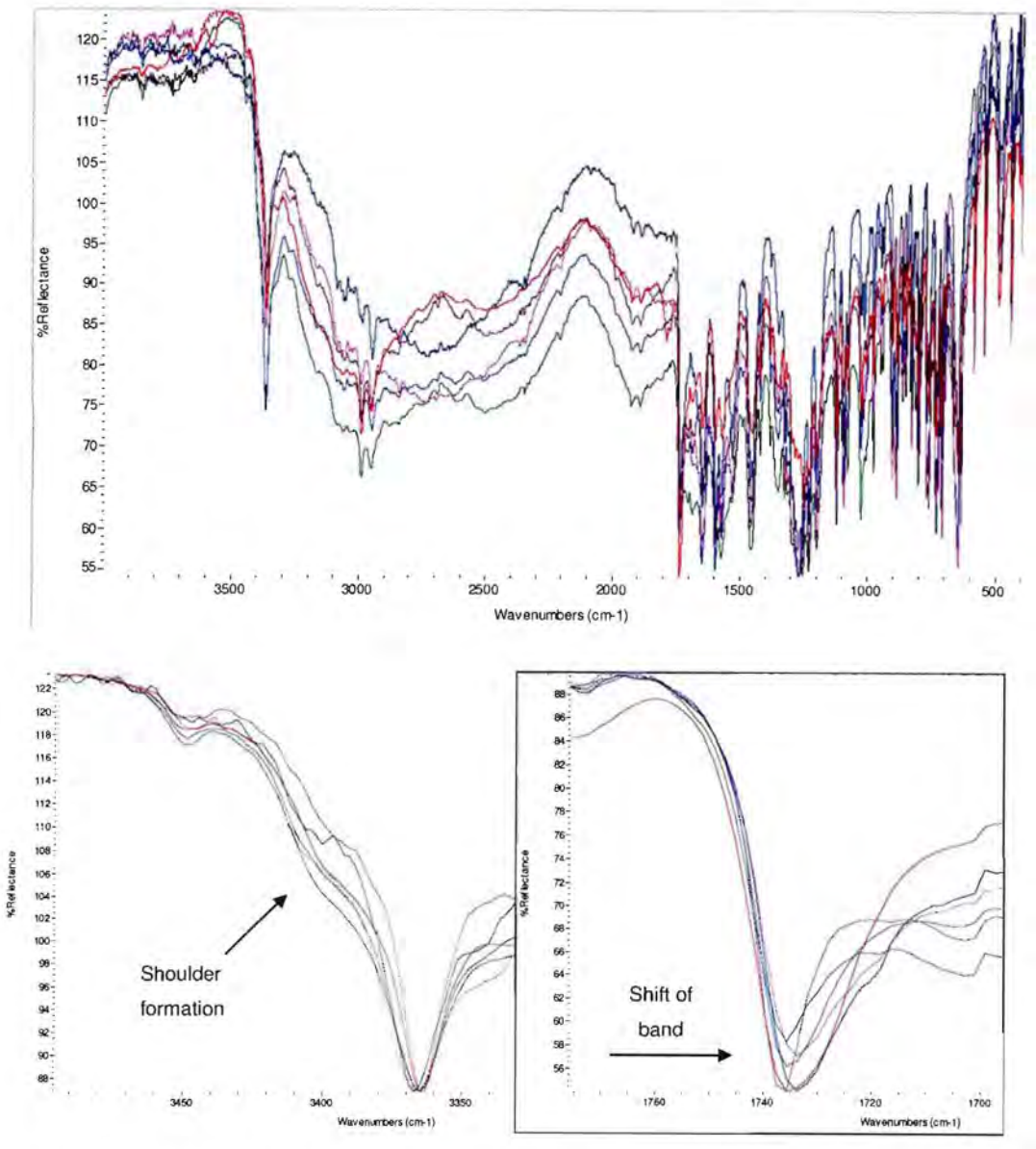

Figure 7.23 (a) Overlay spectra of the mebendazole propionic acid solvate (Form E) stored at 25±2℃ & 60±5 % RH for twenty-eight days. (b and c) Superimposed DRIFT-IR spectra of the main absorptions at the –NH and >C=O stretching frequencies showing polymorphic transition in the sample (initial, 3, 7, 14, 21 and 28 days).

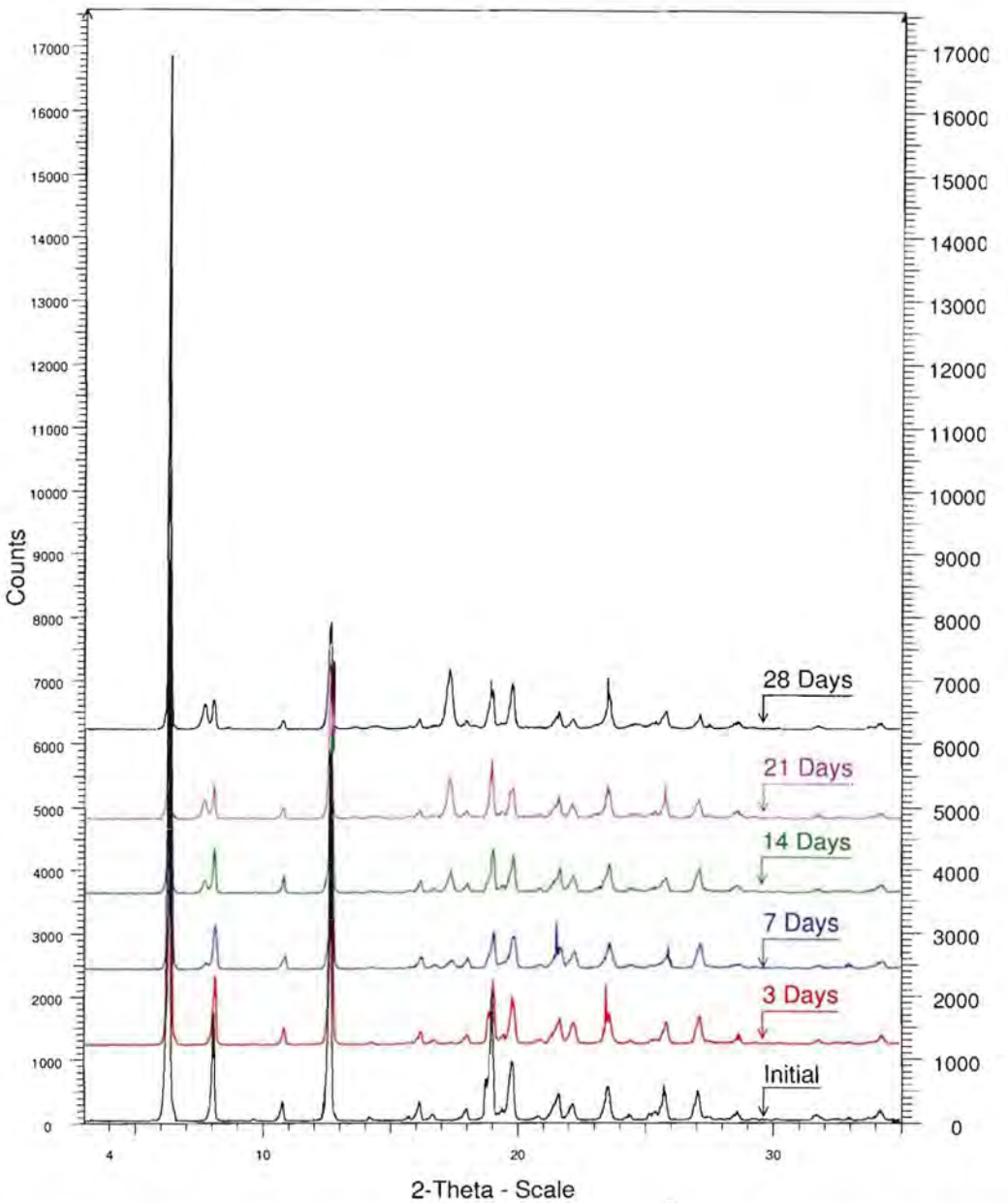

Figure 7.24 XRPD Overlay of the mebendazole propionic acid solvate (Form E) stored at 25±2℃ & 60±5 % RH for twenty-eight days.

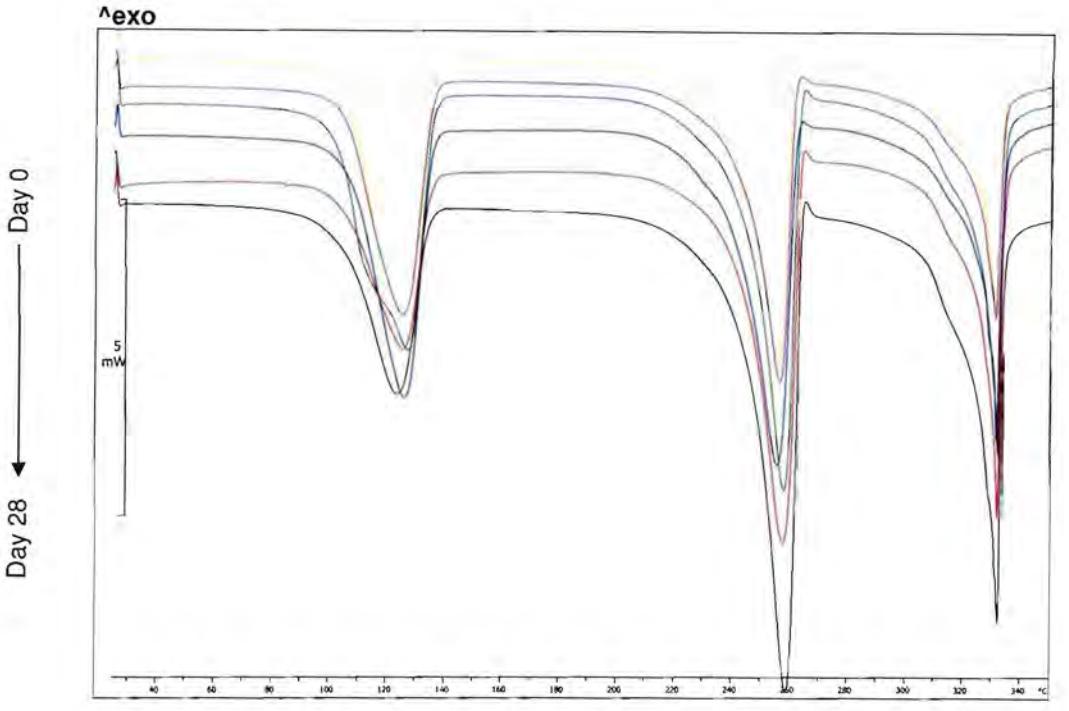

Figure 7.25 DSC thermogram overlay of mebendazole propionic acid solvate (Form E) stored at 25±2℃ & 60±5 % RH for twenty-eight days.

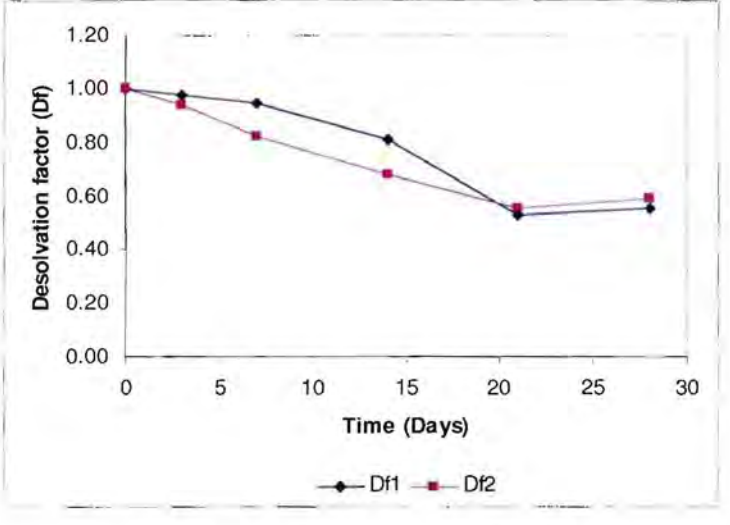

Figure 7.26 Desolvation factors for both DSC and TGA of Form E (25±2℃ & 60±5 % RH) plotted as a function of time (days).

7.3.8 Mebendazole propionic acid solvate (Form E) stored at 40±2°C & 0 % RH

The DRIFT-IR spectra of Form E are shown in Figure 7.27 and the peaks are listed in Table 7.2. The DRIFT-IR-spectra showed strong absorption bands at the 3364 cm^{-1} and 1735 cm^{-1} (characteristic of Form E) during the period: 0 - 14 days. Traces of Form A (formation of a shoulder at 3369 cm^{-1} and peak shift towards 1730 cm^{-1}) were detected after 21 days.

The XRPD patterns of Form E are shown in Figure 7.28 and the main diffraction angles (°2θ) and corresponding peak intensities (*i*) are listed in Table 7.3. The intensities of the characteristic peak of Form E (6.3±0.1 °2θ) showed a minor decrease during the 28 days, while the intensities of the characteristic peaks of Form A (7.8±0.1 °2θ and 17.3±0.1 °2θ) increased after 14 days, confirming the desolvation observed in the DRIFT-IR data.

The DSC thermograms depicted in Figure 7.29 and data listed in Table 7.4 indicated a decrease in the integrated intensity of the desolvation endotherm (178.47 – 128.63 $J.mol^{-1}$) of Form E. The appearance of the two overlapping desolvation and vaporisation endotherms are illustrated in Figure 7.29. The % mass loss of the sample (Table 7.5) decreased from 20.76 - 14.50 % during the 28 days, confirming the continuous desolvation of Form E.

The desolvation factors (D_{f2}) revealed a slight decrease in the D_{f2} value on day 3 (+0.05) with a minimum reached on day 28, confirming the presence of solvated fractions in the sample (as observed with XRPD and DRIFT-IR data). The desolvation factor (D_{f1}) calculated from the DSC data was concurrent with that calculated from the TGA data, indicating by the decrease in the D_{f1} values that the energy required for desolvation of the Form E fraction present in the sample decreased as a function of the solvated fraction present in the samples (Figure 7.30). The appearance of the overlapping desolvation endotherms (in the DSC thermogram) complicated the calculation of the desolvation enthalpy (ΔH_{Di}) and could thus have attributed to the slight differences observed in the D_{f1} and D_{f2} values in Figure 7.30.

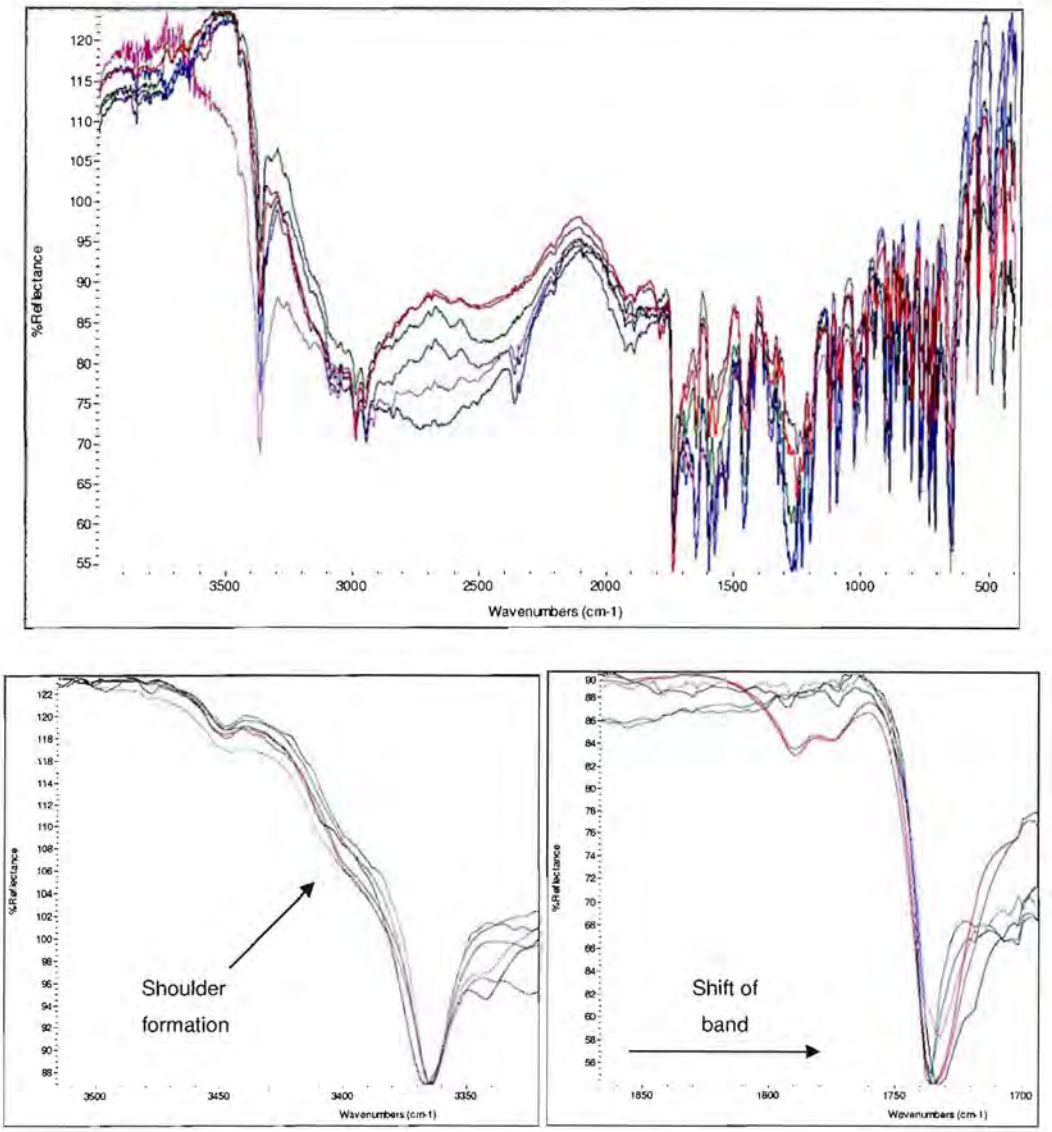

Figure 7.27 (a) Overlay spectra of the mebendazole propionic acid solvate (Form E) stored at 40±2℃ & 0 % RH for twenty-eight days. (b and c) Superimposed DRIFT-IR spectra of the main absorptions at the –NH and >C=O stretching frequencies showing polymorphic transition in the sample (initial, 3, 7, 14, 21 and 28 days).

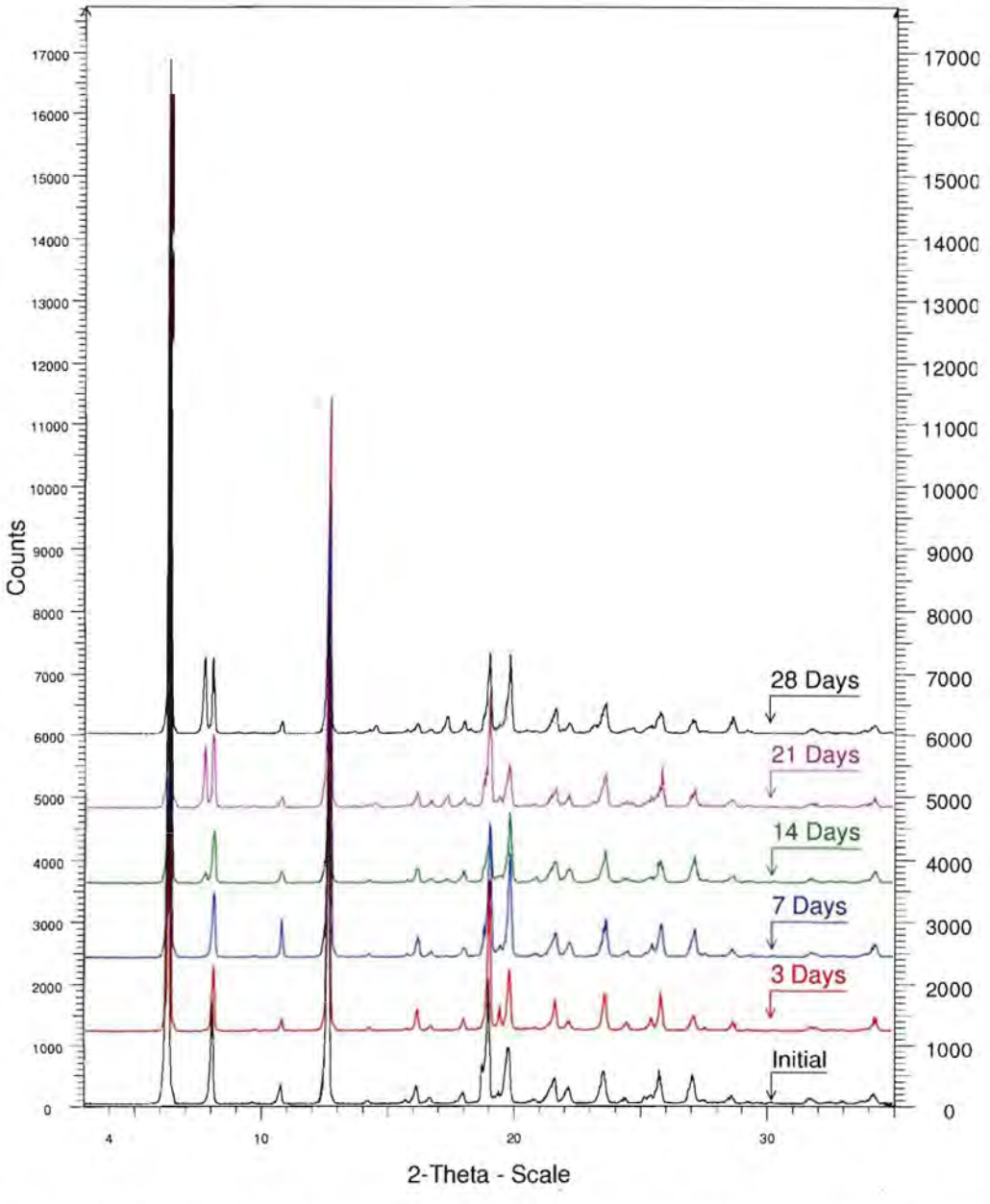

Figure 7.28 XRPD Overlay of the mebendazole propionic acid solvate (Form E) stored at 40±2℃ & 0 % RH for twenty-eight days.

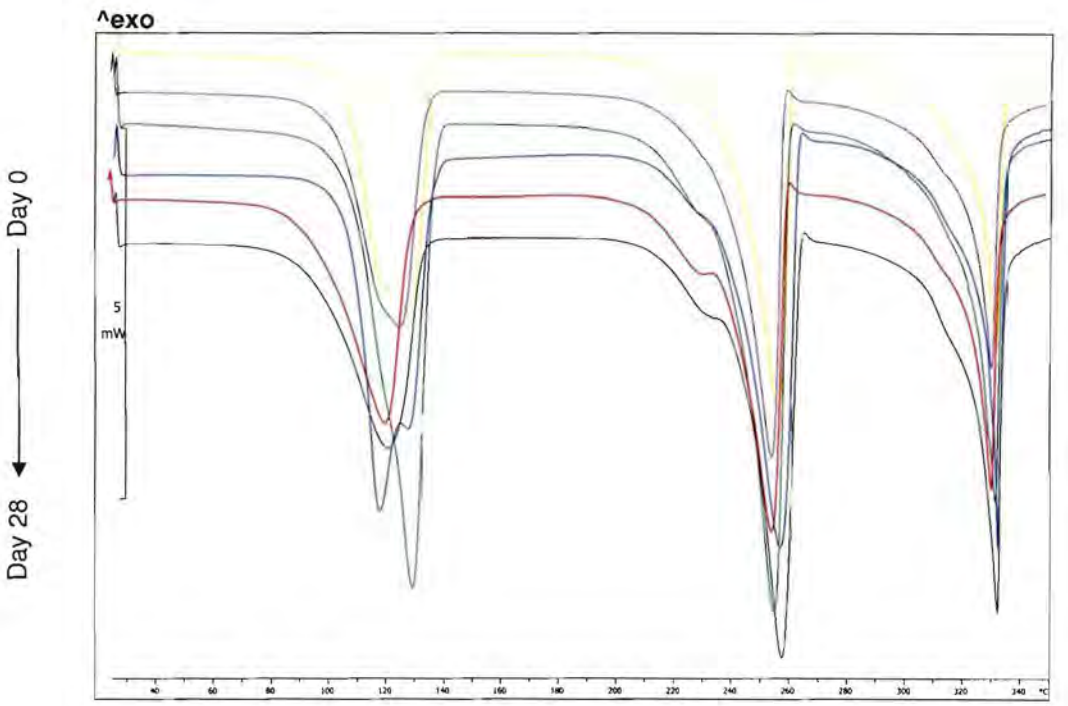

Figure 7.29 DSC thermogram overlay of mebendazole propionic acid solvate (Form E) stored at 40±2℃ & 0 % RH for twenty-eight days.

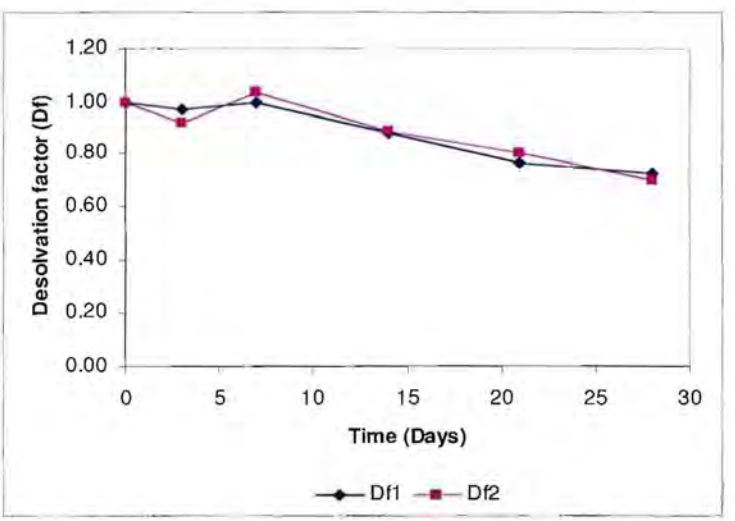

Figure 7.30 Desolvation factors for both DSC and TGA of Form E (40±2℃ & 0 % RH) plotted as a function of time (days).

7.3.9 Mebendazole propionic acid solvate (Form E) stored at 40±2°C & 75±5 % RH

The DRIFT-IR spectra of Form E stored at 40±2°C & 75±5 % RH are shown in Figure 7.31 and the peaks are listed in Table 7.2. The presence of absorption bands at 3369 cm^{-1} and 1730 cm^{-1} (characteristic of Form A) after 3 days and the fact that no traces of Form E were detected, indicated a complete desolvation of Form E when stored at 40±2°C & 75±5 % RH.

The XRPD diffractograms of Form E are shown in Figure 7.32 and the main diffraction angles (°2θ) and corresponding peak intensities (i) are listed in Table 7.3. The disappearance of the characteristic peaks of Form E (6.3±0.1°2θ, 8.0±0.1°2θ and 12.6±0.1°2θ) after 7 days and the appearance of the characteristic peaks of Form A (7.7±0.1°2θ & 17.3±0.1°2θ) after 3 days confirmed the observed desolvation results. The XRPD diffractograms indicated that the desolvation process of Form E was completed after 7 days when stored at 40±2°C & 75±5 % RH. The XRPD diffractograms of the sample on day 14, 21 and 28 were concurrent with the diffractogram of Form A (Figure 2.7).

The DSC thermograms depicted in Figure 7.33 indicated a decrease in the integrated intensity of the desolvation endotherm (178.47 – 0.00 $J.mol^{-1}$) of Form E. No desolvation endotherms were detected after 7 days, indicating that Form E had completely desolvated. The % mass loss during TGA analysis (Table 7.5) decreased from 20.76 – 0.00 % after 7 days, verifying the desolvation process.

The desolvation factors (D_{f2} and D_{f2}) revealed a remarkable decrease (-0.80) after 3 days. After 7 days the desolvation factors (D_{f1} and D_{f2}) reached 0.00, which confirmed XRPD and DRIFT-IR results that Form E was completely desolvated (Figure 7.34).

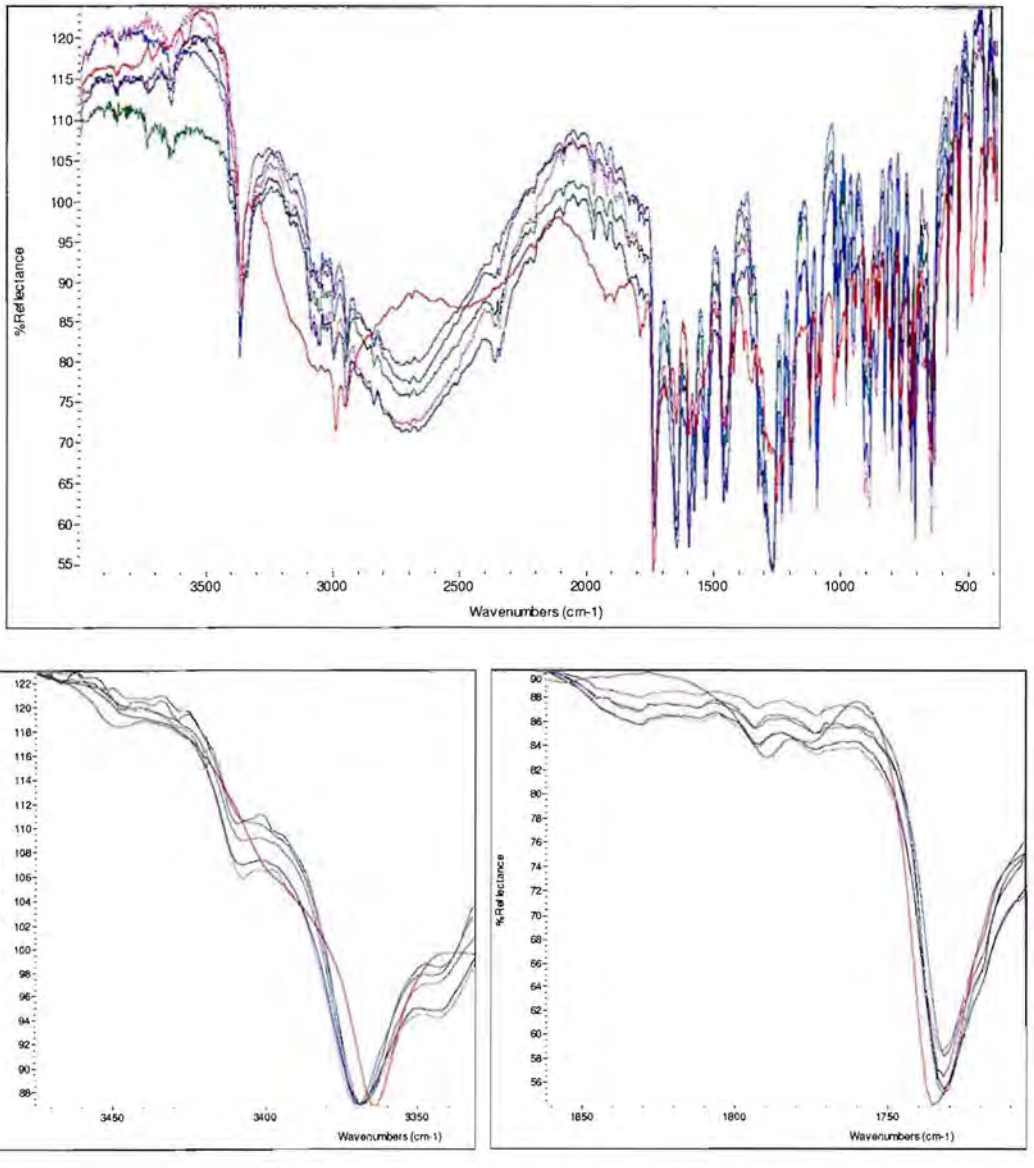

Figure 7.31 (a) Overlay spectra of the mebendazole propionic acid solvate (Form E) stored at 40±2℃ & 75±5 % RH for twenty-eight days. (b and c) Superimposed DRIFT-IR spectra of the main absorptions at the –NH and >C=O stretching frequencies showing polymorphic transition in the sample (initial, 3, 7, 14, 21 and 28 days).

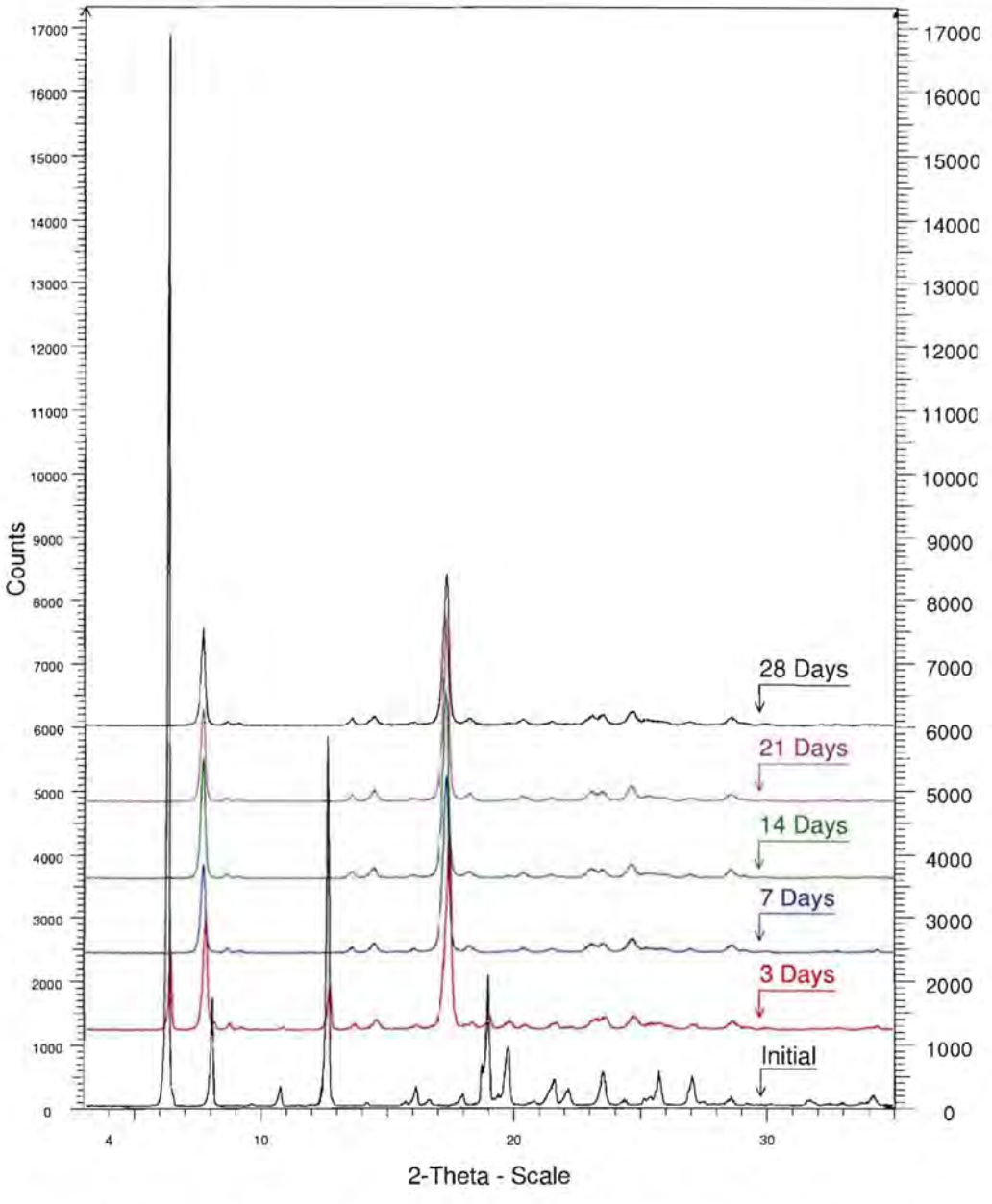

Figure 7.32 XRPD Overlay of the mebendazole propionic acid solvate (Form E) stored at 40±2℃ & 75±5 % RH for twenty-eight days.

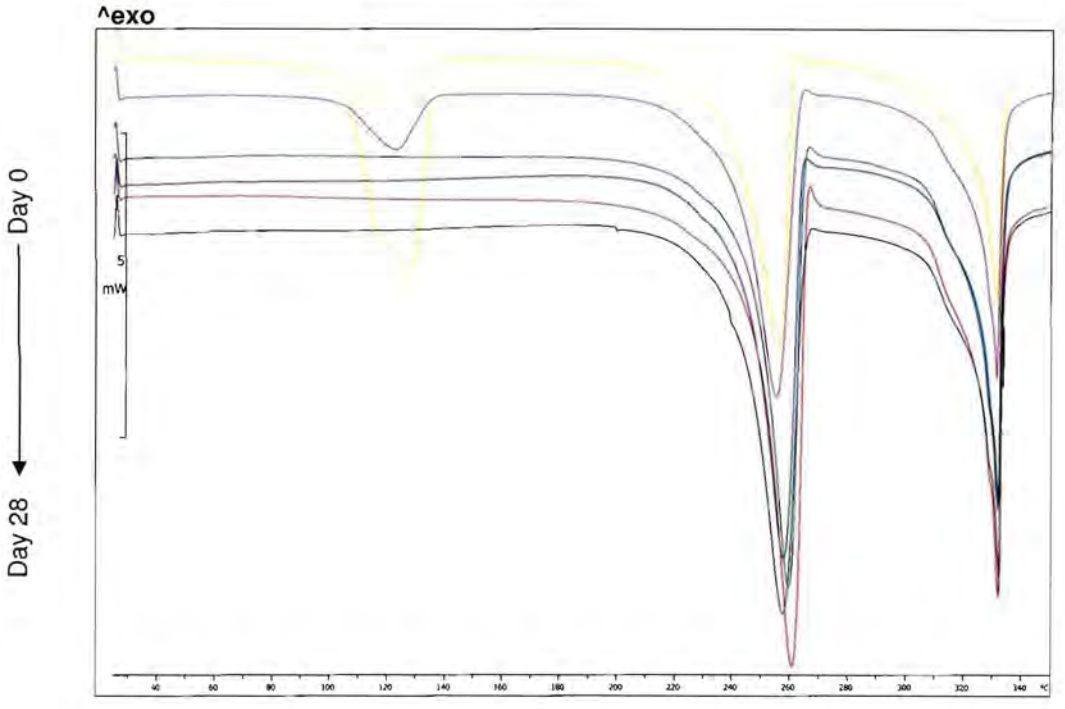

Figure 7.33 DSC thermogram overlay of mebendazole propionic acid solvate (Form E) stored at 40±2℃ & 75±5 % RH for twenty-eight days.

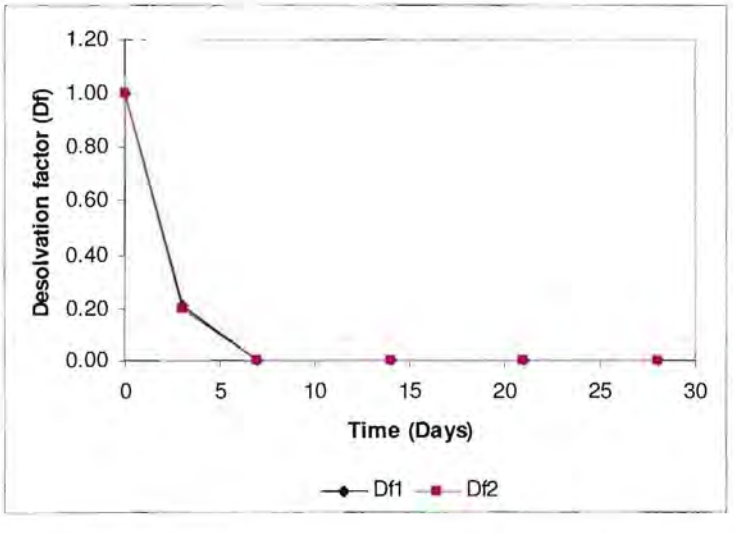

Figure 7.34 Desolvation factors for both DSC and TGA of Form E (40±2℃ & 75±5 % RH) plotted as a function of time (days).

7.4 Quantitative investigation of the desolvation of Form D and conversion to Form A

The relative ratios of Form D and Form A present in the samples during the stability trail, were calculated from the DRIFT-IR data, based on a method proposed by Brits (2008:144-147).

7.4.1 Calculating the ratio of Form A and Form D content relative to the total polymorph content in a sample from DRIFT-IR data

The ratios of Form A and Form D content relative to the total polymorph content in the product were calculated from the DRIFT-IR data using the following equations (Equation 7.7 and Equation 7.8):

$$Form\ A/(A+D) = \frac{AUC_A}{AUC_A + AUC_D} \tag{7.7}$$

$$Form\ D/(A+D) = \frac{AUC_D}{AUC_A + AUC_D} \tag{7.8}$$

Where:

Form A/(A+D):	Ratio of Form A relative to the total mebendazole polymorph content in the sample
Form D/(A+D):	Ratio of Form D relative to the total mebendazole polymorph content in the sample
AUC_A:	Area of the absorption peak present at ≈3370 cm^{-1}, characteristic of Form A
AUC_D:	Area of the absorption peak present at 3353 cm^{-1}, characteristic of Form D

Figure 7.35 illustrates the characteristic frequencies of Form A (3370 cm^{-1}) and Form D (3353 cm^{-1}) respectively as well as the areas thereof observed in the DRIFT-IR spectra of Form D at 0, 3 and 28 days, when stored at 25±2℃ & 0 % RH.

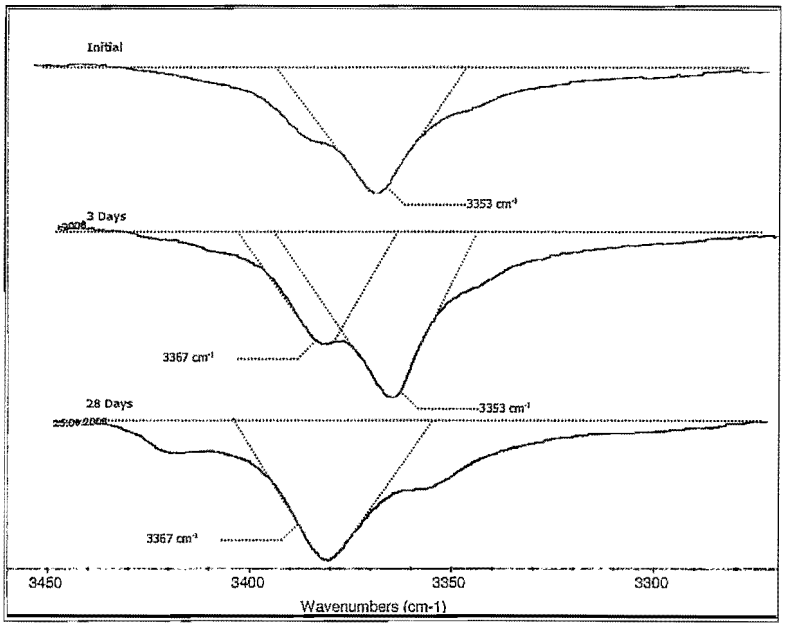

Figure 7.35 Characteristic stretching frequencies (cm^{-1}) and the areas thereof in the DRIFT-IR spectra of Form D (at 25±2°C & 0 % RH) after 0 (top), 3 (middle) and 28 (bottom) days indicating the decreasing Form D and increasing Form A content.

From Figure 7.35 it was clear that there was an overlapping of the characteristic IR-peaks of Form D (3353 cm^{-1}) and Form A (3367 cm^{-1}), which might complicate the analysis. The integrated peak areas were calculated using the sophisticated area-calculation tool of the OMNIC® version 7.3 Software package (Thermo Electon Corporation).

The *Form D/(A+D)* was calculated for Form D at the various temperatures and relative humidities and plotted as a function of time to provide an indication of the Form D fraction present in the samples at a given time interval (Figure 7.36).

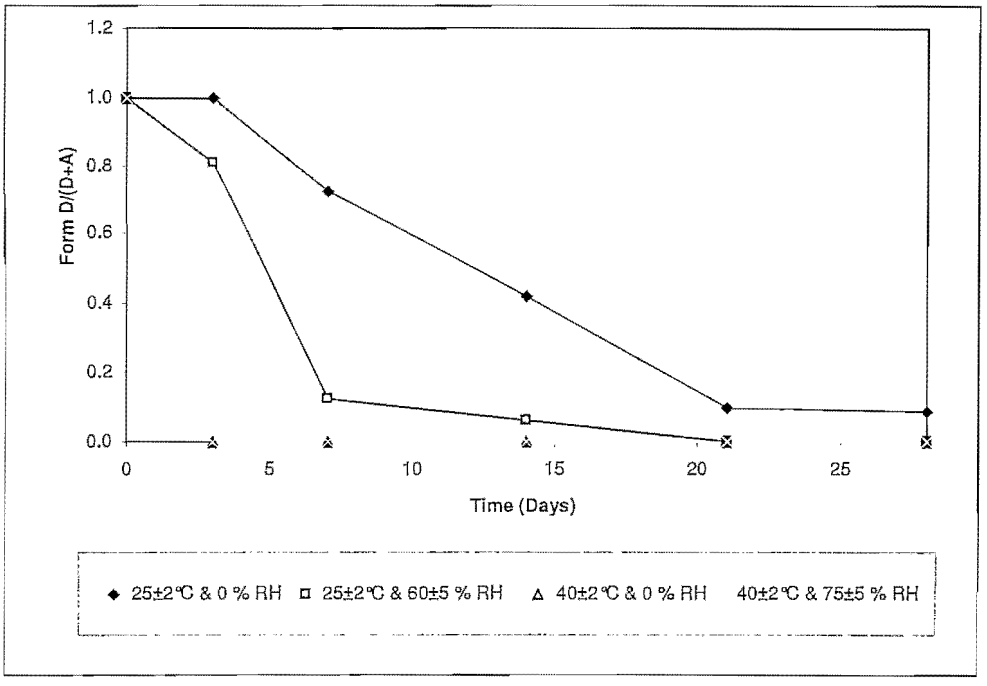

Figure 7.36 Ratio of the Form D content relative to the total mebendazole polymorph content when stored at: 25±2°C & 0 % RH, 25±2°C & 60±5 % RH, 40±2°C & 0 % RH & 40±2°C & 75±5 % RH.

From Figure 7.36 it is clear that the rate for the Form D → Form A conversion was higher at 40°C compared to that observed at 25°C. Form D underwent complete desolvation after 3 days when stored at 40±2°C & 0% RH and 40±2°C & 75±5 % RH, whereas the desolvation at 25±2°C & 60±5 % RH was completed after 21 days. Only 90% of the Form D fraction underwent desolvation when stored at 25±2°C & 0 % RH for 28 days

The fractions of Form A, formed when Form D was stored at 25±2°C & 0 % RH and 25±2°C & 60±5 % RH during the stability trial, were calculated using Equation 7.7 and are illustrated in Figure 7.37.

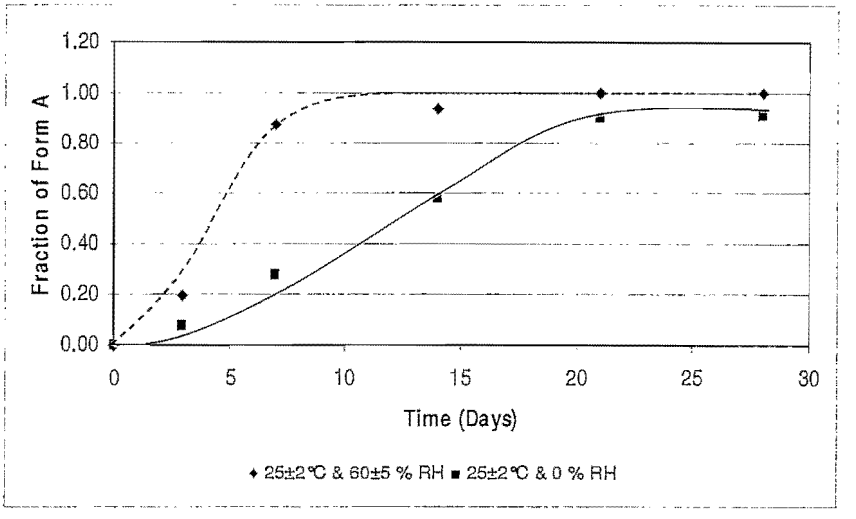

Figure 7.37 Ratio of the Form A content relative to the total mebendazole polymorph content when Form D was stored at: 25±2°C & 0 % RH and 25±2°C & 60±5 % RH.

The formation of Form A at 25±2°C & 60±5 % RH did not reveal any lag time, and produced a first-order like fraction vs. Time-curve. The formation of Form A at 25±2°C & 0 % RH did however reveal a lag time, and produced a sigmoidal like fraction vs. Time-curve.

7.4.2 Models and mechanisms for solid-state kinetics

Brown *et al.* (1980:41-50) stated that the rate equation for solid-state kinetic analysis may be generalised in the derivative form as indicated in Equation 7.9.

$$\frac{d\alpha}{dt} = kf(\alpha) \tag{7.9}$$

Where: α is the fractional extent of the reaction, $d\alpha/dt$ the rate of reaction and k the rate constant.

Equation 7.9 can be integrated to generate Equation 7.10:

$$g(\alpha) = kt + c \tag{7.10}$$

When the fractional extent of the reaction (α) is plotted as a function of time, a unique plot (*α-time curve*) is generated. This plot may be used to determine the model of the kinetic analysis (Brown & Glass, 1999:130). The shape of the α-time curve can be classified as *acceleratory*, *sigmoid*, *constant* or *deceleratory* (Brown & Glass, 1999:130). Figure 7.38 illustrates examples of *acceleratory*, *sigmoid*, *constant* and *deceleratory* isothermal α-time curves.

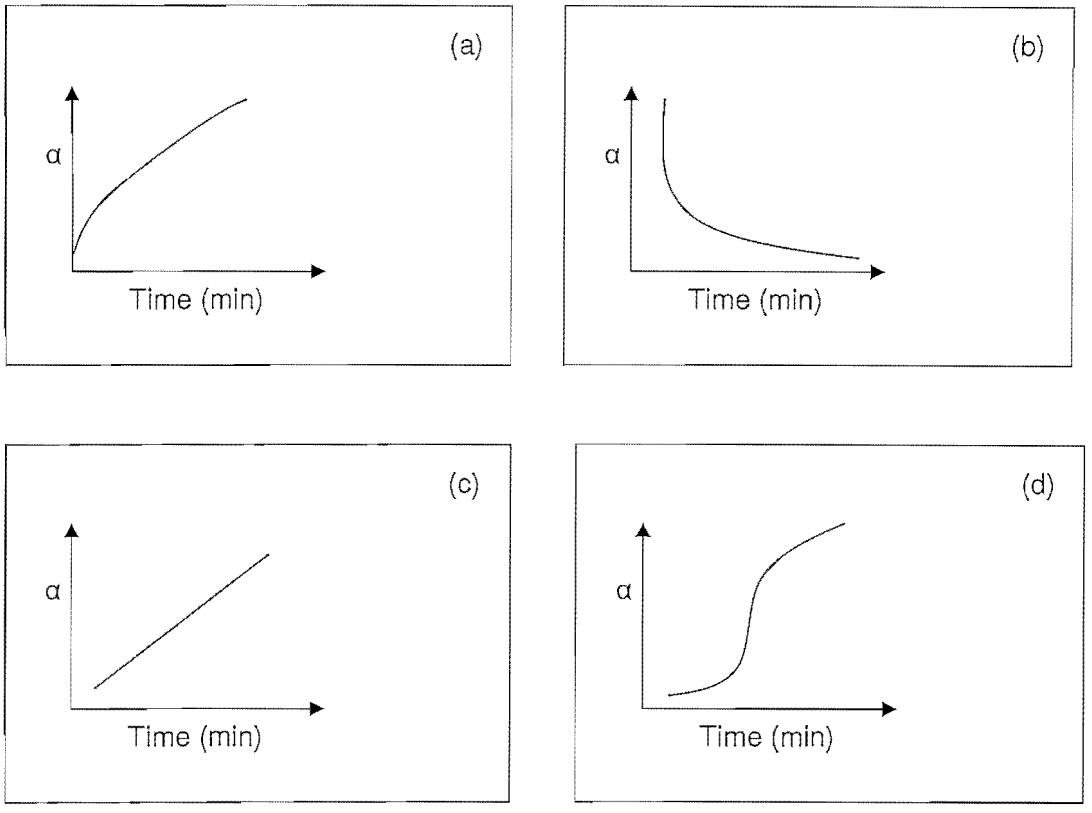

Figure 7.38 Examples of (a) *acceleratory*, (b) *decelerator*y, (c) *constant* and (d) *sigmoid* - isothermal α-time curves (reproduced from Khawam and Flanagan, 2006:17318-17319).

Khawam and Flannagan (2006:17316) defined a *model* as a theoretical or mathematical description of an experimental observation. Numerous models have been postulated for solid-state conversions that are based on certain mechanistic assumptions.

These models can be derived from the generic mathematical form (Equation 7.11) proposed by Sestak and Berggren (1971:1), by assigning values to the three variables (*m*, *n* and *p*):

$$g(\alpha) = \alpha^m (1-\alpha)^n (-\ln(1-\alpha))^p \qquad (7.11)$$

Homogeneous kinetics, (e.g., gas or solution phases) are usually not as complex as heterogeneous kinetics (e.g., solid-state kinetics). For heterogeneous kinetics, a reasonable reaction model is identified based on the correlation coefficient (r^2) for the algebraic expressions of functions. Table 7.6 provides a summary of the mechanisms and their algebraic expressions (Turmanova *et al.*, 2008:137).

Table 7.6 Algebraic expressions of functions g(α) and corresponding mechanism (Turmanova *et al.*, 2008:137)

No.	Sym.	Model	$g(\alpha)$	Rate-determining mechanism
1. Chemical process or mechanism non-invoking equations				
1.	F1/3	One-third order	$1 - (1-\alpha)^{2/3}$	Chemical reaction
2.	F3/4	Three-quarters order	$1 - (1-\alpha)^{1/4}$	Chemical reaction
3.	F3/2	One and a half order	$(1-\alpha)^{-1/2}-1$	Chemical reaction
4.	F2	Second order	$(1-\alpha)^{-1}-1$	Chemical reaction
5.	F3	Third order	$(1-\alpha)^{-2}-1$	Chemical reaction
2. Acceleratory rate equations				
6.	P3/2	Mampel power law	$\alpha^{3/2}$	Nucleation
7.	P1/2	Mampel power law	$\alpha^{1/2}$	Nucleation
8.	P1/3	Mampel power law	$\alpha^{1/3}$	Nucleation
9.	P1/4	Mampel power law	$\alpha^{1/4}$	Nucleation
10.	E1	Exponential law	$\ln \alpha$	Nucleation
3. Sigmoidal rate equations or random nucleation and subsequent growth				
11.	A1,F1	Avrami-Erofeev equation	$-\ln(1-\alpha)$	Assumed random nucleation and its subsequent growth, $n = 1$
12.	A3/2	Avrami-Erofeev equation	$[-\ln(1-\alpha)]^{2/3}$	Assumed random nucleation and its subsequent growth, $n = 1.5$
13.	A2	Avrami-Erofeev equation	$[-\ln(1-\alpha)]^{1/2}$	Assumed random nucleation and its subsequent growth, $n = 2$
14.	A3	Avrami-Erofeev equation	$[-\ln(1-\alpha)]^{1/3}$	Assumed random nucleation and its subsequent growth, $n = 3$
15.	A4	Avrami-Erofeev equation	$[-\ln(1-\alpha)]^{1/4}$	Assumed random nucleation and its subsequent growth, $n = 4$
16.	Au,B1	Prout-Tompkins equation	$\ln[\alpha/(1-\alpha)]$	Branching nuclei

Table 7.6 (Continued)

4. Deceleratory rate equations				
4.1 Phase boundary reactions				
17.	R1,F0,P1	Power law	α	Contracting disk
18.	R2,F1/2	Power law	$1-(1-\alpha)^{1/2}$	Contracting cylinder (Cylindrical symmetry)
19.	R3,F2/3	Power law	$1-(1-\alpha)^{1/3}$	Contracting sphere (Spherical symmetry)
4.2 Based on the diffusion mechanism				
20.	D1	Parabola law	α^2	One-dimensional diffusion
21.	D2	Valensi equation	$\alpha+(1-\alpha)\ln(1-\alpha)$	Two-dimensional diffusion
22.	D3	Jander equation	$[1-(1-\alpha)^{1/3}]^2$	Three-dimensional diffusion, spherical symmetry
23.	D4	Ginstling-Brounstein equation	$1-\frac{2}{3}\alpha-(1-\alpha)^{2/3}$	Three-dimensional diffusion, cylindrical symmetry
24.	D5	Zhuravlev, Lesokin, Tempelman equation	$[(1-\alpha)^{-1/3}-1]^2$	Three-dimensional diffusion
25.	D6	Anti-Jander equation	$[(1+\alpha)^{1/3}-1]^2$	Three-dimensional diffusion
26.	-	Anti-Ginstling-Brounstein equation	$1+\frac{2}{3}\alpha-(1+\alpha)^{2/3}$	Three-dimensional diffusion
27.	-	Anti-Zhuravlev, Lesokin, Tempelman equation	$[(1+\alpha)^{-1/3}-1]^2$	Three-dimensional diffusion

The heterogeneous kinetics for the formation of Form A, expressed as *Form A/(A+D)* - for the desolvation of Form D, (α) was analysed based on the solid-state reaction models reported by Turmanova *et al.*, (2008:137) in Table 7.6. The most reasonable reaction model was identified based on the highest correlation coefficient (r^2) for the algebraic expressions of $g(\alpha)$.

Table 7.7 summarises the correlation coefficients (r^2) for Form D, calculated from the algebraic expressions of $g(\alpha)$.

Table 7.7 Summary of the algebraic expressions of functions $g(\alpha)$ and its corresponding mechanism for Form D when exposed to 25±2℃ & 0 % RH and 25±2℃ & 60±5 % RH

			r^2	
Sym.	**Model**	$g(\alpha)$	**25±2℃ & 60±5 % RH**	**25±2℃ & 0 % RH**
$F_{1/3}$	One-third order	$1 - (1-\alpha)^{2/3}$	0.7716	0.9609
$F_{3/4}$	Three-quarters order	$1 - (1-\alpha)^{1/4}$	0.9347	0.9505
$F_{3/2}$	One and a half order	$(1-\alpha)^{-1/2}-1$	0.9484	0.9573
F_2	Second order	$(1-\alpha)^{-1}-1$	0.9641	0.9381
F_3	Third order	$(1-\alpha)^{-2}-1$	0.9133	0.8971
$P_{3/2}$	Mampel power law	$\alpha^{3/2}$	0.7113	0.9525
$P_{1/2}$	Mampel power law	$\alpha^{1/2}$	0.6070	0.8818
$P_{1/3}$	Mampel power law	$\alpha^{1/3}$	0.5490	0.7881
$P_{1/4}$	Mampel power law	$\alpha^{1/4}$	0.5001	0.7085
E_1	Exponential law	$\ln \alpha$	0.4777	0.8048
A_1, F_1	Avrami-Erofeev equation	$-\ln(1-\alpha)$	0.9028	0.9737
$A_{3/2}$	Avrami-Erofeev equation	$[-\ln(1-\alpha)]^{2/3}$	0.8846	0.9995
A_2	Avrami-Erofeev equation	$[-\ln(1-\alpha)]^{1/2}$	0.8681	0.9832
A_3	Avrami-Erofeev equation	$[-\ln(1-\alpha)]^{1/3}$	0.8247	0.9099
A_4	Avrami-Erofeev equation	$[-\ln(1-\alpha)]^{1/4}$	0.7780	0.8359
A_u	Prout-Tompkins equation	$\ln[\alpha/(1-\alpha)]$	0.7704	0.9610
R_1, F_0, P_1	Power law	α	0.6775	0.9553
$R_2, F_{1/2}$	Power law	$1-(1-\alpha)^{1/2}$	0.8423	0.9590
$R_3, F_{2/3}$	Power law	$1-(1-\alpha)^{1/3}$	0.9144	0.9541
D_1	Parabola law	α^2	0.7416	0.9344
D_2	Valensi equation	$\alpha + (1-\alpha)\ln(1-\alpha)$	0.8571	0.8957
D_3	Jander equation	$[1-(1-\alpha)^{1/3}]^2$	0.928	0.8815
D_4	Ginstling-Brounstein equation	$1 - \frac{2}{3}\alpha - (1-\alpha)^{2/3}$	0.902	0.9024
D_5	Zhuravlev, Lesokin, Tempelman equation	$[(1-\alpha)^{-1/3}-1]^2$	0.9593	0.8500
D_6	Anti-Jander equation	$[(1+\alpha)^{1/3}-1]^2$	0.7173	0.9450
-	Anti-Ginstling-Brounstein equation	$1 + \frac{2}{3}\alpha - (1+\alpha)^{2/3}$	0.7250	0.9419
-	Anti-Zhuravlev, Lesokin, Tempelman equation	$[(1+\alpha)^{-1/3}-1]^2$	0.6951	0.9512

From the results obtained in Table 7.7 it can be postulated that the mechanism for the desolvation of Form D, when exposed to 25±2°C & 60±5 % RH was best described by the second-order reaction (F2-model – Figure 7.39(a)) (r^2 = 0.9641) and when exposed to 25±2°C & 0 % RH by the Avrami-Erofeev reaction (A3/2-model – Figure 7.39 (b)) (r^2 = 0.9995).

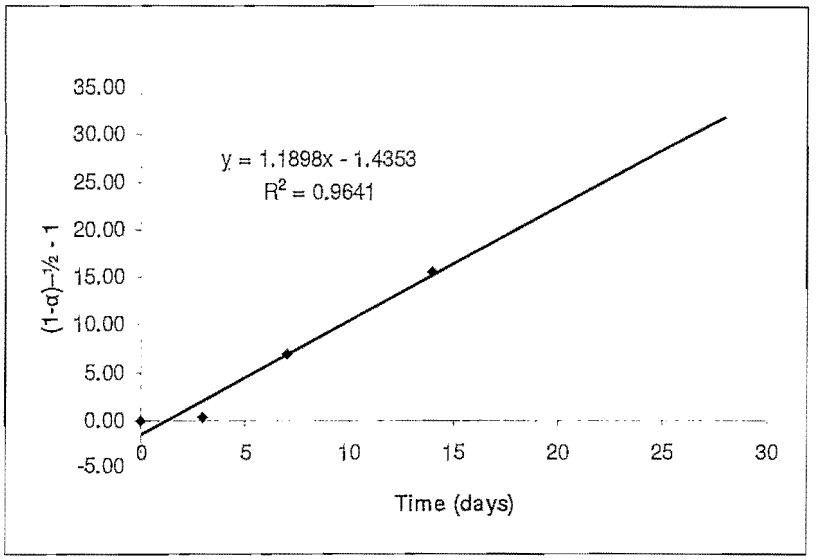

(a)

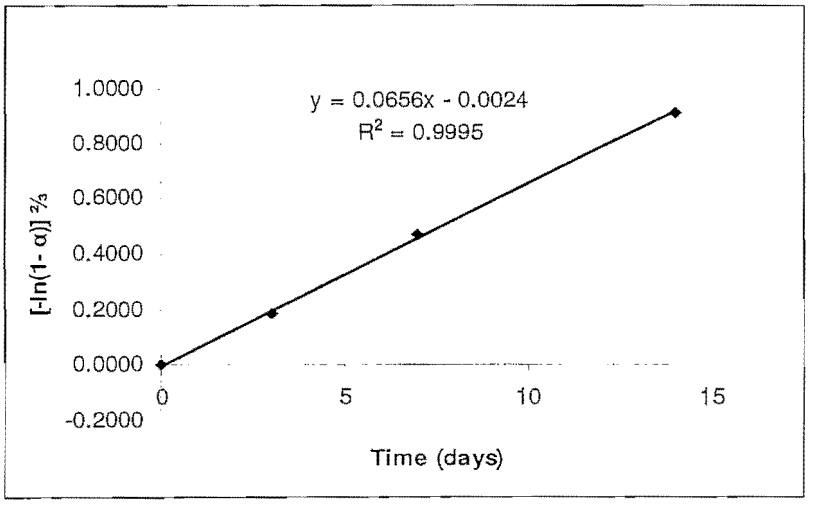

(b)

Figure 7.39 *g(α)* versus time plots for Form D when stored at (a) 25±2°C & 60±5 % RH and (b) 25±2°C & 0 % RH.

Figure 7.40 illustrates the good fit of the experimental data (▲and ■) on the postulated models of desolvation. The plot for Form D when stored at 25±2°C & 0 % RH in Figure 7.40 showed a sigmoid α-time curve, while that for Form D when stored at 25±2°C & 60±5 % RH showed an acceleratory α-time curve.

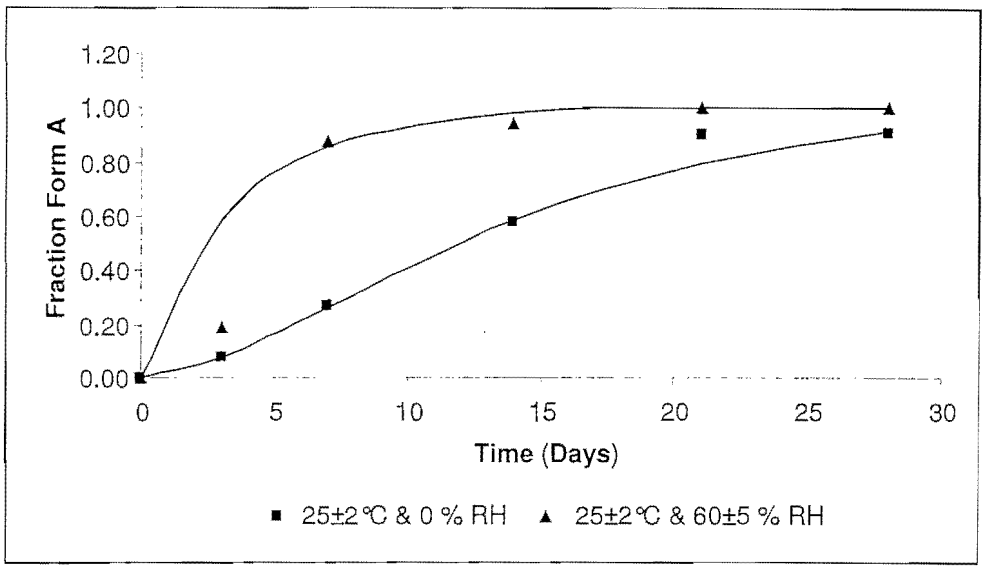

Figure 7.40 Fit of the experimental data (▲and ■) on the postulated models of desolvation for Form D when stored at 25±2°C & 0 % RH and 25±2°C & 60±5 % RH.

The Avrami-Erofeev reaction is based on the principal that the rate of the reaction is governed by the growth of random nuclei in three dimensions that ingest other nuclei (Byrn *et al.*, 1999:444-445).

A desolvation nucleus can be defined as a specific area in / on the crystal lattice, where desolvation is initiated. Bamford & Tipper (1980:120) stated that the formation of a desolvation nucleus is sensitive to superficial imperfections in the crystal. Thus, desolvation will start (a desolvation nucleus will form) in the crystal where the least energy is needed for the removal of the solvent molecule from the solvated lattice (Bamford & Tipper, 1980:120).

7.4.3 The Avrami-Erofeev model and process of nuclei growth

Khawam (2007:53-57) stated that the growth of nuclei could be considered to be a radial growth, and that the nuclei growth rate [G(x)] was represented by the radius formed from the growth (Figure 7.41).

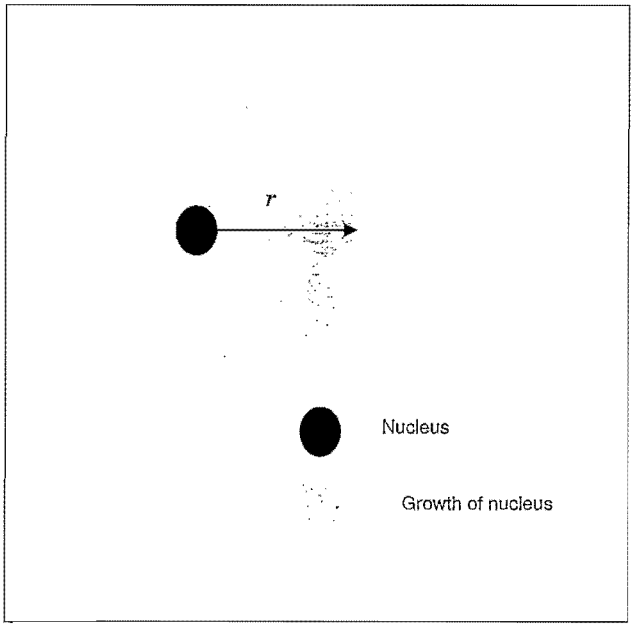

Figure 7.41 Schematic presentation of a nucleus and the radial growth of the nucleus. The radius of the growth is indicated by r.

The nucleus growth (i.e. the radius, r) at time t, ($r(t,t_0)$) was defined by Khawam (2007:53) (Equation 7.12) as:

$$r(t,t_0) = \int_{t_0}^{t} G(x).dx \tag{7.12}$$

Where: G(x) is the rate of nuclei growth and t_0 is the formation time of a growth nucleus (Khawam, 2007:53).

Khawam (2007:54) indicated that the shape (σ) and the growth dimension (λ) influenced the nuclei growth. Once a nucleus has been formed at time (t_0), it will occupy a specific volume $v(t)$ at time, t, which is defined by Equation 7.13.

$$v(t) = \sigma[r(t,t_0)]^{\lambda} \tag{7.13}$$

Where: λ is the number of growth dimensions (i.e., λ =1, 2 or 3), σ is the shape factor (i.e., $4\pi/3$ for a sphere) and r is the radius of a nucleus at time, t (Khawam, 2007:54).

Khawam (2007:54) stated that the total volume occupied by all nuclei ($V(t)$) in a system could be calculated by the combination of the nucleation rate (dN/dt) and growth rate ($v(t,t_0)$) (Equation 7.14):

$$V(t) = \int_0^t v(t)\left(\frac{dN}{dt}\right)_{t=t_0} dt_0 \qquad (7.14)$$

Where: $V(t)$ is the volume of all growth nuclei and dN/dt is the nucleation rate.

Substitution of Equation 7.12 and Equation 7.13 into Equation 7.14 produced Equation 7.15:

$$V(t) = \int_0^t \sigma\left(\int_{t_0}^t G(x).dx\right)^{\lambda}\left(\frac{dN}{dt}\right)_{t=t_0} dt_0 \qquad (7.15)$$

Equation 7.15 may be integrated to produce any of the nucleation and / or growth rate models listed in Table 7.6.

Khawam (2007:56) indicated that there were two restrictions on nuclei growth (illustrated in Figure 7.42):

(1) **Ingestion** – where a potential nucleation site is eliminated by the growth of an existing nucleus;

(2) **Coalescence** – where a loss of the growth product is experienced due to interface when reaction zones of two or more growing nuclei merge.

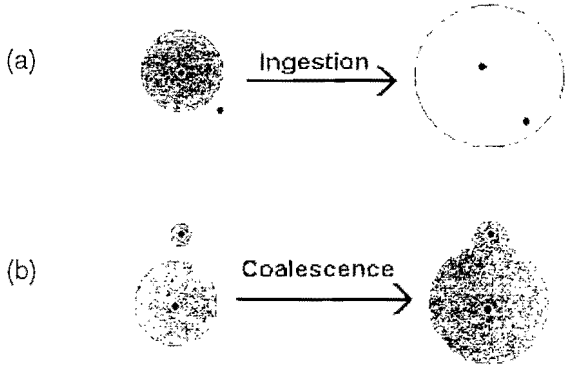

Figure 7.42 Schematic illustration of the two types of growth restrictions: (a) Ingestion and (b) Coalescence. The black dots represent nucleation sites and shaded areas the nuclei growth regions (Khawam, 2007:77).

The volume fraction, α, of the transformed material (if ingestion and coalescence are not considered) has been defined as Equation 7.16 (Khawam, 2007:56):

$$\alpha = \frac{\pi}{3} N v^3 t^4 \tag{7.16}$$

However, if ingestion and coalescence are considered, then the volume fraction is replaced by the *Avrami* equation (Equation 7.17) (Khawam, 2007:57):

$$\alpha = 1 - \exp(-\frac{\pi}{3} N v^3 t^4) \tag{7.17}$$

Therefore, Equation 7.17 represents site saturated three-dimensional growth. However, depending on whether all the nuclei appeared at one time, or grew dimensionally, the general equation for volume transformed transformation would be expressed as (Equation 7.18):

$$\alpha = 1 - \exp(-kt^n) \tag{7.18}$$

Integration of Equation 7.18 produced Equation 7.19, which is known as the Avrami-Erofeev model (Khawam, 2007:57)

$$[-\ln(1-\alpha)]^n = kt \tag{7.19}$$

Table 7.8 Stability parameters calculated using the second order and Avrami-Erofeev models for the desolvation of Form D at 25±2ºC & 0% RH and 25±2ºC & 60±5 % RH

Conditions	k (day^{-1})	$t_{½}$ (days)	t_{90} (days)
25±2℃ & 0 % RH	0.0656	12.0	3.4
25±2℃ & 60±5 % RH	1.1898	2.0	1.3

When the rate constants, k, in Table 7.8 were compared it became evident that the rate of desolvation of Form D at 25±2℃ & 60±5 % RH was 18 times faster in comparison to the desolvation of Form D at 25±2℃ & 0 % RH.

The shelf-life (t_{90}) of a sample has been defined as the period needed to cause a 10% decrease in the original composition of the sample (Winfield, 1999:84). The half-life ($t_{½}$) of a sample can be defined as the period needed to cause a 50% decrease in the original composition of the sample.

The significance of the difference in the rate constants was clearly indicated by the differences in the half-life ($t_{½}$) and the shelf-life (t_{90}) of Form D (Table 7.8). The half-life ($t_{½}$) and the shelf-life (t_{90}) were calculated by substituting $\alpha = 0.5$ (for $t_{½}$) and $\alpha = 0.1$ (for t_{90}) in the $g(\alpha) = kx + c$ – equations derived from Figure 7.39, which fashioned the following equations:

- Half-life ($t_{½}$) for Form D stored at 25±2°C & 0 % RH (Equation 7.20):

$$t_{\frac{1}{2}} = \frac{0.7856}{k} \tag{7.20}$$

- Shelf-life (t_{90}) for Form D stored at 25±2°C & 0 % RH (Equation 7.21):

$$t_{90} = \frac{0.2255}{k} \tag{7.21}$$

- Half-life ($t_{½}$) for Form D stored at 25±2°C & 60±5 % RH (Equation 7.22):

$$t_{\frac{1}{2}} = \frac{2.4353}{k} \tag{7.22}$$

- Shelf-life (t_{90}) for Form D stored at 25±2°C & 60±5 % RH (Equation 7.23):

$$t_{90} = \frac{1.5464}{k} \tag{7.23}$$

The shelf-life of Form D when stored at 25±2°C & 60±5 % RH was 2.6 times lower compared to when Form D was stored at 25±2°C & 0 % RH, suggesting that the presence of moisture facilitated the desolvation process.

According to literature (Swanepoel *et al.*, 2003:346) the recrystallisation of mebendazole using acetic acid as solvent, produced Form A (refer to Chapter 3, Section 3.2.1). However during this study it was revealed that the recrystallisation of mebendazole using acetic acid produced a thermodynamically unstable solvated form (Form D), which underwent rapid desolvation at ambient conditions (Table 7.8 - 25±2°C & 0 % RH) to produce Form A.

Form D did not undergo complete desolvation when stored at 25±2℃ & 0 % RH for 28 days as indicated in Figure 7.40. Based on the kinetic model identified for the desolvation of Form D when stored at 25±2℃ & 0 % RH (Avrami-Erofeev), it was calculated that complete desolvation of Form D at 25±2℃ & 0 % RH would only be achieved after approximately 131.5 days.

7.5 Quantitative investigation of the desolvation of Form E and conversion to Form A

The relative ratios of mebendazole Form E and Form A present in the samples during the stability trail were calculated from the XRPD data based on a method proposed by Brits (2008:142-144).

7.5.1 Calculating the ratio of Form A and Form E content relative to the total polymorph content in a sample from XRPD data

The ratios of Form A and Form E content relative to the total polymorph content in the samples were calculated from the XRPD data using the following equations:

$$Form\ A/(A+E) = \frac{I_A}{I_A + I_E} \tag{7.24}$$

$$Form\ E/(A+E) = \frac{I_E}{I_A + I_E} \tag{7.25}$$

Where:

Form A/(A+E):	ratio of Form A relative to the total mebendazole polymorph content in the sample
Form E/(A+E):	ratio of Form E relative to the total mebendazole polymorph content in the sample
I_A:	Intensity of the 17.3±0.1°2θ diffraction peak, characteristic of Form A
I_E:	Intensity of the 6.3±0.1°2θ diffraction peak, characteristic of Form E

Figure 7.43 illustrates the characteristic diffraction peaks of Form E and Form A and the intensities for Form E when stored at 40±2°C & 75±5 % RH at day: 0, 3 and 28. The decrease in the Form E content, and increase in Form A content is clearly visible in Figure 7.43.

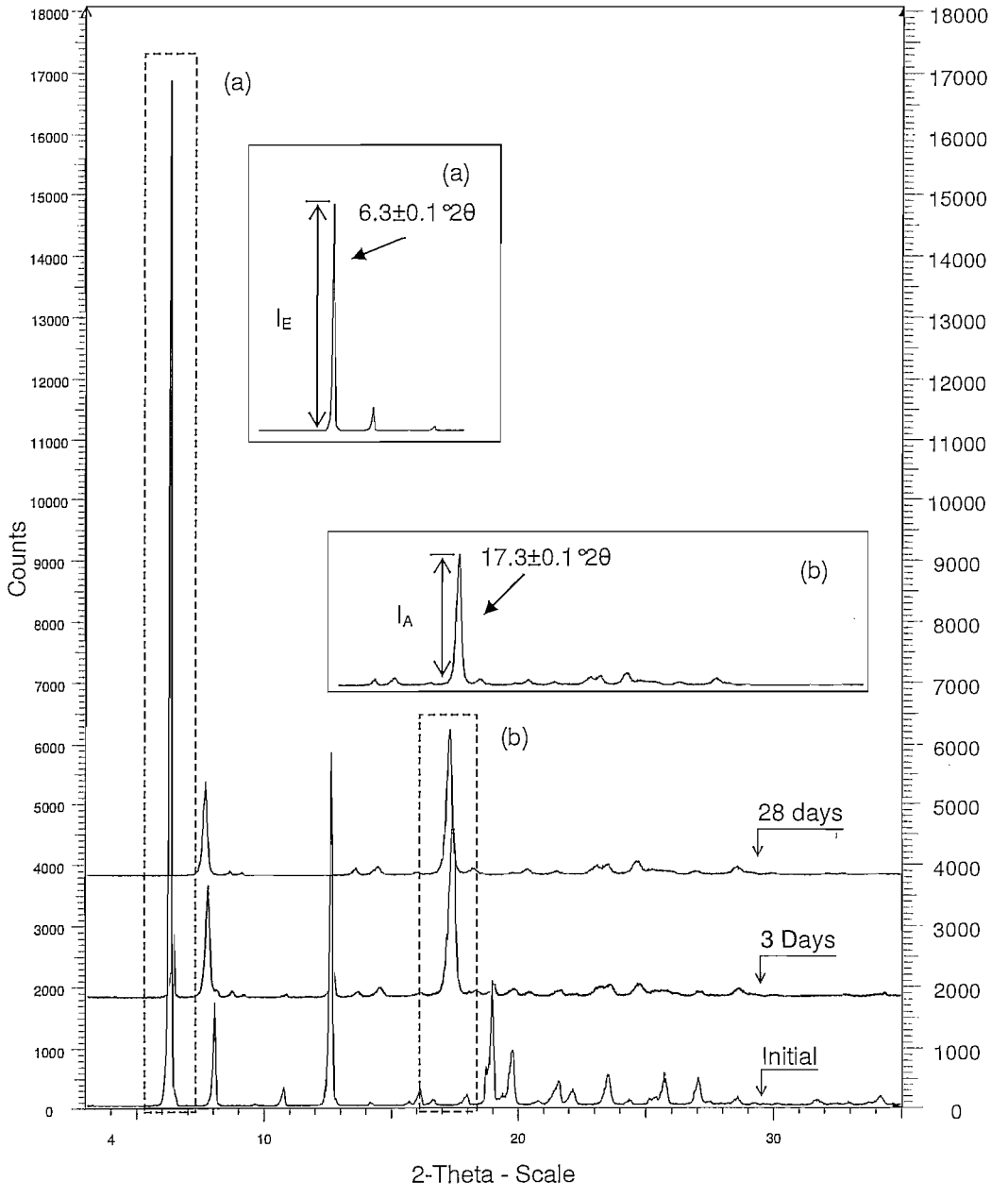

Figure 7.43 Characteristic diffraction peaks and their intensities for mebendazole Forms A and E present in the Form E sample when stored at different intervals at 40±2°C & 75±5 % RH.

The desolvation of Form E was observed when it was stored at 25±2°C & 60±5 % RH, 40±2°C & 0 % RH and 40±2°C & 75±5 % RH. The desolvation of Form E, expressed as *Form E/(A+E)*, was calculated for the mentioned conditions and are illustrated in Figure 7.44.

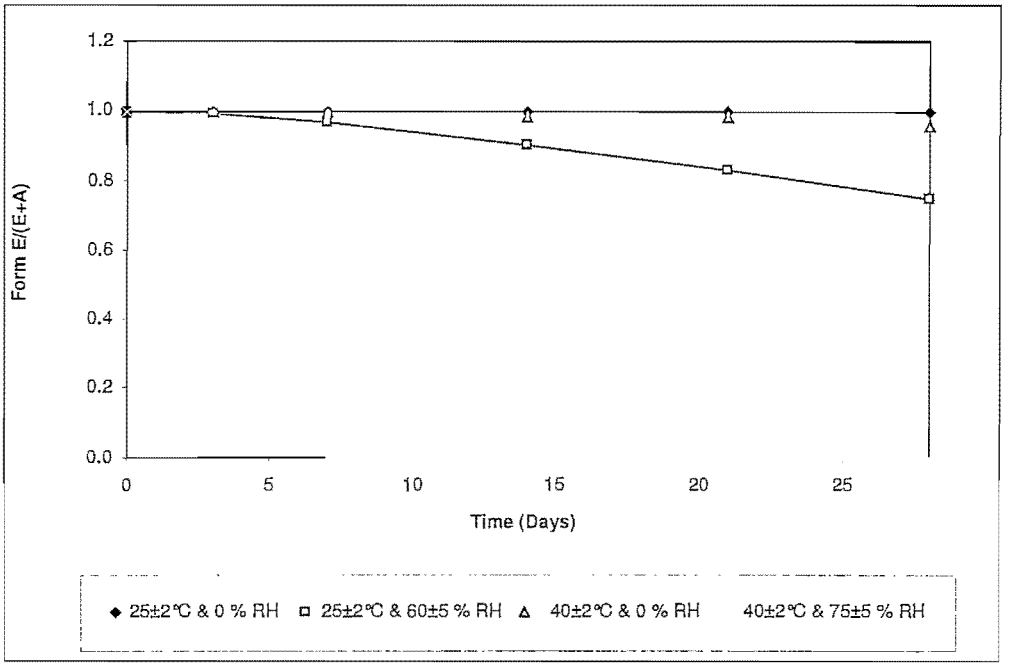

Figure 7.44 Ratio of the Form E content relative to the total mebendazole polymorph content when stored at: 25±2°C & 0 % RH, 25±2°C & 60±5 % RH, 40±2°C & 0 % RH and 40±2°C & 75±5 % RH.

From Figure 7.44 the following observations were made:

- Storage of Form E at 25±2°C & 0 % RH, did not induce any desolvation of Form E.
- Storage of Form E at 25±2°C & 60±5 % RH, 40±2°C & 0 % RH and 40±2°C & 75±5 % RH, did induce the desolvation of Form E, and the rate of desolvation was in the order: 40±2°C & 75±5 % RH > 25±2°C & 60±5 % RH > 40±2°C & 0 % RH, suggesting that moisture could have been a catalyst for the desolvation of Form E. It is known that the adsorption of water enhances the molecular mobility of solids, which may lead to an increase in the solid-state reactivity, thus increase the rate of desolvation(Reutzel-Edens & Newman, 2007:251).
- The extent of desolvation of Form E, when stored at 40±2°C & 0 % RH was found to be insignificant for the investigation of heterogeneous desolvation kinetics (less than 10% after 28 days), and was therefore not investigated.

The fractions of Form A formed when Form E was stored at 40±2°C & 75±5 % RH and 25±2°C & 60±5 % RH, were calculated using Equation 7.24 and illustrated in Figure 7.45

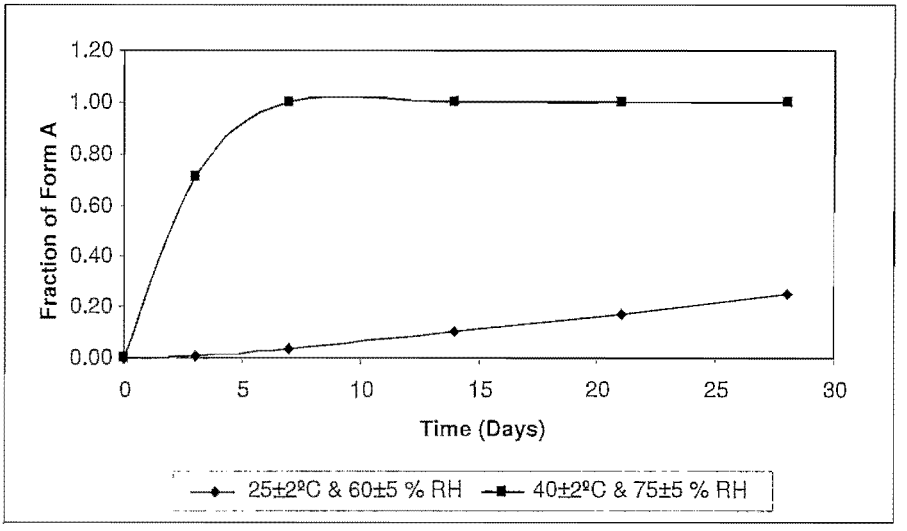

Figure 7.45 Ratio of the Form A content relative to the total mebendazole polymorph content when Form E was stored at 40±2°C & 75±5 % RH and 25±2°C & 60±5 % RH.

The formation of Form A at 40±2°C & 75±5 % RH (Figure 7.45) did not reveal any lag time, however the formation of Form A at 25±2°C & 60±5 % RH did reveal a lag time. Both plots in Figure 7.45 indicated an acceleratory α-time curve.

The heterogeneous kinetics for the formation of Form A, expressed as $Form\ A/(A+E)$ (Equation 7.24) for the desolvation of Form E at 40±2°C & 75±5 % RH and 25±2°C & 60±5 % RH, (α) were analysed, based on the solid-state reaction models reported by Turmanova *et al.*, (2008:137). The most reasonable reaction model was identified based on the highest correlation coefficient (r^2) for the algebraic expressions of $g(\alpha)$. Table 7.9 summarises the calculated correlation coefficient (r^2) for the algebraic expressions of $g(\alpha)$.

Table 7.9 Summary of the algebraic expressions of functions $g(\alpha)$ and corresponding mechanism for Form E when exposed to 25±2℃ & 60±5 % RH and 40±2℃ & 75±5 % RH

			r^2	
Sym.	**Model**	$g(\alpha)$	**25±2℃ & 60±5 % RH**	**40±2℃ & 75±5 % RH**
F1/3	One-third order	$1 - (1-\alpha)^{2/3}$	0.9828	0.5238
F3/4	Three-quarters order	$1 - (1-\alpha)^{1/4}$	0.9795	0.5824
F3/2	One and a half order	$(1-\alpha)^{-1/2}-1$	0.9500	0.1707
F2	Second order	$(1-\alpha)^{-1}-1$	0.9478	0.1707
F3	Third order	$(1-\alpha)^{-2}-1$	0.9434	0.1707
P3/2	Mampel power law	$\alpha^{3/2}$	0.9318	0.5100
P1/2	Mampel power law	$\alpha^{1/2}$	0.9796	0.3912
P1/3	Mampel power law	$\alpha^{1/3}$	0.9159	0.3030
P1/4	Mampel power law	$\alpha^{1/4}$	0.8443	0.3401
E1	Exponential law	$\ln \alpha$	0.0564	0.4071
A1,F1	Avrami-Erofeev equation	$-\ln(1-\alpha)$	0.9773	0.1707
A3/2	Avrami-Erofeev equation	$[-\ln(1-\alpha)]^{2/3}$	0.9987	0.1707
A2	Avrami-Erofeev equation	$[-\ln(1-\alpha)]^{1/2}$	0.9869	0.1091
A3	Avrami-Erofeev equation	$[-\ln(1-\alpha)]^{1/3}$	0.9288	0.1091
A4	Avrami-Erofeev equation	$[-\ln(1-\alpha)]^{1/4}$	0.8593	0.1091
Au	Prout-Tompkins equation	$\ln[\alpha/(1-\alpha)]$	0.0868	0.6048
R1,F0,P1	Power law	α	0.9851	0.4612
R2,F1/2	Power law	$1-(1-\alpha)^{1/2}$	0.9815	0.5529
R3,F2/3	Power law	$1-(1-\alpha)^{1/3}$	0.9802	0.5755
D1	Parabola law	α^2	0.8702	0.5410
D2	Valensi equation	$\alpha + (1-\alpha)\ln(1-\alpha)$	0.8430	0.1091
D3	Jander equation	$[1-(1-\alpha)^{1/3}]^2$	0.8529	0.5844
D4	Ginstling-Brounstein equation	$1 - \frac{2}{3}\alpha - (1-\alpha)^{2/3}$	0.8589	0.5824
D5	Zhuravlev, Lesokin, Tempelman equation	$[(1-\alpha)^{-1/3}-1]^2$	0.8386	0.1091
D6	Anti-Jander equation	$[(1+\alpha)^{1/3}-1]^2$	0.8831	0.5210
-	Anti-Ginstling-Brounstein equation	$1 + \frac{2}{3}\alpha - (1+\alpha)^{2/3}$	0.8789	0.5284
-	Anti-Zhuravlev, Lesokin, Tempelman equation	$[(1+\alpha)^{-1/3}-1]^2$	0.8953	0.4970

From the results obtained in Table 7.9 it can be postulated that the mechanism for the desolvation of Form E when exposed to 25±2°C & 60±5 % RH was best described by the Avrami-Erofeev reaction (A3/2-model – Figure 7.46 (a)) (r^2 = 0.9987), which was also observed for the desolvation of Form D when exposed to 25±2°C & 0 % RH.

None of the correlation coefficients (r^2) calculated for the algebraic expressions of the functions describing the desolvation of Form E (when stored at 40±2°C & 75±5 % RH) were found to be suitable (r^2 < 0.9) for application.

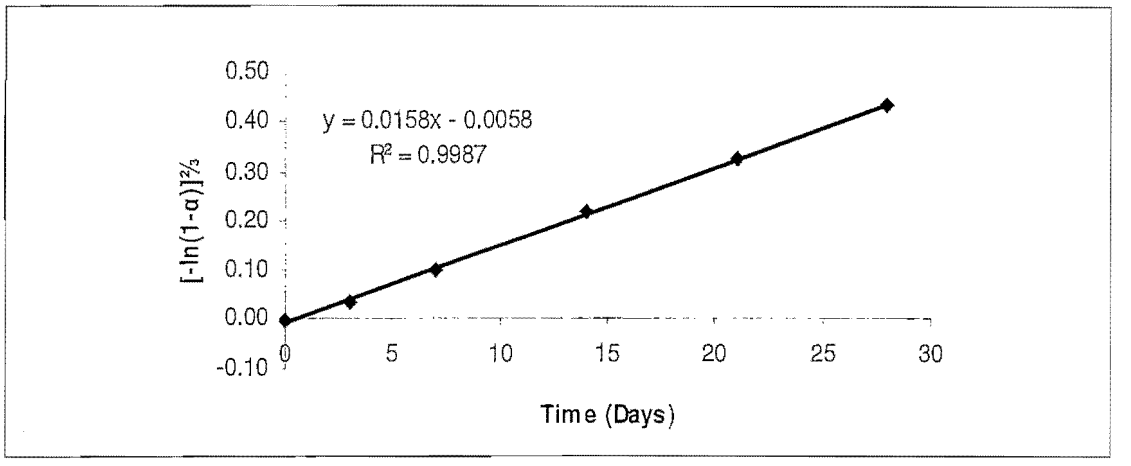

Figure 7.46 *g(α)* versus time plots for Form E when stored at 25±2°C & 60±5 % RH.

Figure 7.47 illustrates the good fit of the experimental data (♦) on the postulated model for the desolvation of Form E when stored at 25±2ºC & 60±5 % RH.

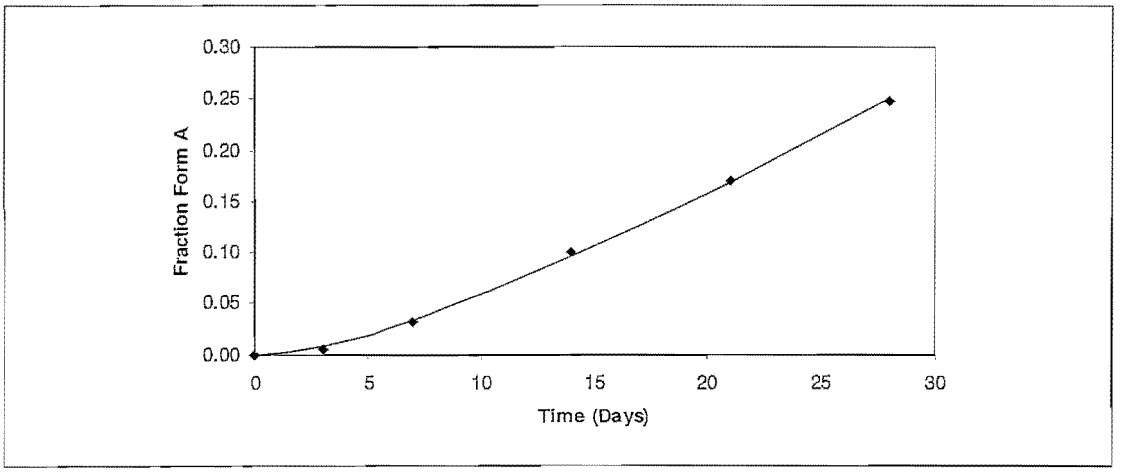

Figure 7.47 Fit of the experimental data (♦) on the postulated model of desolvation for Form E when stored at 25±2°C & 60±5 % RH.

The rate constant, k, in Table 7.10 indicated that the rate of desolvation of Form E at 25±2°C & 60±5 % RH was 0.0158 day^{-1}, which was 4.2 times lower in comparison to the desolvation of Form D at 25±2°C & 60±5 % RH. It can therefore be concluded that Form E was thermodynamically more stable when compared to Form D.

Table 7.10 Stability parameters calculated using the Avrami-Erofeev models for the desolvation of Form E when stored at 25±2°C & 60±5 % RH

Condition	k (day^{-1})	$t_{½}$ (days)	t_{90} (days)
25±2°C & 60±5 % RH	0.0158	49.9	14.5

The half-life ($t_{½}$) and shelf-life (t_{90}) of Form E were calculated by substituting $\alpha = 0.5$ (for $t_{½}$) and $\alpha = 0.1$ (for t_{90}) in the $g(\alpha) = kx + c$ equations derived from Figure 7.46., which fashioned the following equations:

- Half-life ($t_{½}$) for Form E stored at 25±2°C & 0 % RH (Equation 7.26):

$$t_{\frac{1}{2}} = \frac{0.7890}{k} \tag{7.26}$$

- Shelf-life (t_{90}) for Form E stored at 25±2°C & 0 % RH (Equation 7.27):

$$t_{90} = \frac{0.2289}{k} \tag{7.27}$$

7.6 Discussion and conclusion

The stability of mebendazole Form D and Form E when exposed to: **(1)** 25±2 °C & 60±5 % RH, **(2)** 40±2 °C & 75±5 % RH, **(3)** 25±2 °C & 0 % RH and **(4)** 40±2 °C & 0 % RH – was investigated. The rate and extent of desolvation of the forms were investigated using DRIFT-IR, XRPD, DSC and TGA.

Figure 7.48 provides a schematic presentation of the desolvation of Form D (and formation of Form A) detected using DRIFT-IR, when Form D was stored at the mentioned conditions (1) – (4).

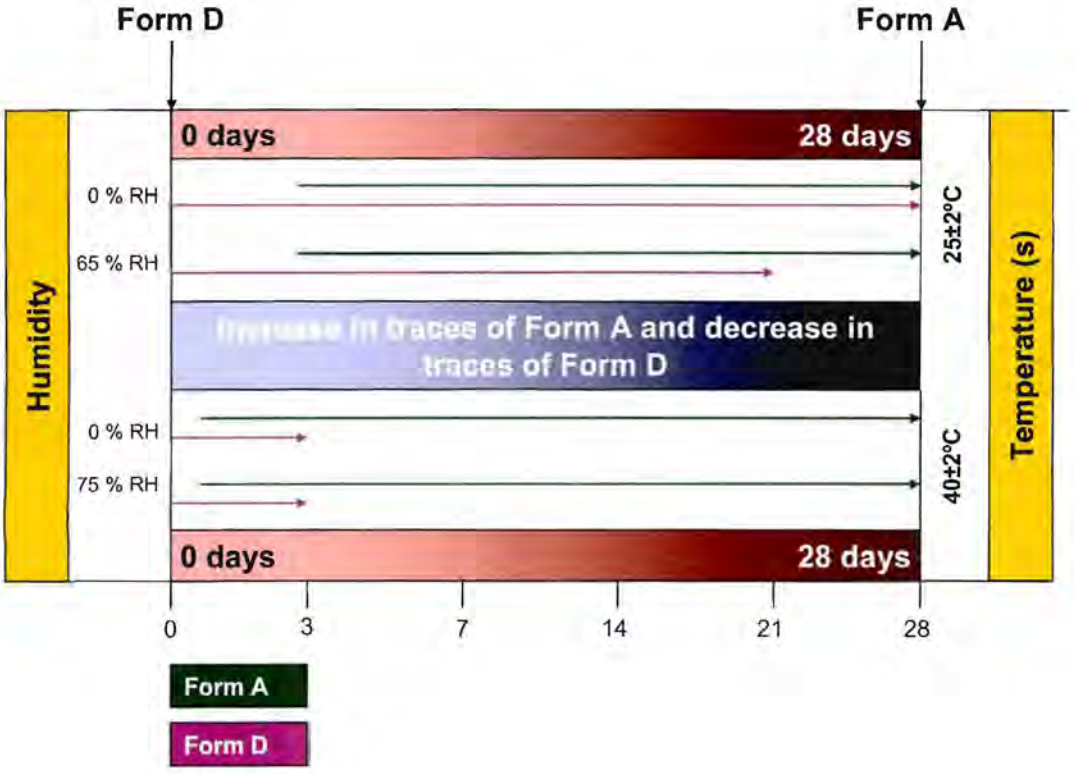

Figure 7.48 Schematic illustration of the conversion of Form D to the stable form, Form A, during a 28 day accelerated stability study.

It was revealed that the rate for the Form D → Form A conversion (in other words the desolvation of Form D) was higher at 40°C compared to that observed at 25°C. Form D underwent complete desolvation after 3 days when stored at 40±2°C & 0% RH and 40±2°C & 75±5 % RH, whereas the desolvation at 25±2°C & 60±5 % RH was completed after 21 days. Only 90% of the Form D fraction underwent desolvation when stored at 25±2°C & 0 % RH for 28 days.

It was postulated that the mechanism for the desolvation of Form D, when exposed to 25±2°C & 60±5 % RH was best described by the second-order reaction (F2-model and when exposed to 25±2°C & 0 % RH, by the Avrami-Erofeev reaction (A3/2-model. The rate of desolvation of Form D at 25±2°C & 60±5 % RH was 18 times faster compared to the desolvation of Form D at 25±2°C & 0 % RH.

The shelf-life of Form D when stored at 25±2°C & 60±5 % RH was 2.6 times lower compared to when Form D was stored at 25±2°C & 0 % RH, suggesting that the presence of moisture facilitated the desolvation process.

Figure 7.49 provides a schematic presentation of the desolvation of Form E (and formation of Form A) detected using XRPD, when Form E was stored at the mentioned conditions (1) – (4). XRPD data was used due to the fact that the IR-absorbancies of Form E (-NH = 3364 cm^{-1}, >C=O = 1735 cm^{-1}) and that of Form A (-NH = 3370 cm^{-1}, >C=O = 1730 cm^{-1}) were closely related and that it was not possible to accurately quantify the desolvation process, due to the overlapping maxima.

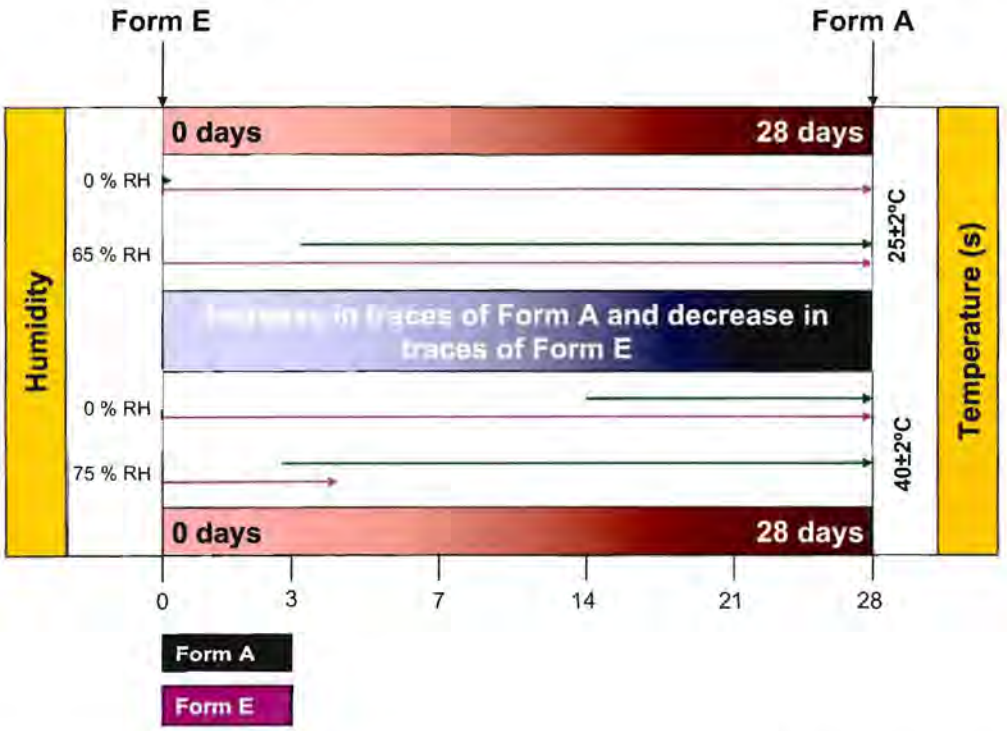

Figure 7.49 Schematic illustration of the conversion of Form E to the stable form, Form A during a 28 day accelerated stability study.

Form E did not desolvate when stored at 25±2℃ & 0 % RH. Desolvation was only detected when Form E was stored at 25±2℃ & 60±5 % RH, 40±2℃ & 0 % RH and 40±2℃ & 75±5 % RH. The rate of desolvation was in the order: 40±2℃ & 75±5 % RH > 25±2℃ & 60±5 % RH > 40±2℃ & 0 % RH, which once again suggested that moisture might have acted as a catalyst for the desolvation of Form E.

The postulated mechanism for the desolvation of Form E when exposed to 25±2℃ & 60±5 % RH was best described by the Avrami-Erofeev reaction (A3/2-model). No suitable desolvation mechanism was identified for the desolvation of Form E, when stored at 40±2℃ & 75±5 % RH

This study indicated that the rate of desolvation of Form E at 25±2℃ & 60±5 % RH was 4.2 times lower in comparison to the desolvation of Form D at 25±2℃ & 60±5 % RH. It can therefore be concluded that Form E was thermodynamically more stable when compared to Form D.

CHAPTER 8

Summary and Conclusion

Solid-state studies of active pharmaceutical ingredients (APIs) play an important role in the research and development of pharmaceutical dosage forms. Knowledge of the solid-state properties of APIs enables pharmaceutical manufacturers to either improve the products currently available on the market, or to develop and validate manufacturing protocols to ensure the efficacy and stability of new innovator products.

In this study, a strategic approach was followed to investigate the solid-state properties and thermodynamic stability of the solvated crystal forms of mebendazole (Figure 8.1).

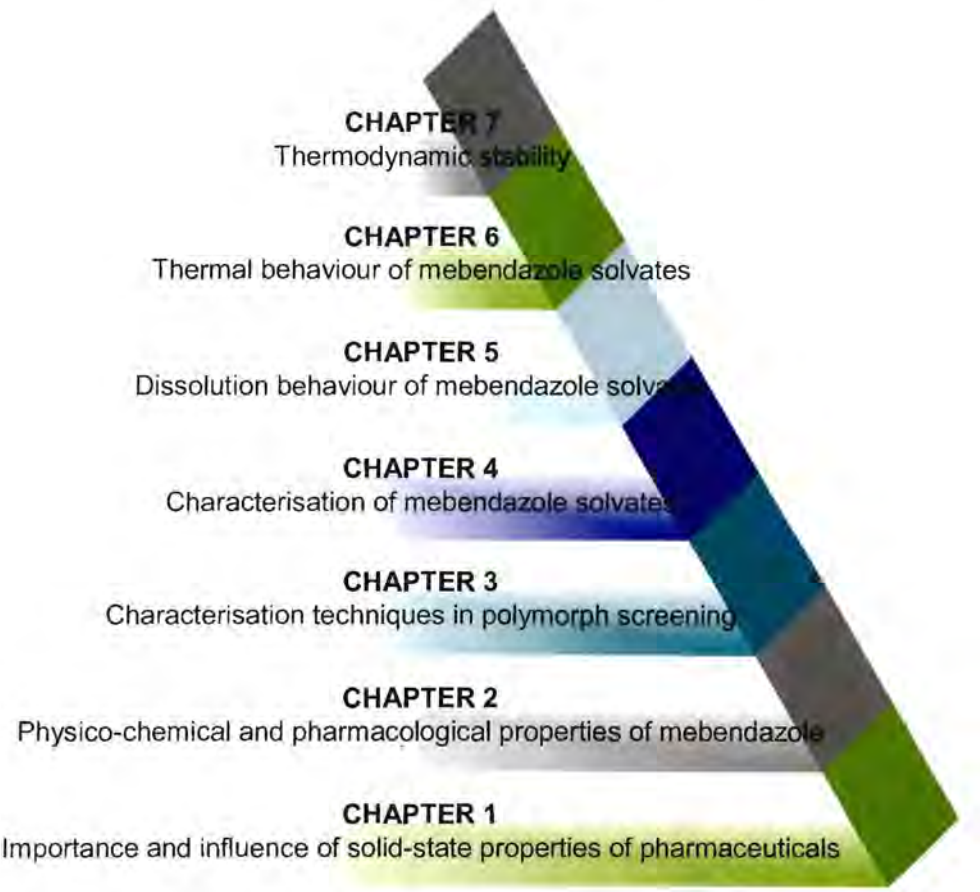

Figure 8.1 Strategic approach followed to investigate the solid-state properties and thermodynamic stability of the solvated crystal forms of mebendazole.

Chapter 1 was the foundation for this study, which provided a general overview of the formation of crystalline solids, the physico-chemical properties that may differ between polymorphic and

pseudo-polymorphic forms of the same chemical entity. By evaluating these properties, pharmaceutical manufacturers can validate the crystallisation techniques used to prepare the preferred polymorphic form of an API, to ensure the safety and efficacy of the dosage form.

Mebendazole is a synthetic benzimidazole and is used as a broad-spectrum anthelmintic against cestodal and nematodal helmintic infestations (Chapter 2). Mebendazole was first introduced into veterinary medicine in 1971 and has since been used as an anthelmintic in modern medicine. Three polymorphic forms of mebendazole have been identified: Forms A, B and C and one pseudo-polymorphic form (mebendazole propionic acid complex). The physico-chemical properties of these polymorphic forms were described in Chapter 2. It is known that Form C is the preferred polymorph for use, due to its low toxicity, increased solubility and efficiency.

Chapter 3 described the methods and experimental techniques utilised during this study for the characterisation and investigation of the thermodynamic stability of the two solvated crystal forms (i.e. Form D and Form E) of mebendazole.

From the literature study on mebendazole (presented in Chapter 2) it was evident that there were some inconsistencies with regards to the thermal behaviour of the polymorphic forms of mebendazole (i.e. Forms A, B and C). This study revealed that those inconsistencies might have been due to the fact that the experimental conditions (during the DSC analysis) differed in the various articles published. The DSC data reported for the mebendazole polymorphs in this study was found to be comparable to the DSC thermograms presented in an article recently published by Kumar *et al.* (2008:138) on the thermal behaviour of mebendazole polymorphs.

In Chapter 4, a novel pseudo-polymorphic form of mebendazole (Form D) was successfully prepared by means of accelerated recrystallisation using acetic-acid as solvent. The same method was utilised (using propionic-acid as solvent) to prepare the mebendazole propionic acid complex (referred to as Form E). This method provided a good yield in a short period of time.

The characteristic physico-chemical properties of the two pseudo-polymorphic forms i.e. Form D and Form E, revealed differences in their DRIFT-IR spectra, XRPD patterns and DSC thermograms. VT-XRPD, DSC, TGA and HSM analysis confirmed that the two crystal forms were solvated forms of mebendazole, and that they desolvated when subjected to increased temperatures. Desolvation of Forms D and E produced Form A.

SEM analysis indicated that the solvated crystal forms of mebendazole (i.e. Form D and Form E) had more distinct crystal habits compared to the true-polymorphic forms of mebendazole (I,e

Forms A, B and C). Both Form D and Form E exhibited definite needle-like habits, whereas the other forms exhibited shapeless particles which showed a tendency to agglomerate.

The dissolution profiles of Form D and Form E in 0.1 N HCl at 37°C differed significantly (f_2 = 16). The powder dissolution profiles of Form D indicated that approximately 51% of the sample dissolved after 120 minutes, whereas 97% of Form E dissolved after 120 minutes in 0.1 N HCl. The difference in the dissolution profiles of Form D and Form E could not be attributed to differences in particle size, but rather to the fact that a fraction of Form D underwent a solvent mediated phase transition (in the dissolution medium) and was transformed to the poorly soluble Form A.

Comparison of the dissolution profiles of the Forms A, B, C, D and E revealed that Form E was the most soluble in 0.1 N HCl (at 37ºC) and Form A the least soluble. Form D was found to be more soluble in 0.1 N HCl (at 37ºC) than Forms A and B. The differences in the dissolution profiles of the solvated forms (Forms D and E) and non-solvated forms (Forms A, B and C) of mebendazole could also be attributed to the decrease in the pH of the dissolution medium caused by the release of solvent molecules from the solvated lattices which facilitated the dissolution (increased the dissolution rate and extend) of Form D and Form E.

Based on the analytical method transfer presented in Chapter 5 it is recommended that quantitative UV-analysis of mebendazole should be performed at 288 nm.

The thermodynamic stability of Form D and Form E was investigated in Chapter 6 and Chapter 7. Exposure of Form D and Form E to increased temperatures (80, 90 & 100°C) caused the desolvation of Form D and Form E. The desolvated lattices were transformed to the thermodynamically stable form, Form A (Figure 8.2).

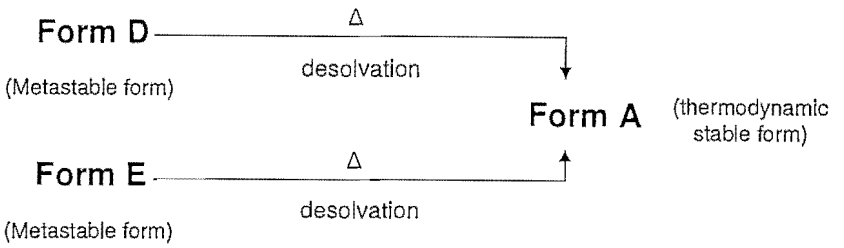

Figure 8.2 Conversion of the metastable solvated forms (Form D and Form E) to the thermodynamically stable form, Form A.

Non-isothermal studies revealed that Form E required 0.3 $kJ.mol^{-1}$ more energy to initiate the desolvation of Form E compared to the activation energy required for the desolvation of Form D. Based on this observation (and the VT-XRPD results) it was concluded that Form D was thermodynamically less stable compared to Form E.

Isothermal studies performed on Form D and Form E revealed that the mechanism of desolvation for Form D and Form E was temperature dependant. The rate of desolvation for Form D and Form E at the mentioned temperatures were found to be in the order: 100°C > 90°C > 80°C.

The stability of mebendazole Form D and Form E when exposed to: (1) 25±2 °C & 60±5 % RH, (2) 40±2 °C & 75±5 % RH, (3) 25±2 °C & 0 % RH and (4) 40±2 °C & 0 % RH – was investigated in Chapter 7.

It was revealed that the desolvation of Form D was higher at 40°C compared to that observed at 25°C. Form D underwent complete desolvation after 3 days when stored at 40±2°C & 0% RH and 40±2°C & 75±5 % RH, whereas the desolvation at 25±2°C & 60±5 % RH was completed after 21 days. Only 90% of the Form D fraction underwent desolvation when stored at 25±2°C & 0 % RH for 28 days.

The mechanism for the desolvation of Form D, when exposed to 25±2°C & 60±5 % RH was best described by the second-order reaction (F2-model) and when exposed to 25±2°C & 0 % RH, by the Avrami-Erofeev reaction (A3/2-model). The rate of desolvation of Form D at 25±2°C & 60±5 % RH was 18 times faster compared to the desolvation of Form D at 25±2°C & 0 % RH.

The shelf-life of Form D when stored at 25±2°C & 60±5 % RH was 2.6 times lower compared to when Form D was stored at 25±2°C & 0 % RH, suggesting that the presence of moisture facilitated the desolvation process.

Form E did not desolvate when stored at 25±2°C & 0 % RH. Desolvation was only detected when Form E was stored at 25±2°C & 60±5 % RH, 40±2°C & 0 % RH and 40±2°C & 75±5 % RH. The rate of desolvation was in the order: 40±2°C & 75±5 % RH > 25±2°C & 60±5 % RH > 40±2°C & 0 % RH, which once again suggested that moisture might have acted as a catalyst for the desolvation of Form E.

The postulated mechanism for the desolvation of Form E when exposed to 25±2°C & 60±5 % RH was best described by the Avrami-Erofeev reaction (A3/2-model). No suitable desolvation mechanism was identified for the desolvation of Form E, when stored at 40±2°C & 75±5 % RH

The desolvation fraction (D_f) was introduced in Chapter 7 as a new means to investigate the relationship between the desolvation enthalpy (ΔH) calculated from the DSC thermogram and the mass loss (m) calculated from the TGA thermogram. The desolvation factors determined from both the DSC (D_{f1}) and TGA (D_{f2}) plotted as a function of time, were successfully applied to complement the DRIFT-IR and XRPD data in the evaluation of the desolvation process of Form D and Form E.

To summarise, the available literature on the polymorphic forms of mebendazole focused on the physico-chemical and pharmacological properties of Forms A, B and C, especially on that of the pharmaceutical preferred Form C. This study revealed that the incorporation of a solvent (propionic acid or acetic acid) induced significant changes to the physico-chemical properties of mebendazole. From the dissolution studies presented it was clear that the incorporation of the solvent molecules into the crystal lattice, caused a significant increase in the dissolution profile of the poorly-soluble mebendazole.

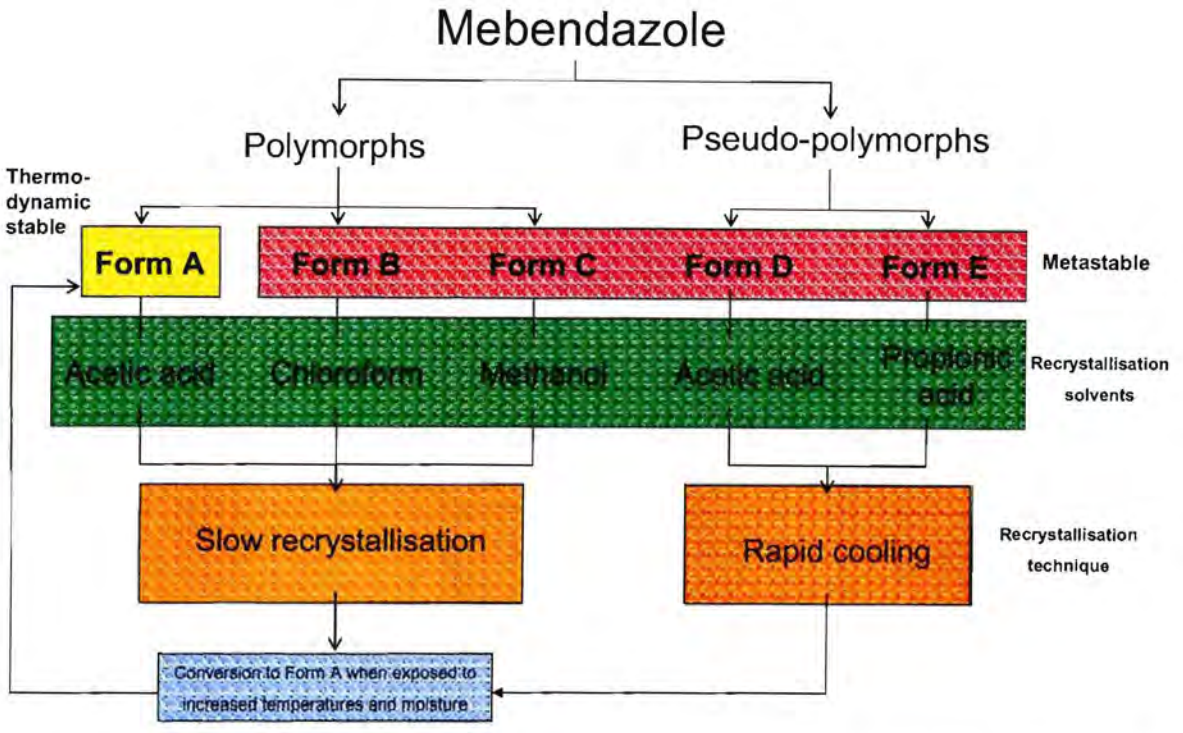

Figure 8.3 Schematic presentation on the preparation of the solid forms of mebendazole.

This study also revealed that the thermodynamic stability of the solvated lattices differed significantly. Figure 8.3 provides a schematic summary of the methods of preparation, differences in thermodynamic stability and desolvation behaviour of the polymorphic and pseudo-polymorphic forms of mebendazole. Table 8.1 provides a concise tool for the identification of the polymorphic and pseudo-polymorphic forms of mebendazole.

Table 8.1 Summary of the physico-chemical properties of the polymorphic and pseudo-polymorphic forms of mebendazole

Technique	Form A	Form B	Form C	Form D	Form E
DRIFT-IR (-NH) (cm^{-1})	3370 [1]	3340 [1]	3410 [1]	3353	3364
DRIFT-IR (>C=O) (cm^{-1})	1730 [1]	1700 [1]	1720 [1]	1738	1735
XRPD (°2θ)	7.6 [2] 17.3 **	5.8 [2]	4.9 [2]	6.6 7.9 13.2	6.3 8.0 12.6
DSC (°C)	250-255 * 330 *	220 [3] * 263 [3] * 330 [3] *	195 [3] * 225 [3] * 253 [3] * 330 [3] *	109.26 255.85 331.35	124.18 253.59 330.46
TGA Mass loss in the temperature range 100-200 °C	N/A	N/A	N/A	15.40%	20.76%
DISSOLUTION Q_{20} (0.1 N HCl at 37 ± 0.2 °C)	Q = 70% [4]	Q = 37% [4]	Q = 20% [4]	Q = 51%	Q = 97%

(*) Thermal behaviour investigation from Chapter 3, Section 3.3.

(**) The 17.30°2θ peak in the XRPD diffractogram of Form A was identified as a strong characteristic peak and utilised in the stability study of Form D and Form E to determine the presence of polymorphic conversion.

[1] Himmelreich *et al.* (1977:123)

[2] Brits (2008:70)

[3] De Villiers *et al.* (2005:438)

[4] Swanepoel *et al.* (2003:347)

BIBLIOGRAPHY

AGATONOVIC-KUSTRIN, S., GLASS, B.D., MANGAN, M. & SMITHSON, J. 2008. Analysing the crystal purity of mebendazole raw material and its stability in a suspension formulation. *International Journal of Pharmaceutics: 1-6.*

ANON. 2007. The University of Oklahoma Crystallography lab: Crystallography. http://xrayweb.chem.ou.edu/notes/crystallography.html. Date of access: 02 Jan. 2008.

ANON. 2006. National institute of general medical sciences – The chemistry of health: Chapter 1 - A special bond. http://publications.nigms.nih.gov/.../chapter1.html. Date of access: 28 Nov. 2007.

ANON. 1978. Mebendazole. McGraw-Hill's Access Medicines. http://www.accessmedicines.com. Date of access: 30 Aug. 2008.

ANON. 1995. Mebendazole (Systemic). Drugs.com – Drug information online. http://www.drugs.com/MMX/mebendazole.html. Date of access: 18 Aug. 2007.

AULTON, A. 2002. Pharmaceutical Dissolution and solubility. (*In* Aulton, A., *ed.* Pharmaceutics – The science of dosage form design. 2nd ed. Churchill Livingstone: Elsevier science limited. 679 p.)

BAMFORD, C.H. & TIPPER, C.F.H. 1980. Decomposition reactions of solids. Chemical kinetics: Reactions in the solid state. New York: Elsevier Scientific Publishing Company. 22:115-136.

BERNSTEIN, J. 2002. Polymorphism in molecular crystals. 1st ed. Oxford University Press: Oxford. 410 p.

BISHOP, M. 2008. Supersaturated: Temperature and solubility of solids. http://www.mpcfaculty.net/mark_bishop/supersaturated.htm. Date of access: 09 Jan. 2008.

BRAITHWAITE, P.A., ROBERTS, M.S., ALLAN, R.J. & WATSON, T.R. 1982. Clinical pharmacokinetics of high dose mebendazole in patients treated for cystic hydatid disease. *European Journal of Clinical Pharmacology*, 22:161-169.

BRITISH PHARMACOPOEIA. 2007. BP2007 Online. Available: http://pharmacopoeia.co.za.

BRITS, M. 2008. Solid-state properties of pharmaceuticals. General methods utilized during studies for characterisation and analytical purposes. Potchefstroom: NWU. (Thesis – PhD) 549p.

BRITTAIN, H.G., *ed.* 1999. Polymorphism in pharmaceutical solids. 1st ed. Marcel Dekker, Inc. New York : Basel. 427 p.

BRITTAIN, H.G. 1997. Spectral methods for the characterisation of polymorphs and solvates. *Journal of Pharmaceutical Sciences,* 86(4):405-412.

BROWN, M.E. & GLASS, B.D. 1999. Pharmaceutical applications of the Prout-Tompkins rate equation. *International Journal of Pharmaceutics,* 190:129-137.

BROWN, M.E., DOLLIMORE, D. & GALWEY, A.K. 1980. Theory of solid state reaction kinetics. (*In* Tipper, C.F.H., *ed.* Chemical kinetics, Amsterdam: Elsevier. p. 41-72).

BRUSAU, E.V., CAMÍ, G.E., NARDA, G.E., CUFFINI, S., AYALA, A.P. & ELLENA, J. 2007. Synthesis and characterisation of a new mebendazole salt: Mebendazole hydrochloride. *Journal of Pharmaceutical Sciences*, 97(1):542-552.

BUERGER, M.J. & BLOOM, M.C. 1937. Crystal polymorphism. *Zeitshrift fur Kristallographie*, 96:182-200.

BUNACIU, A.A., FLESCHIN, S. & ABOUL-ENEIN, H.Y. 2001. Analysis of mebendazole polymorphs by Fourier transform infrared spectrometry using chemometric methods. *Spectroscopy letters*, 34(5):527-536.

BUNACIU, A.A., FLESCHIN, S. & ABOUL-ENEIN, H.Y. 2002. Analysis improvement of drugs using modern methods. *Romanian biotechnology letters*, 7(2):647-654.

BUYS, K. 2003. Formulation and evaluation of mebendazole dosage forms. Potchefstroom: NWU. (Dessertation – M.sc.) 133p.

BYRN, S.R., PFEIFFER, R.R. & STOWELL, J.G., *eds.* 1999. Solid-State chemistry of drugs. 2nd ed. SSCI, Inc : America. 574 p.

BYRN, S.R., SUTTON, P.A., TOBIAS, B., FRYE, J. & MAIN, P. 1988. The crystal structure, solid-state NMR spectra and oxygen reactivity of five crystal forms of prednisolone tert-butylacetatet. *Journal of American Chemical Society*, 110:1609-1614.

CAIRA, M.R., DEKKER, T.G. & LIEBENBERG, W. 1998. Structure of a 1:1 complex between the anthelmintic drug mebendazole and propionic acid. *Journal of Chemical Crystallography*, 28(1):11-15.

CAIRA, M.R., ZANOL, M., PEVERI, T., GAZZANIGA, A. & GIORDANO, F. 1998. Structural characterization of two polymorphic forms of piroxicam pivalate. *Journal of Pharmaceutical sciences*, 87(12):1608-1614.

CAMBRIDGE STRUCTURAL DATABASE AND STRUCTURAL DATABASE SYSTEM. 2002. Version 5.24. Cambridge, UK: Cambridge Crystallographic Data Centre, Univeristy Chemical Laboratory.

CHEN, A.M., ELLISON, M.E., PERESYPKIN, A., WENSLOW, R.M., VARIANKAVAL, N., SAVARIN, C.G., NATISHAM, T.K., MATHRE, D.J., DORMER, P.G., EULER, D.H., BALL, R.G. YE, Z., WANG, Y. & SANTOS, I. 2007. Development of a pharmaceutical cocrystal of a monophosphate salt with phosphoric acid. *The Royal Society of Chemistry: Chemical Communication*, p. 419–421.

CONNOLLY, R.C. 2007. Introduction to x-ray powder diffraction. EPS400-002. Spring 2007. 9p.

COSTA, J., FRESNO, M., GUZMAN, L., IGUAL, A., OLIVA, J., VIDAL, P., PEREZ, A. & PUJOL, A. 1991. Polymorphic forms of mebendazole: Analytical aspects and toxicity. *Circular of Farm*, 49:415-424.

COSTA, P. 2001. An alternative method to the evaluation of similarity factor in dissolution testing. *International Journal of Pharmaceutics*, 220:77-83.

CRAIG, D.Q.M. 2007. Characterisation of polymorphic systems using thermal analysis. (*In* Hilfiker, R., *ed.* Polymorphism in the pharmaceutical industry. Weinham: Wiley-VCH. p.167-210.)

DAWSON, M., ALLAN, R.J. & WATSON, T.R. 1982. The pharmacokinetics and bioavailability of mebendazole in man: A pilot study using [^{3}H]-mebendazole. *Journal of Clinical Pharmaceutics*, 14:453-455.

DAWSON, M., BRAITHWAITE, P.A., ROBERTS, M.S., & WATSON, T.R. 1985. The pharmacokinetics and bioavailability of a tracer dose of [^{3}H]-mebendazole in man. *Journal of Clinical Pharmaceutics*, 19:79-86.

DAYAN, A.D. 2003. Albendazole, mebendazole and praziquantel. Review of non-clinical toxicity and pharmacokinetics. *Acta Tropica*, 86:141-159.

DE VILLIERS, M.M., TERBLANCHE, R.J., LIEBENBERG, W., SWANEPOEL, E. DEKKER, T.G. & SONG, M. 2005. Variable-temperature X-ray powder diffraction analysis of the crystal transformation of the pharmaceutical preferred polymorph C of mebendazole. *Journal of Pharmaceutical and Biomedical Analysis*, 38:435-441.

DOITPOMS. 2007. X-ray diffraction. Doitpoms teaching and learning packages: University of Cambridge. http://www.doitpoms.ac.uk/tlplib/xray-diffraction/bragg.php. Date of access: 6 Sept. 2007.

EMD CHEMICALS INC. 2008. Aquastar: Karl Fischer titration basics. http://www.emdchemicals.com/analytics/literature/LF_Titration_Basics.pdf. Date of access: 29 Sept. 2008.

FLYNN, J.H. & WALL, L.A. 1966. A quick, direct method for the determination of activation energy from thermogravimetric data, *Polymer Letters,* 4:323–328.

FRAYHA, G.J., SMYTH, J.D., GOBERT, J.G. & SAVEL, J. 1997. The mechanisms of action of antiprotozoal and anthelmintic drugs in man. *General Pharmacology*, 28(2):273-299.

FREITAG, G. 2001. Guidelines on dissolution profile comparison. *Drug Information Journal,* 35:865-874.

GIBBON, C.J., *ed.* 2008. Anthelmintics - The South African Medicines Formulary. 8th ed. FA Print : Cape Town. 496-504 p.

GIRON, D. 1995. Thermal analysis and calorimetric methods in the characterisation of polymophs and solvates. *Thermochimica Acta*, 248:1-59.

GRIESSER, U.J. 2007. The importance of solvates. (*In* Hilfiker, R., *ed.* Polymorphism in the pharmaceutical industry. Weinheim: Wiley-VCH. p.221.)

HALEBLIAN, J.K. 1975. Characterization of habits and crystalline modification of solids and their pharmaceutical applications. *Journal of Pharmaceutical science*, 64(8):1269-1288.

HAN, J., GUPTE, S. & SURYANARAYANAN, R. 1998. Applications of pressure differential scanning calorimetry in the study of pharmaceutical hydrates 2: Ampicillin trihydrate. *International Journal of Pharmaceutics*, 170:63-72.

HANCOCK, B.C. & ZOGRAFI, G. 1997. Characteristics and significance of the amorphous state in pharmaceutical solids. *Journal of Pharmaceutical Sciences*, 86(1):1-12.

HILFIKER, R., *ed.* 2007. Polymorphism in the pharmaceutical industry. Weinheim: Wiley-VCH. 414p.

HIMMELREICH, M., RAWSON, B.J. & WATSON, T.R. 1977. Polymorphic forms of mebendazole. *Australian Journal of Pharmaceutical Sciences*, 6(4)123-125.

INTERNATIONAL CONFERENCE ON HARMONISATION OF TECHNICAL REQUIREMENTS FOR REGISTRATION OF PHARMACEUTICALS FOR HUMAN USE. 2005. ICH Harmonised Tripartite Guideline. Validation of analytical procedures: text and methodology Q2(R1). http://www.emea.europe.eu. Date of access: 22 Nov. 2008.

J. SESTAK, J. & BERGGREN, G. 1971. Study of the kinetics of the mechanism of solid-state reactions at increasing temperatures. *Thermochimica Acta*, 3:1–12

JANKOVIĆ, B. ADNAĐEVIĆ, J. & JOVANOVIĆ, J. 2007. Application of model-fitting and model-free kinetics to the study of non-isothermal dehydration of equilibrium swollen poly (acrylic acid) hydrogel: Thermogravimetric analysis. *Thermochimica Acta*, 452:106-115.

JANSSEN-ORTHO. 2004. Product monograph: Vermox®. http://www.janssen-ortho.com/JOI/pdf_files/Vermox_E.pdf. Date of access: 21 Jul. 2007.

KARJALAINEN, M., AIRAKSINEN, S., RANTANEN, J., AALTONEN, J. & YLIRUUSI, Y. 2005. Characterization of polymorphic solid-state changes using variable temperature X-ray powder diffraction. *Journal of Pharmaceutical and Biomedical Analysis*, 39:27–32.

KARKI, S., FRIŠČIČ, T., JONES, W. & MOTHERWELL, W.D.S. 2007. Screening for pharmaceutical cocrystal hydrates via neat and liquid-assisted grinding. *Molecular Pharmaceutics*, 4(3):347-354.

KATZUNG, B.G., ed. 2001. Clinical pharmacology of the anthelmintic drugs. Basic and Clinical Pharmacology. 8th ed. 1217 p.

KHANKARI, R.K. & GRANT, D.J.W. 1995. Pharmaceutical hydrates. *Thermochimica Acta*, 248: 61-79.

KHAWAM, A. & FLANAGAN, D. 2005. Basics and applications of solid-state kinetics: A pharmaceutical perspective. *Journal of Pharmaceutical Sciences*, 95(3):472-498.

KHAWAM, A. & FLANAGAN, D. 2006. Solid-state kinetic models: Basics of mathematical fundamentals. *Journal of Physical Chemistry B*, 110:17315-17328.

KHAWAM, A. & FLANAGAN, D.R. 2005. Role of isoconversional methods in varying activation energies of solid-state kinetics I. isothermal kinetic studies. *Thermochimica Acta*, 429:93-102.

KHAWAM, A. & FLANAGAN, D.R. 2005. Role of isoconversional methods in varying activation energies of solid-state kinetics II. Nonisothermal kinetic studies. *Thermochimica Acta*, 436:101-112.

KHAWAM, A. & FLANAGAN, R.D. 2008. Desolvation kinetics of sulfameter solvates. *Journal of Pharmaceutical Sciences*, 97(6):2160-2175.

KHAWAM, A. 2007. Application of solid-state kinetics to desolvation reactions. University of Iowa. (Thesis – PhD) 349 p.

KULKARNI, G.U., KUMARDHAS, P. & RAO, C.N.R. 1998. Charge density study of the polymorphs of *p*-nitrophenol. *Chemistry of materials,* 10:3498-3505.

KUMAR, S., CHAWLA, G., SOBIA, M.E. & BANSAL, A.K. 2008. Characterization of solid-state forms of mebendazole. *Pharmazie,* 63(2):136-143.

LIEBENBERG, W., DEKKER, T.G., LOTTER, A.P. & DE VILLIERS, M.M. 1998. Identification of the mebendazole polymorphic form present in raw materials and tablets available in South Africa. *Drug Development and Industrial Pharmacy*, 24(5):485-488.

LIESER, K.H. 1969. Teilschritte von fällungsreaktionen. *Angewante Chemie*, 81(6):206-221.

MALLINCKRODT BAKER INC. 2008. Material safety data sheet: Propionic acid. http://jtbaker.com/msds/englishhtml/P6643.htm. Date of access: 23 Sept. 2008.

MARTIN, A. 2003. Physical Pharmacy. 4th ed. Lippincott Williams & Wilkins. 622 p.

McCRONE, W.C. & HALEBLIAN, J. 1969. Pharmaceutical applications of polymorphism. *Journal of Pharmaceutical sciences*, 58(8):911-929.

McCRONE, W.C. 1965. Polymorphism. Physics and chemistry of the organic solid state. Volume 2. New York: Interscience Publishers. 975 p.

MOORE, J.W. & FLANNER, H.H. 1996. Mathematical comparison of dissolution profiles. *Pharmaceutical Technology*, 20(6):64-75, Jun.

MÜNST, G.J., KARLAGANIS, G. & BIRCHER, J. 1980. Plasma concentrations of mebendazole during treatment of echinococcosis. *European Journal of Clinical Pharmacology,* 17:375-378.

NICHOLS, G. 2007. Light microscopy. (In Hilfiker, R., ed. Polymorphism in the pharmaceutical industry. Weinham: Wiley-VCH. p.167-210.)

O'HARE, T., DUNNE, A., BUTLER, J. & DEVANE, J. 1998. A review of methods used to compare dissolution profile data. *PSTT,* 1(5):214-223.

O'NIEL, J., *ed.* 2006. The Merck Index: An encyclopaedia of chemicals, drugs and biologicals. Mebendazole. 14th ed. Merck Research Laboratories. p.5766.

OLIVA, A., LLABREŚ, M. & FARINŇA, J.B. 2006. Data analysis of kinetic modeling used in drug stability studies: Isothermal vs. non-isothermal assays. *Pharmaceutical Research,* 23(11):2595-2602.

OWN, Z., 2000 Inorganic Chemistry: Ionic bonding. http://inorganic.chemistry.pu.edu.tw/first/New/L4/A.html. Date of access: 02 Jan. 2008.

PHIPPS, M.A. & MACKIN, L.A. 2000. Application of isothermal microcalorimetry in solid-state drug development. *PSTT,* 3(1):9-17.

RAZEGHI, M. 2002. Fundamentals of solid state engineering: Crystalline properties of solids. Kluwer Academic publishers, p. 11.

RODANTE, F., VECCHIO, S. & TOMASSETTI, M. 2002. Multi-step decomposition processes for some antibiotics: A kinetic study. *Thermochimica Acta,* 394:7–18.

RODRIGQUEZ-CAABEIRO, F., CRIADO-FORNELIO, A., JIMENEZ-GONZALEZ, A., GUZMAN, L., IGUAL, A., PEREZ, A. & PUJOL, M. 1987. Experimental chemotherapy and toxicity in mice of three mebendazole polymorphic forms. *Chemotherapy,* 33:266-271.

RUNGER, G., CANTER, K., TWIST, J., ROSSI, D. & KIRKHAM, C. 2005. X-ray powder diffraction metrics. http://ww1.ucmss.com/books/LFS/CSREA2006/BIC4130.pdf. Date of access: 4 Sept. 2007.

SANDS, D.E. 1993. Introduction to crystallography. New York: Dover publications Inc. 165 p.

SESTAK, J. & BERGGREN, G. 1971. Study of the kinetics of the mechanism of solid-state reactions at increasing temperatures. *Thermochimica Acta,* 3:1-12.

SINGH, D., MARSHALL, P.V., SHIELDS, L. & YORK, P. 1998. Solid-state characterisation of chlordiazepoxide polymorphs. *Journal of Pharmaceutical Sciences*, 87(5):655-662.

SINGHAL, D. & CURATOLO, W. 2004. Drug polymorphism and dosage form design: a practical perspective. *Advanced Drug Delivery Reviews*, 56:335-347.

SINKO, P.J. 2006. Martin's physical pharmacy and pharmaceutical sciences. 5th ed. Lippincott Williams & Wilkins. Philadelphia. 795 p.

STANIFORTH, J. 2002. Particle-size analysis. (*In* Aulton, M.E., *ed.* Pharmaceutics – The science of dosage form design. 2nd ed. Churchill Livingstone: Elsevier science limited. 679 p.)

STEPHENSON, G.A., FORBES, R.A. & REUTZEL-EDENS, S.M. 2001. Characterisation of the solid state: quantitative issues. *Advanced Drug Delivery Reviews*, 48:67-90.

SWANEPOEL, E., LIEBENBERG, W. & DE VILLIERS, M.M. 2003. Quality evaluation of generic drugs by dissolution test: changing the USP dissolution medium to distinguish between active and non-active mebendazole polymorphs. *European Journal of Pharmaceutics and Biopharmaceutics*, 55:345-349.

SWEETMAN, S., ed. 2007. Mebendazole. Martindale: The complete drug reference. Pharmaceutical Press: London. http://www.medicinescomplete.com/mc/martindale/current/791-z.htm. Date of access: 14 Mar. 2007.

TANAKA, H. 1995. Thermal analysis and kinetics of solid state reactions. *Thermochimica Acta*, 267:29-44.

TIERNEY, L.M., MCPHEE, S.J. & PAPADAKIS, M.A. 2004. Infectious diseases: Protozoal & helmintic. Current Medical Diagnosis and Treatment (CMDT). 43rd ed. McGraw-Hill Companies Inc. 1863 p.

TURMANOVA, S.C., GENIEVA, S.D., DIMITROVA, A.S. & VLAEV, L.T. 2008. Non-isothermal degradation kinetics of filled with rise husk ash polypropene composites. *Polymer Letters*, 2(2):133-146.

USP – see United States Pharmacopeial Convention

UNITED STATES PHARMACOPEIAL CONVENTION. 2007. USP29:NF25 Online. Available: www.uspnf.com.

VAN DER SLUIS, P. & KROON, J. 1989. Solvents and X-ray crystallography. *Journal of Crystal Growth*, 97:645-656.

VERHEYEN, A., VANPARIJS, O., BORGERS, M. & THIENPONT, D. 1978. Scanning electron microscopy observations of *Cysticercus fasciolaris* (= *Taenia taeniaeformis*) after treatment of mice with mebendazole. *The Journal of Parasitology*, 64(3):411-425.

VIPPAGUNTA, S.R., BRITTAIN, H.G. & GRANT, D.J.W. 2001. Crystalline solids. *Advanced Drug Delivery Reviews*, 48:3-26.

VYAZOVKIN, S. & WIGHT, C.A. 1999. Model-free and model-fitting approaches to kinetic analysis of isothermal and non-isothermal data. *Thermochimica Acta*, 340-341:53-68.

WANG, Z., WANG, J. & DANG, L. 2006. Thermal phase transition and spectral studies in erythromycin pseudopolymorphs: dihydrate and acetone solvate. *Crystal Research and Technology*, 41(12):1219 – 1225.

WATERMAN, K.C. & ADAMI, R.C. 2005. Accelerated aging: Prediction of chemical stability of pharmaceuticals. *International Journal of Pharmaceutics*, 293:101-125.

WELLS, J. 2002. Pharmaceutical preformulation: the physicochemical properties of drug substances. (*In* Aulton, M.E., *ed.* Pharmaceutics – The science of dosage form design. 2nd ed. Churchill Livingstone: Elsevier science limited. 679 p.)

WESSELS, P., HOLZ, M., ERNI, F., KRUMMEN, K. & OGORKAL, J. 1997. Statistical evaluation of stability data of pharmaceutical products for specification setting. *Drug Development and Industrial Pharmacy*, 23(5):427-429.

WHITNEY. 2007. Crystal formation. http://www.geo.umn.edu/courses/2301/fall2003/min02.html. Date of access: 12 Feb. 2007.

WHITTINGHAM, M.S. 1989. X-ray analysis of a solid. http://materials.binghamton.edu/labs/xray/xray.html. Date of access: 6 Sept. 2007.

WINFIELD, A.J. 1999. Storage and stability of medicines. (*In* Winfield, A.J. & Richards, R.M.E., *eds.* Pharmaceutical practice. New York: Churchill-Livingstone. p. 83-88.)

YU, L. 2001. Amorphous pharmaceutical solids: preparation, characterisation and stabilisation. *Advanced Drug Delivery Reviews*, 48:27-42.

YU, L., REUTZEL, M. & STEPHENSON, G.A. 1998. Physical characterisation of polymorphic drugs: an integrated characterisation strategy. *PSTT*, 1(3):118-127.

ZHOU, D., SCHMITT, E.A., ZHANG, G.G., LAW, D., VYAZOVKIN, S., WIGHT, C.A. & GRANT, D.J.W. 2003. Crystallization kinetics of amorphous nifedipine studied by model-fitting and model-free approaches. *Journal of Pharmaceutical Sciences*, 92(9):1779-1792.

ACKNOWLEDGEMENTS

"Everything comes from God alone. Everything lives by his power, and everything is for his glory."
Romans 11:36.

I would like to take this opportunity to express my gratefulness and appreciation to the people that stood by me during my studies. If it weren't for your guidance, friendship, love, emotional and physical support, none of this would have been possible.

I would like to thank God for blessing me with the wisdom, strength, love, hope, courage and willpower. I would like to thank Him for walking the path with me, and for guiding me along the way, so that I could find part of my true purpose and strengths in life. I would also like to thank God for providing me with a loving family and friends, for without them nothing would have mattered.

Finally, I would like to thank following:

- To my parents and sister, André, Petro and Jackie, thank you for standing by me during everything. You were always there for me, during good and bad times. You are my foundation and without your love, guidance and teachings, I would not have been able to find my purpose in life or achieve my dreams.
- To my grandparents, Carel and Magda Kleynhans, You have been my role models since I was a child and I was always inspired by your knowledge, skills, achievements and more. Thank you for your constant loving support and believing in me.
- To my very best friends, Petrus Booyens, Denzil Venter, Dewald Venter, Chantelle Diedericks, Danie Gerber, Michelle Rourke, Stephan and Lelanie Smuts and Arulene Smal, thank you for everything. Thank you for believing and standing by me during all these years. You are all an important part of my life and family, and without your loving support and understanding, I would not have been able to find my purpose in life nor achieve my dreams.
- To my aunts and uncles, especially Anna Brits, Derek and Helena de Lange. Thank you for your love and support. You have helped me more than you know. You are the best!
- To the rest of my family, thank you for your love and support.
- To Dr. Marius Brits and Mr. Zak Perold, thank you for all your support and professional guidance throughout this study. The knowledge I gained from you will be valuable to me and put to good use in whatever lies ahead. You are the best!

- To Anriette Pretorius at the NWU library, thank you for your assistance and support. Most of all, thank you for your friendship.

- To the Research Institute for Industrial Pharmacy (RIIP), thank you for the opportunity in allowing me to use your outstanding equipment and facilities. Also, thank you for the valuable knowledge and experience I gained, while working for you. I know that it will serve me well in the future.

- To Dr Erna Swanepoel, Prof. Theo Dekker and Mr. Chris Liebenberg, thank you for all your assistance and support during my studies. I appreciate all that you did.

- To all the personnel at the RIIP, thank you for assisting and supporting me during my studies.

- To the National Research Foundations (NRF), thank you for the financial support that you provided.

Pseudo-polymorphic forms of mebendazole

Carel A. Swartz [1], Zak Perold [1], Marius Brits [1] and Marique Auckamp [1]

[1] Research Institute for Industrial Pharmacy® incorporating CENQAM®, North-West University, Potchefstroom Campus, Potchefstroom, 2520

14 November 2008

Abstract

A new pseudo-polymorphic form of mebendazole (Form D) was prepared and characterised, together with the mebendazole propionic acid complex (Form E) previously reported by Caira *et al.* (3). Single electron microscopy (SEM) was performed on the polymorphic and pseudo-polymorphic forms of mebendazole to evaluate potential differences in the crystal habits. SEM analysis revealed that Forms A, B and C did not exhibit a specific crystalline habit and tended to agglomerate, whilst Forms D and E exhibited well-defined needle-like crystal habits. When exposed to increased temperatures, Form D and Form E underwent desolvation, and transformed into the thermodynamically stable form, Form A. VT-XRPD analysis of the two pseudo-polymorphic forms illustrated that both forms converted to Form A.

Keywords: Mebendazole; pseudo-polymorph, solvate, desolvation, polymorph

1 Introduction

Mebendazole (methyl 5-benzoyl-2-benzimidazolecarbamate, Figure. 1) is a synthetic broad-spectrum anthelmintic drug used in the treatment of nematodal and cestodal infestations [1],[2],[3]. Mebendazole inhibits microtubule synthesis in the parasite, followed by irreversibly blocking glucogen uptake, resulting in immobilisation and death [4],[5],[6].

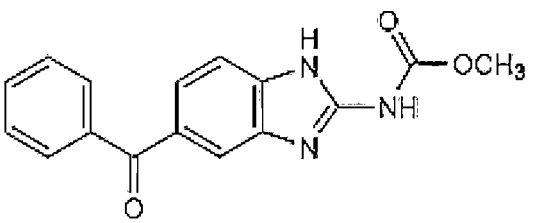

Figure 1 Chemical structure of mebendazole.

Mebendazole is practically insoluble in water, diluted mineral acid solutions, alcohol, chloroform, ether, methylene chloride, and freely soluble in formic acid [7]. Three polymorphic forms have been characterised in the literature (Forms A, B and C) which exhibit different solubility and therapeutic profiles. From clinical studies on the polymorphic forms, Form C is the pharmaceutically preferred form, due to its enhanced solubility profile and therapeutic efficacy [2],[4]. A mebendazole propionic acid complex has been prepared and characterized by Caira *et al.* [3] but very little data is published with regards to the stability of this form.

2 Materials and methods

2.1 Preparation of mebendazole solvated forms

Mebendazole raw material (batch number F10958) was purchased from Rolab (South Africa) and utilised in the recrystallisation of the pseudo-polymorphic forms.

The acetic acid solvate (Form D) was prepared by recrystallisation of mebendazole raw material using glacial acetic acid (analytical grade) as solvent. The solution was heated to approximately 110°C in a fume hood under continues stirring, using a Heidolph MR300K (Heidolph, Germany) magnetic stirrer. Small quantities of solvent were added to the solution to ensure that all the raw material had dissolved, resulting in a supersaturated solution. The supersaturated solution was then removed from the heat source and covered using Parafilm® (Pechiney® plastic packing, Chicago IL, USA). Small holes were pierced in the Parafilm® to allow the solvent to evaporate. Rapid recrystallisation was then induced by cooling the solution in an ice bath. Small quantities of acetone were poured over the ice to allow the temperature to decrease. The recrystallisation vessel was kept in the ice bath for at least 12 hours before it

was removed, after which the crystalline solids were filtered. The crystals were then carefully spread out on filtration paper, to allow residual solvent to evaporate at ambient conditions.

The mebendazole propionic acid solvate (Form E) was prepared using the same method as described for the acetic acid solvate (Form D), using propionic acid as the recrystallisation solvent. Caira *et al.*[3] initially prepared a solution of the mebendazole propionic solvate by dissolving 50 mg of mebendazole in 8 ml of propionic acid, stirred for 25 minutes at 56°C and left to crystallize for 6 months. Contrary to the method described by Caira et al. [3] the recrystallisation of the mebendazole propionic acid solvate (hereafter reffered to as Form E) by means of the alternate method (as used in this study), yielded enough sample for characterisation within a short period of time at the conditions described.

3 Characterisation techniques

3.1 X-ray powder diffraction (XRPD)

X-ray diffraction patterns (XRPD patterns) were recorded using a Bruker D8 Advance diffractometer (Bruker, Germany). The experimental conditions were: target, Cu; voltage, 40kV; current, 30mA; divergence slit, 2 mm; anti-scatter slit, 0.6 mm; detector slit, 0.2 mm; monochromator; scan speed, 2°/min with an increment of 0.025° and a increment time of 1.0 seconds. Samples were prepared by packing the powder into an aluminium sample holder. The aluminium sample holder was placed into the XRPD sample accessory and rotated at 15 revolutions per minute to reduce potential preferred orientation effects of crystals. The peak positions and intensities where extracted from the diffractograms using the Eva® software (version 10.0 revision 1) which is part of the Diffrac^{plus} 2004 software package (Bruker, Germany).

3.2 Variable temperature x-ray powder diffraction (VT-XRPD)

Samples for VT-XRPD analysis were prepared and analysed using the diffractometer setup discussed in section 3.2. Diffraction data were recorded after heating the sample to different temperatures, using an Anton Paar TTK 450 low temperature camera (Anton Paar, Austria) with a heating rate of 10°C/min and maintained at pre-determined temperatures for the duration of the analysis (3 – 40 °2θ).

3.3 Diffuse reflectance infrared Fourier transform spectroscopy (DRIFT-IR)

The infrared spectra of the samples were recorded on a Nicolet Nexus™ 470 Spectrophotometer (Nicolet Instrument Corporation, Madison WI, USA) over a range of 4000 – 400 cm^{-1} with the samples placed in an Avatar Diffuse Reflectance Smart accessory after being mixed and ground with dried KBr (Merck, Darmstadt, Germany). The peak positions and intensities of the spectra recorded were determined using version 7.3 of the OMNIC© software package (Thermo Electron Corporation).

3.4 Differential scanning calorimetry (DSC)

For the purpose of this study 2-5 mg of each sample was placed in a 40 µl aluminium sample pan (Mettler Toledo, Switzerland), crimp sealed with a pierced aluminium lid. The lid was pierced to relieve possible pressure build up which could cause a variation in results. Samples were analysed using a Mettler Toledo DSC823^e (Greifensee, Switzerland) that was calibrated using an indium standard (Mettler Toledo, Switzerland). Samples were analysed at temperatures ranging between 25 - 350°C with a heating rate of 10°C/min and a nitrogen gas purge flow rate of 80 ml/min. The melting points (and other data) were calculated from the thermograms using the STAR^e Software programme (version 9.0*x*) (Mettler Toledo, Switzerland).

3.5 Thermogravimetric analysis (TGA)

For the purpose of this study 10-15 mg of each sample was placed in a 100 µl aluminium pan and covered with a pierced lid (not crimped sealed). Samples were analysed using a calibrated Mettler Toledo TGA/SDTA851^e (Greifensee, Switzerland), with the samples heated between 25 - 200°C at a heating rate of 10°C/min and a nitrogen gas flow rate of 80 ml/min. The weight loss of the sample was calculated using the STAR^e Software programme (version 9.0*x*) (Mettler Toledo, Switzerland).

3.6 Scanning electron microscopy (SEM)

Samples for SEM analysis were prepared by covering the SEM pin with carbon tape and sample, mounted onto a metal stub and coated with a gold-palladium film (Eiko engineering ion coater IB-2, Japan) in a vacuum. The samples were placed in the microscope sample holder and analysed using a FEI Quanta 200 ESEM & Oxford INCA 400 EDS microscope system (FEI Corporation, Hillsboro OR, USA).

3.7 Karl Fischer analysis (KF)

During this study a Metrohm 701 KF Titrino (Herisau, Switzerland) was utilised. The instrument was calibrated with distilled water and validated using sodium tartrate dihydrate (Riedel-de Haën, Germany)

4 Results and discussion

The infrared (IR) spectra of the two solvated forms are shown in Figure 2 (a). The spectra showed similarities, but closer investigation of the -NH stretching frequency and >C=O stretching frequency revealed remarkable differences between the two solvated forms and the reported polymorphic forms of mebendazole. Form D showed unique absorption bands at 3352 cm^{-1} and 1737 cm^{-1} where as Form E showed unique absorption bands at 3364 cm^{-1} and 1735 cm^{-1}. No traces of Forms A, B or C were detected. A comparison of the IR absorption peaks used in the identification of the mebendazole polymorphic and pseudo-polymorphic forms are listed in Table 1 and illustrated in Figure 2 (b) [1]. [2]. [3], [4].

Table 1 Main characteristic IR peaks at corresponding Wavenumbers (cm^{-1}) of mebendazole Forms A, B, C, D and E

IR	Form A	Form B	Form C	Form D	Form E
-NH (cm^{-1})	3370	3340	3410	3352	3364
>C=O (cm^{-1})	1730	1700	1720	1737	1735

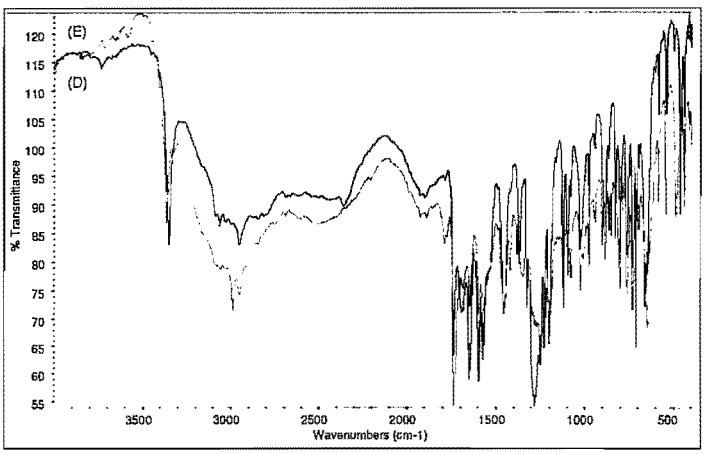

(a)

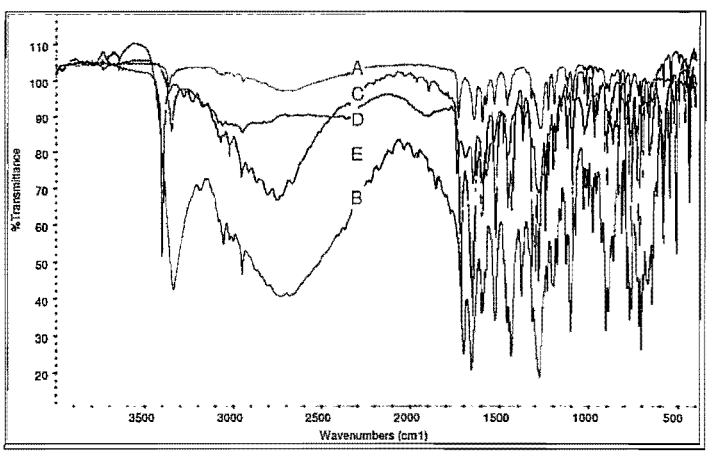

(b)

Figure 2 (a) DRIFT-IR spectra of the solvated (pseudo-polymorphs) of mebendazole. (b) An overlay of the DRIFT-IR spectra of the polymorphic and pseudo-polymorphic forms of mebendazole.

Comparison of the XRPD patterns of the two pseudo-polymorphic forms (Forms D and E) (Figure 3), revealed differences between the diffraction peaks of Form D and Form E. Form D showed a slight shift in the peaks between the regions of 5-9±0.1 °2θ with the appearance of additional peaks at 16.3±0.1 °2θ, 17-18±0.1 °2θ and 22.1±0.1 °2θ and the absence of peaks at 9.6±0.1 °2θ, 19.0±0.1 °2θ and 25.8±0.1 °2θ, when compared to the XRPD pattern of Form E. Although minor similarities were detected in the XRPD patterns of Form D and Form E, they can not be considered as iso-structural pseudopolymorphs.

Table 2 Main XRPD peaks and corresponding diffraction angles (°2θ) of mebendazole Forms A, B, C, D and E

Form A	Form B	Form C	Form D	Form E
7.6±0.1	5.8±0.1	4.9±0.1	6.6±0.1 7.9±0.1 13.2±0.1	6.3±0.1 8.0±0.1 12.6±0.1

With reference to the main XRP diffraction peaks of Forms A, B and C, it is clear that the crystal structure of the two pseudo-polymorphic forms differed from that of the known polymorphic forms, Forms A, B and C (Table 2 and Table 3) [4].[7].

Table 3 The main diffraction angles (°2θ) and corresponding relative intensity values (I/I_0) of Form D and Form E

Main peaks	Form D		Form E	
	°2θ	I/I_0 %	°2θ	I/I_0 %
1	6.6	86.7	6.3	100
2	7.9	95.4	8.0	10.1
3	10.9	31.8	10.7	1.9
4	13.2	100	12.6	34.6
5	15.8	43.7	18.7	3.9
6	17.8	22.3	19.0	12.2
7	20.4	40.9	19.8	5.5
8	21.7	40.9	23.5	3.2
9	22.6	13.4	25.8	3.3
10	27.3	26.9	27.1	2.8

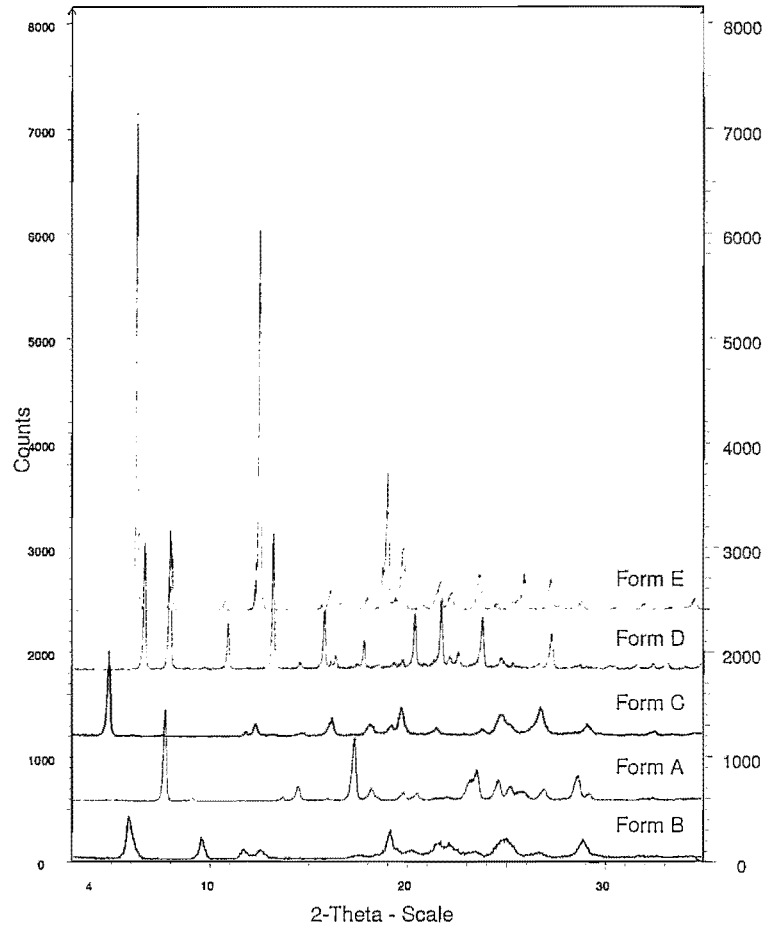

Figure 3 XRPD overlay of mebendazole polymorphs (Forms A, B and C) and pseudo-polymorphs (Forms D and E).

The DSC thermogram (Figure 4) of Form D exhibited three sharply defined endothermic transition events at 109°C, 256°C and 331°C. It is reported in the literature that mebendazole melts at temperatures exceeding 270°C, followed by decomposition. The endothermic event for Form D at 109°C is evident of desolvation.

Table 4 Thermal events in the DSC thermograms of Form D and Form E

Form	Desolvation endotherm (°C)	Thermal endotherms (°C)	
Form D	109	256	331
Form E	124	254	331

The DSC thermogram (Figure 4) of Form E exhibited three sharply defined endothermic events at 124°C, 254°C and 331°C, respectively. The endotherm at 124°C is evident of the desolvation. The desolvation process of Form D and Form E was verified by hot-stage microscopy (HSM). The thermal events of Form D and Form E are listed in Table 4.

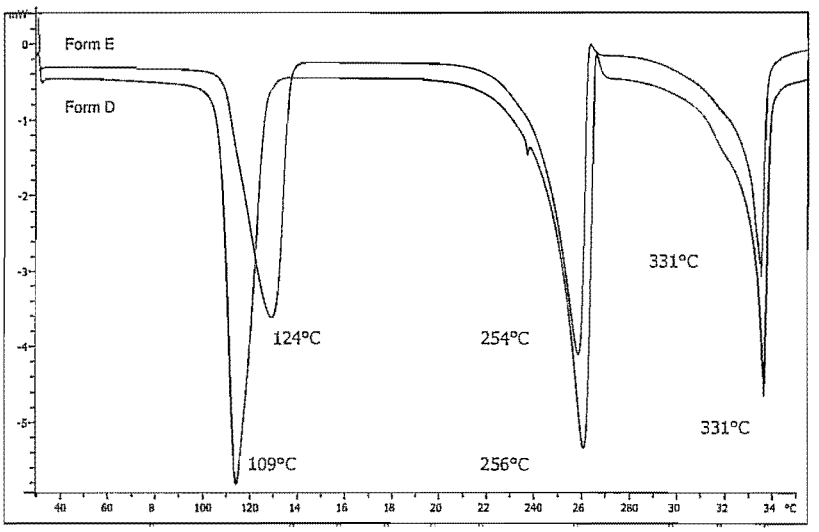

Figure 4 DSC thermograms of Form D and Form E.

Thermogravimetric analysis (Figure 5) of Form D revealed a one-step mass loss of 15.40% in the temperature range 100-150°C (theoretical mass loss of 17.00% calculated using Equation 1, confirming the possibility of a 1:1 mebendazole-acetic acid complex. Form E (Figure 5) revealed a two-step mass loss of 10.01% and 20.76% respectively (theoretical mass loss of 20.05%).

$$\%\ Weight\ loss = \frac{Molecular\ weight\ (solvent)}{Molecular\ weight\ \ (solvent) + Molecular\ weight\ (API)} \times 100\% \quad (1)$$

From the literature it was reported that the mebendazole propionic acid complex underwent a one-step desolvation process of 19.85% in the temperature range of 100-150°C [3]. Unfortunately no data was published describing the mass loss detected in the temperature range of 25-100°C.

Karl Fischer (KF) analysis was utilised to determine whether the mass loss detected on the TGA thermogram of Form E (10.01%) in the temperature range of 25-100°C was due to the presence of water or solvent adsorbed onto the surface of the crystal structure. The KF results

revealed that the sample contained 0.40% (m/m) water which was too low for the % mass loss (determined as 10.01%) detected in the 25-100°C temperature region of Form E, Therefore the change in mass in this region, may be attributed to solvent adsorbed onto the surface of the crystals. It may therefore be concluded that only the second step showed characteristic properties of desolvation [3].

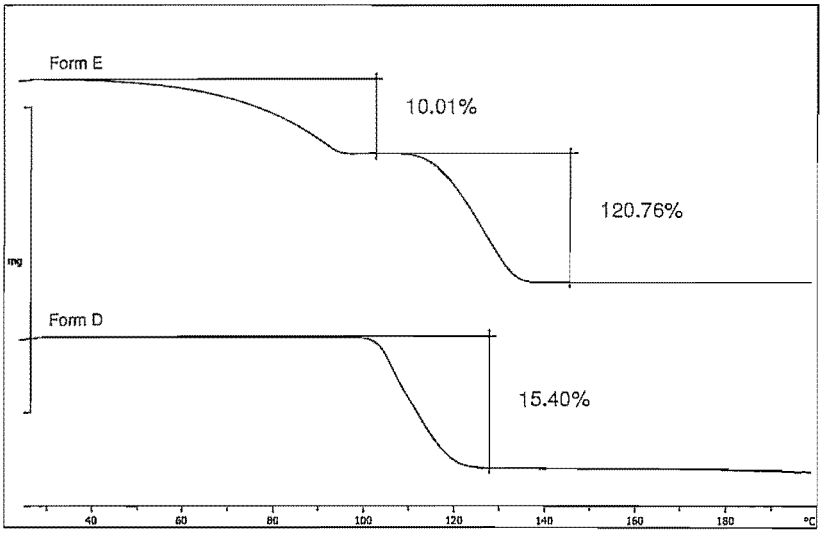

Figure 5 TGA thermograms of Form D and Form E.

Scanning electron microscopy (SEM) was used to investigate the morphology of the two solvated forms of mebendazole. Both Form D and Form E exhibited needle-like shapes with acicular crystalline habits. SEM photographs were also taken for mebendazole Forms A, B and C (Figure 6) to contribute to the available literature. From the SEM photomicrographs it was evident that Forms A, B and C showed no distinct crystal morphology, although the powders appeared to agglomerate.

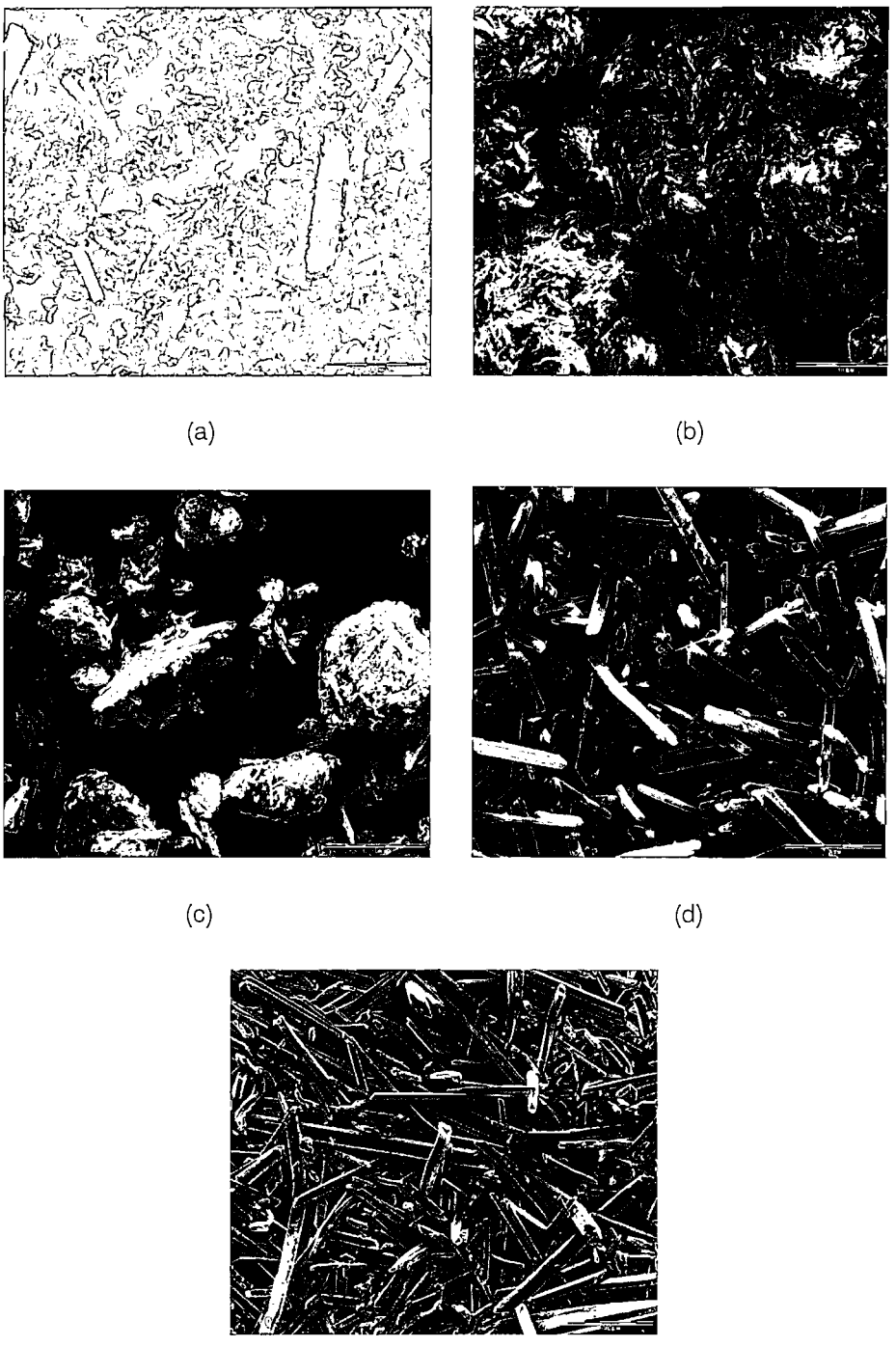

Figure 6 SEM microphotographs of the polymorphic and pseudo-polymorphic forms of mebendazole. (a) Form A, (b) Form B, (c) Form C, (d) Form D and (e) Form E.

VT-XRPD analysis revealed Form D to be stable between 25-75°C with no crystal transitions detected in the temperature range. The desolvation effect was detected from 75°C by the the decrease in the intensity of the 6.6±0.1°2θ peak, characteristic to Form D (Figure 7). At 100°C the diffractogram of Form D showed transition to the stable Form A with the appearance of the 7.6±0.1°2θ peak (characteristic of Form A). As the temperature was increased, the peaks at 7.6±0.1°2θ and 17.3±0.1°2θ increased in intensity, while the characteristic peaks of Form D at 6.3±0.1°2θ and 13.2±0.1°2θ disappeared after 100°C. The transition of the Form D to the stable crystal form (Form A) was completed at 110°C with no further transitions detected. The sharp endotherm detected on the DSC at 109°C indicated the presence of a solvate (temperature of desolvation) and transition of Form D to Form A. The VT-XRPD results confirm the findings of the DSC analysis.

The VT-XRPD analysis of Form E indicated that Form E was stable between 25-85°C with no crystal transitions (desolvation) detected in the temperature range (Figure 8). At 95°C the diffractogram of Form E showed a transition to the stable Form A with the appearance of the 7.6±0.1°2θ and 17.3±0.1°2θ peaks (characteristic of Form A). As the temperature was increased the peak at 7.6±0.1°2θ and 17.3±0.1°2θ increased in intensity while the characteristic peak of Form E at 6.3±0.1°2θ decreased. The transition of Form E to the stable crystal form (Form A) was completed at temperatures ranging between 110 and 120°C with no further transitions detected. The sharp endotherm detected on the DSC at 124.18° indicated the presence of a solvate (temperature of desolvation) and transition of Form E to Form A. The VT-XRPD results confirm the findings of the DSC analysis.

The XRPD patterns of Form D and Form E after heating of the sample to ±130°C were comparable with the XRPD pattern of mebendazole Form A, indicating full transition to the stable polymorphic form.

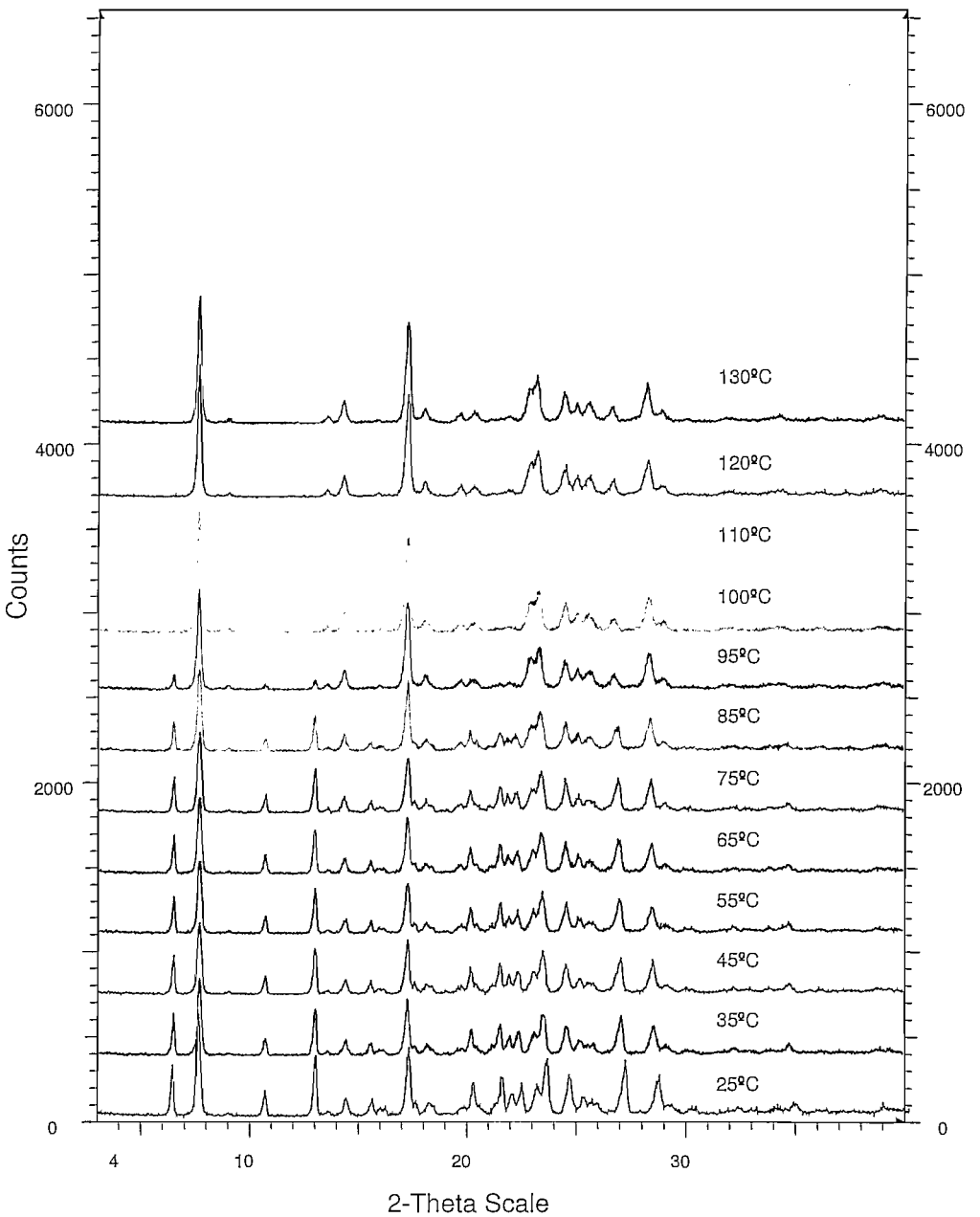

Figure 7 VT-XRPD diffractograms of mebendazole Form D.

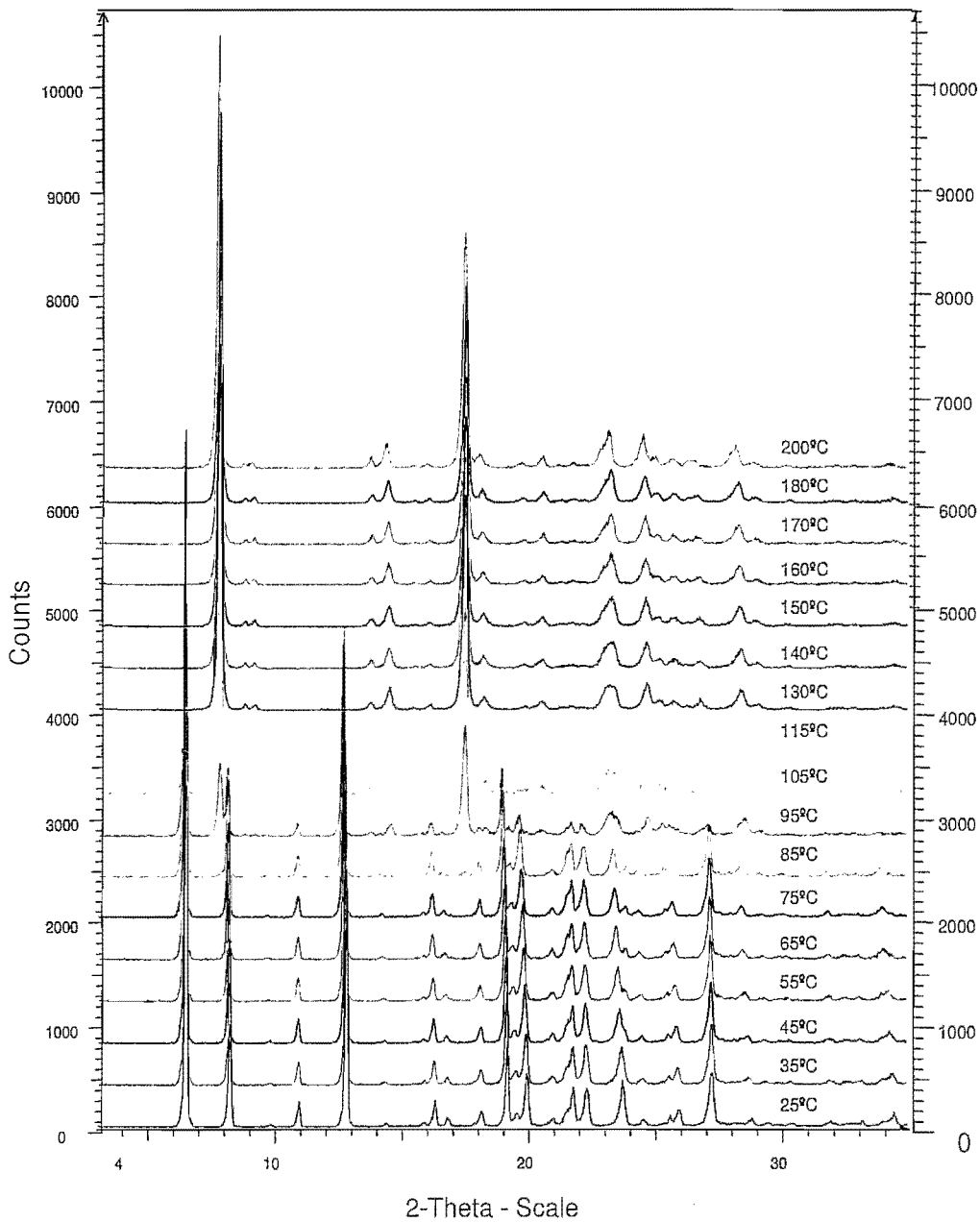

Figure 8 VT-XRPD diffractograms of mebendazole Form E.

Table 5 provides a summary of the characteristic physico-chemical properties of the mebendazole polymorphic and pseudo-polymorphic forms [1],[4],[7].

Table 5 Summary of the characteristic differences between the polymorphic and pseudo-polymorphic forms of mebendazole

Technique	Form A	Form B	Form C	Form D	Form E
DRIFT-IR (-NH) (cm^{-1})	3370	3340	3410	3353	3364
DRIFT-IR (>C=O) (cm^{-1})	1730	1700	1720	1738	1735
XRPD (°2θ)	7.6 17.30	5.8	4.9	6.6 7.9 13.2	6.3 8.0 12.6
DSC (°C)	250-255 330	220 263 330	195 225 253 330	109 256 331	124 254 331
TGA Range: 100-200°C	N/A	N/A	N/A	15.40%	20.76%

5 Summary and conclusion

A new pseudo-polymorphic form of mebendazole (acetic acid solvate) was recrystallised by means of a rapid recrystallisation method. The same method was used to recrystallise the mebendazole propionic acid complex (using propionic acid as recrystallisation solvent).

Both the pseudo-polymorphs were characterised by DSC, TGA, HSM and VTXRPD and classified as solvated forms of mebendazole. The DRIFT-IR and XRPD analysis of the two forms revealed some resemblances.

Form D and Form E exhibited needle-like crystalline habits. When the solvated forms (Form D and Form E) were exposed to increased temperatures, the solvent entrapped within the crystalline lattices were released and the desolvated crystal lattices transformed into the thermodynamically stable form, Form A.

VT-XRPD analysis of Form D and Form E revealed the two solvated forms to be stable at temperatures below 75°C and 85°C individually. When exposed at temperatures above these temperatures, Form D and Form E showed polymorphic transitioning to the stable Form A.

References

1. **HIMMELREICH, M., RAWSON, B.J. & WATSON, T.R.** 1977. Polymorphic forms of mebendazole. *Australian Journal of Pharmaceutical Sciences*, 6(4)123-125.

2. **SWANEPOEL, E., LIEBENBERG, W. & DE VILLIERS, M.M.** 2003. Quality evaluation of generic drugs by dissolution test: changing the USP dissolution medium to distinguish between active and non-active mebendazole polymorphs. *European Journal of Pharmaceutics and Biopharmaceutics*, 55:345-349.

3. **CAIRA, M.R., DEKKER, T.G. & LIEBENBERG, W.** 1998. Structure of a 1:1 complex between the anthelmintic drug mebendazole and propionic acid. *Journal of Chemical Crystallography*, 28(1):11-15.

4. **DE VILLIERS, M.M., TERBLANCHE, R.J., LIEBENBERG, W., SWANEPOEL, E. DEKKER, T.G. & SONG, M.** 2005. Variable-temperature X-ray powder diffraction analysis of the crystal transformation of the pharmaceutical preferred polymorph C of mebendazole. *Journal of Pharmaceutical and Biomedical Analysis*, 38:435-441.

5. **FRAYHA, G.J., SMYTH, J.D., GOBERT, J.G. & SAVEL, J.** 1997. The mechanisms of action of antiprotozoal and anthelmintic drugs in man. *General Pharmacology*, 28(2):273-299.

6. **KATZUNG, B.G.**, ed. 2001. Clinical pharmacology of the anthelmintic drugs. Basic and Clinical Pharmacology. 8th edition:903-922. 1217p.

7. **BRITS, M.** 2008. Solid-state properties of pharmaceuticals. Potchefstroom: NWU. (Thesis – PhD) 549p.